AD-A181 776 SLOPING FLOAT BREAKWATER STUDY OREGON INLET NORTH CAROLINA COASTAL MODEL INVESTIGATION(U) COASTAL ENGINEERING RESEARCH CENTER VICKSBURG MS 1/3

UNCLASSIFIED R D CARVER ET AL. APR 87 CERC-TR-87-5 F/G 13/2 NL

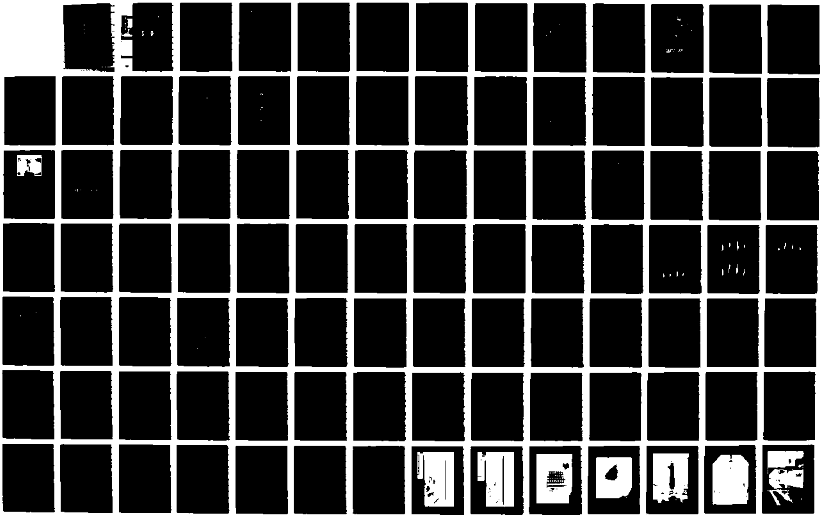

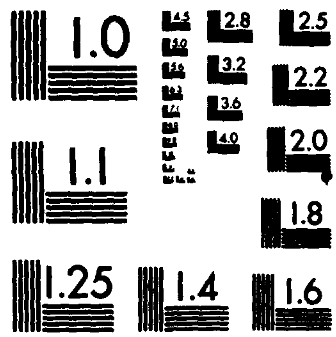

MICROCOPY RESOLUTION TEST CHART
NATIONAL BUREAU OF STANDARDS-1963-A

(12)

S Army Corps
Engineers

AD-A181 776

TECHNICAL REPORT CERC-87-5

SLOPING FLOAT BREAKWATER STUDY OREGON INLET, NORTH CAROLINA

Coastal Model Investigation

by

Robert D. Carver, Dennis G. Markle, Willie G. Dubose,
Robert E. Jensen

Coastal Engineering Research Center

DEPARTMENT OF THE ARMY
Waterways Experiment Station, Corps of Engineers
PO Box 631, Vicksburg, Mississippi 39180-0631

April 1987

Final Report

Approved For Public Release; Distribution Unlimited

Prepared for US Army Engineer District, Wilmington
Wilmington, North Carolina 28042

Unclassified
SECURITY CLASSIFICATION OF THIS PAGE

AD-A181 776

REPORT DOCUMENTATION PAGE

Form Approved
OMB No 0704-0188
Exp Date Jun 30, 1986

1a. REPORT SECURITY CLASSIFICATION Unclassified	1b. RESTRICTIVE MARKINGS
2a. SECURITY CLASSIFICATION AUTHORITY 2b. DECLASSIFICATION/DOWNGRADING SCHEDULE	3. DISTRIBUTION/AVAILABILITY OF REPORT Approved for public release; distribution unlimited
4. PERFORMING ORGANIZATION REPORT NUMBER(S) Technical Report CERC-87-5	5. MONITORING ORGANIZATION REPORT NUMBER(S)
6a. NAME OF PERFORMING ORGANIZATION USAEWES, Coastal Engineering Research Center 6b. OFFICE SYMBOL (If applicable)	7a. NAME OF MONITORING ORGANIZATION
6c. ADDRESS (City, State, and ZIP Code) PO Box 631 Vicksburg, MS 39180-0631	7b. ADDRESS (City, State, and ZIP Code)
8a. NAME OF FUNDING/SPONSORING ORGANIZATION US Army Engineer District, Wilmington 8b. OFFICE SYMBOL (If applicable)	9. PROCUREMENT INSTRUMENT IDENTIFICATION NUMBER
8c. ADDRESS (City, State, and ZIP Code) PO Box 1890 Wilmington, NC 28042	10. SOURCE OF FUNDING NUMBERS PROGRAM ELEMENT NO. / PROJECT NO. / TASK NO. / WORK UNIT ACCESSION NO

11. TITLE (Include Security Classification)

Sloping Float Breakwater Study, Oregon Inlet, North Carolina: Coastal Model Investigation

12. PERSONAL AUTHOR(S)

Carver, Robert D., Markle, Dennis G., Dubose, Willie G., Jensen, Robert E.

13a. TYPE OF REPORT	13b. TIME COVERED	14. DATE OF REPORT (Year, Month, Day)	15. PAGE COUNT
Final report	FROM Jan '81 TO Jul '84	April 1987	221

16. SUPPLEMENTARY NOTATION

Available from National Technical Information Service, 5285 Port Royal Road, Springfield, VA 22161.

17. COSATI CODES			18. SUBJECT TERMS (Continue on reverse if necessary and identify by block number)	
FIELD	GROUP	SUB-GROUP	Barges	Mooring lines
			Floating breakwaters	Oregon Inlet, North Carolina
			Hydraulic models	Waves

19. ABSTRACT (Continue on reverse if necessary and identify by block number)

Two-dimensional (2-D) and three-dimensional (3-D) hydraulic model investigations were conducted at an undistorted linear scale of 1:25 (model to prototype) to acquire data on transmitted wave heights, mooring line forces, intermodule connector forces, bottom impact velocities, and barge angularities as a function of wave climate. These data were needed as input to optimize the design of the sloping float breakwater (SFB) concept whose function would be to protect floating dredges being used for sand bypassing at Oregon Inlet, N. C.

The 2-D tests indicated that for the 89.6- and 118.4-ft SFB's (a) the transmission response of both structures is strongly dependent on wave period; (b) increasing the water depth significantly decreases the wave-attenuating capabilities of both structures; (c) for most wave conditions, mooring forces are similar for both SFB lengths and tend to

(Continued)

20. DISTRIBUTION/AVAILABILITY OF ABSTRACT ☒ UNCLASSIFIED/UNLIMITED ☐ SAME AS RPT ☐ DTIC USERS	21. ABSTRACT SECURITY CLASSIFICATION Unclassified
22a. NAME OF RESPONSIBLE INDIVIDUAL	22b. TELEPHONE (Include Area Code) / 22c. OFFICE SYMBOL

DD FORM 1473, 84 MAR — 83 APR edition may be used until exhausted. All other editions are obsolete.

SECURITY CLASSIFICATION OF THIS PAGE
Unclassified

19. ABSTRACT (Continued).

increase with increasing depth; and (d) peak flow velocities under the structure are generally higher for the longer SFB.

The 3-D tests revealed that the existing barge connector concept would be subjected to extremely high forces during impact on a rigid bottom. A softer seafloor condition greatly reduced the connector forces, but since a soft bottom condition could not be guaranteed at all prototype sites, it was determined that the design of the existing connector system for highly rigid bottom-impact forces was not economically feasible. A connector system design that is isolated from these highly rigid bottom-impact forces is feasible, but needs further indepth study.

PREFACE

The model investigations reported herein were requested by the US Army Engineer District, Wilmington (SAW), during a December 1979 telephone conversation with the US Army Engineer Waterways Experiment Station (WES) Coastal Engineering Research Center (CERC). Funding authorization was granted by SAW on Intra-Army Order No. SAWEN-PC-80-225 dated 1 April 1980 and Change Orders numbers 1 through 8 dated 22 December 1980, 8 January 1982, 23 March 1982, 22 July 1982, 12 October 1982, 10 November 1982, 27 January 1983, and 30 November 1983, respectively.

Model tests were conducted at WES during the period January 1981 to July 1984, under the general direction of Mr. H. B. Simmons, former Chief, Hydraulics Laboratory, Dr. J. R. Houston, Chief, CERC, and Mr. C. C. Calhoun, Jr., Assistant Chief, and Mr. C. E. Chatham, Chief, Wave Dynamics Division, and Mr. D. D. Davidson, Chief, Wave Research Branch. The Wave Dynamics Division and its personnel were transferred to the Coastal Engineering Research Center under the direction of Dr. R. W. Whalin, Chief of CERC on 1 July 1983. The model tests were planned and conducted by Messrs. R. D. Carver and D. G. Markle, Research Hydraulic Engineers, and Mr. W. G. Dubose, Engineering Technician, with the assistance of Mr. C. L. Lewis, Engineering Technician, Mr. K. A. Turner, Computer Specialist, Mr. H. C. Greer, Electronics Engineer, and Messrs. L. B. Smithhart, S. W. Guy, and L. L. Friar, Electronics Technicians. Prototype information was provided by and model test plans were coordinated through Messrs. Tom Jarrett, Bill Dennis, and Lim Vallianos, SAW. Additional technical assistance was provided by Messrs. Bob Taylor and Don Jones, Naval Civil Engineering Laboratory and Drs. Maxwell Cheung and Charles Babcock, MCA Engineers, Inc. Dr. Robert Jensen prepared Part III of this report. The remainder of this report was prepared by Messrs. Carver, Markle, and Dubose.

Liaison was maintained during the course of the investigation by means of conferences, progress reports, and telephone conversations.

Commander and Director of WES during the preparation and publication of this report was COL Dwayne G. Lee, CE. Technical Director was Dr. Robert W. Whalin.

CONTENTS

CONVERSION FACTORS, NON-SI TO SI (METRIC) UNITS OF MEASUREMENT

Non-SI units of measurement used in this report can be converted to SI (metric) units as follows:

Multiply	By	To Obtain
feet	0.3048	metres
feet per second	0.3048	metres per second
feet per second per second	0.3048	metres per second per second
inches	25.4	millimetres
kips	4448.222	newtons
knots (international)	0.5144444	metres per second
pounds (force)	4.448222	newtons
pounds (force) per inch	175.1268	newtons per metre
pounds (mass)	0.4535924	kilograms
pounds (mass) square feet	0.028317	kilograms square metres

SLOPING FLOAT BREAKWATER STUDY

OREGON INLET, NORTH CAROLINA

Coastal Model Investigation

PART I: INTRODUCTION

Background

1. Oregon Inlet (Figure 1), the northernmost opening through the barrier reef of the North Carolina coast, is of major hydrological significance in that it is the only existing communicator between the sounds of northeastern North Carolina and the Atlantic Ocean. The area immediately adjacent to Oregon Inlet includes all of Dare County. Principal economic activities include services, recreation, commercial fishing, seafood processing, and boat building.

2. The existing project channel depth of 14 ft* across the ocean bar at Oregon Inlet is neither deep enough nor stable enough for safe navigation by operators of commercial fishing vessels from North Carolina and other out-of-state ports. In an effort to provide safe passage for commercial fishing craft and other commercial ships, the US Army Engineer District, Wilmington (SAW), has proposed a channel improvement and stabilization project for Oregon Inlet. The proposed project will include a 20-ft-deep and 400-ft-wide channel through the ocean bar at Oregon Inlet. Protection for the new channel will be provided by rubble-mound jetties.

3. It is anticipated that net differences in north-south longshore transport rates will necessitate bypassing (dredging) significant quantities of sand. The primary system for sand bypassing at Oregon Inlet would involve the use of a conventional cutter-suction pipeline dredge to remove material directly from the accretion fillet that would form updrift of the stabilized inlet. Due to the severity of the wave climate in the project area, the efficiency of the sand bypassing operation would be maximized through the use of a transportable breakwater that would be deployed seaward of the fillet borrow

---

* A table of factors for converting non-SI units of measurement to SI (metric) units is presented on page 3.

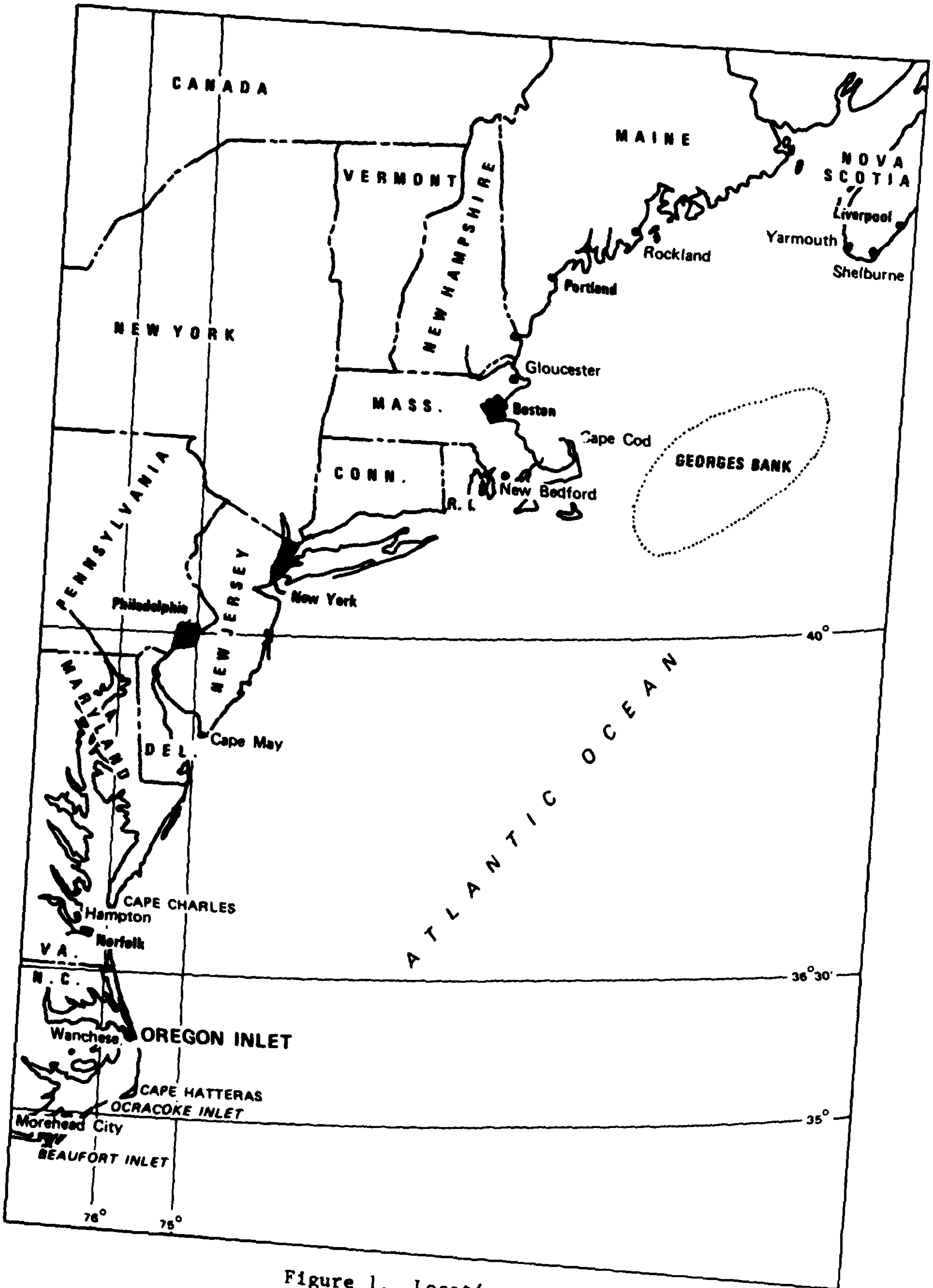

Figure 1. Location map

area. The breakwater would remain onsite during the dredging operation after which it would be removed and stored in a protected area or possibly used at other project sites. Advantage would be taken of the seasonal variability of the wave climate by scheduling sand bypassing during the low wave energy period that extends from May to August of each year. Based on an extensive literature review and analysis of available model and prototype performance data, SAW determined that the sloping float breakwater (SFB) concept (Patrick 1951, Raichlen and Lee 1978, and Raichlen 1981) is the most promising alternative available.

Description of the SFB Concept

4. The SFB is a wave barrier that consists of a row of flat slabs or panels whose weight distribution is such that each panel rests with one end above the water surface and the other end on the bottom. Various types of construction are possible; however, hollow steel or concrete barges appear to have the most promise (Jones 1980). Deployment would consist of assembling unballasted modules at the surface and then partially flooding the barges so the stern sinks and rests on the bottom and the bow floats above the water surface. The height of protrusion of the bow above the water surface (freeboard) is controlled by flooding a selected number of pontoons or barge compartments. Barges are positioned so that the bow faces into the primary direction of wave attack and mooring lines are attached between the barge and a bottom anchor. Figure 2 shows two barges moored together and Figure 3 illustrates a possible arrangement for groups of eight barges.

Purpose of Model Study

5. A need for hydraulic model tests arose from the intent of SAW to select a SFB configuration which is optimum in terms of cost-effectiveness; (i.e., the selection of breakwater length, positioning, connectors, and mooring system is to be based on a least-cost alternative in terms of combined capitalized initial construction costs and expected annual operational and maintenance costs). Determination of these costs necessitated as inputs the determination of transmitted wave heights, mooring line forces, intermodule connector forces, bottom impact velocities, and barge angularities as a

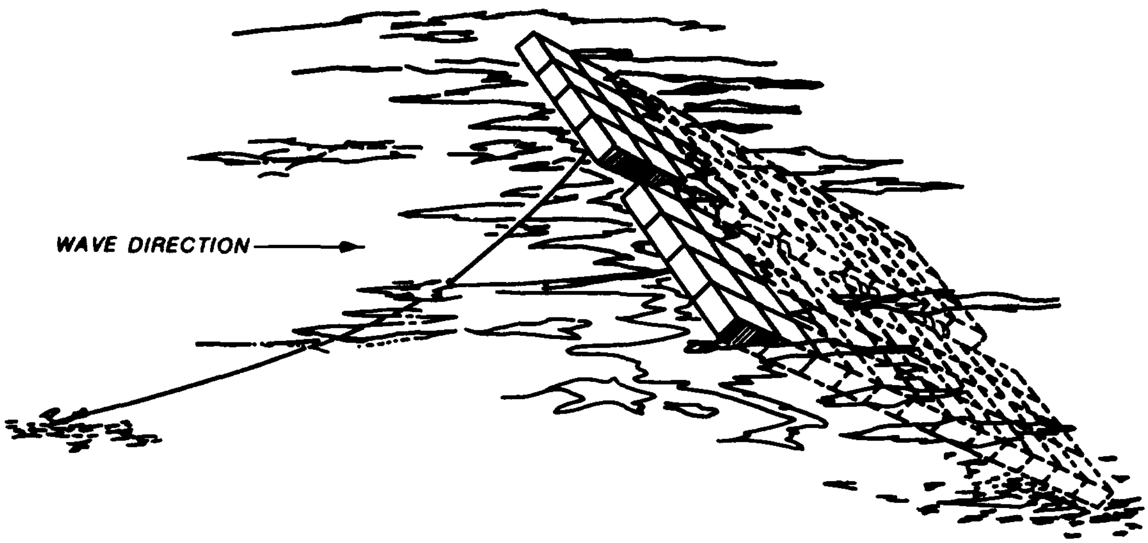

Figure 2. The SFB--an artist's conception

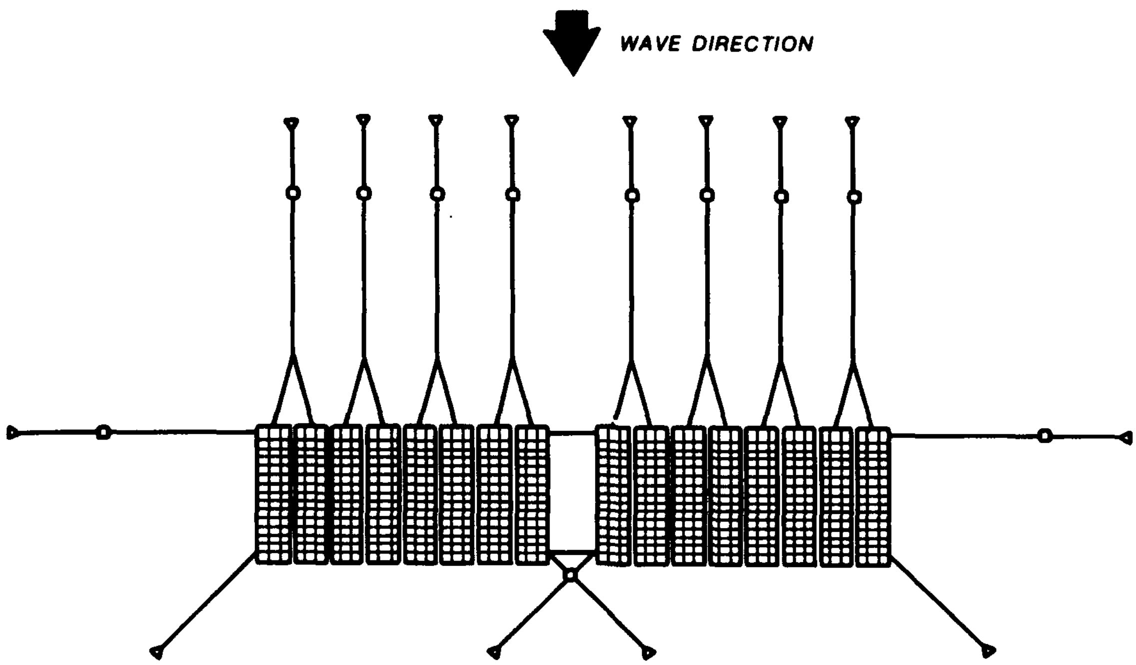

Figure 3. Two groups of SFB's

function of wave climate. The purposes of the model studies were to conduct a sufficient number of tests, both two-dimensional (2-D) (functional tests) and three-dimensional (3-D) (side-connector tests), to provide the data required for this design optimization.

PART II: THE MODELS

Design of Models

Scale selection

6. It is imperative in any model investigation of wave structure interaction that model dimensions (i.e., model scales) are made large enough to preclude any significant scale effects. Descriptions of numerous floating breakwater model studies are found in the literature; however, no comprehensive investigation of possible scale effects has been performed. Prototype flow phenomena and structure motions are primarily controlled by gravitational forces; consequently, models of this type are designed and operated in accordance with Froude's model law, while Reynolds numbers are not in similitude. This dissimilarity has no effect on the validity of test results if model Reynolds numbers are large enough to ensure turbulent flow for all test conditions. Since the Reynolds number is directly proportional to the product of a characteristic length and velocity, its values are maximized by making the model as large as possible.

7. Considering (a) capabilities (wave board velocities, electronic control accuracy, etc.) of the largest monochromatic/spectral wave generators available for the study, (b) maximum stable wave convergence, and (c) the required range of test conditions it was determined that a scale ratio of 1:25 was the largest practical value to use (most importantly, this value would ensure turbulent flow for all test conditions). Based on Froude's model law and the linear scale of 1:25, the following model-to-prototype relations were derived for the 2-D and 3-D models:

Characteristic	Dimension	Model-to-Prototype Scale Relation
Length	L	$L_r = 1:25$
Area	L^2	$A_r = L_r^2 = 1:625$
Volume	L^3	$V_r = L_r^3 = 1:15625$
Time	T	$T_r = L_r^{1/2} = 1:5$
Weight	F	$W_r = L_r^3(64/62.4) = 1:16026$

Dimensions are in terms of force (F), length (L), and time (T).*

* Symbols and abbreviations are listed in the Notation (Appendix A).

Design of model SFB's (functional tests)

8. The functional model tests were conducted with SFB's that simulated Navy Lightered (NL) pontoon-type barges that measured 72.3, 89.6, and 118.4 ft long. The barges are 21 ft wide and 5 ft deep. Bow and stern pontoons are 7 ft by 7 ft in plan and those comprising the interior rows are 5 ft by 7 ft. All pontoons are 5 ft deep. Structural steel assembly angles (6 by 6 by 1/2 in. thick) are used to connect the pontoons. Exact geometric details of the prototype barges, needed for model design, were obtained from "Pontoon Gear Handbook Navy Lightered (NL) Equipment P-Series" (Naval Facilities Engineering Command 1974). The NL pontoon structures were initially considered since the previous developmental work by the Navy, which included some field tests of prototype units, was based on the use of modified pontoon barges.

9. As previously discussed, the bow freeboard and the angle of inclination are controlled by flooding a specified number of pontoons. The structures tested herein represented ballasted conditions that allowed for about 5 ft of free-board. Required ballasting was as follows:

SFB	Number of Rows of Pontoons		Weight, lb		
Length, ft	Total	Flooded	Unballasted SFB	Ballast	Total
72.3	12	8	108,000	266,000	374,000
89.6	15	11	134,000	366,000	500,000
118.4	20	14	177,000	467,000	644,000

10. Important geometric and dynamic details of the prototype barge were considered in the design and the construction of the model sections. Overall prototype dimensions were precisely reproduced and all major parameters that control dynamic response (i.e., weight, center of gravity, mass moments of inertia, and angle of inclination) were reproduced within ±1.0 percent. It should be noted that the model structures were 2.96 ft wide. Thus, a prototype width of 74.0 ft (or 3.5, 21-ft-wide barges) was represented. Because of the 2-D nature of the tests, this dissimilarity had no effect on model results even though the model structures represent 3.5 widths of a 21-ft-wide barge. All model results are presented relative to a normal 21-ft-wide barge. The model SFB's were constructed from marine plywood, aluminum plate, and styrofoam. Photos 1 and 2 show the 89.6- and 118.4-ft model structures, respectively.

Design of model SFB's (side-connector tests)

11. Based on both technical and economic analyses of data gathered during the Navy field tests and the 2-D functional model tests, the structural design of the SFB was changed to a prestressed concrete barge that measured 130 ft wide, 90 ft long, and 5.5 ft deep with consideration given to possibly connecting two such barges along their 90-ft sides (Figure 4). Connectors would be located 6.75 ft inward from the bow and stern and at the center of the 90-ft sides. The bow and stern connectors would resist vertical loads and loads along the 130-ft barge axis while the center connector would resist loads along the 90-ft length. These connectors would give the two barges freedom of movement analogous to a door hinge. The barge interior would be compartmentalized and a portion of the compartments toward the stern of the barge would be ballasted with seawater so that one of its 130-ft-long sides (stern) would rest on the seafloor while the other (bow) would be above water and facing the open ocean. Each of the barges would have ballasted and unballasted weights of 3,566,600 and 2,175,000 lb, respectively. Mass moments of inertia and centers of gravity would be as shown in Figure 4. This amount of ballast will cause the SFB to float at an angle of 14.5 deg relative to the horizontal when the stern of the SFB is placed in a 20-ft water depth.

12. The model barges were constructed of aluminum plates of various thicknesses and alloy types (Photos 3 and 4). The model barges were designed and constructed so they could be ballasted and deballasted with fresh water and were scaled to reproduce the overall geometry, weight, mass moments of inertia, and centers of gravity of the ballasted and unballasted prototype barges.

13. The model SFB barges were connected by two instrumented connectors that were centered on the 5.5-ft (prototype) dimension of the barges and located 6.75 ft (prototype) from the bow and stern (Figures 4-7 and Photo 5). The spacing between the prototype barges was not specified prior to model construction. Guidelines from SAW only specified that the connectors be kept as compact as possible. The resulting assembled model connector length corresponded to a prototype barge spacing of 4.7 ft. The model did not incorporate the third connector, but, instead, simulated its resistance in the other two model connectors. Thus, forces along the 90-ft axes could be measured at the two simulated connectors and then the loadings could be

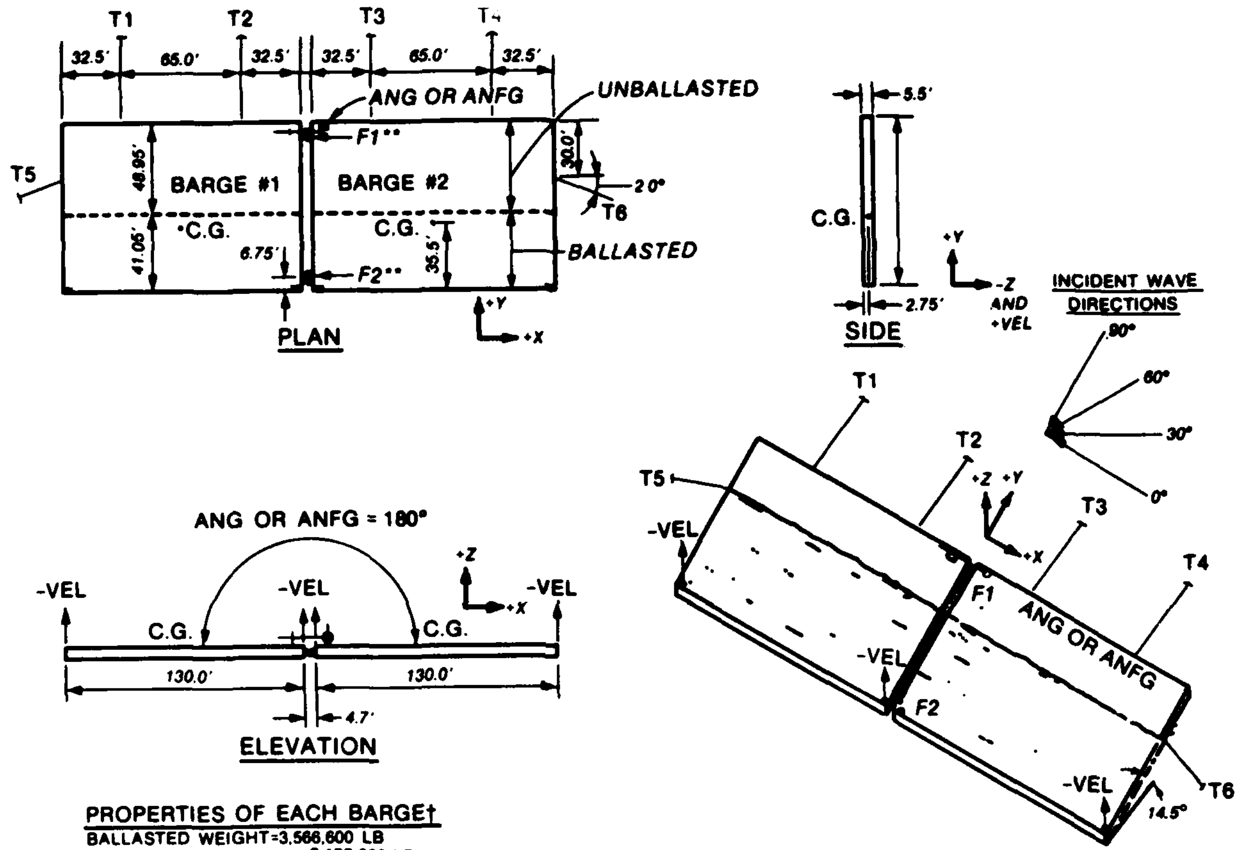

PROPERTIES OF EACH BARGE†

BALLASTED WEIGHT=3,566,600 LB
UNBALLASTED WEIGHT= 2,175,000 LB
MASS MOMENTS OF INERTIA ABOUT AXES PASSING THROUGH THE CENTER OF GRAVITY (C.G.)

I_{mX} = 2,167,060,000 $LB_m FT^2$
I_{mY} = 5,000,660,000 $LB_m FT^2$
I_{mZ} = 7,151,620,000 $LB_m FT^2$

† ALL PROPERTIES ARE GIVEN IN PROTOTYPE TERMS

LEGEND

T1 - T6	MOORING LINES
F1 & F2	BARGE CONNECTORS
ANG OR ANFG	ANGULARITY OF BARGES
VEL	STERN VELOCITY *

* VELOCITY POSITIVE IN NEGATIVE Z DIRECTION
** INSTRUMENTED PORTION OF CONNECTORS ATTACHED TO BARGE # 1

Figure 4. SFB characteristics, mooring line locations, and title and locations of model data channels

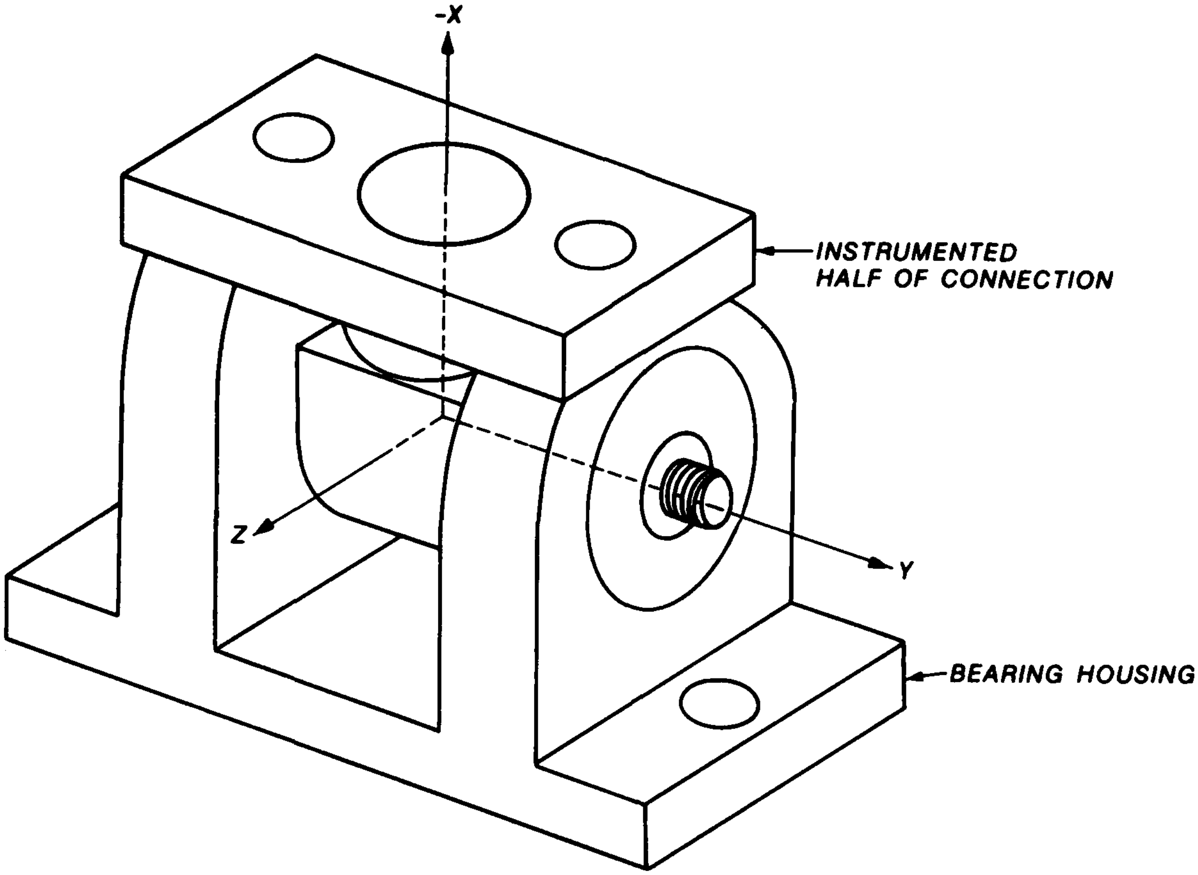

Figure 5. Model connector assembly

numerically transferred to the proper location (center of the 90-ft sides) during the analysis of the model data.

Model mooring system (functional tests)

14. The functional model tests were conducted with a mooring system that simulated a 150-ft-long, 8-in. circumference, double braided nylon rope. The breaking strength of this line is 230,000 lb. With one line attached to each 21-ft-wide NL pontoon barge, the breaking strength of the mooring line per foot of breakwater width was about 11,000 lb/ft. The stress-strain diagram for this material is nonlinear; therefore, restoring force characteristics are also nonlinear.

15. The nonlinear restoring force characteristics of the nylon line were simulated with a series of four linear springs (see Photo 6). The spring system was designed and fabricated by Dr. Fredric Raichlen, California Institute of Technology, and a detailed description of design considerations and procedures is presented in "Experiments with a Sloping Float Breakwater in

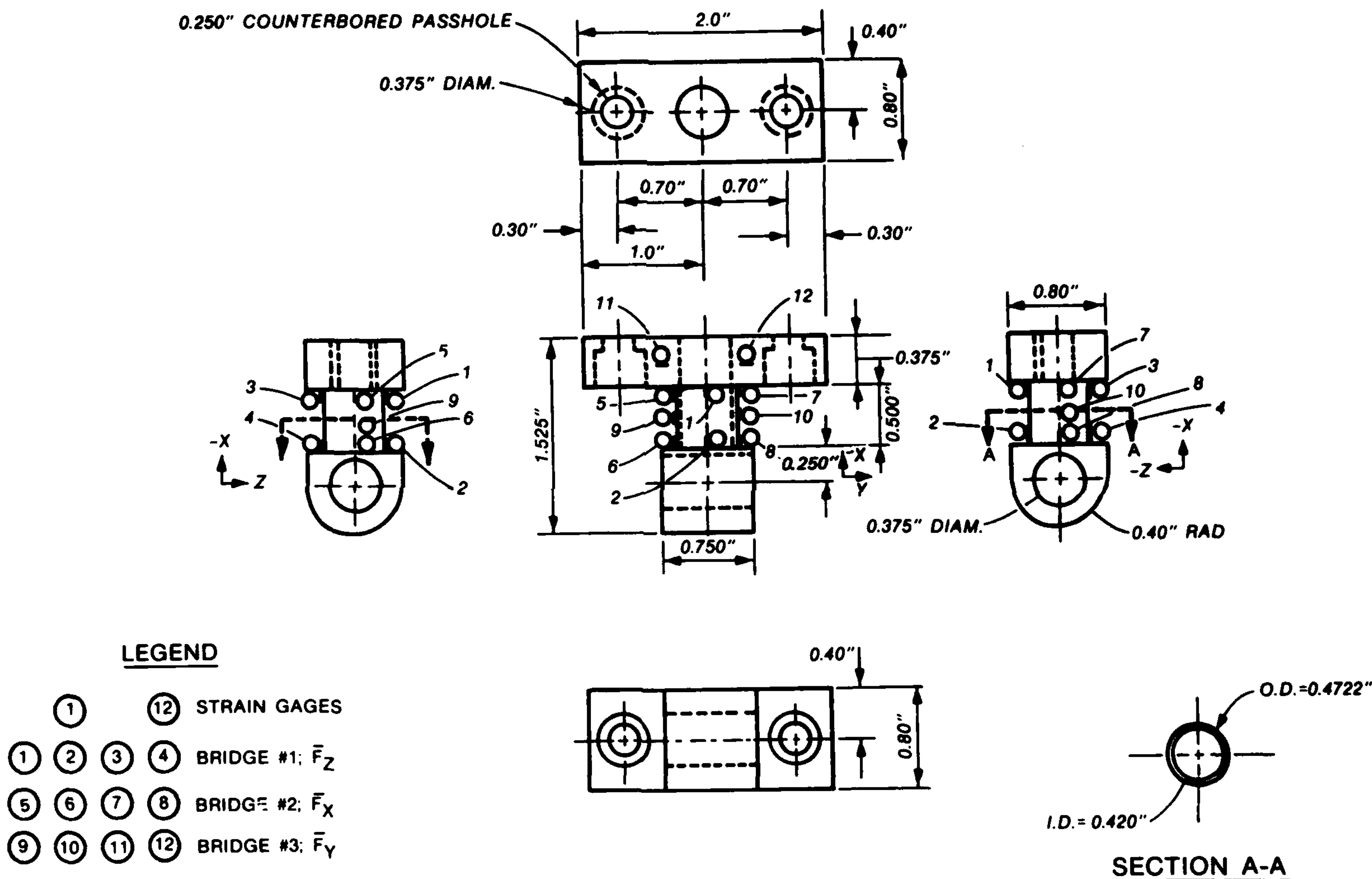

NOTE: CONSTRUCTED OF STRUCTURAL STEEL AND NONINSTRUMENTED AREAS WERE ELECTROLESS NICKEL PLATED TO PREVENT CORROSION.

Figure 6. The instrumented half of the model connector

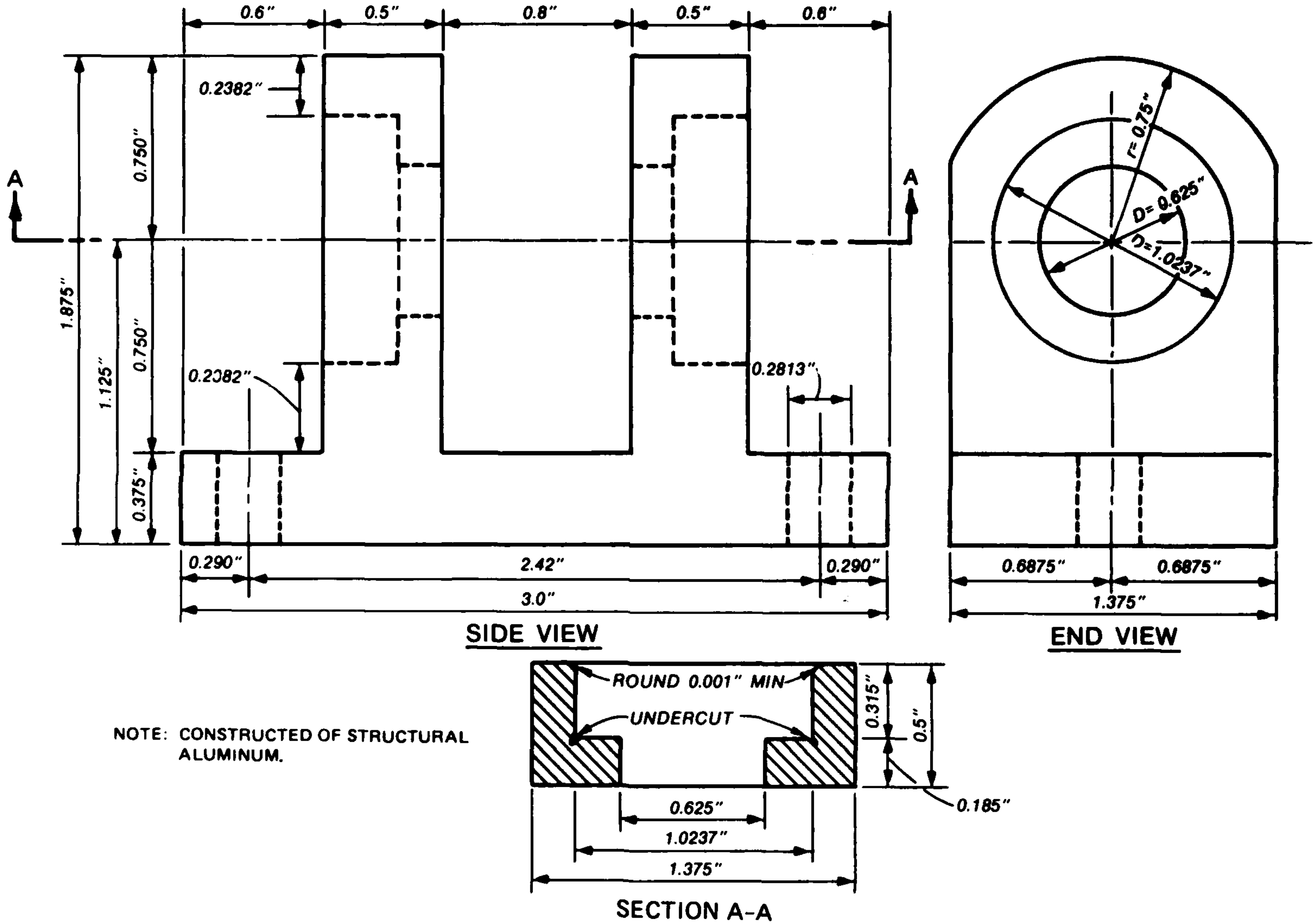

Figure 7. Bearing housing half of model connector

Water Waves-Phase I" (Raichlen 1981). The spring system functions as follows: for small deflections all springs act in series; however, after a predetermined deflection a stop is reached and only three of the springs can deflect further. After the system deflects a certain additional amount another stop is reached and two springs act. Finally, a third stop is reached and only one spring continues to elongate.

16. The spring system with the intermediate stops was calibrated by attaching weights and measuring the deflection. Results of calibration were in excellent agreement with the desired force-displacement relationship (±2.0 percent).

Model mooring system
<u>(side-connector tests)</u>

17. As previously noted, the structural design of the SFB was changed to a 130-ft-wide post-tensioned concrete barge prior to the initiation of the 3-D side connector tests. In addition, the mooring arrangement was modified from that used in the 2-D functional test and consisted of six mooring lines arranged as shown in Figure 4. Each mooring line would be 245 ft long and composed of 110 ft of steel chain and 135 ft of 20-in. circumference, 2 in 1 braided nylon rope. The nylon rope has wet and dry breaking strengths of 992,000 lb and 1,050,000 lb, respectively. Based on the wet breaking strength of the nylon rope, the breaking strength of the mooring system was equivalent to 14,200 lb/ft of breakwater or slightly stronger than the breaking strength used in the functional tests. Six spring systems were designed, constructed, and calibrated to simulate the elasticity of the 135-ft-long nylon portion of the prototype mooring line. A spring system was installed on each of the six mooring lines. It was necessary to suspend the spring systems above the water; therefore, a pulley was designed and constructed of Plexiglas and Teflon. The pulleys were attached to the flume floor in positions that corresponded to the prototype anchor weight locations, and a monofilament line was attached between the barges and each spring system. Due to the limited space in the test facility, the model mooring line length between the barge and pulley corresponded to a prototype length of 150 ft. This represented 15 ft of chain and 135 ft of nylon line.
The use of the shorter overall length of the mooring line did not impact on the test results since the elasticity of the mooring system had been simulated.

Test Facilities and Equipment

Test facility (functional tests)

18. All tests were conducted in a 260-ft-long concrete wave flume (Figure 8) which converges from a width of 10.1 ft at the wave generator to a width of 3.2 ft in the area of the test sections (Photo 7). Filters were installed immediately shoreward of the generator to minimize reflected wave heights. The location of test sections was 160 ft from the wave generator. Local prototype bathymetry was represented by a 1V-on-50H slope for a simulated prototype distance of 1,500 ft (60 ft, model) seaward of the test section. The flume was equipped with a horizontal displacement hydraulic-actuated wave generator capable of producing both monochromatic and spectral wave conditions.

Test facility (side-connector tests)

19. All tests were conducted in a T-shaped wave basin 164 ft long, 43 and 15 ft wide at the top and bottom of the T, respectively, and 3.3 ft deep (Figure 9). The flume was equipped with a horizontal displacement, hydraulic-actuated wave generator capable of producing both monochromatic and spectral waves. Like the functional tests, prototype bathymetry was represented by a 1V-on-50H slope for a simulated prototype distance of 1,500 ft (60 ft, model) seaward of where the stern of the prototype barge would rest on the seafloor in a 20-ft water depth. This placed the stern of the model barge approximately 130 ft (model) from the generator.

Data Acquisition and Control System (Both Models)

20. Because of the complexity of the study and anticipated volume of model data to be collected, an automated data acquisition and control system (ADACS) with supporting software for model control, data acquisition, and analyses was used. Important characteristics and capabilities of the system are as follows:

a. Model wave characteristics.

   (1) Wave frequencies as high as 2 Hz (wave period range of 0.50 to 25.00 sec).

   (2) Wave heights in an operating range of 0.01 to 1.0 ft.

   (3) Wave-height accuracy of ±0.001 ft.

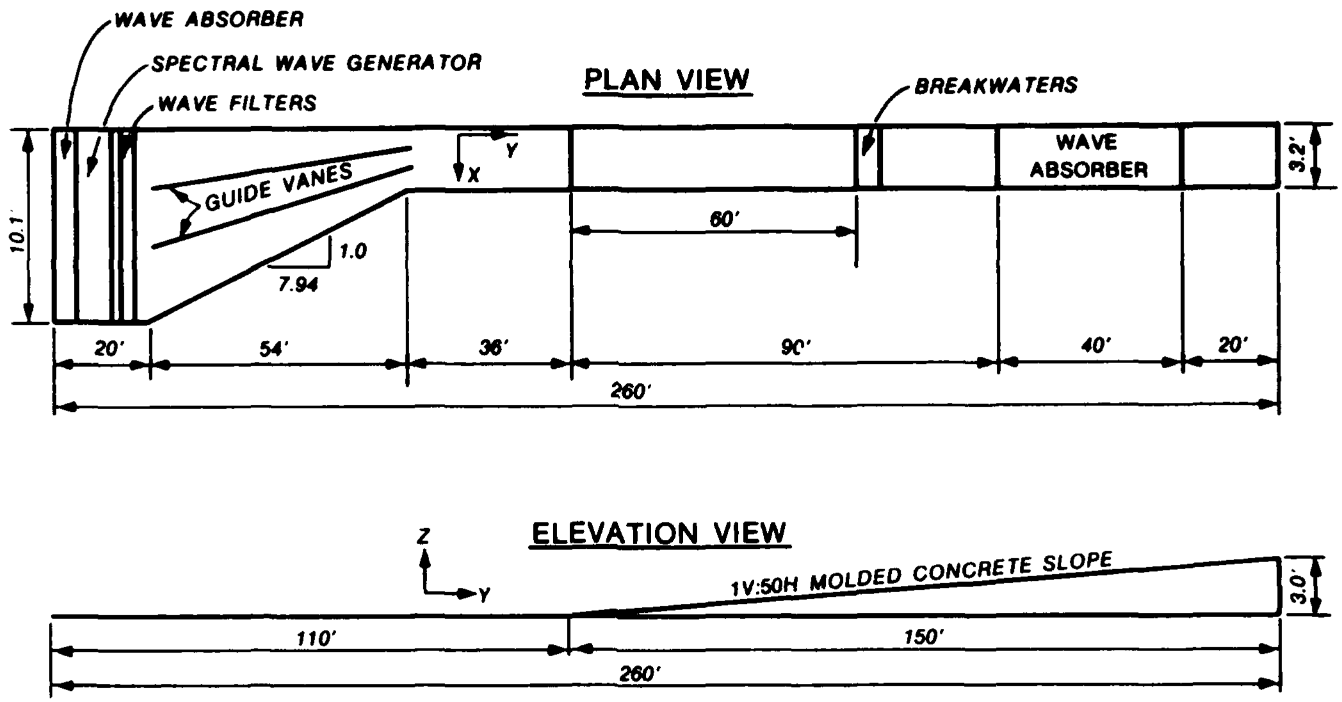

NOTE: X AND Z DISTANCES ARE AMPLIFIED 4 TIMES (RELATIVE TO Y DISTANCES) TO ENHANCE DETAIL

Figure 8. Test facility layout (functional tests)

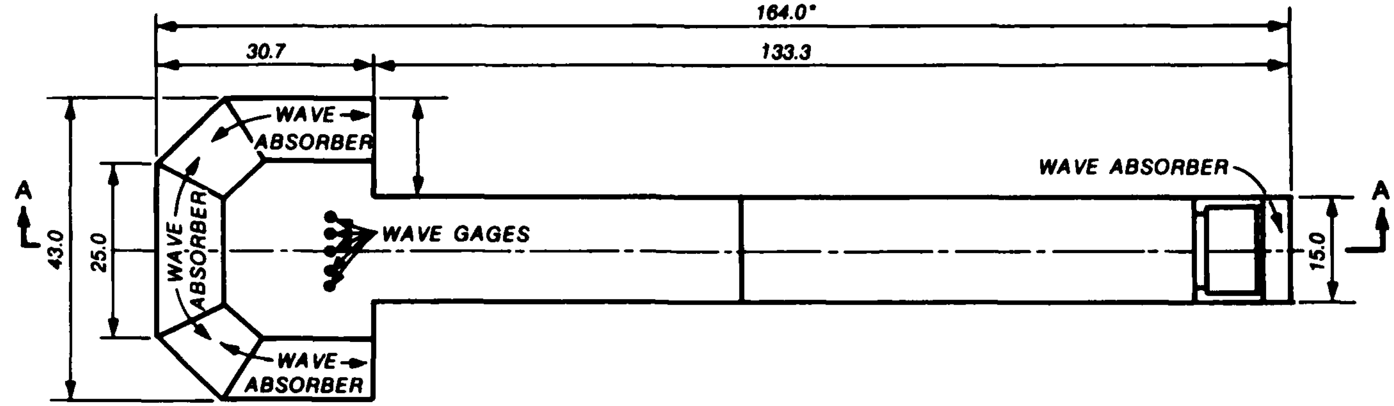

PLAN

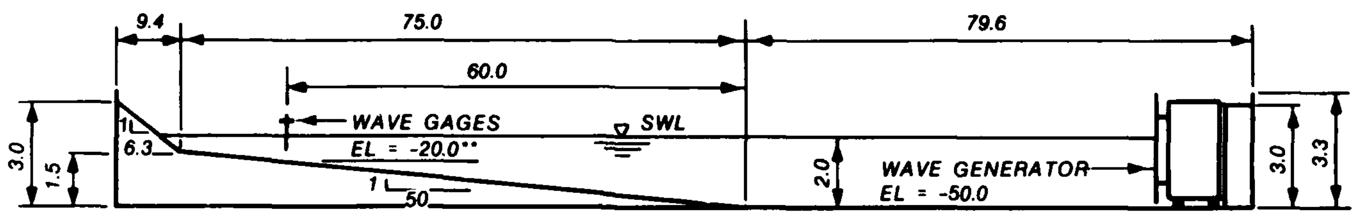

SECTION A-A

* LINEAR DIMENSIONS ARE IN MODEL FEET
** ELEVATIONS ARE IN PROTOTYPE FEET REFERRED TO NATIONAL GEODETIC VERTICAL DATUM

Figure 9. Test flume geometry and wave gage locations (side-connector tests)

b. Sampling techniques.

(1) Data collected over at least 150 wave periods.

(2) Sampling frequency variable and high enough to define the first three harmonics of the 2-Hz wave frequency (minimum sampling rate of 60 samples per cycle).

(3) Minimum time delay (not to exceed 6 m/sec) between sampling digitally the first and last wave gage during any one scan of the gages, and this time delay should be constant and independent of the sampling frequency.

(4) Time interval between scans of all gages should be controlled to within a few microseconds.

c. Recording modes.

(1) Digital recording of data from all channels in binary code with provisions for BCD recording of specific information regarding test identification and data analysis.

(2) Digital data recorded on 9-track magnetic tape with IBM compatible record format.

(3) Continuous analog recording of all channels.

(4) Time correlation of digital and analog recording modes.

d. Calibration of wave gages.

(1) Efficient and accurate means of calibrating the wave gages before a series of wave tests.

(2) Recording of calibration data in digital and analog modes.

21. The system configuration (Figure 10) of ADACS consists of the following subsystems:

a. Digital data recording and controls.

b. Analog recorders and channel selection circuits.

c. Wave and force sensors and interfacing equipment.

d. Wave generator unit and control equipment.

22. The analog recording subsystem acts as a backup for ADACS and a visual display for operator inspection of analog signals from wave sensors. This subsystem has manual or automated selection and control of five 12-channel oscillographs.

Test Procedures

Calibration of test facility (both models)

23. The normal procedure at the US Army Engineer Waterways Experiment Station (WES) is to calibrate the wave facility without the test section in

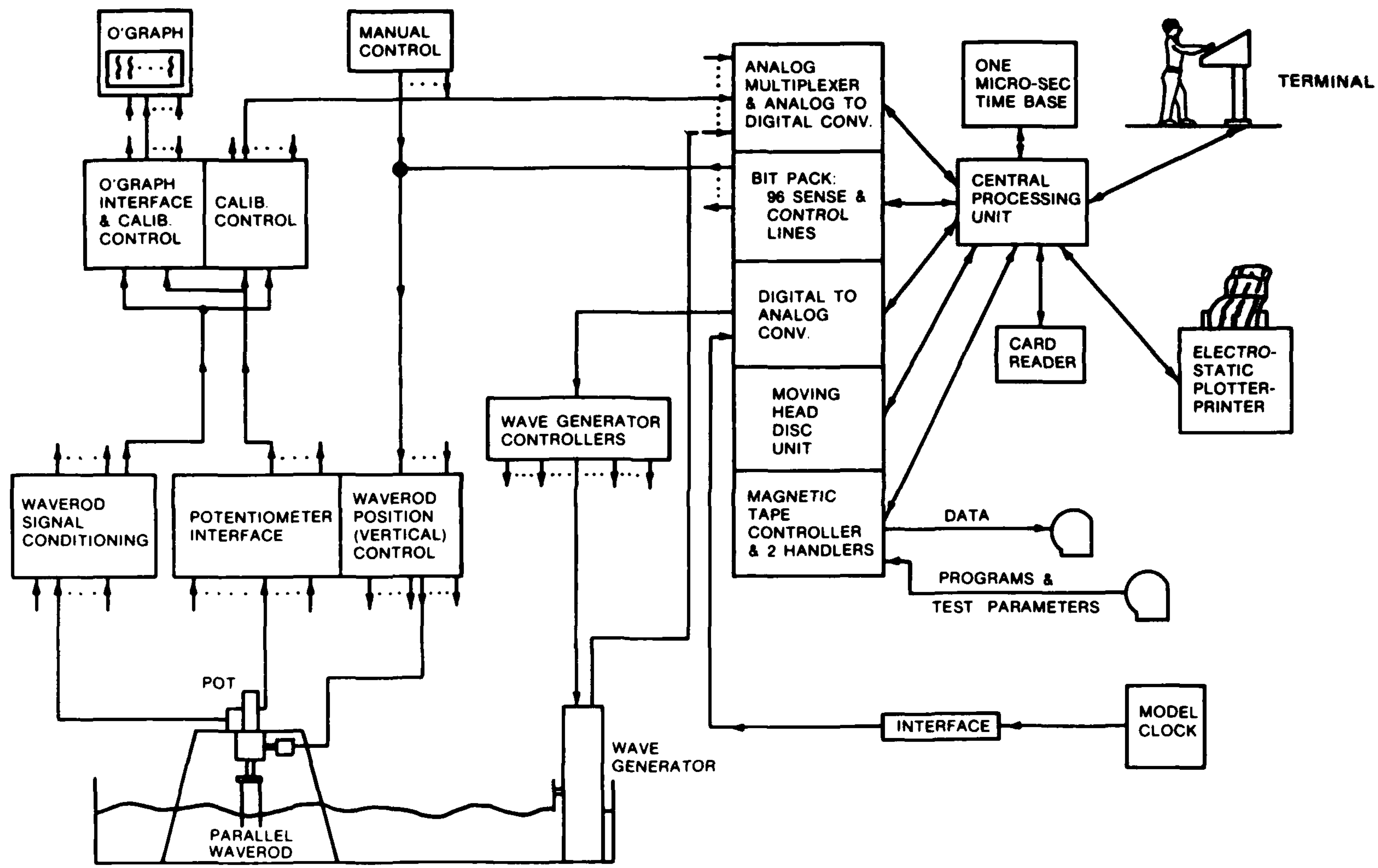

Figure 10. ADACS for hydraulic wave models

the facility. This is the most accurate means of calibrating and is analogous to the prototype conditions for which the measured and/or hindcast wave data were determined. In both test facilities, electrical resistance-type wave gages were positioned in the wave flume at a point that would coincide with the location of the proposed breakwater, and the wave generator was calibrated for various selected wave conditions.

24. Monochromatic wave calibration was achieved by simply varying the amplitude of the wave board motion for various frequencies, thus obtaining wave height as a function of wave board amplitude and frequency of motion. An iterative procedure was used in the spectral wave calibration. For each combination of peak spectral wave period T_p, spectrally based wave height H_{mo}, and energy-frequency distribution, a command signal was generated that assumed the amplitude of the wave board motion was equal to the wave height. Characteristics of the resulting spectrum were measured, compared with the desired distribution, and the command signal modified. This procedure was repeated until the desired wave characteristics were obtained at the wave gages. Typically, four or five iterations per spectral condition were required to obtain the final wave board command signals. Part III presents a detailed description of how the spectra wave conditions were selected and developed.

<u>Test setup (functional tests)</u>

25. The mooring system of the SFB's was represented by the linear spring system described in paragraphs 14-16. Mooring forces were measured by a load cell (Force Gage 1) connected to the spring mooring system and a load link (Force Gage 2) which was part of an inextensible line extending from the spring system through a laboratory-quality Teflon pulley and, finally, to the bow of the barge. Photo 7 shows a general view of the model setup. Photo 6 shows a close-up view of Force Gage 1 and the spring mooring system and Photo 8 shows a close-up view of Force Gage 2.

26. Wave heights were measured by water-surface piercing, parallel-rod wave gages (visible in the background of Photos 6 and 7). Each wave gage was connected to a Wheatstone bridge (Figure 11) which measured the conductance of the water. The output of each gage was routed through shielded cables to its signal conditioning equipment where it was processed for recording. The output of the signal conditioning equipment was connected through shielded cables to analog oscillographs where an analog time history was recorded and to the analog multiplexer of the digital recording subsystem where it was digitized

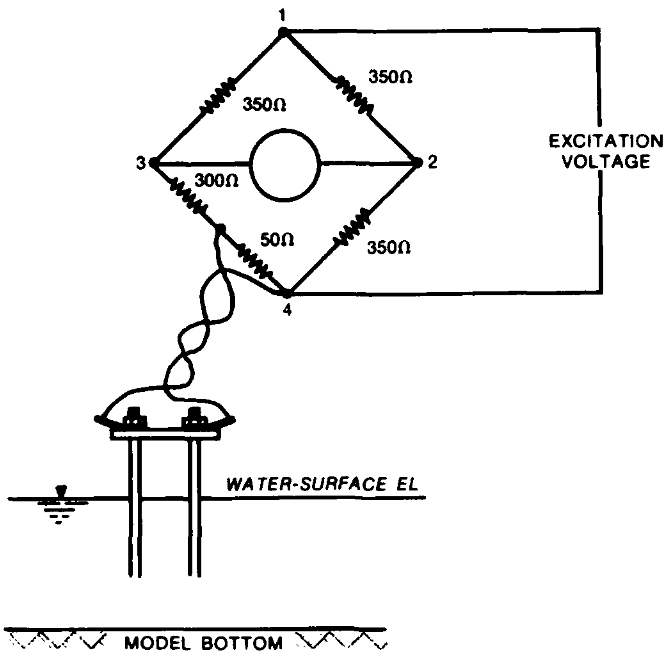

Figure 11. Schematic of parallel-rod Wheatstone bridge transducer

and recorded in a binary format on magnetic tape and/or disc. The signal conditioning equipment (Figure 12) consists of a carrier amplifier and various power supplies. This system can detect changes in water-surface elevations to an accuracy of ±0.001 ft. Wave gages, to measure transmitted wave heights, were positioned at locations that correspond to one half of the wavelength shoreward of the SFB for the various wave periods investigated.

27. Velocities were obtained with a Teledyne Gurley Model 700 flow meter. The sensor was positioned about 1 ft (prototype) shoreward of the SFB and about 1.25 ft (prototype) above the flume bottom.

Test setup (side-connector tests)

28. The barge connectors described in paragraph 13 were composed of an instrumented section and a bearing housing section. The instrumented portions of the connectors (Figure 6 and Photo 9) were strain gaged and calibrated in such a manner that positive and negative loads in the x-, y-, and z-directions (Figures 4-7) could be resolved based on output voltages of three Wheatstone bridges incorporated into the connectors' instrumented circuitry.

29. A potentiometer was connected to the bow of one barge to measure the time history of the angularity of the barges relative to one another during their exposure to wave attack (Figure 4 and Photo 5). An angle of 180 deg

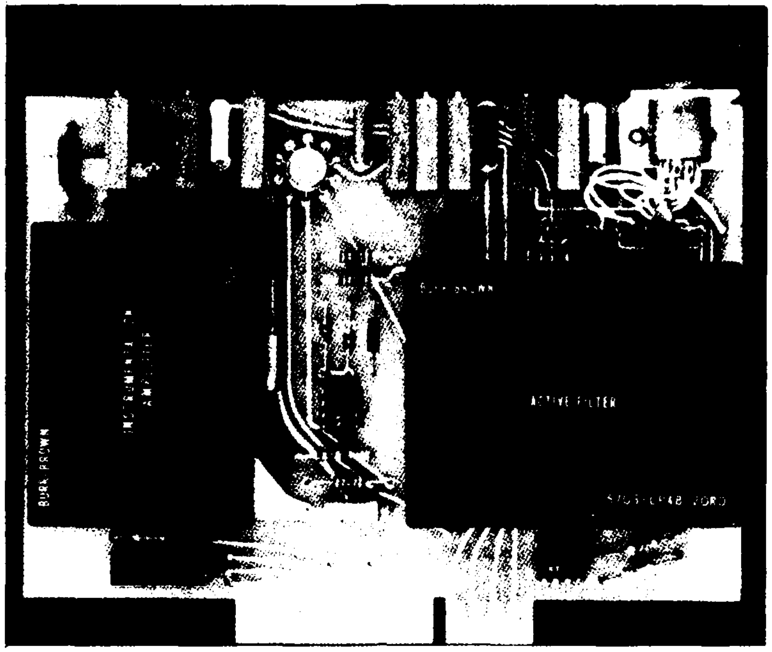

Figure 12. Signal conditioning equipment for wave rod amplifiers

(Figure 4) was defined as the static reference angle. Angle measurements less than or greater than 180 deg were defined as corresponding to the barges being concave upward and downward, respectively.

30. In order to measure the impact velocity of the stern of either barge on the model floor, a velocity transducer was positioned over and connected to the model barges by means of a monofilament line. The velocity transducer was positioned so that the line connecting it to the model barge was as close as possible to perpendicular to the top of the barge at the time of bottom impact. Thus, the output voltage of the velocity transducer corresponded to the velocity component that was perpendicular to the barge top just prior to bottom impact. Attachment points were provided on the stern corners of the model barges (Figure 4 and Photo 5). This allowed impact velocity measurements at either the inside or outside corners of either of the connected model barges.

31. In order to measure tensions in the mooring line systems described in paragraph 17, strain gaged load links were incorporated into a nonexpanding monofilament line that connected the spring systems to the barges. These load links were calibrated prior to installation on the model, and, thus, their output voltages could be transformed to mooring line tensions. Photos 10

and 11 show the SFB installed in the facility for testing with an incident wave direction of 90 deg.

32. Wave height measurements made during calibration of the side-connector test facility were carried out in the same manner as described in paragraphs 24 and 26 for the functional tests.

33. During the SFB testing, the mooring line tensions, SFB angularities, connector forces, and stern impact velocities were defined with sampling rates that varied from 100 to 300 times per second. Thus, for each data channel (labeling of data channels is defined in the legend of Figure 4) a time history of its responses to each test condition was defined and plotted. Figure 13 shows an example of a time history plot of the forces measured in the

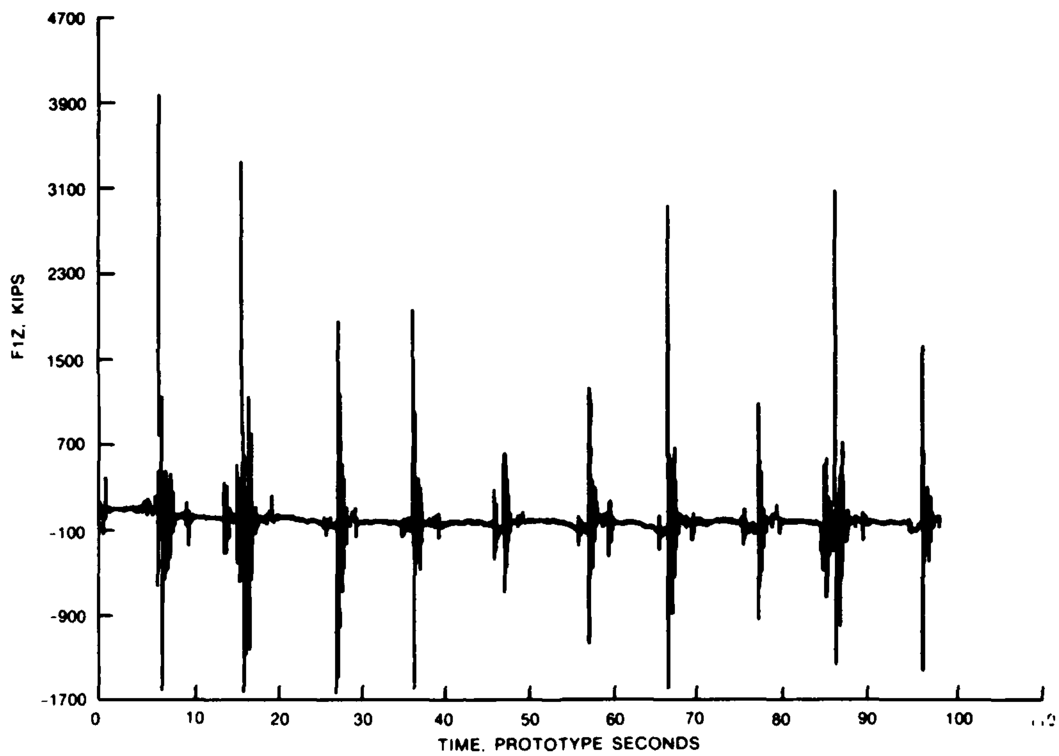

Figure 13. Typical time history plot of data channel for side-connector tests (Test 1, Table 1)

z-direction of connector F1 during the SFB's exposure to 10 sec, 10-ft monochromatic waves from 90 deg (Test 1, Table 1). In addition to plotted time histories, a data analysis routine was developed that defined the maximum and minimum value found in each time history and when these values occurred during a test. When a maximum or minimum value was found in a data channel, all values in the other data channels being monitored were defined at that same

instant in time. Figure 14 is the output data for the analysis of the time-history shown in Figure 13. A maximum value in the positive z-direction was found in connector F1 at 7.2 sec into the test run; this was extracted from the data and printed out along with the corresponding values in all the other data channels at that same instant in time. The lower portion of Figure 14 shows where a minimum value (maximum negative value) in the z-direction for connector F1 was found at 28.3 sec into the test.

GAGE F1Z

TIMES IN PROTOTYPE SEC IN THE ANALYZED DATA THAT MAXIMUMS WERE FOUND

POSITIVE MAXIMUM -- TIME 7.2000

GAGE	MODEL		PROTOTYPE		
>F1Z	247.5440	LB	3967.0503	KIPS	MAXIMUM FORCE IN F1 IN POSITIVE Z-DIRECTION
F1Y	18.1433	LB	290.7574	KIPS	VALUES OF OTHER DATA CHANNELS AT POINT IN TIME WHEN MAXIMUM POSITIVE F1Z WAS FOUND
F1X	-44.1376	LB	-707.3329	KIPS	
F2Z	-251.9656	LB	-4037.9106	KIPS	
F2Y	13.2062	LB	211.6374	KIPS	
F2X	-125.0584	LB	-2004.1416	KIPS	
T1	.0800	LB	1.2821	KIPS	
T2	.0797	LB	1.2772	KIPS	
T3	.0000	LB	.0000	KIPS	
T4	.0871	LB	1.3963	KIPS	
T5	2.4166	LB	38.7281	KIPS	
T6	.8670	LB	13.8935	KIPS	
ANG	180.6472	DEGREES	180.6472	DEGREES	

NOTE: INDICATORS PLACED BY ANALYSIS PROGRAM TO SHOW WHICH MAXIMUM VALUES ARE BEING DEFINED ON EACH OUTPUT PAGE

NEGATIVE MAXIMUM -- TIME 28.3000

GAGE	MODEL		PROTOTYPE		
>F1Z	-101.7035	LB	-1629.8633	KIPS	MAXIMUM FORCE IN F1 IN NEGATIVE Z-DIRECTION
F1Y	-19.4748	LB	-312.0967	KIPS	VALUES OF OTHER DATA CHANNELS AT POINT IN TIME WHEN MAXIMUM NEGATIVE F1Z WAS FOUND
F1X	-38.6046	LB	-618.6632	KIPS	
F2Z	-19.9233	LB	-319.2833	KIPS	
F2Y	5.3746	LB	86.1317	KIPS	
F2X	12.1595	LB	194.8637	KIPS	
T1	.5700	LB	9.1346	KIPS	
T2	.8169	LB	13.0911	KIPS	
T3	.3327	LB	5.3324	KIPS	
T4	.2227	LB	3.5683	KIPS	
T5	2.5658	LB	41.1187	KIPS	
T6	.0797	LB	1.2776	KIPS	
ANG	181.5609	DEGREES	181.5609	DEGREES	

Figure 14. Example of numerical data extracted from analysis of the time history plot in Figure 13. No impact velocities were measured (side-connector Test 1, Table 1)

PART III: SPECTRAL WAVE SIMULATION

Selection of Spectral Shapes

34. Spectral wave tests were conducted with a T_p range of 6 to 14 sec for H_{mo} of 2, 4, 6, and 8 ft. This range of wave conditions would provide a database that would allow (a) selection of an optimum SFB length in terms of total cost as a function of wave protection received, (b) final mooring line and anchoring selection, (c) estimation of bottom-scour potential at the stern of the SFB, and (d) load determination for the design of barge connectors.

35. Measured shallow-water wave spectra, obtained at a depth of 16.4 ft, were available from Thompson (1980) for Nags Head, N. C. The Nags Head data could reasonably be used to develop the energy-frequency distributions needed in the present investigation because of (a) the geographic proximity of Nags Head and Oregon Inlet, (b) intermediacy of the 16.4-ft depth relative to the proposed testing depths, and (c) observations that, based on available measured wave spectra, energy-frequency distributions do not appear to vary significantly along that portion of the North Carolina Coast.

36. The selection of spectral wave conditions plays a critical role in studies of this type. Extensive research has been performed in scientific and engineering communities to quantify a consistent shallow-water spectral form (Vincent 1982). The basis of this work is derived from similarity principles between deep- and shallow-water spectral shapes in wave number space (Kitaigordskii et al. 1975). Comparisons between measured (laboratory and field) spectral shapes and the theoretical shape have been found to be very similar (Goda 1974, Thornton 1977, Ou 1980, Iwata 1980, Vincent 1982, and Jensen 1983). The equilibrium range in the spectrum of wind-generated surface waves is defined by

$$E(f) = \alpha g^2 (2\pi)^{-4} f^{-5} \psi \left(\frac{f}{f_m}\right) \Phi(\omega_d) \qquad f > f_m \tag{1}$$

where

$E(f)$ = the energy density at a given frequency f

α = Phillip's equilibrium constant

g = acceleration due to gravity

$\psi\left(\frac{f}{f_m}\right)$ = spectral shape function dependent on f and f_m (peak frequency), the frequency at which the maximum energy density occurs

$\Phi(\omega_d)$ = a nondimensional dispersion function dependent on ω_d given by

$$\omega_d = 2\pi f\left(\frac{d}{g}\right)^{1/2} \tag{2}$$

37. The function $\Phi(\omega_d)$ in its complete form (Grosskopf and Vincent 1982) is a transcendental equation that can be solved through trial and error procedures. In deep water the function $\Phi(\omega_d)$ approaches 1.0; when ω_d is less than 1.0, $\Phi(\omega_d)$ can be approximated by

$$\Phi(\omega_d) \cong \frac{1}{2}\,\omega_d^2$$

and therefore,

$$E(f) = \frac{1}{2}\,\alpha g d(2\pi)^{-2} f^{-3}\psi\left(\frac{f}{f_m}\right) \qquad f > f_m \tag{3}$$

The spectral shape changes from an f^{-5} to an f^{-3} in the tail of the energy density spectrum and, more importantly, becomes a function of the water depth.

38. The forward face of the spectrum is represented by

$$E(f) = \alpha g^2(2\pi)^{-4} f_m^{-5} \exp\left[1 - \left(\frac{f}{f_m}\right)^{-4}\right] \Phi'(\omega_d) \qquad f \le f_m \tag{4}$$

where $\Phi'(\omega_d)$ is evaluated from the ω_d defined at f_m. Equation 4 has been shown to generate very consistent results when compared with field wave data (Garcia and Jensen 1983, and Jensen 1983).

39. The only unknowns involved in the evaluation of the spectral shape are the peak frequency, Phillips' equilibrium constant, and the total energy E_o. The peak frequency is given by the design specifications requested by SAW. The peak frequency will shift toward a lower frequency from deep to

shallow water. The mechanisms that cause this change are derived from the nonlinear transfers of energy, or wave-wave interactions (Hasselmann 1962). The energy transfers act conservatively, although a portion of the energy is transferred into the high frequency end of the spectrum and is lost because of wave breaking (like "white capping"). Phillips' equilibrium constant is related (nondimensionally) to the fetch length, wind speed, and peak frequency. A wind speed of approximately 40 knots is selected as a reasonable estimate for wind conditions occurring in a storm passing the area. Therefore, α is given as a function of peak wave period, derived from Vincent (1982) in the following tabulation

f_m 1/sec	T_p sec	α*
0.167	6	0.0166
0.125	8	0.0131
0.100	10	0.0117
0.083	12	0.0100
0.071	14	0.0093

* For wind speeds equal to 40 knots.

40. The remaining unknown E_o (total energy), is related to the significant wave height H_{mo} by the following equation:

$$H_{mo} = 4\sqrt{E_o} \tag{5}$$

where

$$E_o = \int_0^\infty E(f)df \tag{6}$$

Since the range of H_{mo} was specified by SAW (of 2, 4, 6, and 8 ft), it becomes a matter of distributing the energy over the frequency range of the spectrum (Equations 3 and 4).

41. The theoretical spectrum is evaluated for each discrete frequency band (knowing f_m and α), and then integrated over the range of frequencies (Equation 6). The resulting total energy is then scaled according to the

total energy obtained from the H_{mo} desired conditions. That ratio (desired H_{mo}/theoretical H_{mo}) is reapplied to the spectrum, and the resulting spectrum is now referenced with respect to the desired H_{mo} wave conditions for a particular f_m. The derived spectral shape represents the "true" shape sought in the model study.

42. During preliminary model testing, problems were encountered as the peak frequency decreased to 0.083 Hz. The measured spectral shape would not correspond to the theoretically derived spectral shape (Equations 3 and 4). From the measured spectra (in 15 ft), the model was "excited" in frequency bands just above the peak frequency. The energy level was nearly as high as that observed at f_m. Between the two peaks was a significant drop in the spectral energy as if an energy sink existed somewhere in the wave tank. This selective removal of energy from discrete frequency bands and the transformation of the single peaked spectra into two-peaked spectra could not be explained. Therefore, an alternate method of solution was adopted to control the excitation and thus produce a single peaked spectrum in shallow water.

43. Two alternate solution techniques could be adopted to model the long-period wave condition found at Oregon Inlet. The first technique would assume that swell waves could be approximated by a monochromatic, unidirectional wave form (for example, Hasselmann et al. (1973) and Jensen (1983)). A wave train with a single frequency and wave height could be input (linear wave train) at the deep-water section and, through shoaling and refraction (caused by convergence of the side walls in the wave tank) effects, a single wave train would result in shallow water. The second solution technique requires the specification of some spectral shape that would transform into a distribution represented by Equations 3 and 4 without adversely exciting the wave tank producing a double peaked spectrum. The deep-water (at the forcing end where d = 50 ft) spectral shape is governed by the form given below:

$$E(f) = \lambda \alpha g^2 (2\pi)^{-4} f_m^{-8} \exp \left[1 - \left(\frac{f}{f_m} \right)^{-6} \right] \quad f \leq f_m \qquad (7a)$$

$$= \lambda \alpha g^2 (2\pi)^{-4} f^{-8} \quad f > f_m \qquad (7b)$$

The constant λ balances out the dimensions on the righthand side of the equation set so that $E(f)$ is given in the form of length^2-time. The justification for Equations 7a,b is found through comparisons of the resulting laboratory spectral shapes in shallow water (15 ft) with swell-dominated prototype data observed at Nags Head, N. C. (Thompson 1977). Many alternate shapes were used (varying the powers of f, f_m, and the ratio of f/f_m). It was found that the resulting shallow-water spectral shape derived from Equations 7a,b reproduced the expected theoretical shape, as well as the prototype data, more consistently than any other approximated form.

Initialization

44. The actual input conditions to the wave generator are given in deep water. However, wave spectra must be estimated from shallow-water design conditions. The problem is easily solved because the model study is simulating conservative processes of wave refraction (constricted wave tank), shoaling (sloping bottom), and nonlinear transfers of energy (wave-wave interactions, although a portion of the energy is lost in the high frequency end of the spectrum). The spectral shape can be transformed into deep water by employing the linear wave theory as a basis to compute the individual phase speeds (dependent on each discrete frequency) and the group celerity (assumed to be derived from the peak frequency). The generation of deep-water swell spectra does not pose significant problems since the spectral shape is computed for deep-water conditions. The deep-water total energy of these tests is controlled by an *a priori* knowledge of the expected H_{mo} in the 15-ft-water depth, again using linear theory to estimate refraction and shoaling effects.

Comparisons

45. Comparisons were made between the wave spectra measured in the model and theoretically derived spectra, for wave conditions in a water depth of 15 ft. These tests verify that: (a) the given "sea" wave spectra conform to the assumed shape in a 15-ft-water depth, and (b) the input description of the "swell" wave spectra collapse into a similar water-depth-dependent spectral shape given in Equations 3 and 4. The test series employing an H_{mo} equal to 6.0 ft is used to demonstrate the consistency of test results.

46. Figure 15 shows results of the measured and theoretical spectra for the 6.0-sec peak-period wave test. The energy density is plotted against a nondimensional frequency based on f_m. Unlike the monochromatic tests, the peak period is not conserved (i.e. remaining constant) from deep water (d = 50 ft at the wave paddle) to shallow water (d = 15 ft at the gage). The nonlinear transfers will shift f_m to a lower frequency (as shown in Figure 16). Rather than attempt to control the transfer rate (and the shift in f_m) from deep to shallow water, it was decided to input the specified f_m at the wave generator and allow for the shift in peak frequency. The maximum error between the required f_m and the measured f_m was 5.0 percent (with a mean error of 2.7 percent). Returning to Figure 15 one notices that the measured data follow the theoretically derived data quite closely. There is a small overestimation in the measured data set near the spectral peak and a strong divergence between E(f) values near $f/f_m = 2.0$. The reason for this trend is unknown.

47. The second verification test involves H_{mo} and T_p conditions of 6.0 ft and 8.0 sec, respectively. As shown in Figure 17, the measured data nearly replicate theoretical results. Minor oscillations exist in the measured data above and below the computed spectral shape, but, in general, the trends are very similar. The last locally generated "sea" wave condition (Figure 18) is for H_{mo} equal to 5.9 ft, and f_m equal to 0.11 Hz ($T_p \cong 9$ sec). As in the three previous cases, the measured E(f) corresponds to the theoretical spectral shape. There is a small underestimation of the energy density near the spectral peak, but it is only on the order of -7.0 percent. There is a lobe of energy at the base of the forward face of the measured spectra, probably caused by a cross oscillation in the wave channel or created by the convergence in the sidewalls of the tank. However, the amount of energy in the lobe is small compared to the energy in the primary spectra and therefore contamination in the test results from the added energy packet was insignificant.

48. The final two tests (Figures 19 and 20) are used as examples to simulate distant swell wave conditions. As previously discussed, the swell spectral tests are performed using a slightly different procedure. An assumed deep-water spectral shape is specified as input conditions, and the spectrum is allowed to transform into a stable shape at the 15-ft water depth. Applying similarity principles (Kitaigordskii et al. 1975), a theoretical spectral

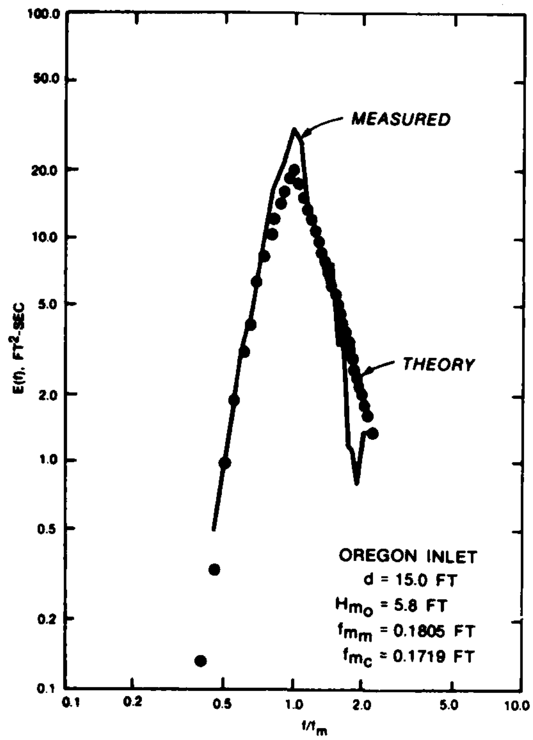

Figure 15. Theoretical and measured spectra for 6-sec peak period

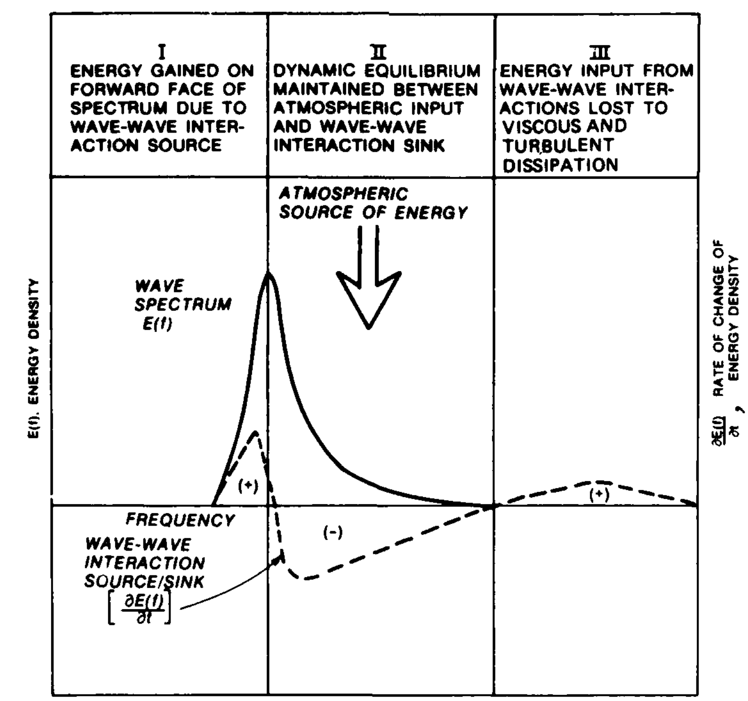

Figure 16. Shifting of f_m to a lower frequency caused by nonlinear transfers

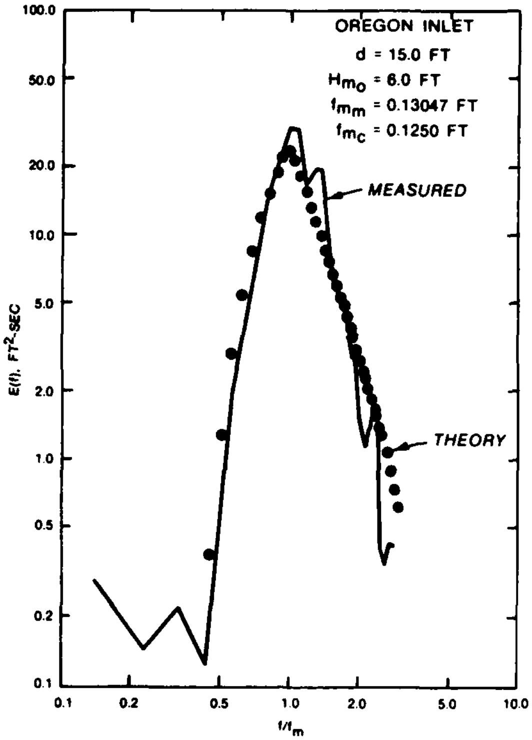

Figure 17. Theoretical and measured spectra for the 8-sec peak period

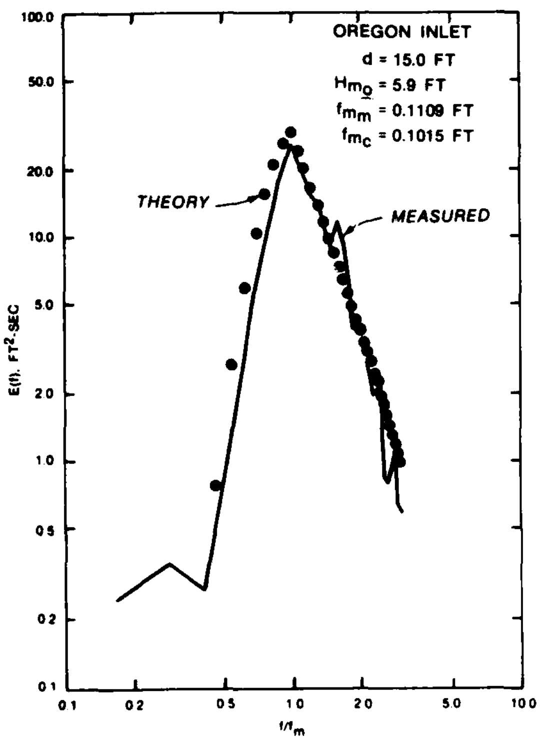

Figure 18. Theoretical and measured spectra for the 10-sec peak period

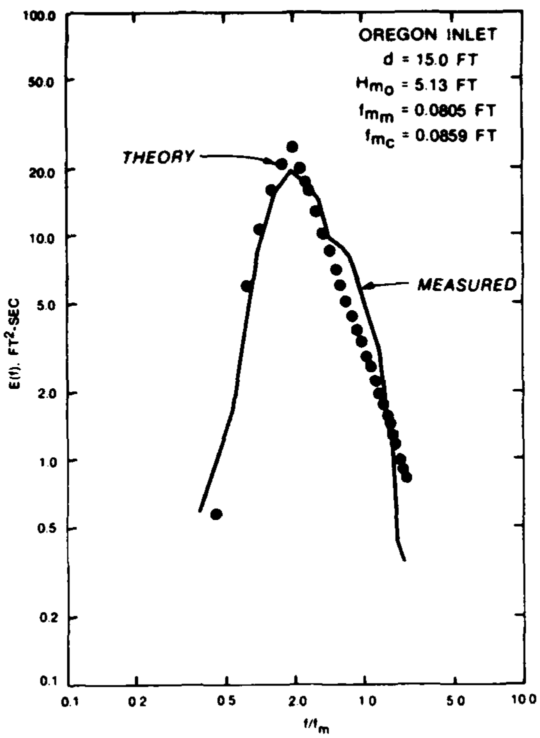

Figure 19. Theoretical and measured spectra for the 12-sec peak period

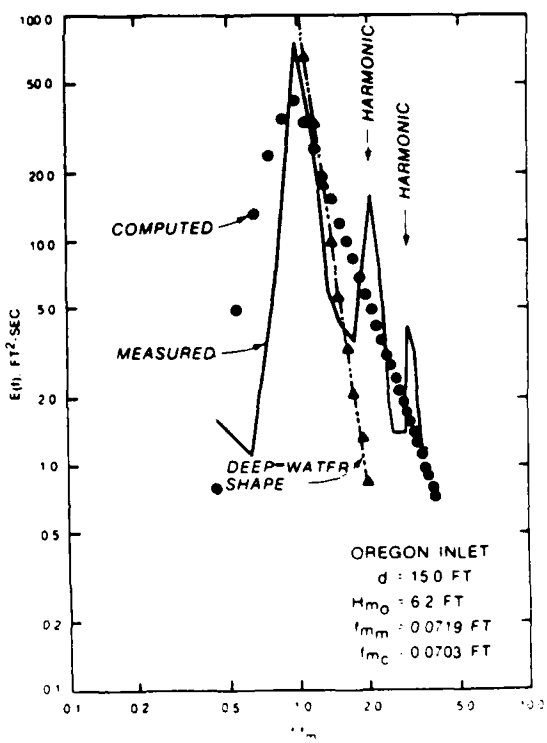

Figure 20. Theoretical and measured spectra for the 14-sec peak period

shape can be generated and compared with the measured spectra. Although the "fine-tuning" of the measured spectral shape is based on the deep-water version, the shallow-water shape must be consistent with the theoretical data set. Figure 19 represents an H_{mo} condition equal to 5.1 ft and a T_p condition equal to 12.4 sec. The measured spectral results compare very favorably with the theoretical data set. There appears to be a divergence in the measured spectral shape for $f/f_m > 2.5$ where the slope is approximately twice as steep for similar conditions found in the theoretical shape. In all other regions, the measured E(f) is of the same form represented in the theoretical spectral shape verifying the consistency in the model results for spectral conditions in 15-ft water depths. The final test (Figure 20) displays the theoretical and measured spectral shapes for H_{mo} and T_p wave conditions of 6.2 ft and 14 sec, respectively. The comparisons between theory and measured results are not favorable as in previous tests. The reason for the poor comparison is based principally on the processes occurring in the wave channel. The input wave spectrum is nearly of the form of a monochromatic wave train (i.e. a spectrum with all of its energy concentrated in a single frequency band). As the spectrum propagates into shallow water, an energy exchange occurs that has been caused by the nonlinear interactions. Since the spectrum is very narrow banded (relative to all others tested), there will be a strong decomposition of that shape splitting the energy between the primary and secondary harmonics. The "spikes" found in the measured spectrum are a result of these processes. However, the theory employed cannot resolve the resonant interaction between primary and secondary harmonics; thus, a poor comparison between measured and theoretical data sets is shown. The measured spectral shape remains nearly unchanged from its input shape (excluding the secondary harmonics). The theoretical spectral shape found in Figure 18 (closed circles) represents a scaled (via H_{mo}), saturated, swell wave condition in 15-ft-water depths. The measured spectral energy is approximately 1.5 times less than saturated conditions in that particular water depth. Therefore, the measured data should not reflect the saturated spectral shape, but remain nearly unchanged from a deep-water condition. Hence, the model test for the long-period (defined here as swell) spectral wave shapes is also well represented.

PART IV: TESTS AND RESULTS FOR THE FUNCTIONAL MODEL

Monochromatic Wave Tests

Performance tests

49. Monochromatic performance tests were conducted with the 89.6-ft SFB exposed to 2-, 4-, and 6-ft waves for periods from 4 to 14 sec. Specific test conditions and corresponding values of relative depth (d/L), wave steepness (H/L), relative wave height (H/d), and relative structure length (L_{SFB}/L) are presented in Table 2. Typical test views for 6-, 10-, and 14-sec waves are presented in Photos 12-17. All tests were conducted on a 1V:50H bottom slope in a water depth of 15.0 ft (measured at the stern of the SFB). Tests were conducted in a 3.20-ft-wide flume and the model SFB was 2.96-ft wide; consequently, when the SFB was centered between flume walls, a gap of about 1.5 in. existed between the structure and walls. Initially, it was felt that this gap (Condition 1; 1.5-in. gaps without absorber) would not have a significant effect on tests results. However, to quantify the effect of the 1.5-in. gaps on experimental results, tests were conducted for Condition 2 (1.5-in. gaps filled with fibrous wave absorber) and results were compared with those of Raichlen (1981).

50. Wave attenuation test results are presented in Table 3 for the three modeling conditions. Data for Conditions 1 and 2 were obtained in the present investigation; Condition 3 data were extracted from "Experiments with a Sloping Float Breakwater in Water Waves - Phase I" (Raichlen 1981). Transmission coefficients, C_t , from Table 3 are graphically depicted as functions of wave period (Plates 1 and 2) and relative structure width (Plate 3). These data show that

- a. Condition 2 generally yielded lower values of C_t than Condition 1; however, when C_t is plotted as a function of L_{SFB}/L , the differences are small.
- b. Condition 3 C_t's are generally less than either Condition 1 or 2 but some specific values are significantly larger (4-sec, 6-ft and 8-sec, 4-ft waves).
- c. There is relatively little difference in the maximum C_t for a given value of L_{SFB}/L .
- d. The general quality of experimental data for Conditions 1 and 2 appears to be more consistent than for Condition 3 since there is less variation of C_t for constant values of L_{SFB}/L .

51. For direct comparison with Raichlen's data, all mooring force data reported herein are expressed as the force that would exist on one mooring line for the case of a single 21-ft-wide barge. Mooring force test results, obtained from Force Gage 1, are presented in Table 4 and Plates 4 and 5. These data show that (a) in general, Condition 1 produced the highest mooring forces followed by Conditions 2 and 3, respectively; and (b) model data obtained for Conditions 1 and 2 appear to be more consistent (force increasing with increasing wave height) than those obtained for Condition 3 (note in Table 4, Condition 3 test results for 8-, 10-, and 12-sec wave periods). Force Gage 2 test results are presented in Table 5. Recalling that Force Gages 1 and 2 were connected in series and separated by the Teflon pulley, it would be expected that results are the same for both gages, except for a small frictional loss at the pulley. Comparisons of Tables 4 and 5 show this expectation is realized.

52. Flow velocity measurements for modeling Conditions 1 and 2 are shown in Table 6 and Plates 6 and 7. The minimum, average, and maximum values presented therein were obtained from the maximum velocities observed for each wave cycle of a specific incident wave condition; thus, depending on wave period, flow velocity measurements represent the distribution of 10 to 40 individual readings. The large differences (spread) between the minimums and maximums are not unexpected when one considers the highly turbulent and unsteady flow conditions under the SFB.

53. In summary, it is recommended that test results for Condition 1 be used for design purposes. Discussions with SAW personnel revealed that each module might be moored separately or in small groups of modules producing a condition more analogous to Condition 1, which resulted in the largest forces and transmission coefficients. When one considers the small differences in maximum C_t's , mooring forces, and velocities, it becomes apparent that any of the modeling conditions will yield nearly the same design values. For Condition 1 a maximum C_t of 0.75 was observed for 14-sec, 2-ft waves; the maximum peak mooring force of 24.7 kips was observed at Force Gage 2 during attack of 12-sec, 6-ft waves; and a maximum peak velocity of 8.0 ft/sec was recorded during attack of 8- and 10-sec, 6-ft waves.

Survival (storm wave) tests

54. Limited tests were conducted to aid in determination of the survival probabilities of the SFB, should it be subjected to storm wave

conditions. Reviews of historical wave data for Nags Head showed the largest storm of record occurred in 1966 and had a significant wave height of 15.5 ft at a significant period of about 10 sec. Therefore, monochromatic tests were conducted with the 10-sec period for wave heights up through the maximum, depth-limited breaking wave height ($H = 12.7$ ft) that could be supported in the 15-ft depth. Tests conditions are listed in Table 7.

55. Based on previous performance test results, it was decided to consider only Model Condition 1 (1.5-in. gap with no absorber) during the storm wave tests. Transmitted wave heights, mooring forces, and flow velocities are presented in Tables 8-10 and Plates 8-10. Maximum transmitted wave heights and mooring forces of 7.5 ft and 27.0 kips were observed. Both occurred during attack of 12.7-ft waves. A maximum flow velocity of 11.0 ft/sec was produced by the 10-ft wave condition.

56. During both performance and survival tests, large amounts of lift were observed at the structure's stern (see Photos 18 and 19 for examples of extreme conditions). Based on model observations, maximum vertical lifts were estimated to be 1 to 2 ft for the 4- and 6-ft waves and 3 to 4 ft for the 10- to 12.7-ft waves.

Spectral Wave Tests

57. Spectral tests were conducted using 72.3-, 89.6-, and 118.4-ft-long SFBs anchored in water depths of 13, 15, 18, and 21 ft. The 89.6- and 118.4-ft-long structures were tested in all depths; however, the 72.3-ft-long structure was tested only in the 15-ft depth as its wave-attenuating capabilities proved inadequate to make it a viable alternative. Breakwaters were anchored with a 150-ft-long mooring line which had a breaking strength of 230 kips (with the exception of limited mooring line length effect tests, which are described in a later section of this part). Peak periods T_p of the spectra ranged from 6 to 14 sec and the significant wave heights H_{mo} were 2, 4, 6, and 8 ft.

Wave attenuation tests

58. Wave attenuation test results are presented in Tables 11-14 and Plates 11-19. These data show that transmitted wave heights are consistently lower for the 118.4-ft SFB, and the transmission response of the structures is strongly dependent on wave period. The transmission coefficient variations

for a given wave period tend to be slightly larger for the 118.4-ft SFB. Performance of the structures decreased as the water depth increased.

59. Photos 20-37 show the model breakwaters under attack of 6-sec, 4- and 6-ft waves and 10- and 14-sec, 4- and 8-ft waves in the 15-ft depth. It should be noted that every possible effort was made to take the photos at a point in the test where the barges were under attack of a wave that approximated the significant height of the spectrum. However, for a given spectral condition, photos of the structures were not necessarily taken at exactly the same point in the wave train; therefore, they are generally illustrative of the SFB's responses, but exact comparisons of displacement and wave height should not be attempted.

Mooring force tests

60. Mooring force data are presented in Tables 15-18 and Plates 20-28. These data show average and, particularly, peak mooring forces are dependent on wave period, wave height, and water depth. For a constant wave period, peak mooring forces increased with increasing wave height, and for a constant wave height (with the exception of the 2-ft height) peak mooring forces generally increased with increasing wave period. The deviation of results for the 2-ft spectra from the trends observed for the 4-, 6-, and 8-ft spectra merits explanation. For wave heights of 4 ft and greater, the structures are alternately lifted from and dropped back to the seafloor. Thus, mooring forces result from both a shoreward translation of the SFB and rotation about the bottom contact point. However, 2-ft waves do not significantly lift the structures, and most of the mooring force results from rotation about the bottom contact point. Based on model observations, rotation appears to increase as the wave period is increased from 6 to 10 sec and then decrease at the 12- and 14-sec periods. This trend is approximately reflected in the mooring force data. For most wave conditions, mooring forces are similar for both SFB lengths and tend to increase with increasing depth. The 14-sec, 8-ft spectrum produced the highest peak mooring forces (64.4 and 61.6 kips for the 89.6 and 118.4-ft structures, respectively) of all conditions investigated.

Flow velocity tests

61. Results of flow velocities tests are presented in Tables 19-22 and Plates 29-32. Examination of these data shows that (a) peak flow velocities are dependent on SFB length, wave height, wave period, and water depth; (b) for constant structure length and wave period, flow velocities generally

increase with increasing wave height; (c) for constant structure length and wave height, flow velocities generally increase with increasing wave period; and (d) peak flow velocities are generally higher for the 118.4-ft SFB. Maximum values of 11.0, 12.5, and 15.5 ft/sec were observed for the 72.3-, 89.6-, and 118.4-ft structures, respectively.

Mooring line length effect tests

62. Limited tests were conducted to investigate effects of increasing the mooring line length from 150 to 250 ft. Prior to initiation of testing, it was hypothesized that the longer mooring line, because of its increased elasticity, might decrease average and peak mooring forces for the higher wave heights without adversely affecting wave attenuation at the lower wave heights.

63. Tests were conducted with both monochromatic and spectral waves. The monochromatic conditions (10-sec, 10-, 12-, 14-, and 15-ft waves) were representative of observed prototype storm conditions. Spectral tests encompassed peak periods of 6 to 14 sec for wave heights of 4 and 8 ft. SFB lengths of 89.6 and 118.4 ft were investigated. The structures were anchored in a water depth of 21 ft using 150- and 250-ft-long mooring lines which had a breaking strength of 230 kips.

64. Wave attenuation, mooring force, and flow velocity results for the monochromatic wave tests are presented in Tables 23-25, respectively. Transmitted wave height is presented as a function of incident wave height in Plate 33. Plate 34 depicts peak mooring force as a function of incident wave height. These data show that for the 250-ft line, as opposed to the 150-ft line, (a) transmitted wave heights are slightly lower; (b) average mooring forces are similar, but peak mooring forces are consistently reduced with the relative reduction being greater for the 118.4-ft SFB; and (c) peak flow velocities tend to be slightly lower.

65. Spectral wave attenuation results are summarized in Table 26 and coefficients of transmission are presented as a function of wave period in Plates 35 and 36. These data show that the wave-attenuating capability of the breakwaters is essentially unaffected when the mooring line length is increased from 150 to 250 ft. Average and peak mooring forces are listed in Table 27. Peak mooring forces are depicted as a function of wave period for the 89.6- and 118.4-ft structures in Plates 37 and 38, respectively. These data show that in general both average and peak mooring forces are reduced

when the mooring line length is increased with the reduction being the most significant for the peak forces observed at the 8-ft wave heights. Table 28 presents flow velocities observed at the stern of the structures. These results are generally similar for both mooring line lengths with the 250-ft line appearing to have a slight advantage for a few specific wave conditions.

Summary of spectral wave test results

66. As evidenced in the preceding sections, coefficients of transmission are relatively insensitive to wave height (for 2- to 8-ft waves and constant wave period). Therefore, it is felt that the average coefficient of transmission $\bar{C}_t$ is representative of SFB performance. Plates 39 and 40 present $\bar{C}_t$ as a function of water depth and wave period. These data show that the performance of the SFB decreases as the wave period and/or water depth increases, and the longer SFB performs consistently better than the shorter structure.

67. Peak mooring force is presented as a function of wave period and water depth in Plates 41-48 for 2-, 4-, 6-, and 8-ft incident wave heights. These plots show that peak mooring force generally increases with increasing wave period and/or water depth, and the largest values occur for 14-sec, 8-ft waves at the 21-ft depth. It is interesting to note that the largest value observed (64.4 kips) is only 28 percent of the mooring line's breaking strength.

68. Peak flow velocity is depicted as a function of wave period and water depth in Plates 49-54 for 4-, 6-, and 8-ft waves. These data show that peak flow velocities generally increase with increasing wave period and/or wave height and tend to decrease as the water depth increases. Also, the data become more narrow banded as the wave height increases; i.e., effects of wave period are less pronounced for larger wave heights.

69. Based on the data presented herein, it appears that wave attenuation will be at a maximum and peak mooring forces will be at a minimum when the SFB is moored in 13 ft of water. The purpose of testing the SFB in variable water depths was to define its performance over a complete range of tide.

Nondimensionalized wave attenuation test results

70. Examination of wave attenuation test results shows that coefficients of transmission appear to primarily depend on wave period or length, SFB length, and water depth, i.e.,

$$C_t = f(L_p, L_{SFB}, d)$$

The variables L_p , L_{SFB} , and d are defined as the wavelength of the peak spectral period, length of the SFB, and water depth, respectively. Values of C_t and relative SFB length (L_{SFB}/L_p) are given in Tables 29 through 32, and Plates 55 through 58 present C_t as a function of L_{SFB}/L_p for constant depths. These data show that, for the range of SFB lengths investigated, the value of C_t associated with a given value of L_{SFB}/L_p is independent of SFB length. Therefore, these plots could be used to predict the performance of an intermediate SFB length over the range of wave conditions investigated.

71. It should be noted that Plates 55-58 also show that for the range of conditions tested, relative mass moments of inertia do not significantly influence SFB performance over the range of lengths investigated. Since the mass moment of inertia varies with L_{SFB}^2 (approximately), a dependence of C_t on the relative mass moments of inertia would have necessitated a family of curves when C_t was plotted as a function of L_{SFB}/L_p .

PART V: TESTS AND RESULTS FOR SIDE-CONNECTOR TESTS

Test Conditions

72. The side-connector tests were conducted with the SFB's moored in a 20-ft water depth. The use of the 20-ft mooring depth allowed the side-connected SFB's to be subject to the following rather severe monochromatic and spectral wave condition:

Monochromatic Waves

Wave Period sec	Wave Height ft
10	10
10	12.5
10	15
12	10
12	12.5
12	15
14	10
14	12.5
14	15

Spectral Waves

Period of Peak Energy Density, T_p sec	Wave Height $H_{mo} = 4\sqrt{E}$* ft
6	6
8	6
8	8
10	6
10	8
12	6
12	8
14	6
14	8

* E = total energy of spectrum (defined by the area under the curve of the spectral energy density versus frequency plots).

The test program was initiated in order to expose the side-connected SFB to waves from the four incident wave directions described in Figure 4.

Monochromatic Wave Tests

73. A total of 20 tests were run with monochromatic waves incident from 90 deg (Table 1). For all tests, the barges were ballasted, connected together, and floated at an angle of 14.5 deg relative to the horizontal with their sterns resting on the bottom in a 20-ft water depth. Photos 38 and 39 show the model SFB during monochromatic wave attack (90-deg incident wave direction).

74. Tests 1-9 covered the full range of monochromatic waves with all mooring lines attached. Time histories of the output for all but the stern impact velocity data channel were recorded. The time histories for stern impact velocities were only recorded for what were observed to be the most severe bottom impact conditions. Plates 59-72 are typical examples of the time histories recorded for all tests. These examples are taken from Test 2. The time histories were then analyzed for maximums and minimums by using the method described in paragraph 33 and Figure 14. Plates 73-86 are the analyses outputs for Test 2. Because of the massive amount of data plots and tabulations created by these tests, the maximums for the connector forces, mooring line tensions, and impact velocities; and range of barge angularities were extracted and are presented in Table 33.

75. With the possibility of mooring line breakage, concern arose as to the effect this would have on tension in the remaining mooring lines, forces in the connectors, stern impact velocities, and barge motion (angularity time history). For this reason, Tests 10-13 were conducted using 15-ft waves with periods of 12 and 14 sec, as these wave conditions appeared to be the most severe for the 90-deg wave direction. The results of these tests are summarized in Table 33. During Test 11, the load in connector F2 exceeded its model design load which resulted in a slight deformation in the thin wall portion of the connector. This was not found until the end of the day when Tests 10-13 had been completed. Thus, the offset in the calibration for connector F2, due to it being overloaded, could not be compensated for. For this reason, the validity of the magnitudes of the forces measured in connector F2 are questionable for these latter tests, but since the connector was damaged, it is known that the load was quite high (equal to or greater than the -6,854 kips reported in Table 33 for F2Z).

76. Following Test 13, the calibrations of connector F2 were corrected in order to compensate for the offset which occurred during Test 11. By doing this, and with the assumption that the set was minor enough to not cause nonlinearity in the connector calibrations, some degree of confidence could be placed in data gathered with connector F2 as long as no additional yielding of the connector occurred. In an effort to avoid additional connector damage, the remaining tests were conducted with 10-ft, 10- and 14-sec monochromatic waves.

77. A discussion arose during the review of Tests 1-13 as to what effect, if any, the mass weights suspended from the spring systems were having on the mooring line tension measurements. Depending on the spring constant and the design of a spring, some magnitude of initial tension needs to be exceeded before elongation of the spring is initiated. The mass weights were suspended from the spring system so that when the mooring line tension exceeded a magnitude of zero, no matter how small the tension, spring elongation began. This assured that the spring system would respond immediately, but it failed to take into consideration the inertial effects of the mass weights.

78. It was observed in the data from Tests 1-13 that the maximum connector forces coincided with the instant in time when the stern of the barges impacted on the concrete floor of the test flume. Some discussion arose as to conservatism in this condition relative to the prototype where the barges would be in contact with a sand bottom. Maxwell Cheung and Associates, Inc. (MCA), provided a theoretical force deflection curve that they felt would be representative of the barges as they impacted and dug into a prototype sand bottom.

79. MCA felt that if they had some idea of the natural frequency of the connected free floating ballasted barges, it would aid them in their analysis of the side-connector force data.

80. Tests 14-20 (Table 1) were conducted to help answer the questions discussed in the four previous paragraphs. Tests 14 and 15 were run as control tests with no modifications in the sterns or spring systems. With calibrations for connector F2 being modified because of yielding during Test 11, these tests provided data for comparison with the data to be gathered with the modified spring systems and bumpered barge sterns. A summary of the maximum connector forces, mooring line tensions, impact velocities, and barge angularities measured during Tests 14 and 15 are presented in Table 33.

81. Test 16, referred to as the "ping test," was conducted to look at the natural frequency of the connected, ballasted, and moored barges. During Test 16, a small rubber hammer was used to ping barge number 1 along the top of its bow. The barge was pinged twice on the outside corner, then the middle, and lastly the inside corner (nearest the connectors). During the ping test, the barges were connected and floating in the water; all mooring lines were attached; and the inside and outside stern corners of each barge were positioned on 1/4-in.-diam steel rods. As an example of the data gathered, Plates 87 and 88 show the response of connector F1 in the z-direction during the ping test. To aid in the measurement of the frequencies, the x-axis prototype time scales were expanded for the second pings on the outside and middle and first ping on the inside corner and are presented on Plates 89-91, respectively.

82. Prior to Tests 17 and 18 (Table 1), the mass weights were removed from the model mooring line spring systems and the spring systems were recalibrated. The calibration curve for the modified spring system was slightly stiffer than the original spring system, which in turn was slightly stiffer than the 135-ft length of the 20-in. circumference 2-in-1 braided nylon line which it was representing (Figure 21). Table 33 shows the maximums recorded for all the data channels during these tests. Figures 22-27 and 28-33 are the time histories of the mooring line tensions for a portion of Tests 15 and 18, respectively. Comparison of these plots and the data in Table 33 shows that removal of the mass weights eliminated the higher frequencies in the mooring line data.

83. Five bumpering materials were developed and tested to see how well they would represent the force-compression equation provided by MCA (Figure 34). Up to a load level of 15 lb/in. of model bumper, material C had the closest fit to the theoretical force-compression curve. Assuming that the load would not exceed 15 lb/in. in the model, a 1-in.-wide strip of bumper material C was added to the bottom of the sterns of both barges, and Tests 19 and 20 were conducted with the modified spring systems. The softening of the barge impact on the concrete floor resulted in a significant reduction in the forces measured in the connectors (Table 33).

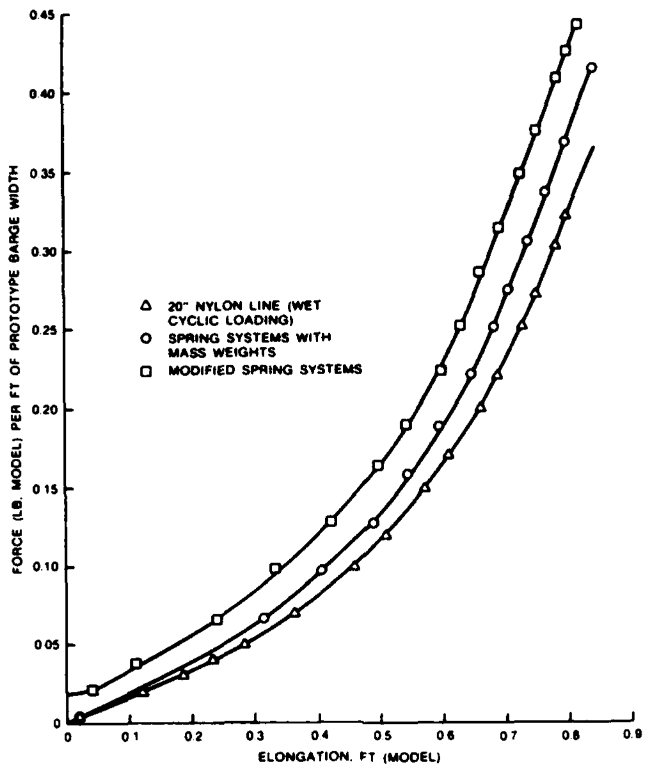

Figure 21. Force-elongation curves for side-connector tests, model mooring line spring systems

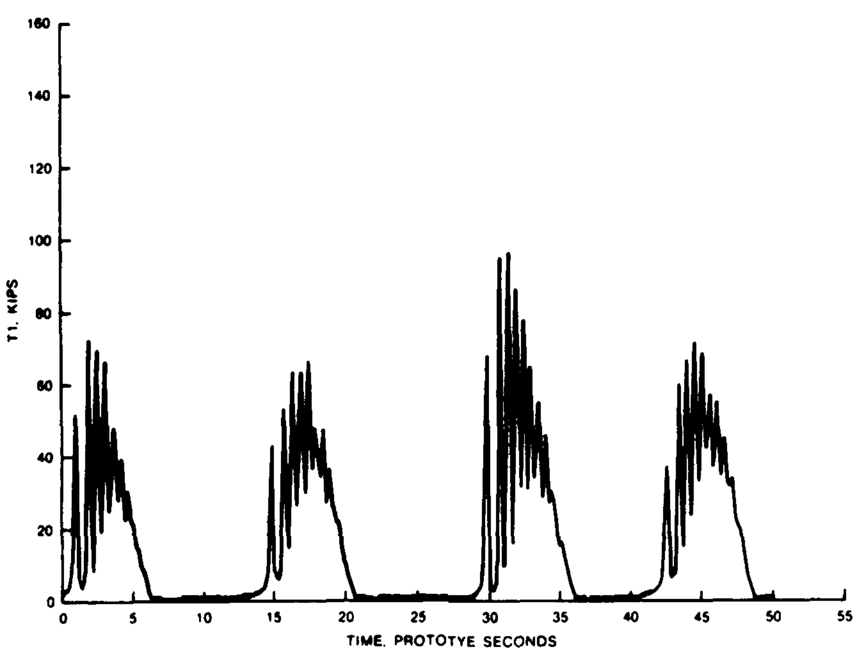

Figure 22. Mooring line T1's tension time history for Test 15 of side-connector tests

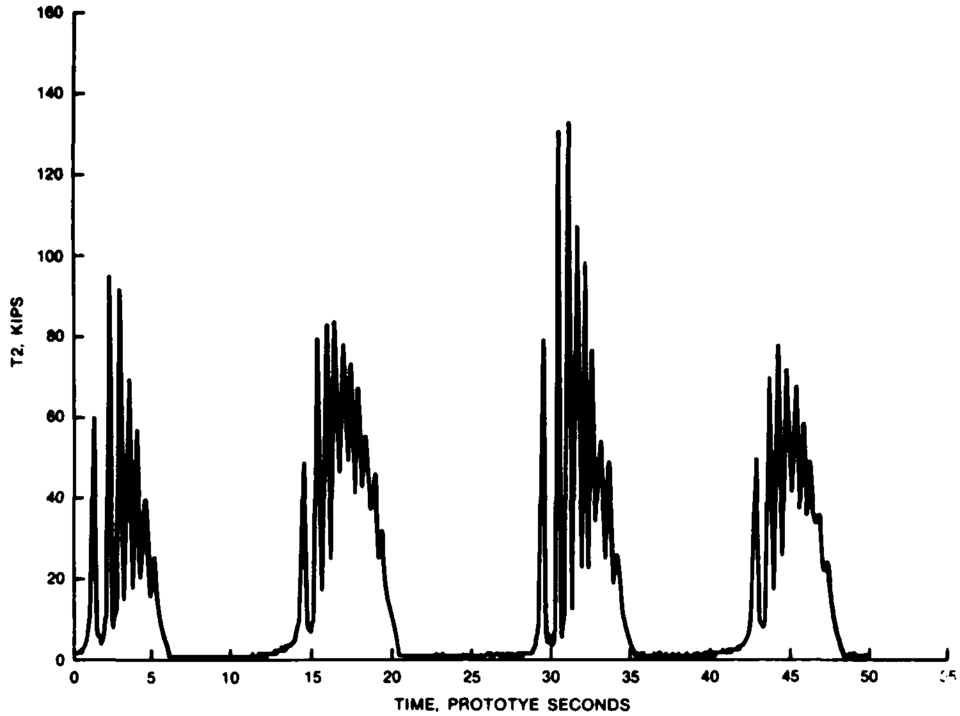

Figure 23. Mooring line T2's tension time history for Test 15 of side-connector tests

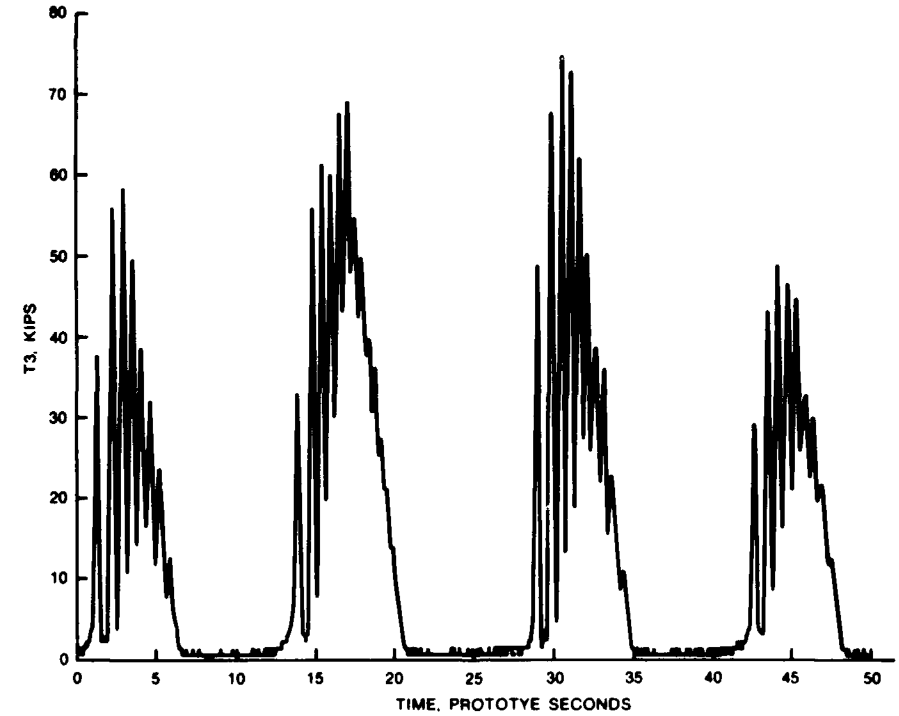

Figure 24. Mooring line T3's tension time history for Test 15 of side-connector tests

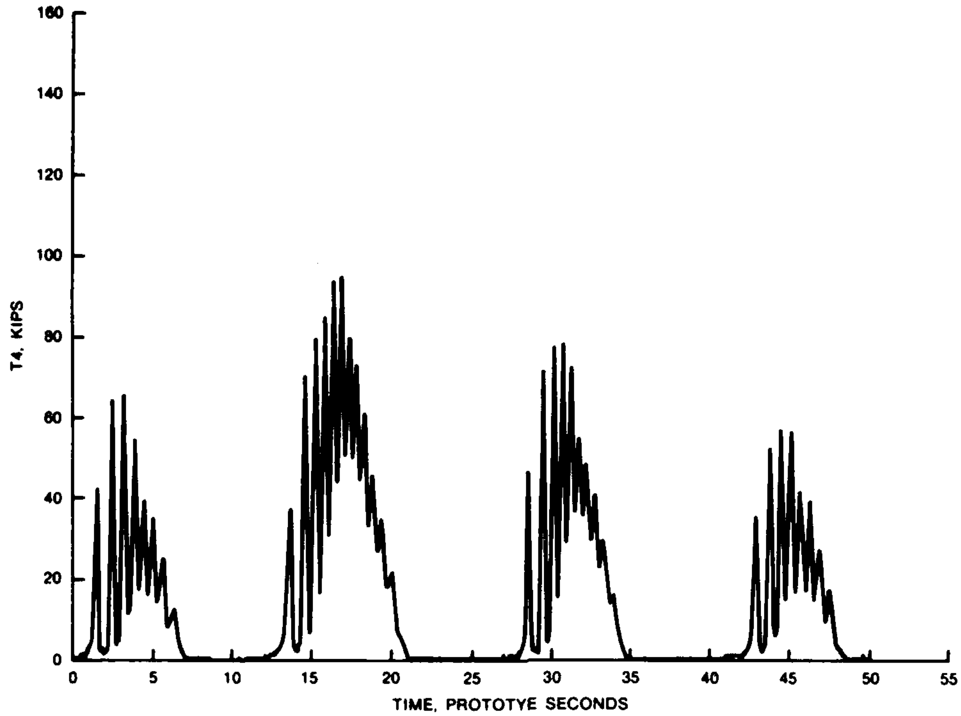

Figure 25. Mooring line T4's tension time history for Test 15 of side-connector tests

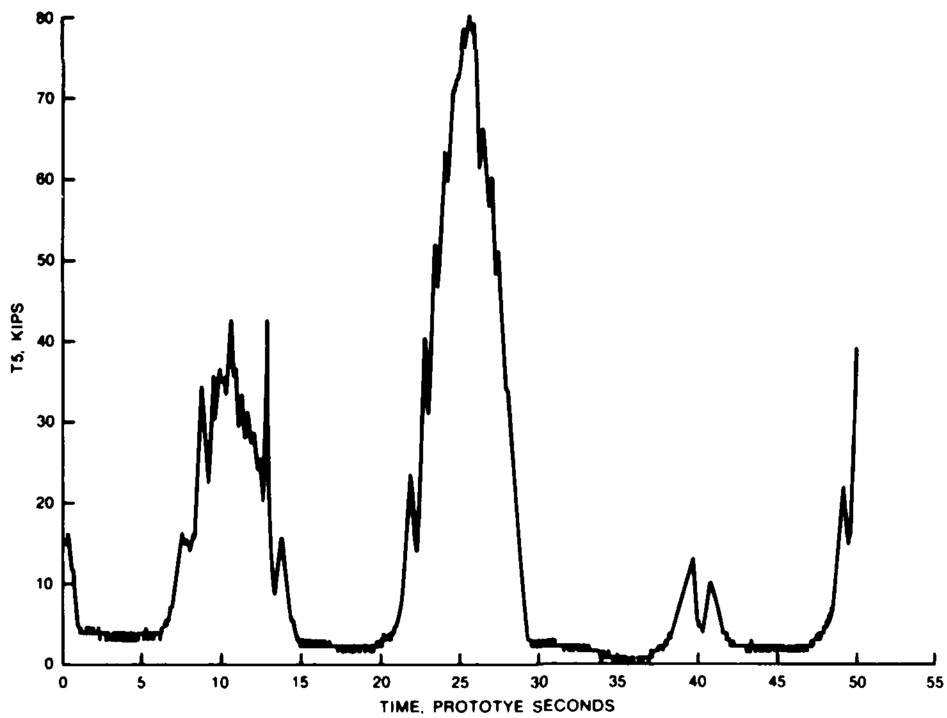

Figure 26. Mooring line T5's tension time history for Test 15 of side-connector tests

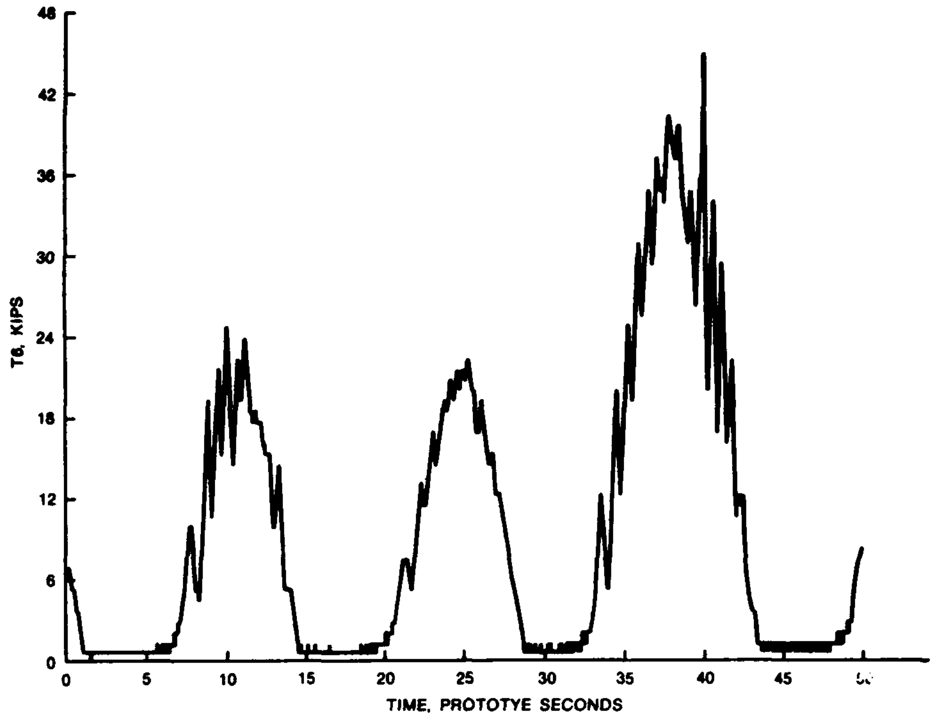

Figure 27. Mooring line T6's tension time history for Test 15 of side-connector tests

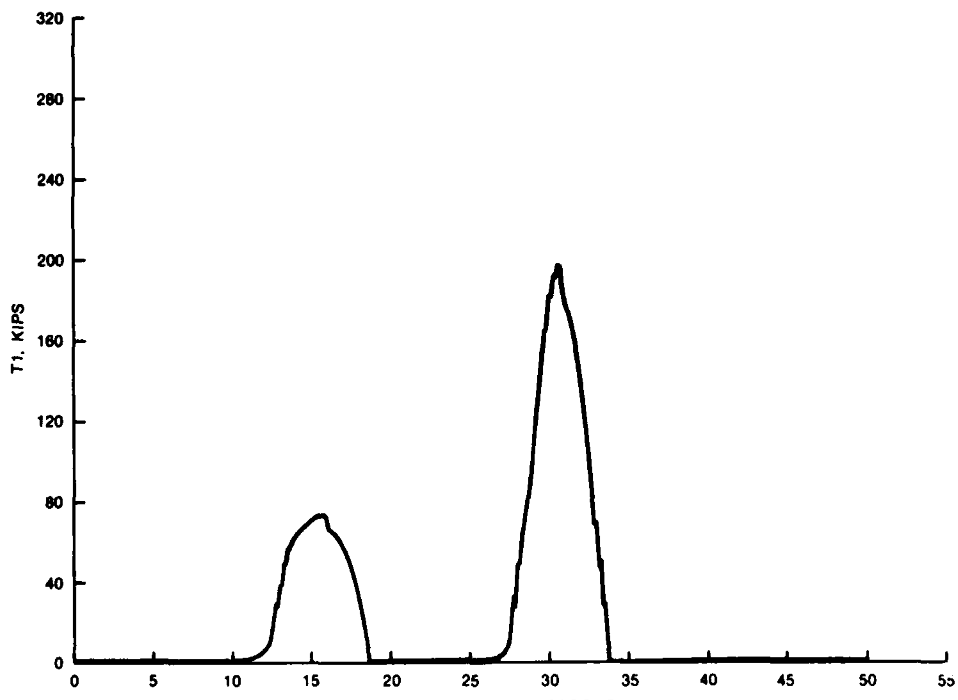

Figure 28. Mooring line T1's tension time history for Test 18 of side-connector tests

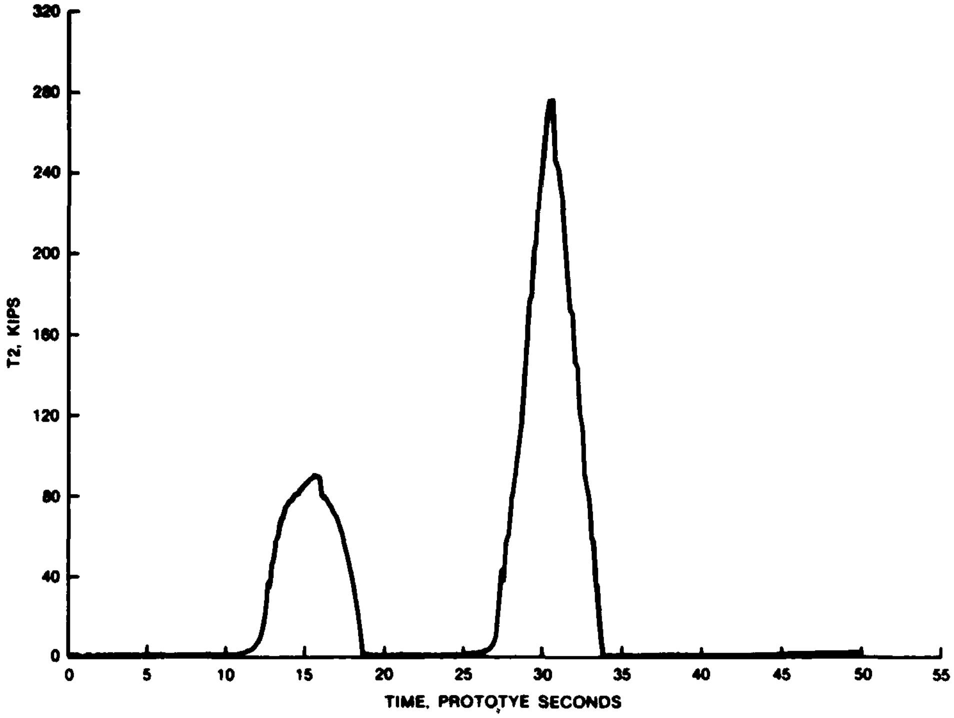

Figure 29. Mooring line T2's tension time history for Test 18 of side-connector tests

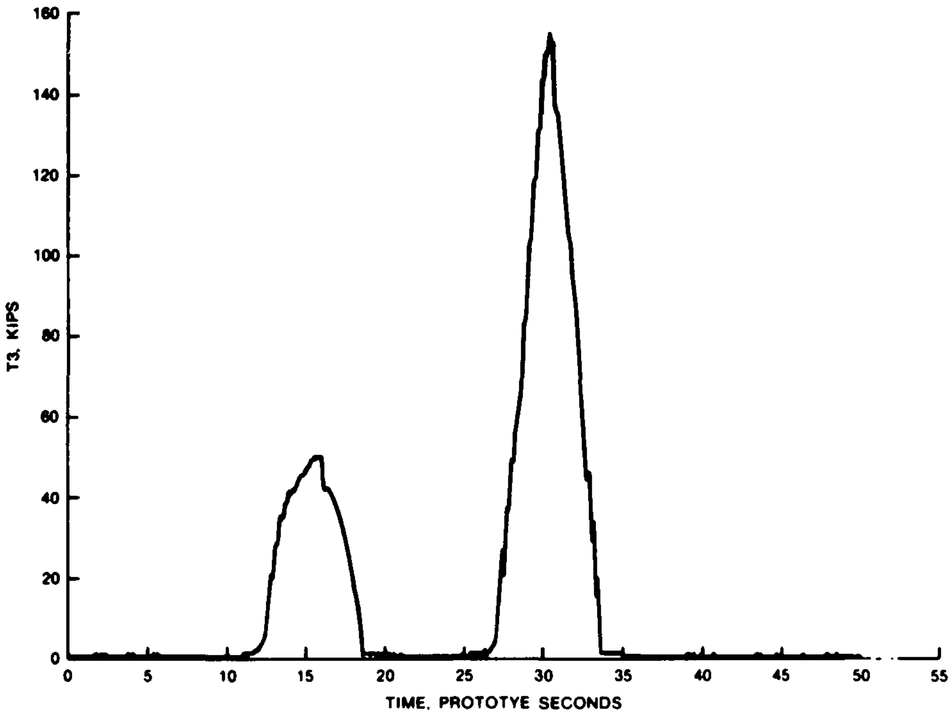

Figure 30. Mooring line T3's tension time history for Test 18 of side-connector tests

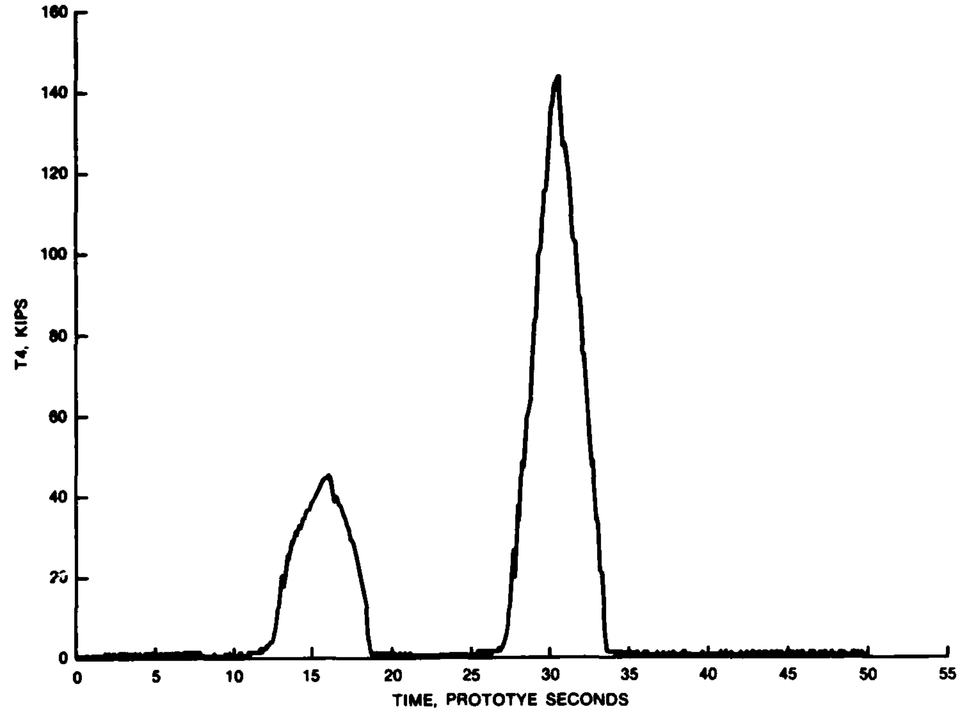

Figure 31. Mooring line T4's tension time history for Test 18 of side-connector tests

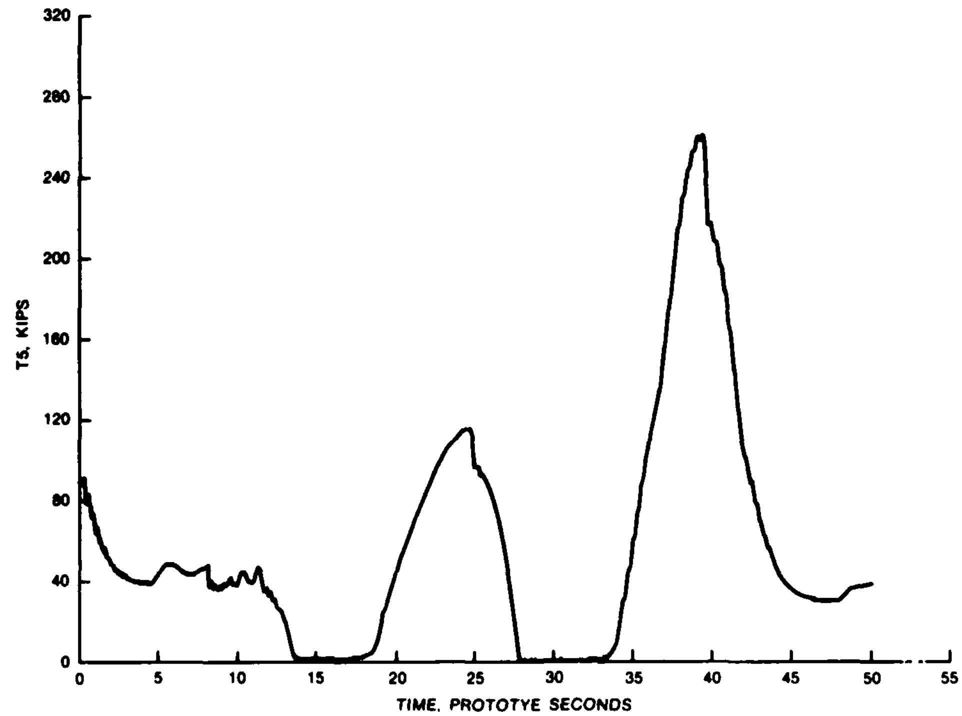

Figure 32. Mooring line T5's tension time history for Test 18 of side-connector tests

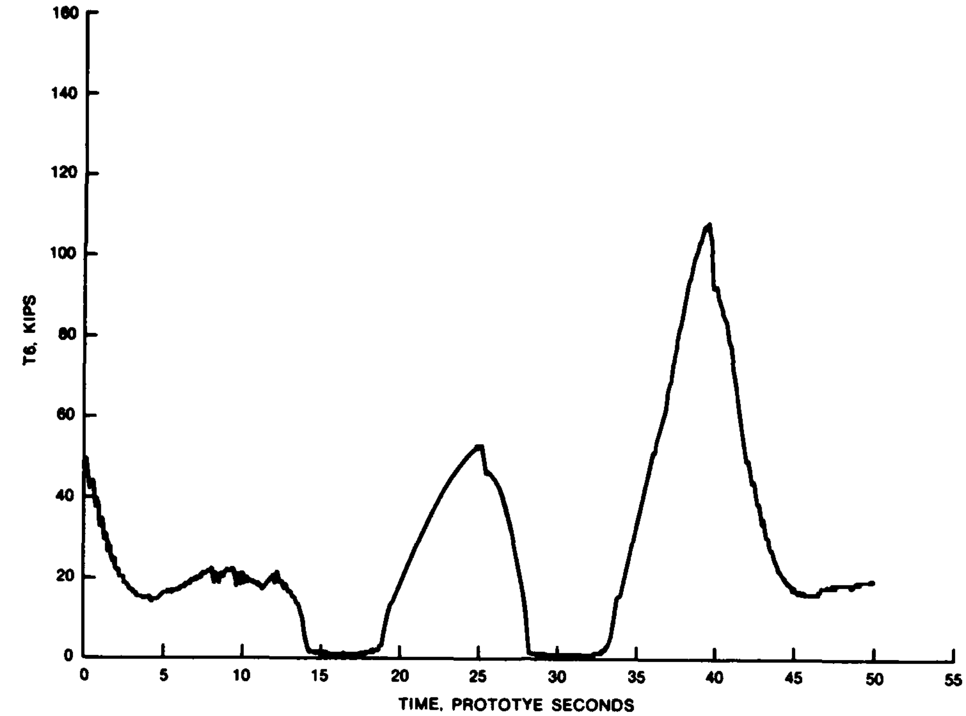

Figure 33. Mooring line T6's tension time history for Test 18 of side-connector tests

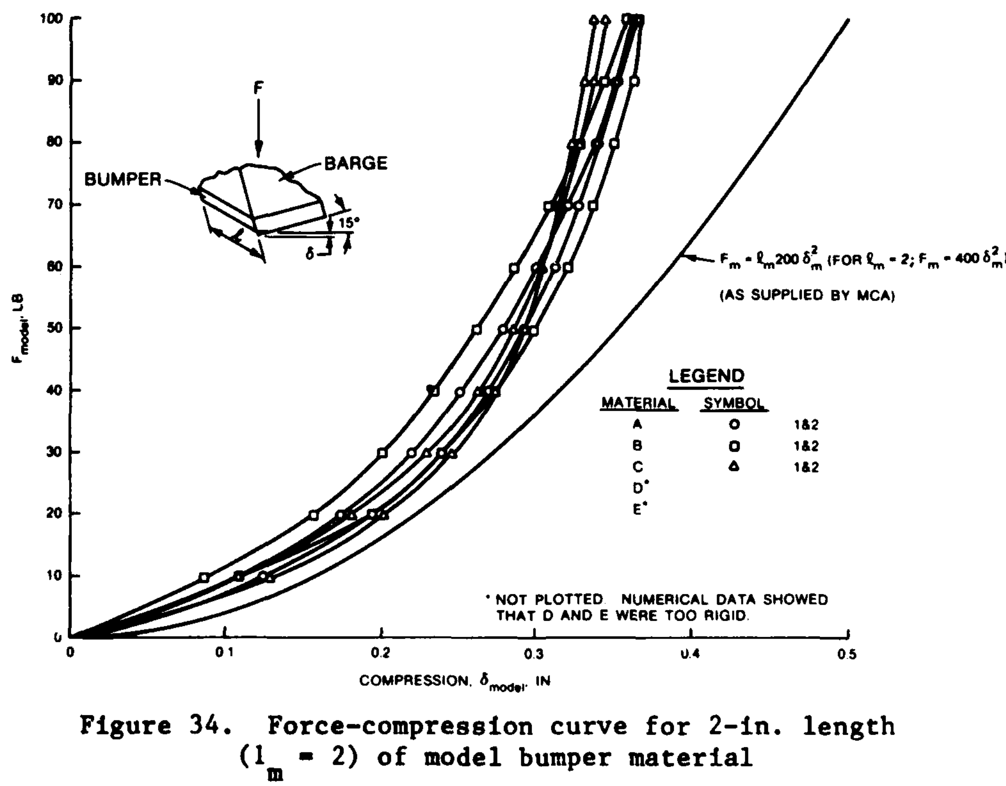

Figure 34. Force-compression curve for 2-in. length (l_m = 2) of model bumper material

PART VI: CONCLUSIONS

84. Based on assumptions, tests, and results reported herein, it is concluded from the functional tests that:

a. For an 89.6-ft SFB moored in 15 ft of water using a mooring line length of 150 ft and subjected to monochromatic waves:

   (1) Test results from Model Condition 1 (1.5-in. gap with no absorber beside SFB) should be used for design purpose.

   (2) For maximum wave heights of 6 ft in a wave period range of 4 to 14 sec, maximum C_t's , mooring forces, and flow velocities were 0.75, 1.18 kips/ft of breakwater, and 8.0 ft/sec, respectively.

   (3) Exposure of the SFB to the maximum possible wave height in a 15-ft water depth for a 10-sec wave period results in a maximum transmitted wave height of 7.5 ft, a peak mooring force of 1.29 kips/ft of breakwater, and an extreme flow velocity of 11.0 ft/sec.

b. For 89.6- and 118.4-ft SFBs moored in 13, 15, 18, and 21 ft of water using a mooring line length of 150 ft and subjected to spectral waves:

   (1) Transmitted wave heights are consistently lower for the 118.4-ft SFB, and the transmission response of both structures is strongly dependent on wave period.

   (2) Increasing the water depth significantly decreases the wave-attenuating capabilities of both structures.

   (3) For most wave conditions, mooring forces are similar for both SFB lengths and tend to increase with increasing depth.

   (4) The 14-sec, 8-ft spectrum produced the highest peak mooring forces (3.07 and 2.93 kips/ft of breakwater for the 89.6-ft and 118.4-ft structures, respectively) of all conditions investigated.

   (5) Peak flow velocities are generally higher for the longer SFB, and maximum values of 12.5 and 15.5 ft/sec were observed for the 89.6- and 118.4-ft structures, respectively.

c. For the 250-ft mooring line, as opposed to the 150-ft mooring line:

   (1) For attack of 10-sec, 10- to 15-ft storm waves:

      (a) Transmitted wave heights are slightly lower.

      (b) Average mooring forces are similar and peak mooring forces are consistently reduced.

      (c) Peak flow velocities are slightly lower.

   (2) For subjection to 6- to 14-sec, 4- and 8-ft spectral waves:

(a) Wave attenuation is essentially unaffected.

(b) Generally, both average and peak mooring forces are reduced with the reduction being the most significant for the peak forces associated with the 8-ft wave heights.

(c) Peak flow velocities are similar for most wave conditions; however, the longer mooring line appears to have a slight advantage for a few specific conditions.

85. Based on the test conditions, test results, and the test data analysis carried out and reported on by MCA Engineers, Inc. (MCA 1984), for Tests 1-20 of the side-connector tests, it is concluded that:

a. The mooring line test data are valid for all tests. The mass weights in the model mooring line spring systems did not have an affect on the mean peak mooring line tensions recorded during Tests 1-15.

b. The connector forces measured during the rigid bottom tests (Tests 1-15, 17 and 18) are of such a large magnitude that it does not appear to be economically feasible to design the connector type used in these tests if the rigid-bottom impact case is a design requirement.

c. The bumpering, which simulated a soft seafloor condition, reduced the connector forces to values that would make the connector design a feasible task, but the connector system design would only be adequate for seafloor conditions equal to or softer than the condition simulated in the model tests. Since this seafloor condition cannot be guaranteed for all prototype site conditions, it would be essential to provide a bumper or fendering system on the stern of the barges. A fendering system had been considered as a method of alleviating structural loadings in the barges, but it was ruled out as being too complicated.

d. With the barges being adequately designed to withstand impact loadings, the connector loads could possibly be reduced through the incorporation of an absorber in the connector design that would reduce the impact-induced connector forces. This is a feasible alternative, but it requires further in-depth study.

e. Since major modifications of the connector design were deemed essential, it was decided that testing of the existing connector design for other angles of wave attack and with spectral wave conditions was not needed.

REFERENCES

Garcia, A. W., and Jensen, R. E. 1983 (Jun). "Wave Data Acquisition and Hindcast for Saginaw Bay," Technical Report HL-83-14, US Army Engineer Waterways Experiment Station, Vicksburg, Miss.

Goda, Y. 1974. "Estimation of Wave Statistics from Spectral Information," Proceedings, International Symposium on Ocean Wave Measurement and Analysis; American Society of Civil Engineers, Vol 1, pp 320-337.

Grosskopf, W. G., and Vincent, C. L. 1982 (Feb). "Energy Losses of Waves in Shallow Water," Rep. CETA 82-2, US Army Coastal Engineering Research Center, CE, Fort Belvoir, Va.

Hasselmann, K. 1962. "On the Non-Linear Energy Transfer in a Gravity Wave Spectrum-General Theory," Journal of Fluid Mechanics, Vol 12, Part 1, pp 481-500.

Hasselmann, K., et al. 1973. "Measurements of Wind-Wave Growth and Swell Decay During the Joint North Sea Wave Project JONSWAP," Dtsch, Hydrogr. Z., Vol 8, Supplement A8, No. 12.

Iwata, K. 1980. "Wave Spectrum Changes due to Shoaling and Breaking; I - Minus - Three - Power - Law of Frequency Spectrum," Osaka University, Technical Report, Vol 30, No. 1517-1550, pp 269-278.

Jensen, R. E. 1983 (April). "Mississippi Sound Wave Hindcast Study," Technical Report HL-83-8, US Army Engineer Waterways Experiment Station, Vicksburg, Miss.

__________. 1983 (Sep). "Methodology for the Calculation of a Shallow-Water Wave Climate," WIS Report 8, US Army Engineer Waterways Experiment Station, Vicksburg, Miss.

Jones, D. B. 1980. "Sloping Float Breakwater: Interim Data Summary," TN No. N-1568, Civil Engineering Laboratory, Naval Construction Battalion Center, Port Hueneme, Calif.

Kitaigordskii, S. A., Krasitskii, V. P., and Zaslavaskii, M. M. 1975 (Jul). "On Phillips' Theory of Equilibrium Range in the Spectra of Wind-Generated Gravity Waves," Journal of Physical Oceanography, Vol 5, No. 3, pp 410-420.

MCA Engineers, Inc. 1984. "Sloping Float Breakwater Three Dimensional Connector Tests," MCA Engineers, Inc., Newport Beach, Ca. 92660.

Naval Facilities Engineering Command. 1974. "Pontoon Gear Handbook Navy Lightered (N.L.) Equipment P-Series," Report No. NAVFAC P-401, Department of Navy, Washington, D.C.

Ou, Shan-Hwei. 1980 (Sep). "The Equilibrium Range in the Frequency Spectra of the Wind Generated Gravity Waves," Proceedings, 4th Conference on Ocean Engineering in the Republic of China.

Patrick, D. A. 1951. "Model Study of Amphibious Breakwaters," Report 3-332, Institute of Engineering Research, University of California at Berkeley, Berkeley, Calif.

Raichlen, F. 1981. "Experiment with a Sloping Float Breakwater in Water Waves - Phase I," Pasadena, Calif.

Raichlen, F., and Lee, J. J. 1978. "The Behavior of an Inclined Pontoon Breakwater in Water Waves," PO No. N62583/78 M R552, Civil Engineering Laboratory, Naval Construction Battalion Center, Port Hueneme, Calif.

Thompson, E. F. 1977 (Jan). "Wave Climate at Selected Locations Along U. S. Coasts," Technical Report No. 77-1, US Army Coastal Engineering Research Center, CE, Fort Belvoir, Va.

__________. 1980 (Feb). "Energy Spectra in Shallow U. S. Coastal Waters," Technical Paper No. 80-2, US Army Coastal Engineering Research Center, CE, Fort Belvoir, Va.

Thornton, E. B. 1977. "Rederivation of the Saturation Range in a Frequency Spectrum of Wind-Generated Gravity Waves," Journal of Physical Oceanography, Vol 7, pp 137-140.

Vincent, C. L. 1982 (May). "Shallow Water Wave Modeling," 1st International Conference on Meteorology and Air-Sea Interaction in the Coastal Zone, The Hague.

Table 1

Wave Conditions and Test Setup for Side-Connector Tests

Monochromatic Waves, 90 deg

Test No.	Wave Period, sec	Wave Height, ft	Mooring Line(s) Unhooked	Spring Systems, Modified (M) or Unmodified (U)	SFB Stern, Rigid (R) or Bumpered (B)
1	10	10.0	--	U	R
2	10	12.5	--	U	R
3	10	15.0	--	U	R
4	12	10.0	--	U	R
5	12	12.5	--	U	R
6	12	15.0	--	U	R
7	14	10.0	--	U	R
8	14	12.5	--	U	R
9	14	15.0	--	U	R
10	14	15.0	T6	U	R
11	12	15.0	T6	U	R
12	12	15.0	T4 & T6	U	R
13	14	15.0	T4 & T6	U	R
14	10	10.0	--	U	R
15	14	10.0	--	U	R
16	Ping tests		--	U	R
17	10	10.0	--	M	R
18	14	10.0	--	M	R
19	10	10.0	--	M	B
20	14	10.0	--	M	B

Table 2

Characteristics of Monochromatic Test Waves; d = 15.00 ft

T, sec	H, ft	d/L	H/L	H/d	L_{SFB}/L
4.0	2.0	0.2107	0.0281	0.133	1.237
4.0	4.0	0.2107	0.0562	0.267	1.237
4.0	6.0	0.2107	0.0843	0.400	1.237
6.0	2.0	0.1244	0.0166	0.133	0.731
6.0	4.0	0.1244	0.0332	0.267	0.731
6.0	6.0	0.1244	0.0498	0.400	0.731
8.0	2.0	0.0896	0.0119	0.133	0.526
8.0	4.0	0.0896	0.0239	0.267	0.526
8.0	6.0	0.0896	0.0358	0.400	0.526
10.0	2.0	0.0705	0.0094	0.133	0.414
10.0	4.0	0.0705	0.0188	0.267	0.414
10.0	6.0	0.0705	0.0282	0.400	0.414
12.0	2.0	0.0581	0.0077	0.133	0.341
12.0	4.0	0.0581	0.0155	0.267	0.341
12.0	6.0	0.0581	0.0232	0.400	0.341
14.0	2.0	0.0495	0.0066	0.133	0.291
14.0	4.0	0.0495	0.0132	0.267	0.291
14.0	6.0	0.0495	0.0198	0.400	0.291

Table 3

Wave-Attenuating Capabilities of 89.6-ft SFB;

Monochromatic Waves; d = 15.0 ft

Incident Wave		Condition 1		Condition 2		Condition 3	
T, sec	H, ft	H_t, ft	C_t	H_t, ft	C_t	H_t, ft	C_t
4.0	2.0	0.50	0.25	0.45	0.23	0.25	0.13
4.0	4.0	1.30	0.33	0.60	0.15	0.95	0.24
4.0	6.0	1.55	0.26	0.80	0.13	2.30	0.38
6.0	2.0	0.40	0.20	0.45	0.23	0.35	0.18
6.0	4.0	1.05	0.26	0.80	0.20	1.00	0.25
6.0	6.0	2.20	0.37	1.80	0.30	1.30	0.22
8.0	2.0	0.65	0.33	0.50	0.25	0.30	0.15
8.0	4.0	1.40	0.35	1.15	0.29	1.50	0.38
8.0	6.0	2.65	0.44	2.40	0.40	2.20	0.37
10.0	2.0	1.25	0.63	1.10	0.55	0.70	0.35
10.0	4.0	2.15	0.54	1.90	0.48	1.45	0.36
10.0	6.0	3.25	0.54	3.10	0.52	2.80	0.47
12.0	2.0	1.35	0.68	1.40	0.70	1.25	0.63
12.0	4.0	2.70	0.68	2.40	0.60	1.85	0.46
12.0	6.0	4.05	0.68	3.55	0.59	2.90	0.48
14.0	2.0	1.50	0.75	1.35	0.68	1.30	0.65
14.0	4.0	2.50	0.63	2.30	0.58	2.25	0.56
14.0	6.0	3.20	0.53	3.20	0.53	3.60	0.60

NOTES: Condition 1 tests were conducted with a 1.5-in. gap between the SFB's edge and the flume walls.

Condition 2 was the same as Condition 1 except the 1.5-in. gap was filled with a fibrous wave absorber.

Condition 3 tests were conducted with a 0.25-in. gap between the SFB's edge and the flume walls (Raichlen 1981).

Table 4

Average and Peak Mooring Forces Observed at Gage 1; 89.6-ft SFB; Monochromatic Waves; d = 15.0 ft

Incident Wave		Mooring Force, kips/21-ft Barge Width					
		Condition 1		Condition 2		Condition 3	
T, sec	H, ft	Average	Peak	Average	Peak	Average	Peak
4.0	2.0	1.3	1.5	1.4	1.6	*	2.2
4.0	4.0	2.2	2.3	4.8	5.2	*	4.8
4.0	6.0	4.3	5.0	5.3	5.9	*	3.0
6.0	2.0	3.3	3.7	1.9	2.6	*	5.8
6.0	4.0	12.9	13.9	12.0	12.4	4.8	5.4
6.0	6.0	12.9	14.4	11.1	11.7	3.0	8.6
8.0	2.0	12.5	14.2	12.8	13.6	8.0	10.0
8.0	4.0	17.2	17.4	15.8	16.1	8.0	8.8
8.0	6.0	20.2	20.7	16.4	16.9	4.0	15.2
10.0	2.0	16.7	17.4	12.4	13.1	*	13.8
10.0	4.0	20.6	21.3	19.4	19.9	11.6	12.0
10.0	6.0	20.8	22.9	18.9	20.2	7.4	13.6
10.0	2.0	12.8	13.8	5.0	6.1	*	11.8
12.0	4.0	20.0	21.3	19.2	20.5	*	15.2
12.0	6.0	21.2	22.9	20.3	21.3	10.0	13.6
14.0	2.0	8.1	8.2	6.2	6.3	*	6.8
14.0	4.0	20.7	21.0	20.7	21.2	*	16.8
14.0	6.0	21.8	22.8	20.5	21.0	14.2	20.4

NOTES: Condition 1 tests were conducted with a 1.5-in. gap between the SFB's edge and the flume walls.

Condition 2 was the same as Condition 1 except the 1.5-in. gap was filled with a fibrous wave absorber.

Condition 3 tests were conducted with a 0.25-in. gap between the SFB's edge and the flume walls (Raichlen 1981).

* No value reported.

Table 5

Average and Peak Mooring Forces Observed at Gage 2; 89.6-ft SFB; Monochromatic Waves; d = 15.0 ft

Incident Wave		Mooring Force, kips/21-ft Barge Width			
		Condition 1		Condition 2	
T, sec	H, ft	Average	Peak	Average	Peak
4.0	2.0	1.4	1.7	1.5	1.7
4.0	4.0	2.3	2.5	5.1	5.5
4.0	6.0	4.6	5.4	5.5	6.2
6.0	2.0	3.5	3.9	2.3	3.0
6.0	4.0	13.8	14.8	12.6	13.0
6.0	6.0	13.4	15.0	11.7	12.3
8.0	2.0	12.9	14.6	13.5	14.2
8.0	4.0	19.0	19.5	16.5	16.8
8.0	6.0	21.3	21.8	16.8	17.4
10.0	2.0	17.8	18.6	12.9	13.6
10.0	4.0	22.1	22.8	20.2	20.7
10.0	6.0	22.1	24.4	19.6	21.0
12.0	2.0	13.7	14.6	5.2	6.3
12.0	4.0	21.5	23.0	19.9	21.3
12.0	6.0	22.7	24.7	21.0	22.1
14.0	2.0	8.7	8.8	6.4	6.5
14.0	4.0	22.1	22.5	21.3	21.8
14.0	6.0	22.8	24.0	21.4	21.9

NOTES: Condition 1 tests were conducted with a 1.5-in. gap between the SFB's edge and the flume walls.

Condition 2 was the same as Condition 1 except the 1.5-in. gap was filled with a fibrous wave absorber.

Table 6

Peak Flow Velocities Observed at Stern of SFB; 89.6-ft SFB; Monochromatic Waves; d = 15.0 ft

Incident Wave		Peak Flow Velocity, ft/sec					
		Condition 1			Condition 2		
T, sec	H, ft	Minimum	Average	Maximum	Minimum	Average	Maximum
4.0	4.0	1.5	1.9	2.5	1.0	1.6	2.0
4.0	6.0	2.0	2.7	3.0	1.5	2.6	3.0
6.0	4.0	3.0	3.8	4.5	3.0	3.4	4.0
6.0	6.0	3.5	4.7	6.0	3.0	4.4	5.5
8.0	4.0	3.0	4.1	4.5	3.0	3.7	4.5
8.0	6.0	5.0	6.7	8.0	5.5	6.9	7.5
10.0	4.0	2.5	3.9	5.0	3.0	4.0	5.5
10.0	6.0	4.0	6.2	8.0	4.5	5.8	8.0
12.0	4.0	3.5	4.2	5.5	4.0	4.8	6.0
12.0	6.0	4.0	5.5	7.0	4.0	6.1	8.0
14.0	4.0	3.5	4.4	5.5	4.5	5.6	6.5
14.0	6.0	4.0	5.6	7.0	4.5	5.5	8.0

NOTES: Condition 1 tests were conducted with a 1.5-in. gap between the SFB's edge and the flume walls.

Condition 2 was the same as Condition 1 except the 1.5-in. gap was filled with a fibrous wave absorber.

Table 7

Characteristics of Monochromatic Storm Waves; d = 15.0 ft; T = 10.0 sec*

H, ft	H/L	H/d
2.0	0.0094	0.133
4.0	0.0188	0.267
6.0	0.0282	0.400
8.0	0.0376	0.533
10.0	0.0470	0.667
11.0	0.0517	0.733
12.0	0.0564	0.800
12.5	0.0588	0.833
12.7	0.0597	0.847

* $d/L = 0.0705$; $L_{SFB}/L = 0.414$.

Table 8

Wave-Attenuating Capabilities of 89.6-ft SFB; Monochromatic Storm Waves; $d = 15.0$ ft; $T = 10$ sec (Survival Tests)

H, ft	H_t, ft	C_t
2.0	1.25	0.63
4.0	2.15	0.54
6.0	3.25	0.54
8.0	4.20	0.53
10.0	6.15	0.62
11.0	6.60	0.60
12.0	7.10	0.59
12.5	7.40	0.59
12.7	7.50	0.59

Table 9

Average and Peak Mooring Forces; Monochromatic Storm Waves; 89.6-ft SFB; $d = 15.0$ ft; $T = 10$ sec (Survival Tests)

	Mooring Force, kips/21-ft Barge Width			
	Gage 1		Gage 2	
H, ft	Average	Peak	Average	Peak
2.0	16.7	17.4	17.8	18.6
4.0	20.6	21.3	22.1	22.8
6.0	20.8	22.9	22.1	24.4
8.0	19.8	22.2	20.4	22.7
10.0	17.9	21.0	18.4	21.9
11.0	18.3	22.0	18.7	22.9
12.0	17.4	23.9	18.5	24.6
12.5	17.6	26.0	17.9	27.0
12.7	17.8	26.3	18.3	27.0

Table 10

Peak Flow Velocities Observed at Stern of SFB;

Monochromatic Storm Waves; 89.6 ft SFB;

d = 15.0 ft; T = 10 sec

(Survival Tests)

	Peak Flow Velocity, ft/sec		
H, ft	Minimum	Average	Maximum
4.0	2.5	3.9	5.0
6.0	4.0	6.2	8.0
8.0	6.0	8.1	9.5
10.0	7.0	9.0	11.0
11.0	7.0	8.9	10.5
12.0	7.0	9.0	10.5
12.5	6.5	8.4	10.0
12.7	6.5	8.4	9.5

Table 11

Wave Attenuation Test Results; Spectral Waves; d = 13.0 ft

		Transmitted Wave Heights and Coefficients of Transmission for Indicated SFB Length			
Incident Spectrum		89.6 ft		118.4 ft	
T_p, sec	H_{mo}, ft	H_t, ft	C_t	H_t, ft	C_t
6.0	2.0	0.50	0.25	0.30	0.15
6.0	4.0	1.05	0.26	0.75	0.19
6.0	6.0	2.10	0.35	1.75	0.29
8.0	2.0	0.70	0.35	0.45	0.23
8.0	4.0	1.45	0.36	1.10	0.28
8.0	6.0	2.75	0.46	2.25	0.38
8.0	8.0	3.90	0.49	3.45	0.43
10.0	2.0	0.95	0.48	0.65	0.33
10.0	4.0	1.90	0.48	1.40	0.35
10.0	6.0	3.15	0.53	2.50	0.42
10.0	8.0	4.65	0.58	3.90	0.49
12.0	2.0	1.25	0.63	0.80	0.40
12.0	4.0	2.45	0.61	1.75	0.44
12.0	6.0	3.65	0.61	2.95	0.49
12.0	8.0	4.95	0.62	4.30	0.54
14.0	2.0	1.45	0.73	1.15	0.58
14.0	4.0	2.55	0.64	2.05	0.51
14.0	6.0	3.90	0.65	3.30	0.55
14.0	8.0	5.20	0.65	4.80	0.60

Table 12

Wave Attenuation Test Results; Spectral Waves; d = 15.0 ft

Incident Spectrum		Transmitted Wave Heights and Coefficients of Transmission for Indicated SFB Length					
		72.3 ft		89.6 ft		118.4 ft	
T_p, sec	H_{mo}, ft	H_t, ft	C_t	H_t, ft	C_t	H_t, ft	C_t
6.0	2.0	0.85	0.43	0.55	0.28	0.40	0.20
6.0	4.0	1.65	0.41	1.15	0.29	0.85	0.21
6.0	6.0	2.65	0.44	2.20	0.37	1.90	0.32
8.0	2.0	1.10	0.55	0.80	0.40	0.55	0.28
8.0	4.0	2.05	0.51	1.60	0.40	1.15	0.29
8.0	6.0	3.35	0.56	2.90	0.48	2.15	0.36
8.0	8.0	4.85	0.61	4.25	0.53	3.50	0.44
10.0	2.0	1.30	0.65	1.10	0.55	0.80	0.40
10.0	4.0	2.45	0.61	2.10	0.53	1.55	0.39
10.0	6.0	3.65	0.61	3.20	0.53	2.55	0.43
10.0	8.0	5.45	0.68	4.80	0.60	4.05	0.51
12.0	2.0	1.50	0.75	1.45	0.73	1.25	0.63
12.0	4.0	2.95	0.74	2.50	0.63	1.95	0.49
12.0	6.0	4.40	0.73	3.70	0.62	3.25	0.54
12.0	8.0	5.75	0.72	5.10	0.64	4.55	0.57
14.0	2.0	1.45	0.73	1.45	0.73	1.40	0.70
14.0	4.0	2.95	0.74	2.75	0.69	2.35	0.59
14.0	6.0	4.40	0.73	4.05	0.68	3.55	0.59
14.0	8.0	5.95	0.74	5.65	0.71	5.35	0.67

Table 13

Wave Attenuation Test Results; Spectral Waves; d = 18.0 ft

Incident Spectrum		Transmitted Wave Heights and Coefficients of Transmission for Indicated SFB Length			
		89.6 ft		118.4 ft	
T_p, sec	H_{mo}, ft	H_t, ft	C_t	H_t, ft	C_t
6.0	2.0	0.65	0.33	0.45	0.23
6.0	4.0	1.40	0.35	0.90	0.23
6.0	6.0	2.55	0.43	1.80	0.30
8.0	2.0	1.00	0.50	0.65	0.33
8.0	4.0	1.90	0.48	1.25	0.31
8.0	6.0	3.20	0.53	2.40	0.40
8.0	8.0	5.05	0.63	3.90	0.49
10.0	2.0	1.30	0.65	0.90	0.45
10.0	4.0	2.30	0.58	1.70	0.43
10.0	6.0	3.80	0.63	2.90	0.48
10.0	8.0	5.60	0.70	4.60	0.58
12.0	2.0	1.65	0.83	1.40	0.70
12.0	4.0	3.20	0.80	2.45	0.61
12.0	6.0	4.55	0.76	3.85	0.64
12.0	8.0	6.35	0.79	5.35	0.67
14.0	2.0	1.75	0.88	1.60	0.80
14.0	4.0	3.35	0.84	2.85	0.71
14.0	6.0	5.10	0.85	4.25	0.71
14.0	8.0	6.50	0.81	5.85	0.73

Table 14

Wave Attenuation Test Results; Spectral Waves; d = 21.0 ft

Incident Spectrum		Transmitted Wave Heights and Coefficients of Transmission for Indicated SFB Length			
		89.6 ft		118.4 ft	
T_p, sec	H_{mo}, ft	H_t, ft	C_t	H_t, ft	C_t
6.0	2.0	0.75	0.38	0.55	0.28
6.0	4.0	1.50	0.38	1.05	0.26
6.0	6.0	2.60	0.43	1.75	0.29
8.0	2.0	1.15	0.58	0.80	0.40
8.0	4.0	2.15	0.54	1.55	0.39
8.0	6.0	3.35	0.56	2.50	0.42
8.0	8.0	5.20	0.65	4.20	0.53
10.0	2.0	1.40	0.70	1.10	0.55
10.0	4.0	2.60	0.65	1.95	0.49
10.0	6.0	3.90	0.65	3.10	0.52
10.0	8.0	5.70	0.71	4.90	0.61
12.0	2.0	1.75	0.88	1.50	0.75
12.0	4.0	3.50	0.88	2.90	0.73
12.0	6.0	4.75	0.79	4.05	0.68
12.0	8.0	6.55	0.82	5.55	0.69
14.0	2.0	1.80	0.90	1.70	0.85
14.0	4.0	3.60	0.90	3.15	0.79
14.0	6.0	5.20	0.87	4.50	0.75
14.0	8.0	6.90	0.86	6.00	0.75

Table 15

Average and Peak Mooring Forces; Spectral Waves; d = 13.0 ft

Incident Spectrum		Average and Peak Mooring Forces, kips/21-ft Barge Width, for Indicated SFB Length			
		89.6 ft		118.4 ft	
T_p, sec	H_{mo}, ft	Average	Peak	Average	Peak
6.0	2.0	4.1	9.5	1.2	2.5
6.0	4.0	10.9	15.3	7.5	11.0
6.0	6.0	9.4	16.5	6.7	16.2
8.0	2.0	9.9	14.3	1.6	3.2
8.0	4.0	13.0	16.9	11.5	15.7
8.0	6.0	12.0	21.5	10.2	19.7
8.0	8.0	13.2	27.9	12.9	22.3
10.0	2.0	7.7	15.8	2.5	7.2
10.0	4.0	16.2	20.9	12.9	17.7
10.0	6.0	15.6	27.8	14.0	22.6
10.0	8.0	15.6	42.4	15.6	38.1
12.0	2.0	10.8	19.1	9.7	16.3
12.0	4.0	19.8	23.6	16.9	20.3
12.0	6.0	18.3	29.6	18.3	25.2
12.0	8.0	16.9	34.2	16.5	30.4
14.0	2.0	13.5	18.0	11.4	14.5
14.0	4.0	19.9	22.9	19.5	23.5
14.0	6.0	17.9	32.3	17.8	35.9
14.0	8.0	16.3	46.4	17.3	44.6

Table 16

Average and Peak Mooring Forces; Spectral Waves; d = 15.0 ft

Incident Spectrum		Average and Peak Mooring Forces, kips/21-ft Barge Width, for Indicated SFB Length					
		72.3 ft		89.6 ft		118.4 ft	
T_p, sec	H_{mo}, ft	Average	Peak	Average	Peak	Average	Peak
6.0	2.0	10.0	14.4	3.7	7.5	2.7	5.4
6.0	4.0	13.5	18.8	12.5	17.3	11.5	15.1
6.0	6.0	15.0	21.3	12.7	19.4	11.4	16.2
8.0	2.0	12.9	17.2	11.8	16.4	9.4	13.9
8.0	4.0	15.6	22.9	15.3	19.4	13.8	17.0
8.0	6.0	17.0	27.2	14.8	21.7	14.0	19.3
8.0	8.0	18.0	39.6	16.2	27.9	15.9	24.6
10.0	2.0	12.5	18.1	10.0	17.8	10.1	15.5
10.0	4.0	16.4	24.7	17.3	26.0	15.6	19.7
10.0	6.0	17.8	34.4	17.6	28.3	16.2	22.2
10.0	8.0	19.2	44.3	19.1	43.3	19.0	41.7
12.0	2.0	8.6	18.3	11.8	19.9	14.7	18.8
12.0	4.0	17.1	27.7	19.8	24.7	18.3	22.8
12.0	6.0	19.8	43.0	20.8	34.8	19.9	27.9
12.0	8.0	20.3	47.2	19.3	37.1	19.3	45.2
14.0	2.0	15.0	18.6	9.7	19.8	15.2	19.5
14.0	4.0	18.6	27.5	20.4	24.5	19.8	23.6
14.0	6.0	20.6	34.7	21.3	32.4	20.0	28.3
14.0	8.0	20.9	54.6	18.9	56.0	21.1	52.0

Table 17

Average and Peak Mooring Forces; Spectral Waves; d = 18.0 ft

Incident Spectrum		Average and Peak Mooring Forces, kips/21-ft Barge Width, for Indicated SFB Length			
		89.6 ft		118.4 ft	
T_p, sec	H_{mo}, ft	Average	Peak	Average	Peak
6.0	2.0	4.7	14.6	2.2	6.0
6.0	4.0	16.6	22.6	15.1	19.5
6.0	6.0	16.4	25.4	15.4	20.8
8.0	2.0	14.9	20.0	8.8	13.6
8.0	4.0	18.9	26.0	17.7	22.0
8.0	6.0	19.8	30.3	19.0	28.1
8.0	8.0	20.8	37.3	20.0	34.0
10.0	2.0	9.1	19.9	10.5	17.4
10.0	4.0	20.7	28.3	20.1	24.7
10.0	6.0	24.0	34.5	20.4	28.4
10.0	8.0	23.3	49.1	21.9	44.3
12.0	2.0	4.6	10.8	13.0	21.0
12.0	4.0	21.7	31.0	24.4	29.1
12.0	6.0	23.9	39.0	26.1	36.1
12.0	8.0	26.4	54.5	26.3	51.2
14.0	2.0	2.2	3.5	2.7	7.3
14.0	4.0	23.0	30.4	25.0	32.0
14.0	6.0	25.5	41.7	27.7	42.6
14.0	8.0	24.7	61.4	29.2	59.5

Table 18

Average and Peak Mooring Forces; Spectral Waves; d = 21.0 ft

Incident Spectrum		Average and Peak Mooring Forces, kips/21-ft Barge Width, for Indicated SFB Length			
		89.6 ft		118.4 ft	
T_p, sec	H_{mo}, ft	Average	Peak	Average	Peak
6.0	2.0	9.5	14.0	1.5	5.5
6.0	4.0	17.1	23.1	19.3	21.8
6.0	6.0	18.3	26.4	18.9	23.7
8.0	2.0	12.6	19.5	10.5	16.1
8.0	4.0	19.4	27.2	21.4	26.5
8.0	6.0	21.4	33.1	22.5	38.0
8.0	8.0	21.6	42.9	25.3	43.5
10.0	2.0	6.3	14.8	10.3	17.2
10.0	4.0	21.2	30.3	23.8	30.5
10.0	6.0	21.4	35.5	24.6	36.4
10.0	8.0	23.2	56.7	25.6	47.0
12.0	2.0	3.9	7.9	9.2	16.6
12.0	4.0	22.0	31.0	29.0	35.5
12.0	6.0	24.7	43.2	31.2	42.3
12.0	8.0	25.0	60.1	31.4	51.9
14.0	2.0	0.8	1.7	3.6	6.9
14.0	4.0	21.9	33.0	28.5	35.9
14.0	6.0	24.9	44.3	31.4	47.9
14.0	8.0	27.3	64.4	32.6	61.6

Table 19

Peak Flow Velocities Observed at Stern of SFB; Spectral Waves; d = 13.0 ft

Incident Spectrum		Peak Flow Velocity, ft/sec, for Indicated SFB Length	
T_p, sec	H_{mo}, ft	89.6 ft	118.4 ft
6.0	4.0	4.0	1.0
6.0	6.0	6.5	4.5
8.0	4.0	5.5	6.0
8.0	6.0	7.0	9.0
8.0	8.0	9.5	11.5
10.0	4.0	7.5	8.0
10.0	6.0	9.0	11.5
10.0	8.0	11.0	13.5
12.0	4.0	8.0	12.5
12.0	6.0	10.0	15.0
12.0	8.0	12.0	14.5
14.0	4.0	9.0	13.0
14.0	6.0	11.5	15.0
14.0	8.0	12.5	14.5

Table 20

Peak Flow Velocities Observed at Stern of SFB; Spectral Waves; d = 15.0 ft

Incident Spectrum		Peak Flow Velocity, ft/sec, for Indicated SFB Length		
T_p, sec	H_{mo}, ft	72.3 ft	89.6 ft	118.4 ft
6.0	4.0	3.0	4.0	1.5
6.0	6.0	6.0	7.0	4.5
8.0	4.0	6.0	6.5	4.5
8.0	6.0	6.5	8.0	9.0
8.0	8.0	8.0	8.5	11.5
10.0	4.0	6.0	7.5	6.0
10.0	6.0	7.0	9.0	9.5
10.0	8.0	9.0	11.5	13.0
12.0	4.0	6.0	8.0	12.0
12.0	6.0	9.0	10.5	15.5
12.0	8.0	10.0	11.0	14.5
14.0	4.0	9.0	9.5	12.0
14.0	6.0	11.0	12.0	15.0
14.0	8.0	11.0	12.0	14.0

Table 21

Peak Flow Velocities Observed at Stern of SFB; Spectral Waves; d = 18.0 ft

Incident Spectrum		Peak Flow Velocity, ft/sec, for Indicated SFB Length	
T_p, sec	H_{mo}, ft	89.6 ft	118.4 ft
6.0	4.0	4.5	3.0
6.0	6.0	6.5	5.5
8.0	4.0	5.5	4.5
8.0	6.0	7.5	9.0
8.0	8.0	9.0	11.0
10.0	4.0	7.0	6.0
10.0	6.0	9.5	11.0
10.0	8.0	10.5	12.0
12.0	4.0	7.0	10.0
12.0	6.0	9.5	14.0
12.0	8.0	10.0	14.0
14.0	4.0	6.0	10.5
14.0	6.0	11.0	14.5
14.0	8.0	12.0	13.5

Table 22

Peak Flow Velocities Observed at Stern of SFB; Spectral Waves; d = 21.0 ft

Incident Spectrum		Peak Flow Velocity, ft/sec, for Indicated SFB Length	
T_p, sec	H_{mo}, ft	89.6 ft	118.4 ft
6.0	4.0	4.5	4.0
6.0	6.0	7.0	6.0
8.0	4.0	6.0	5.0
8.0	6.0	8.0	9.5
8.0	8.0	10.5	11.0
10.0	4.0	5.5	7.0
10.0	6.0	8.0	10.0
10.0	8.0	9.0	11.5
12.0	4.0	6.0	10.0
12.0	6.0	9.5	13.5
12.0	8.0	10.0	13.5
14.0	4.0	6.0	8.5
14.0	6.0	11.0	13.0
14.0	8.0	11.0	13.5

Table 23

Mooring Line Length-Effect Tests; Monochromatic Wave Attenuation

Results; d = 21.0 ft; T = 10.0 sec

Incident Wave Height, ft	Transmitted Wave Heights and Coefficients of Transmission for Indicated Mooring Line Length: 150.0 ft		250.0 ft	
	H_t, ft	C_t	H_t, ft	C_t
	89.6-ft SFB			
10.0	8.05	0.81	7.00	0.70
12.0	9.40	0.78	8.70	0.73
14.0	11.30	0.81	11.00	0.79
15.0	11.60	0.77	11.70	0.78
	118.4-ft SFB			
10.0	5.50	0.55	5.35	0.54
12.0	7.35	0.61	6.80	0.57
14.0	9.40	0.67	9.00	0.64
15.0	10.45	0.70	10.05	0.67

Table 24

Mooring Line Length-Effect Tests; Average and Peak Mooring Forces; Monochromatic Waves; d = 21.0 ft; T = 10.0 sec

Incident Wave Height, ft	Average and Peak Mooring Forces, kips/21-ft Barge Width for Indicated Mooring Line Length: 150.0 ft Average	150.0 ft Peak	250.0 ft Average	250.0 ft Peak
	89.6-ft SFB			
10.0	30.1	37.2	29.9	31.7
12.0	28.8	35.8	27.9	33.1
14.0	23.7	35.9	24.1	32.1
15.0	21.0	36.7	23.9	34.8
	118.4-ft SFB			
10.0	37.5	41.1	31.6	33.3
12.0	36.0	38.6	32.2	34.1
14.0	32.8	40.1	31.1	33.3
15.0	31.1	40.4	30.2	34.0

Table 25

Mooring Line Length-Effect Tests; Peak Flow Velocities Observed at Stern of SFB; Monochromatic Waves; d = 21.0 ft; T = 10.0 sec

Incident Wave Height, ft	Peak Flow Velocity, ft/sec, for Indicated Mooring Line Length: 150.0 ft	250.0 ft
	89.6-ft SFB	
10.0	10.5	9.5
12.0	11.0	11.0
14.0	12.0	11.5
15.0	11.5	11.5
	118.4-ft SFB	
10.0	11.0	11.0
12.0	11.0	10.5
14.0	12.0	11.5
15.0	12.0	11.0

Table 26

Mooring Line Length-Effect Tests; Spectral Wave Attenuation Results; d = 21.0 ft

Incident Spectrum		Transmitted Wave Heights and Coefficients of Transmission for Indicated Mooring Line Length			
		150.0 ft		250.0 ft	
T_p, sec	H_{mo}, ft	H_t, ft	C_t	H_t, ft	C_t
		89.6-ft SFB			
6.0	4.0	1.50	0.38	1.55	0.39
8.0	4.0	2.15	0.54	2.10	0.53
10.0	4.0	2.60	0.65	2.60	0.65
12.0	4.0	3.50	0.88	3.45	0.86
14.0	4.0	3.60	0.90	3.55	0.89
8.0	8.0	5.20	0.65	5.15	0.64
10.0	8.0	5.70	0.71	5.80	0.73
12.0	8.0	6.55	0.82	6.50	0.81
14.0	8.0	6.90	0.86	6.65	0.83
		118.4-ft SFB			
6.0	4.0	1.05	0.26	1.05	0.26
8.0	4.0	1.55	0.39	1.45	0.36
10.0	4.0	1.95	0.49	1.90	0.48
12.0	4.0	2.90	0.73	2.85	0.71
14.0	4.0	3.15	0.79	3.10	0.78
8.0	8.0	4.20	0.53	4.05	0.51
10.0	8.0	4.90	0.61	4.80	0.60
12.0	8.0	5.55	0.69	5.65	0.71
14.0	8.0	6.00	0.75	6.00	0.75

Table 27

Mooring Line Length-Effect Tests; Average and Peak

Mooring Forces; Spectral Waves; d = 21.0 ft

Incident Spectrum		Average and Peak Mooring Forces, kips/21-ft Barge Width, for Indicated Mooring Line Length			
		150.0 ft		250.0 ft	
T_p, sec	H_{mo}, ft	Average	Peak	Average	Peak
		89.6-ft SFB			
6.0	4.0	17.1	23.1	17.9	22.9
8.0	4.0	19.4	27.2	19.4	25.3
10.0	4.0	21.2	30.3	20.3	25.2
12.0	4.0	22.0	31.0	20.8	28.9
14.0	4.0	21.9	33.0	21.2	29.3
8.0	8.0	21.6	42.9	20.6	36.1
10.0	8.0	23.2	56.7	20.6	43.5
12.0	8.0	25.0	60.1	22.9	47.2
14.0	8.0	27.3	64.4	23.8	56.0
		118.4-ft SFB			
6.0	4.0	19.3	21.8	16.8	19.2
8.0	4.0	21.4	26.5	19.5	24.6
10.0	4.0	23.8	30.5	20.4	25.6
12.0	4.0	29.0	35.5	24.5	29.6
14.0	4.0	28.5	35.9	24.0	28.4
8.0	8.0	25.3	43.5	22.0	29.7
10.0	8.0	25.6	47.0	23.6	36.6
12.0	8.0	31.4	51.9	27.3	41.4
14.0	8.0	32.6	61.6	25.5	52.0

Table 28

Mooring Line Length-Effect Tests; Peak Flow Velocities Observed at Stern of SFB; Spectral Waves; d = 21.0 ft

Incident Spectrum		Peak Flow Velocity, ft/sec, for Indicated Mooring Line Length	
T_p, sec	H_{mo}, ft	150.0 ft	250.0 ft
	89.6-ft SFB		
6.0	4.0	4.5	4.0
8.0	4.0	6.0	6.0
10.0	4.0	5.5	5.0
12.0	4.0	6.0	6.0
14.0	4.0	6.0	4.5
8.0	8.0	10.5	9.5
10.0	8.0	9.0	10.0
12.0	8.0	10.0	10.0
14.0	8.0	11.0	9.5
	118.4-ft SFB		
6.0	4.0	4.0	3.5
8.0	4.0	5.0	5.0
10.0	4.0	7.0	6.0
12.0	4.0	10.0	8.5
14.0	4.0	8.5	9.0
8.0	8.0	11.0	10.0
10.0	8.0	11.5	10.5
12.0	8.0	13.5	11.5
14.0	8.0	13.5	12.0

Table 29

Coefficients of Transmission and Relative SFB Lengths;

Spectral Waves; d = 13.0 ft

Incident Spectrum		Values of C_t and L_{SFB}/L_p for Indicated SFB Length			
		89.6 ft		118.4 ft	
T_p, sec	H_{mo}, ft	C_t	L_{SFB}/L_p	C_t	L_{SFB}/L_p
6.0	2.0	0.25	0.79	0.15	1.04
6.0	4.0	0.26	0.79	0.19	1.04
6.0	6.0	0.35	0.79	0.29	1.04
8.0	2.0	0.35	0.57	0.23	0.75
8.0	4.0	0.36	0.57	0.28	0.75
8.0	6.0	0.46	0.57	0.38	0.75
8.0	8.0	0.49	0.57	0.43	0.75
10.0	2.0	0.48	0.45	0.33	0.59
10.0	4.0	0.48	0.45	0.35	0.59
10.0	6.0	0.53	0.45	0.42	0.59
10.0	8.0	0.58	0.45	0.49	0.59
12.0	2.0	0.63	0.37	0.40	0.49
12.0	4.0	0.61	0.37	0.44	0.49
12.0	6.0	0.61	0.37	0.49	0.49
12.0	8.0	0.62	0.37	0.54	0.49
14.0	2.0	0.73	0.32	0.58	0.42
14.0	4.0	0.64	0.32	0.51	0.42
14.0	6.0	0.65	0.32	0.55	0.42
14.0	8.0	0.65	0.32	0.60	0.42

Table 30

Coefficients of Transmission and Relative SFB Lengths; Spectral Waves; d = 15.0 ft

Incident Spectrum		Values of C_t and L_{SFB}/L_p for Indicated SFB Length					
		72.3 ft		89.6 ft		118.4 ft	
T_p, sec	H_{mo}, ft	C_t	L_{SFB}/L_p	C_t	L_{SFB}/L_p	C_t	L_{SFB}/L_p
6.0	2.0	0.43	0.60	0.28	0.74	0.20	0.98
6.0	4.0	0.41	0.60	0.29	0.74	0.21	0.98
6.0	6.0	0.44	0.60	0.37	0.74	0.32	0.98
8.0	2.0	0.55	0.43	0.40	0.54	0.28	0.71
8.0	4.0	0.51	0.43	0.40	0.54	0.29	0.71
8.0	6.0	0.56	0.43	0.48	0.54	0.36	0.71
8.0	8.0	0.61	0.43	0.53	0.54	0.44	0.71
10.0	2.0	0.65	0.34	0.55	0.42	0.40	0.56
10.0	4.0	0.61	0.34	0.53	0.42	0.39	0.56
10.0	6.0	0.61	0.34	0.53	0.42	0.43	0.56
10.0	8.0	0.68	0.34	0.60	0.42	0.51	0.56
12.0	2.0	0.75	0.28	0.73	0.35	0.63	0.46
12.0	4.0	0.74	0.28	0.63	0.35	0.49	0.46
12.0	6.0	0.73	0.28	0.64	0.35	0.54	0.46
12.0	8.0	0.72	0.28	0.64	0.35	0.57	0.46
14.0	2.0	0.73	0.24	0.73	0.30	0.70	0.39
14.0	4.0	0.74	0.24	0.69	0.30	0.59	0.39
14.0	6.0	0.73	0.24	0.68	0.30	0.59	0.39
14.0	8.0	0.74	0.24	0.71	0.30	0.67	0.39

Table 31

Coefficients of Transmission and Relative SFB Lengths;

Spectral Waves; d = 18.0 ft

Incident Spectrum		Values of C_t and L_{SFB}/L_p for Indicated SFB Length			
		89.6 ft		118.4 ft	
T_p, sec	H_{mo}, ft	C_t	L_{SFB}/L_p	C_t	L_{SFB}/L_p
6.0	2.0	0.33	0.69	0.23	0.91
6.0	4.0	0.35	0.69	0.23	0.91
6.0	6.0	0.43	0.69	0.30	0.91
8.0	2.0	0.50	0.49	0.33	0.65
8.0	4.0	0.48	0.49	0.31	0.65
8.0	6.0	0.53	0.49	0.40	0.65
8.0	8.0	0.63	0.49	0.49	0.65
10.0	2.0	0.65	0.39	0.45	0.51
10.0	4.0	0.58	0.39	0.43	0.51
10.0	6.0	0.63	0.39	0.48	0.51
10.0	8.0	0.70	0.39	0.58	0.51
12.0	2.0	0.83	0.32	0.70	0.42
12.0	4.0	0.80	0.32	0.61	0.42
12.0	6.0	0.76	0.32	0.64	0.42
12.0	8.0	0.79	0.32	0.67	0.42
14.0	2.0	0.88	0.27	0.80	0.36
14.0	4.0	0.84	0.27	0.71	0.36
14.0	6.0	0.85	0.27	0.71	0.36
14.0	8.0	0.81	0.27	0.73	0.36

Table 32

Coefficients of Transmission and Relative SFB Lengths; Spectral Waves; d = 21.0 ft

Incident Spectrum		Values of C_t and L_{SFB}/L_p for Indicated SFB Length			
		89.6 ft		118.4 ft	
T_p, sec	H_{mo}, ft	C_t	L_{SFB}/L_p	C_t	L_{SFB}/L_p
6.0	2.0	0.38	0.65	0.28	0.86
6.0	4.0	0.38	0.65	0.26	0.86
6.0	6.0	0.43	0.65	0.29	0.86
8.0	2.0	0.58	0.46	0.40	0.61
8.0	4.0	0.54	0.46	0.39	0.61
8.0	6.0	0.56	0.46	0.42	0.61
8.0	8.0	0.65	0.46	0.53	0.61
10.0	2.0	0.70	0.36	0.55	0.48
10.0	4.0	0.65	0.36	0.49	0.48
10.0	6.0	0.65	0.36	0.52	0.48
10.0	8.0	0.71	0.36	0.61	0.48
12.0	2.0	0.88	0.30	0.75	0.39
12.0	4.0	0.88	0.30	0.73	0.39
12.0	6.0	0.79	0.30	0.68	0.39
12.0	8.0	0.82	0.30	0.69	0.39
14.0	2.0	0.90	0.25	0.85	0.33
14.0	4.0	0.90	0.25	0.79	0.33
14.0	6.0	0.87	0.25	0.75	0.33
14.0	8.0	0.86	0.25	0.75	0.33

Table 33

Maximum Connector Forces, Mooring Line Tensions, Barge Angularities, and Impact Velocities

Side-Connector Tests

Test No.	F1X* kips	F1Y kips	F1Z kips	F2X* kips	F2Y kips	F2Z kips	T1 kips	T2 kips	T3 kips	T4 kips	T5 kips	T6 kips	ANG or ANFG deg	VEL ft/sec
1	137	674	3,967	1,419	476	2,862	129	149	98	107	94	26	183.6	--
	-1,831	-1,164	-1,630	-2,004	-432	-4,038							177.7	--
2	764	825	4,232	1,819	486	4,058	171	235	119	144	95	34	183.9	1.8**
	-2,821	-1,624	-4,976	-825	-1,277	-2,921							177.0	--
3	356	798	4,820	1,647	479	3,189	248	189	154	106	106	47	183.8	--
	-2,228	-728	-2,772	-1,651	-580	-4,087							177.5	--
4	621	550	2,850	1,353	396	2,805	165	114	127	76	90	35	182.6	1.4**
	-2,293	-362	-2,586	-807	-240	-2,957							177.7	--
5	967	683	3,378	1,248	512	5,625	179	135	120	143	136	57	183.1	--
	-3,262	-573	-5,564	-2,193	-1,016	-5,122							176.4	--
6	892	1,057	3,574	2,234	842	4,437	307	323	133	144	163	61	182.9	1.8**
	-2,969	-2,102	-4,554	-1,432	-569	-3,867							177.3	--
7	2,048	528	2,698	1,172	255	4,300	136	178	98	91	132	77	182.8	--
	-1,758	-474	-3,788	-969	-718	-1,937							176.9	--
8	331	589	3,003	1,306	218	3,373	323	360	174	121	233	102	182.8	--
	-2,093	-608	-3,753	-969	-604	-2,748							176.7	--
9	301	538	2,741	906	242	3,301	394	525	259	245	314	142	184.9	0.8**
	-1,318	-464	-3,073	-858	-540	-2,196							176.7	--
10	624	1,081	4,573	1,467	667	5,649	244	312	166	171	131	Unhooked	183.4	2.0**
	-3,385	-1,332	-5,569	-1,328	-638	-4,782							177.0	2.0†

(Continued)

* The validity of data is questionable for these two channels. During calibration, these two channels reacted when loading was purely in the y- or z-axis.

** Stern impact velocity measured at inside corner of Barge No. 2.

† Stern impact velocity measured at outside corner of Barge No. 2.

Table 33 (Concluded)

Test No.	F1X* kips	F1Y kips	F1Z kips	F2X* kips	F2Y kips	F2Z kips	T1 kips	T2 kips	T3 kips	T4 kips	T5 kips	T6 kips	ANG or ANFG deg	VEL ft/sec
11	1,142	1,262	4,129	1,901††	1,159††	4,766††	200	247	139	160	77	Unhooked	183.5	2.8**
	-2,804	-1,233	-3,751	-1,800††	-778††	-6,854††							177.2	—
12	280	440	2,691	308††	169††	††	147	257	249	Unhooked	71	Unhooked	182.3	1.3**
	-3,111	-505	-6,294	-1,015††	-1,056††	††							177.1	—
13	312	696	1,537	931††	402††	††	143	257	264	Unhooked	106	Unhooked	184.0	2.2**
	-2,348	-524	-4,695	-917††	-739††	††							177.8	—
14	1,414	871	3,327	1,845	608	2,539	150	180	95	89	96	26	183.9	1.5**
	-2,632	-958	-3,745	-1,100	-649	-3,331							177.3	—
15	670	273	1,507	1,221	466	1,664	136	140	76	95	103	45	180.5	0.6**
	-1,407	-539	-3,272	0	-1,495	-1,218							176.9	—
16	Ping Tests													
17	948	412	3,214	2,193	1,167	2,692	138	173	102	97	102	46	182.4	1.58**
	-3,495	-483	-5,060	-1,215	-1,828	-3,314							177.2	—
18	287	353	2,659	2,292	1,011	4,102	197	276	155	144	261	108	183.0	1.35**
	-2,079	-261	-2,449	0	-1,670	-3,305							177.4	—
19	86	179	1,036	661	204	521	‡	176	123	80	‡	46	‡‡	1.55**
	-554	-131	-929	0	-154	-1,064								—
20	188	162	767	406	97	281	‡	316	132	125	‡	90	182.5	1.02**
	-416	-69	-350	0	-77	-705							177.5	—

* The validity of data is questionable for these two channels. During calibration, these two channels reacted when loading was purely in the y- or z-axis.

** Stern impact velocity measured at inside corner of Barge No. 2.

†† Validity of data is questionable due to offset that occurred in connector F2 during Test 11.

‡ Gage inoperable.

‡‡ Gage malfunctioned.

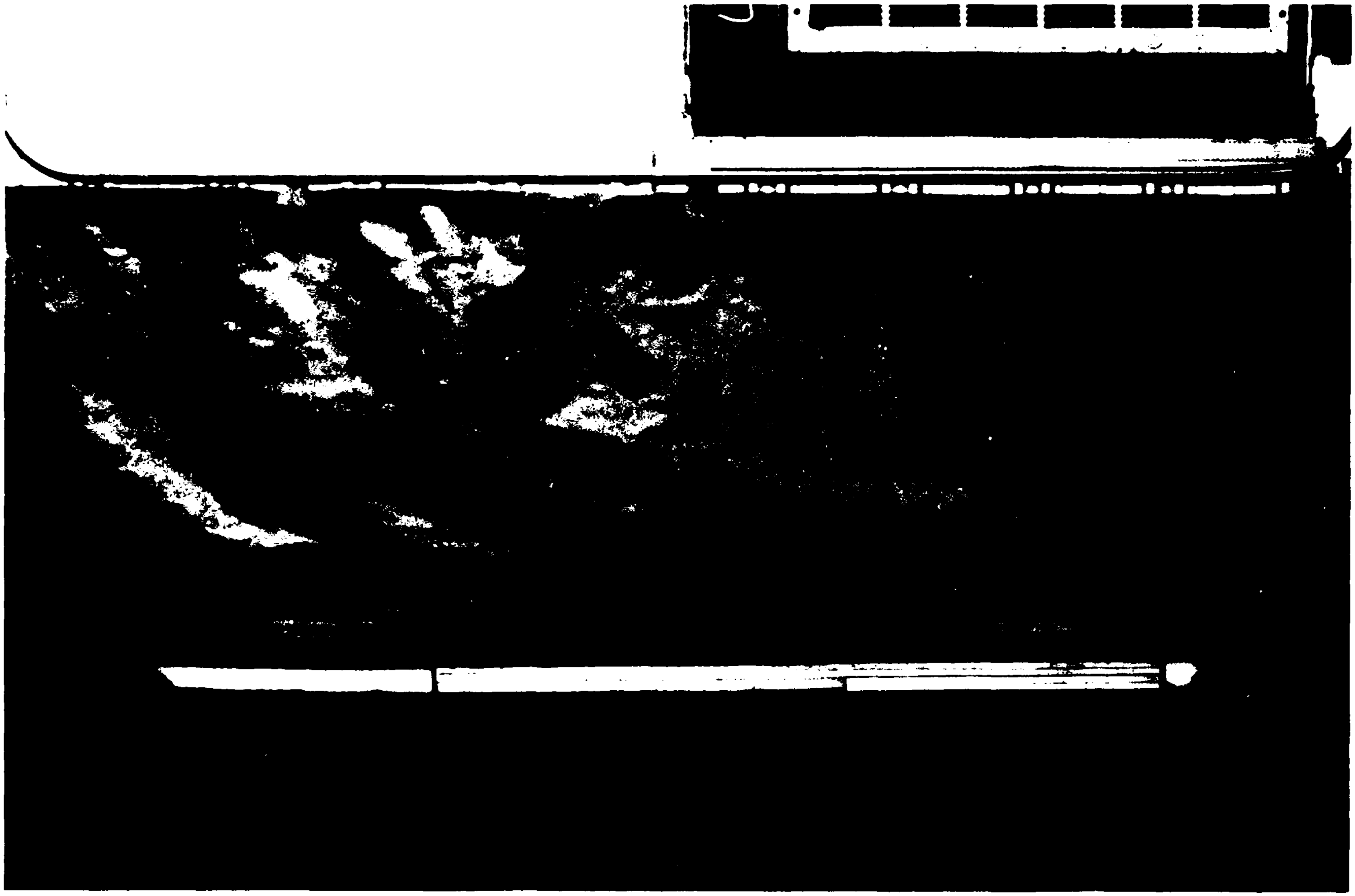

Photo 1. Side view of 89.6-ft SFB

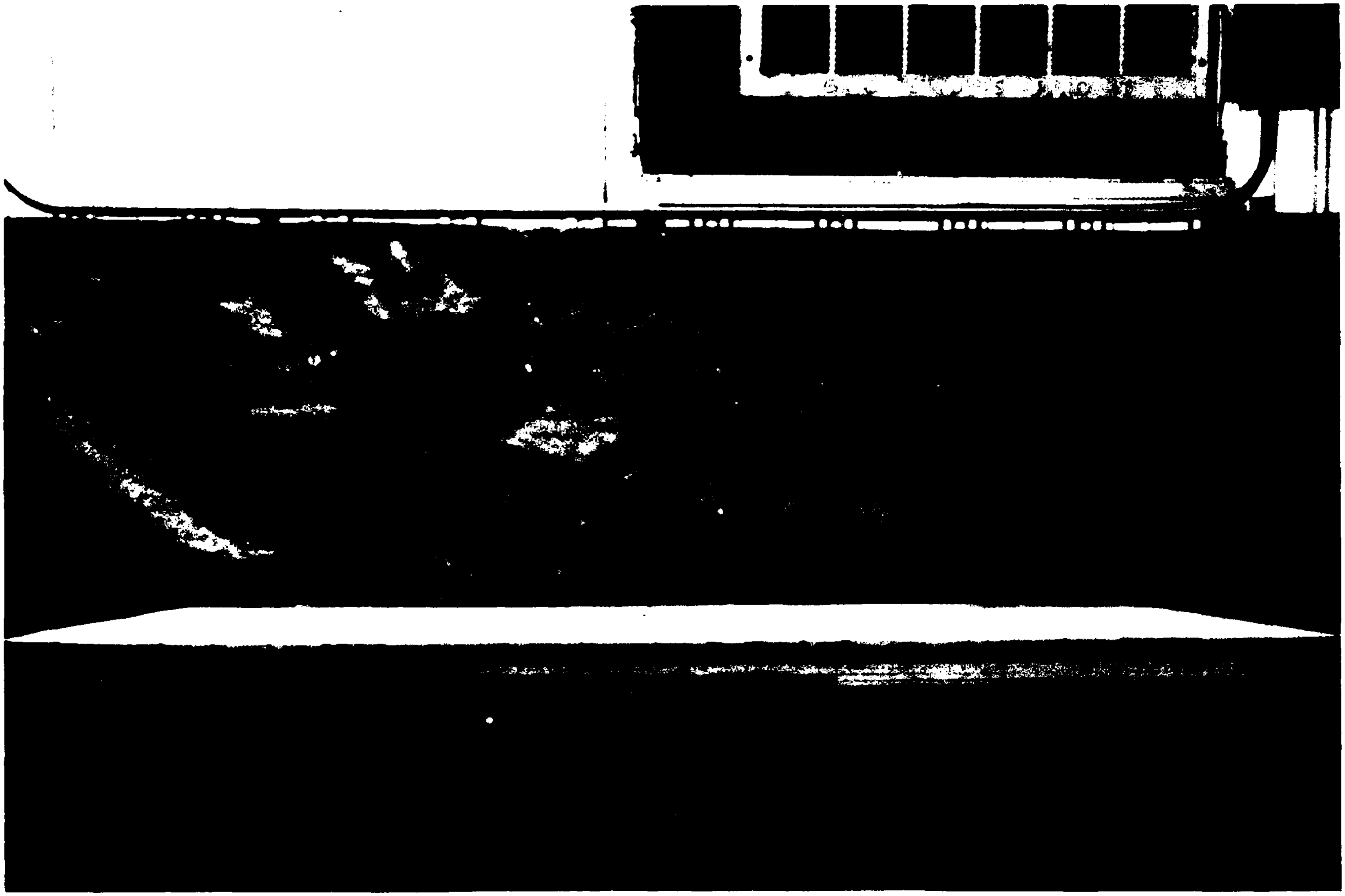

Photo 2. Side view of 118.4-ft SFB

Photo 3. View of model barges with and without the top decks attached (side-connector tests)

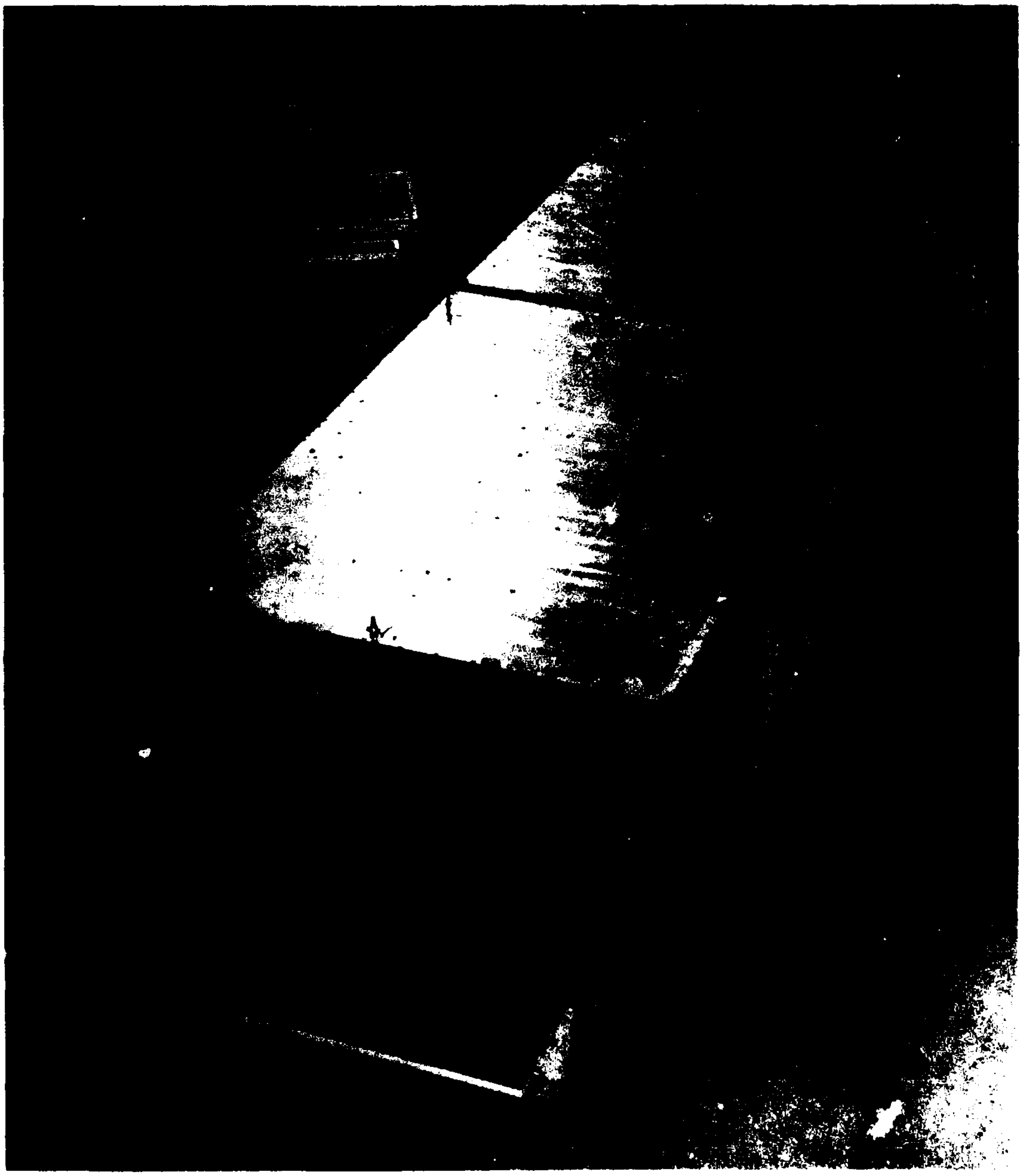

Photo 4. View of model barges with top decks in place (side-connector tests)

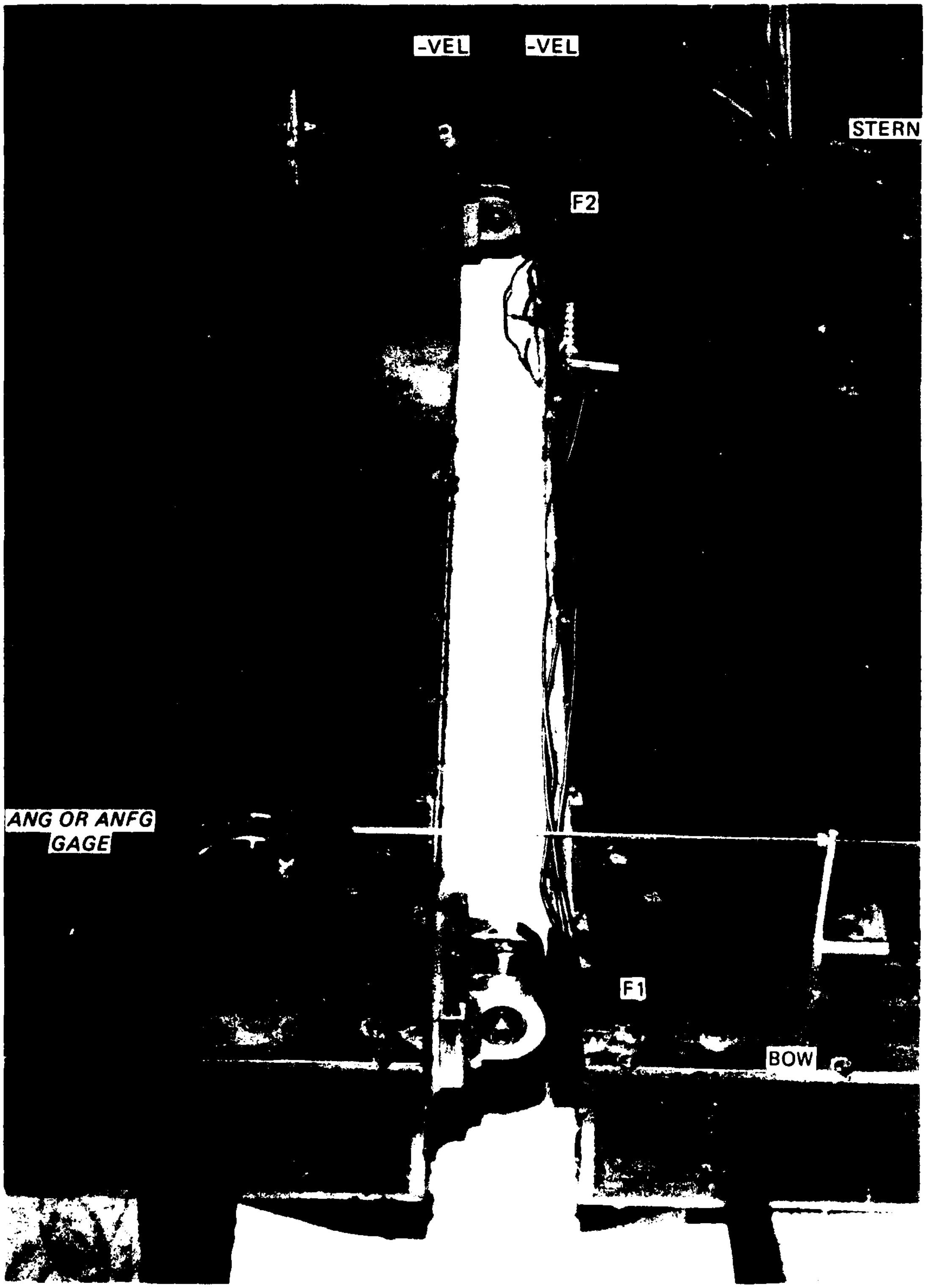

Photo 5. Bow view of model barge connectors and angularity gage (side-connector tests)

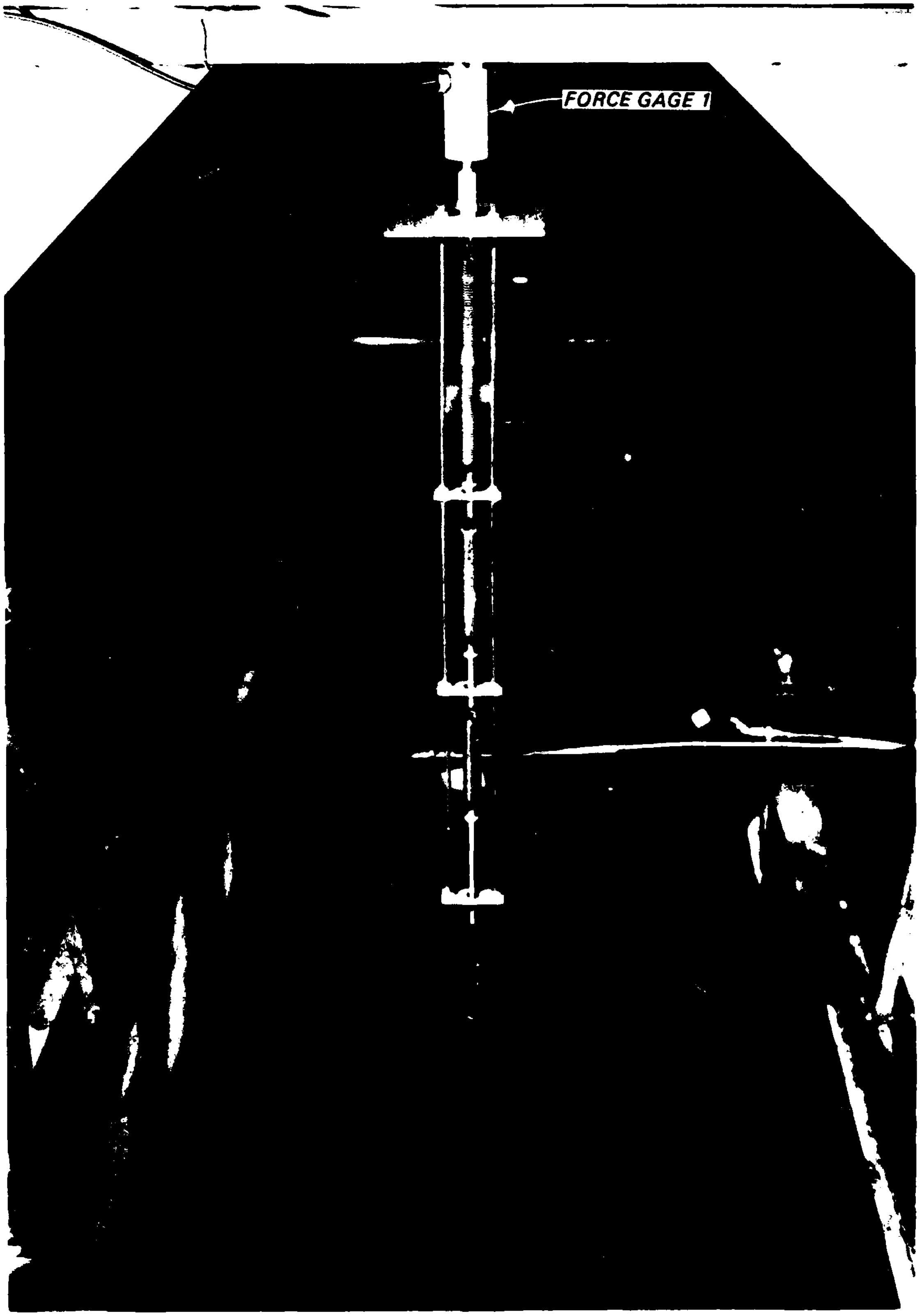

Photo 6. Close-up view of Force Gage 1 and spring mooring system

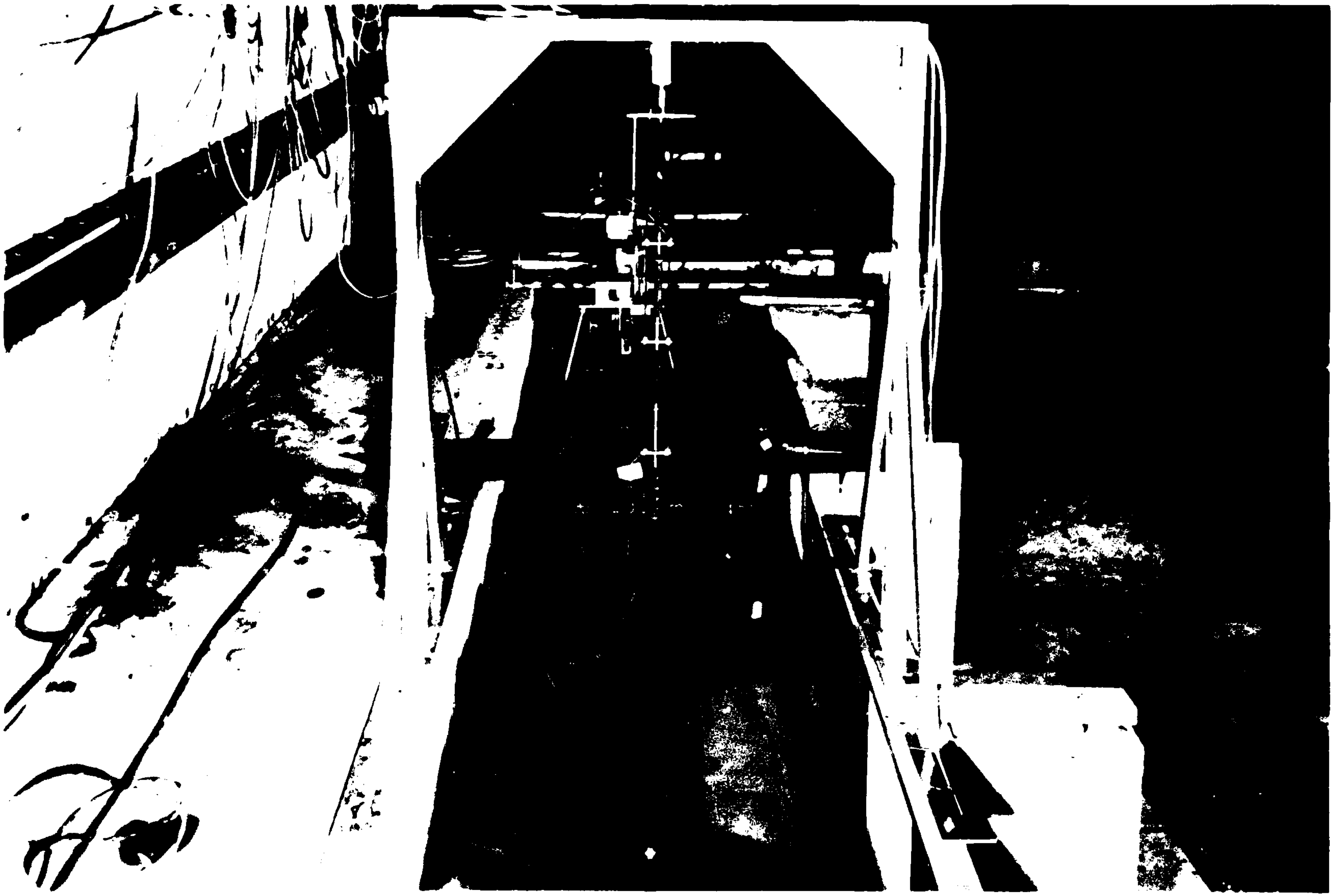

[illegible]. General view of test setup for functional tests

AD-A181 776 SLOPING FLOAT BREAKWATER STUDY OREGON INLET NORTH CAROLINA COASTAL MODEL INVESTIGATION(U) COASTAL ENGINEERING RESEARCH CENTER VICKSBURG MS 2/3

UNCLASSIFIED R D CARVER ET AL. APR 87 CERC-TR-87-5 F/G 13/2 NL

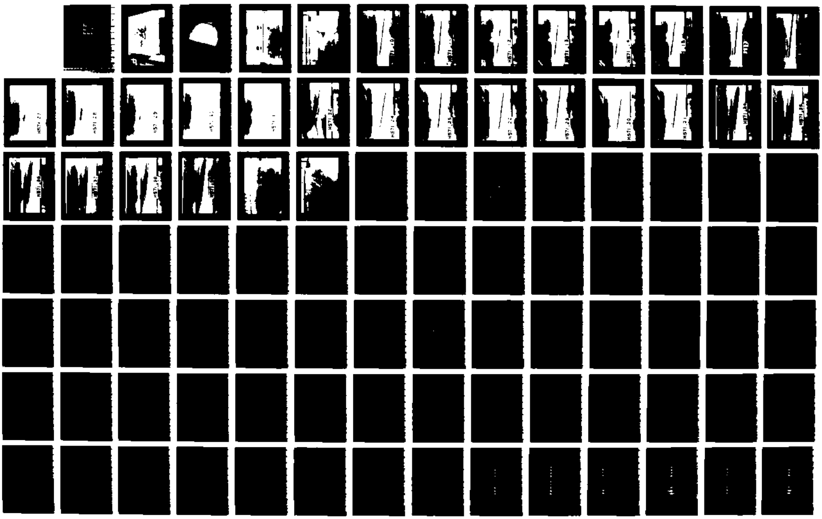

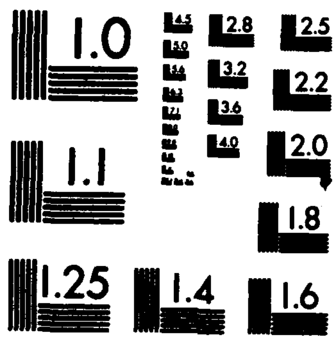

MICROCOPY RESOLUTION TEST CHART
NATIONAL BUREAU OF STANDARDS-1963-A

Photo 8. Close-up view of Force Gage 2

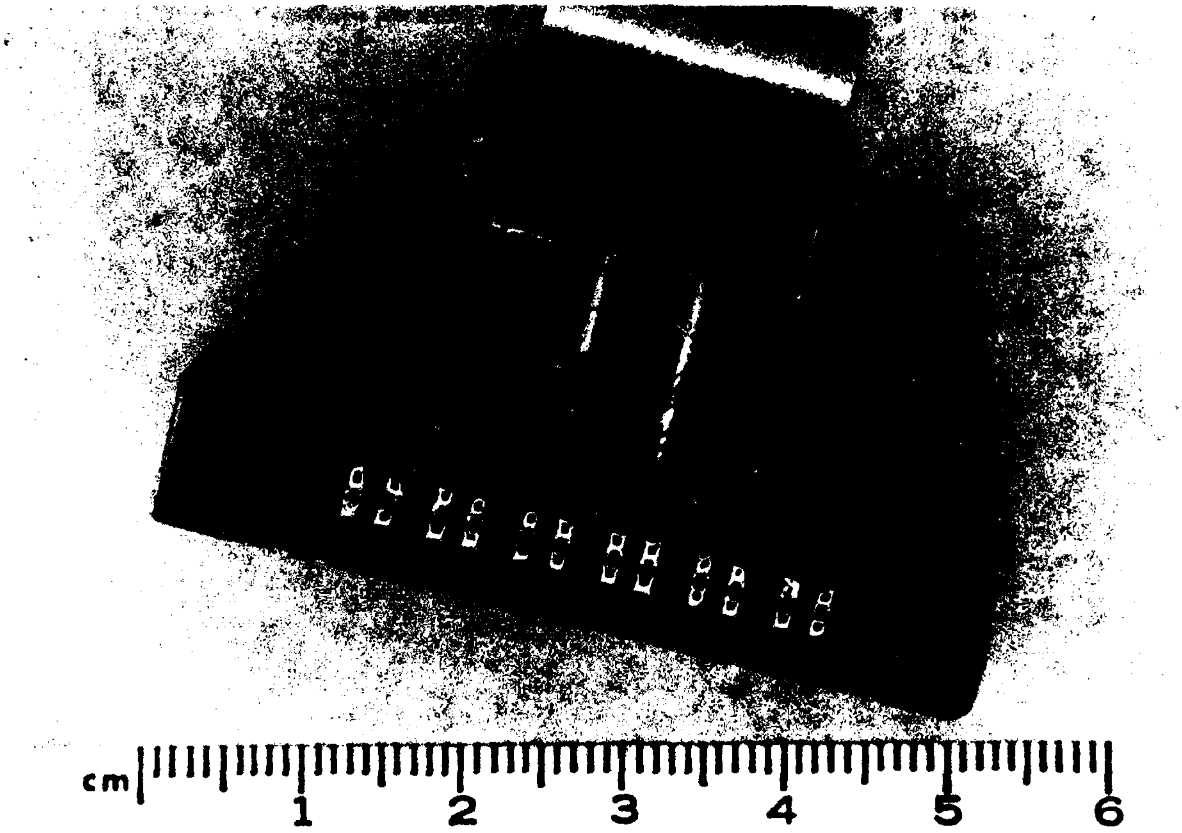

Photo 9. Instrumented half of model barge connector prior to placement of waterproofing sealer (side-connector tests)

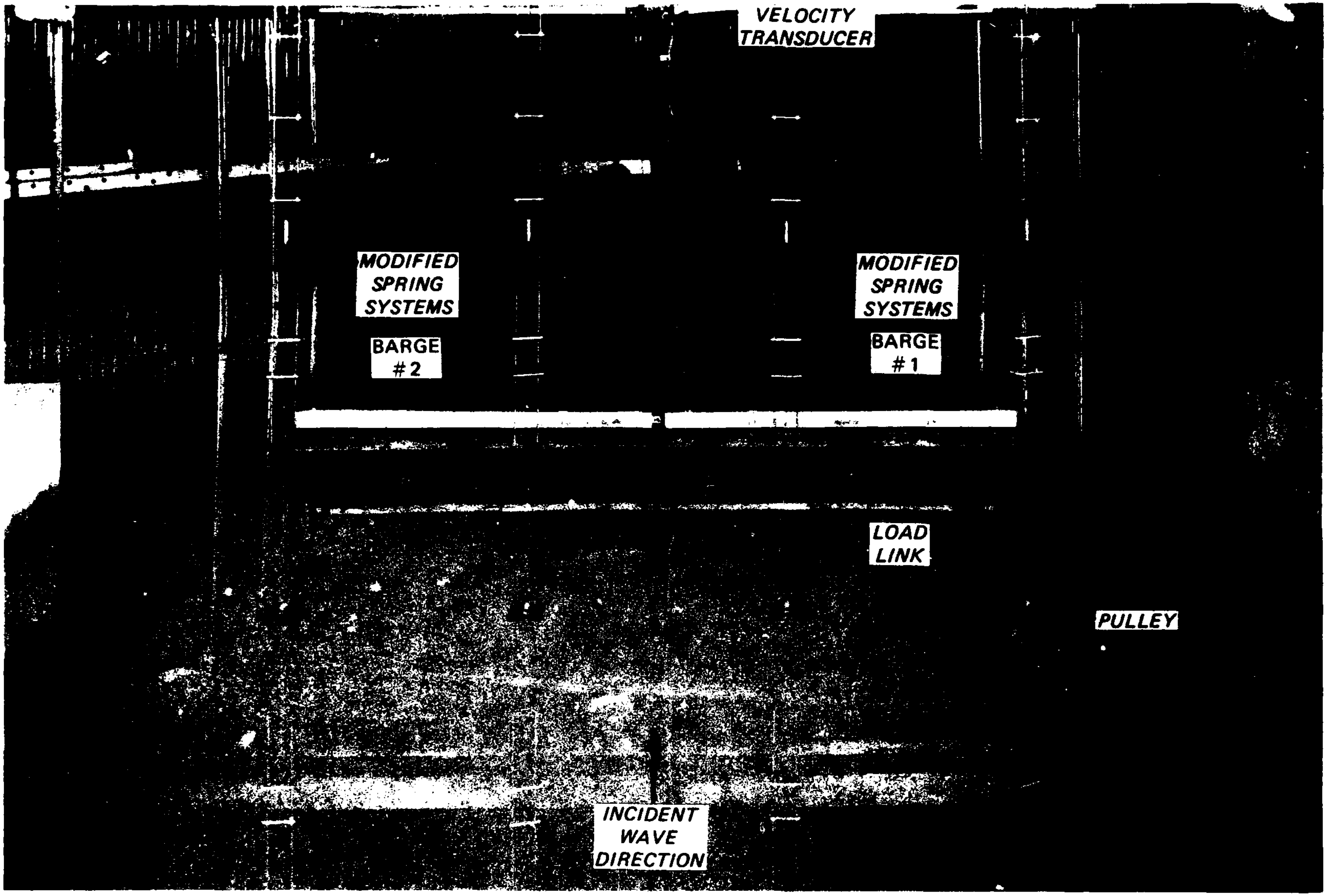

Photo 10. Seaside view of the SFB setup for 90-deg wave attack (side-connector tests)

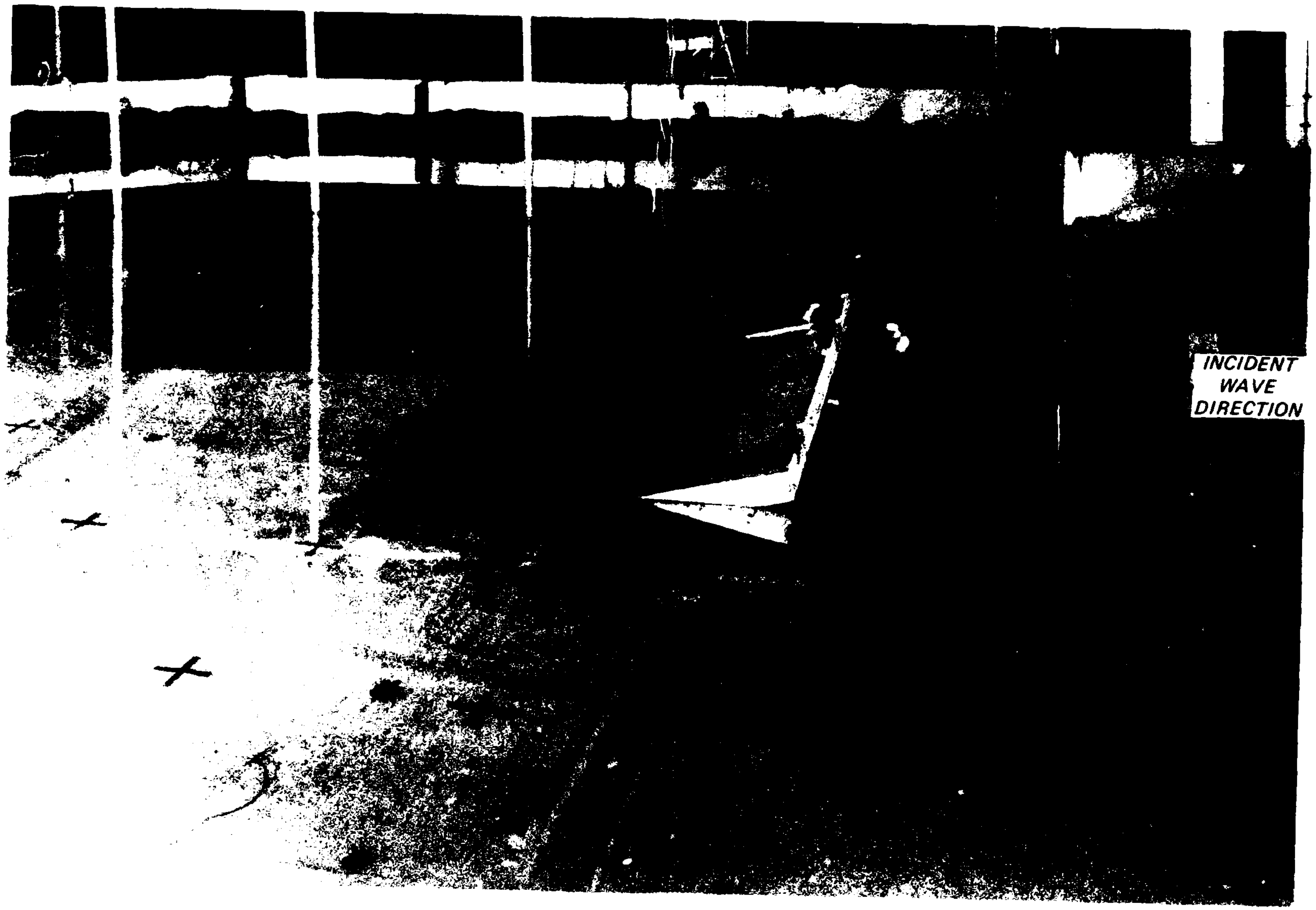

Photo 11. Side view of the SFB setup for 90-deg wave attack (side-connector tests)

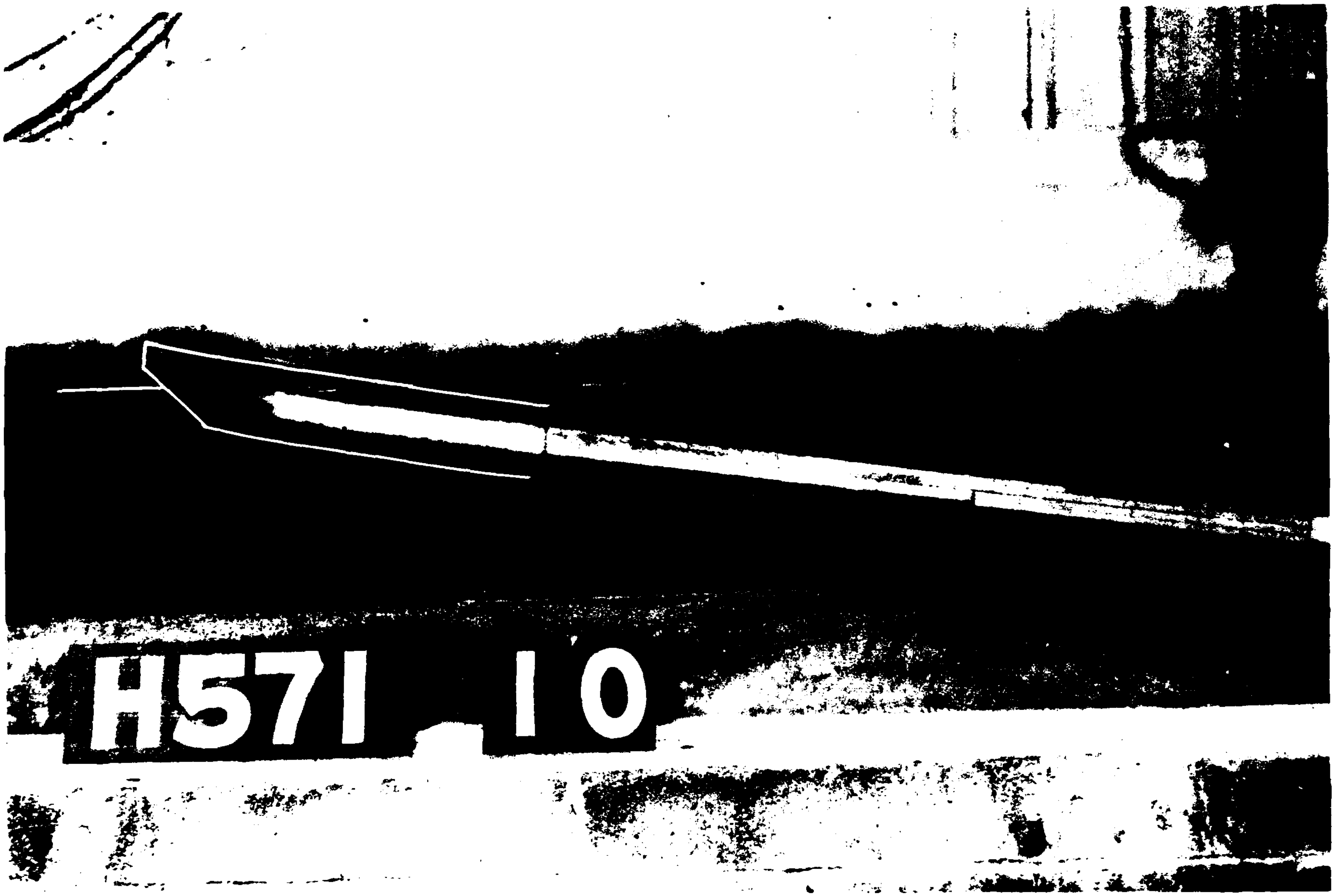

Photo 12. Side view of 89.6-ft SFB under attack of 6-sec, 4-ft monochromatic waves in a water depth of 15 ft

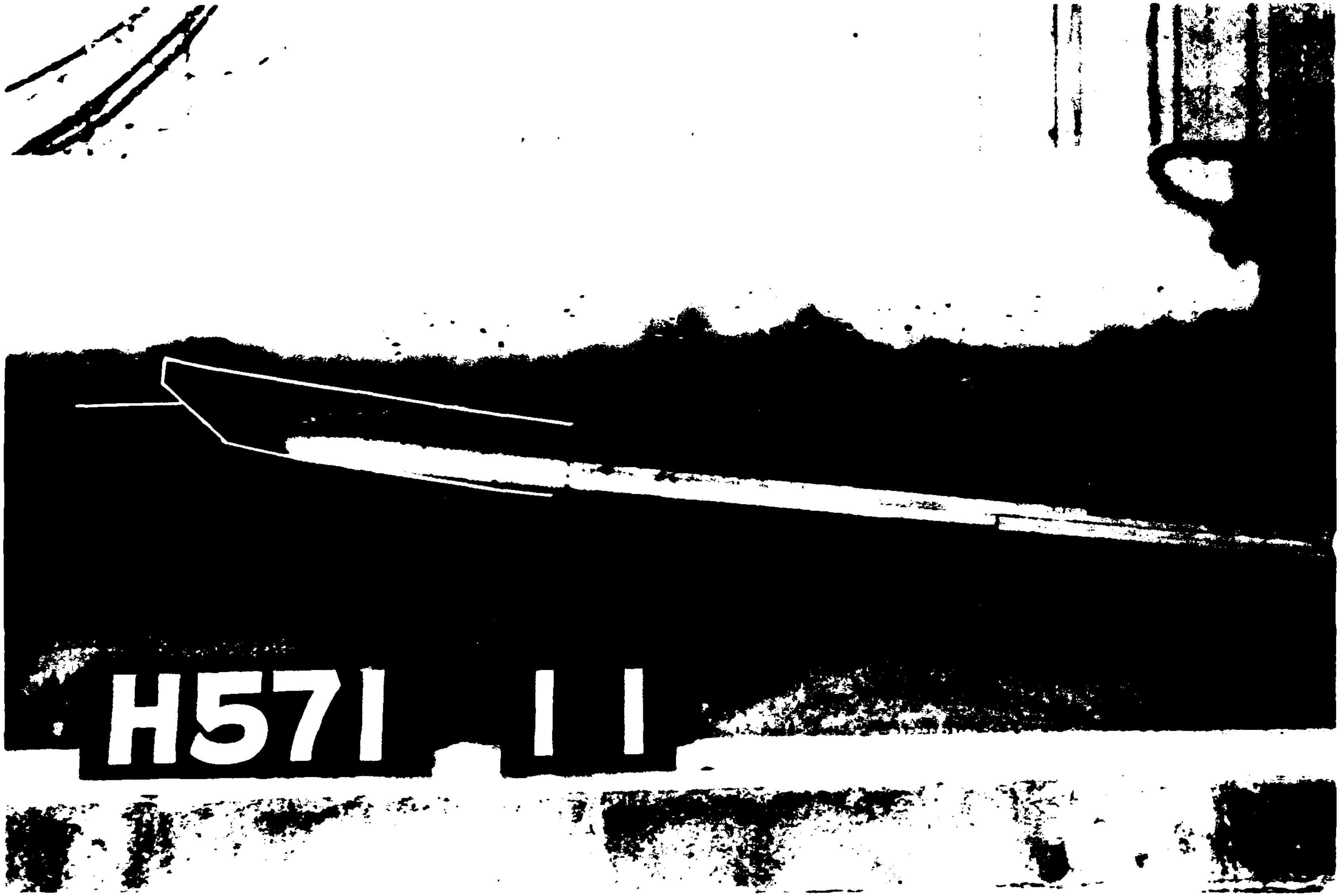

Photo 13. Side view of 89.6-ft SFB under attack of 6-sec, 6-ft monochromatic waves in a water depth of 15 ft

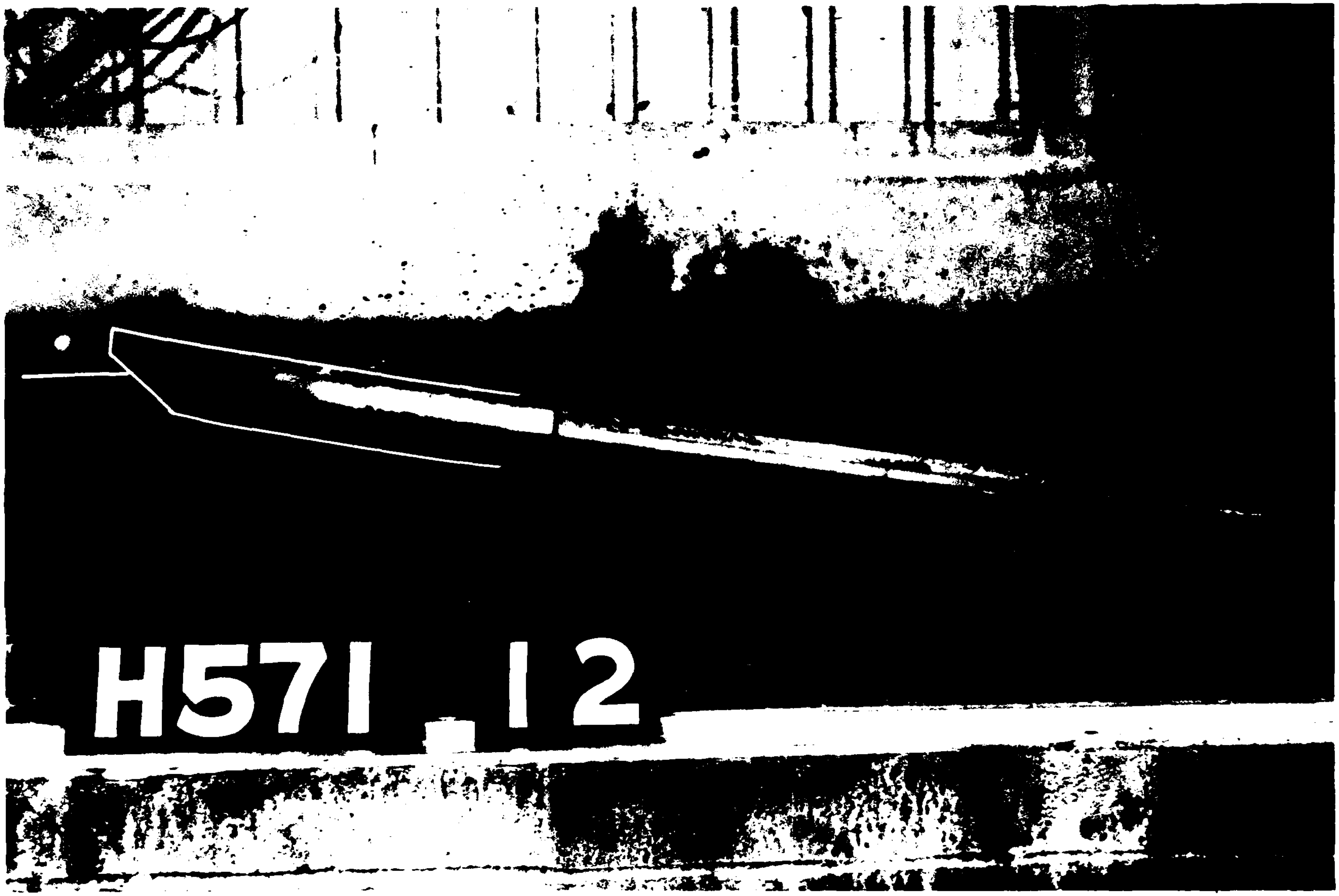

Photo 14. Side view of 89.6-ft SFB under attack of 10-sec, 4-ft monochromatic waves in a water depth of 15 ft

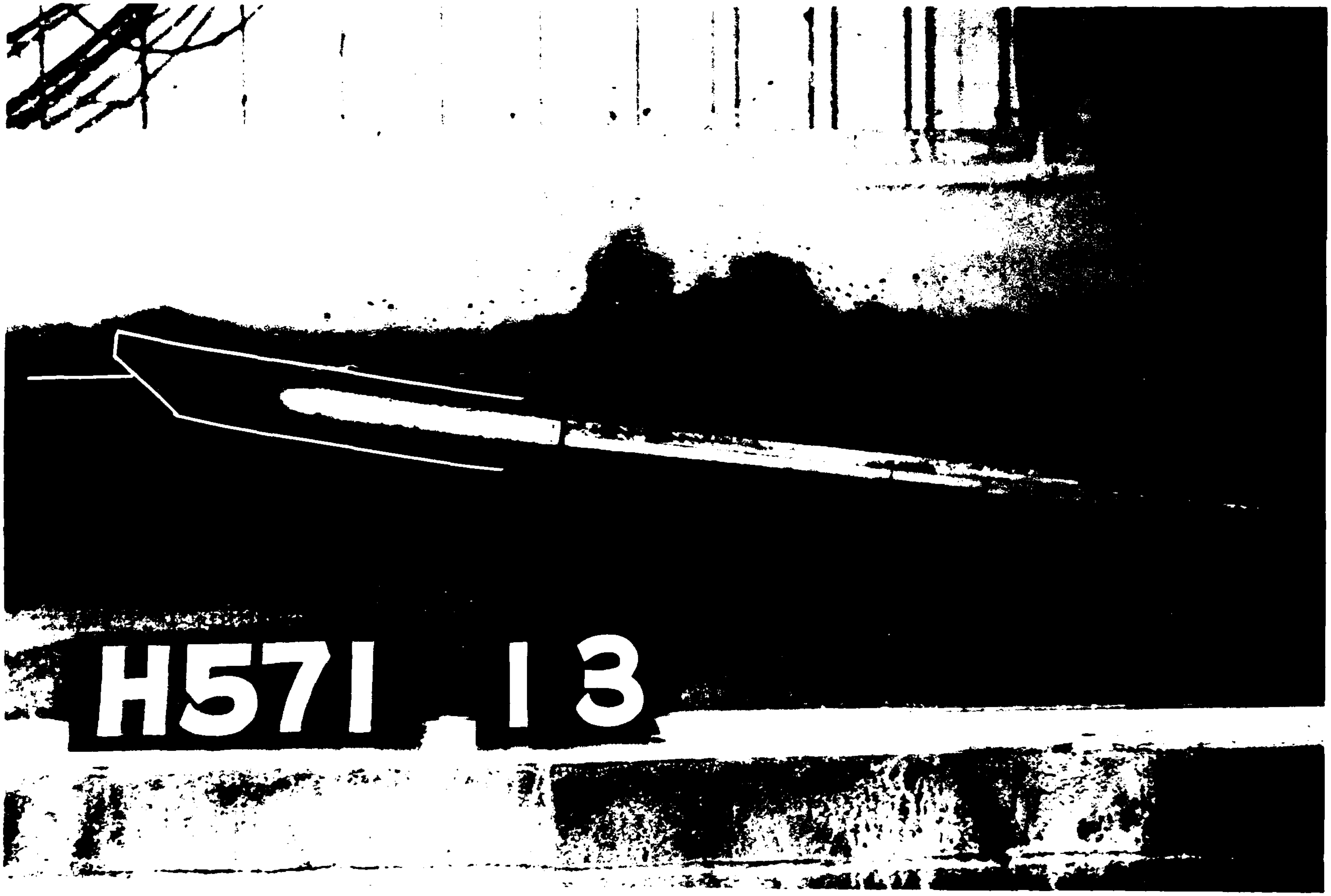

Photo 15. Side view of 89.6-ft SFB under attack of 10-sec, 6-ft monochromatic waves in a water depth of 15 ft

Photo 16. Side view of 89.6-ft SFB under attack of 14-sec, 4-ft monochromatic waves in a water depth of 15 ft

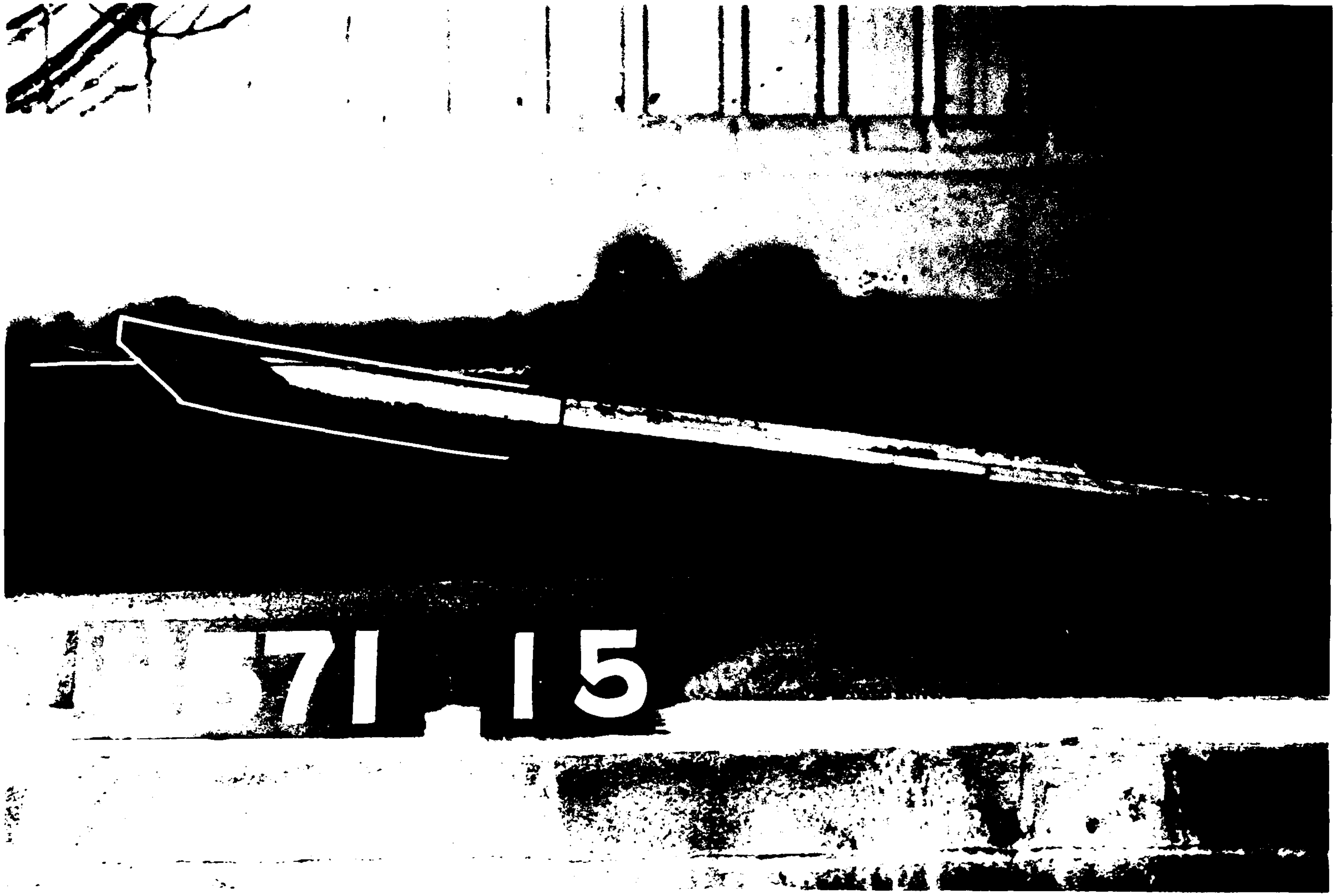

Photo 17. Side view of 89.6-ft SFB under attack of 14-sec, 6-ft monochromatic waves in a water depth of 15 ft

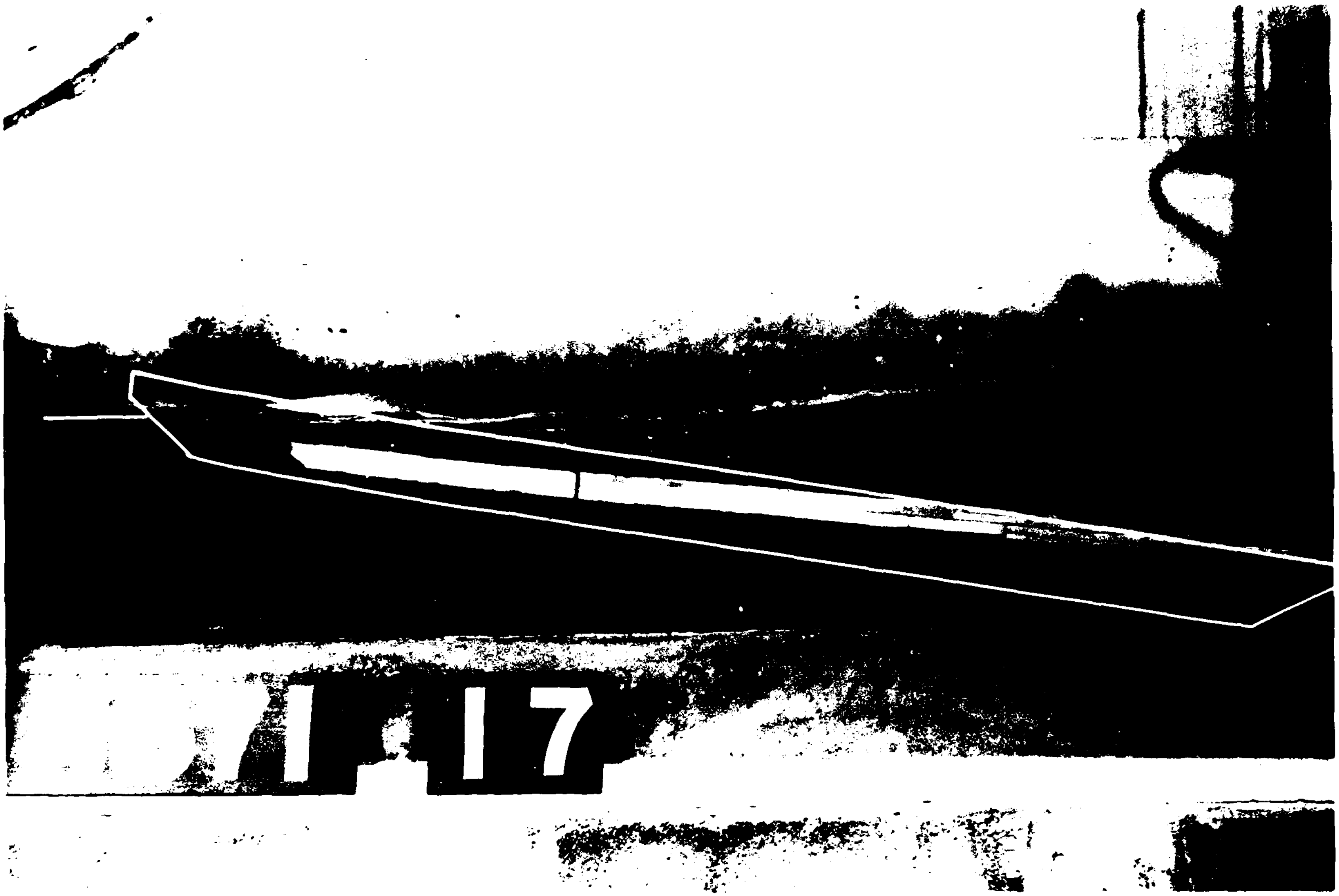

Photo 18. Side view of 89.6-ft SFB under attack of 10-sec, 10-ft monochromatic waves in a water depth of 15 ft

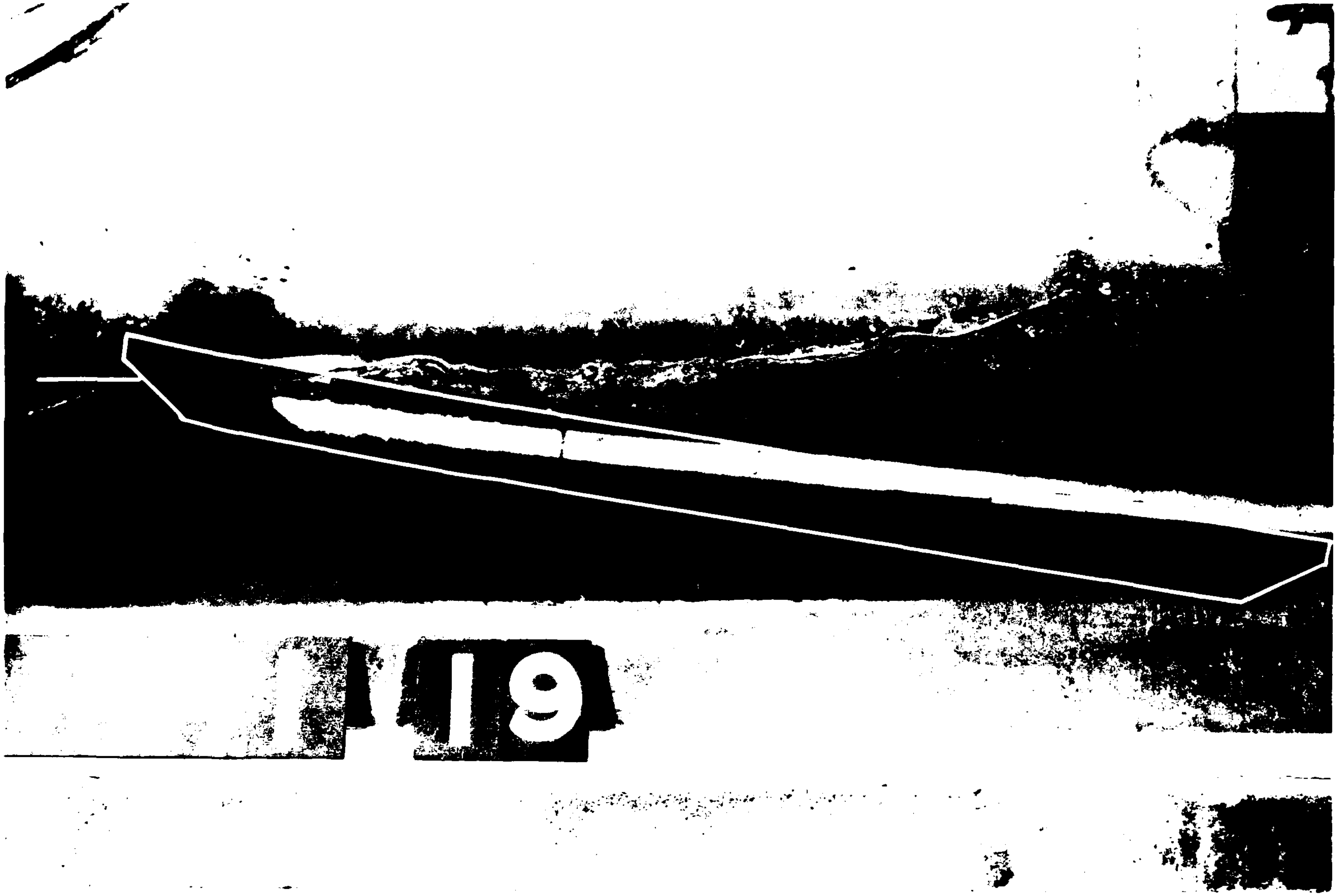

Photo 19. Side view of 89.6-ft SFB under attack of 10-sec, 12-ft monochromatic waves in a water depth of 15 ft

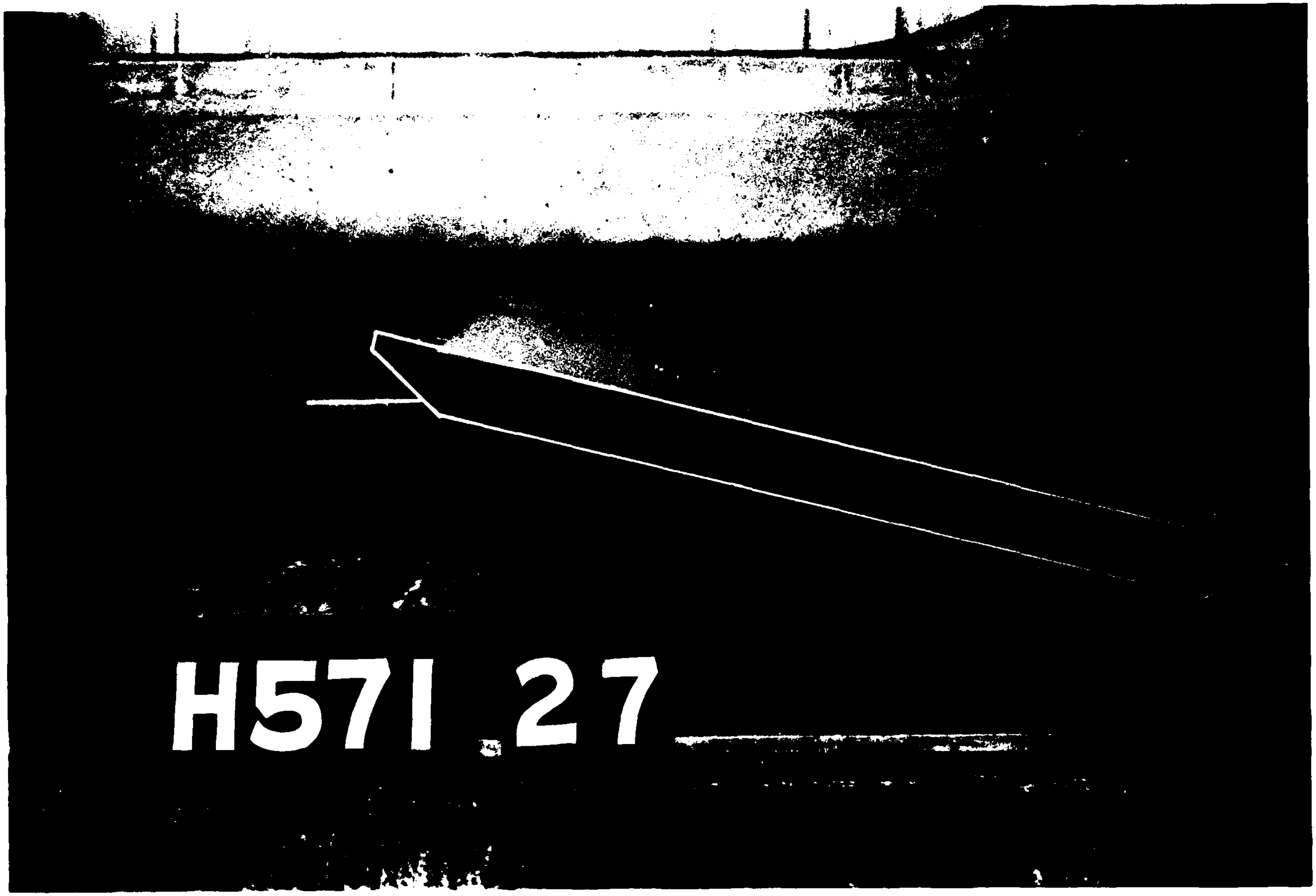

Photo 20. Side view of 72.3-ft SFB under attack of 6-sec, 4-ft spectral waves in a water depth of 15 ft

Photo 21. Side view of 72.3-ft SFB under attack of 6-sec, 6-ft spectral waves in a water depth of 15 ft

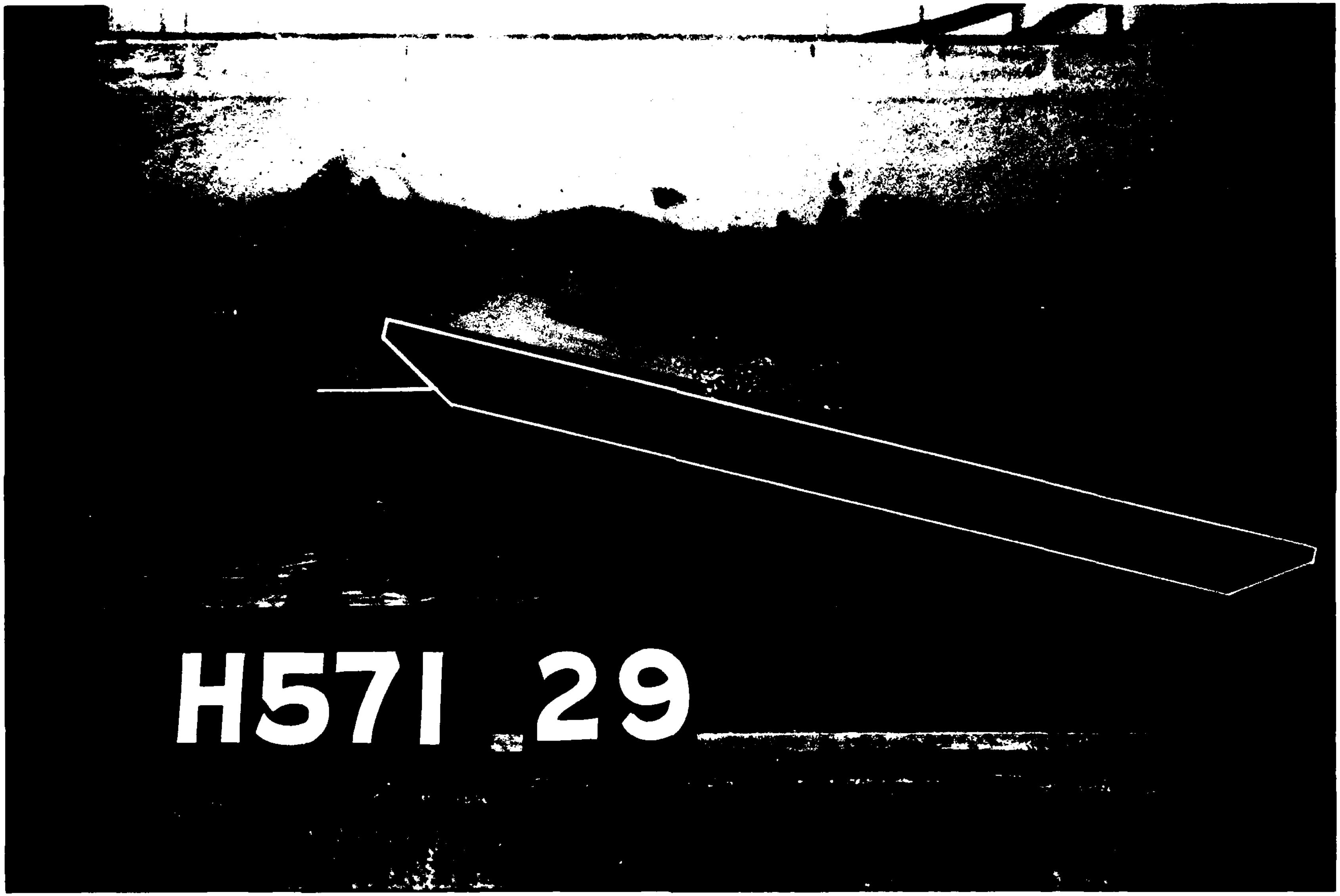

Photo 22. Side view of 72.3-ft SFB under attack of 10-sec, 4-ft spectral waves in a water depth of 15 ft

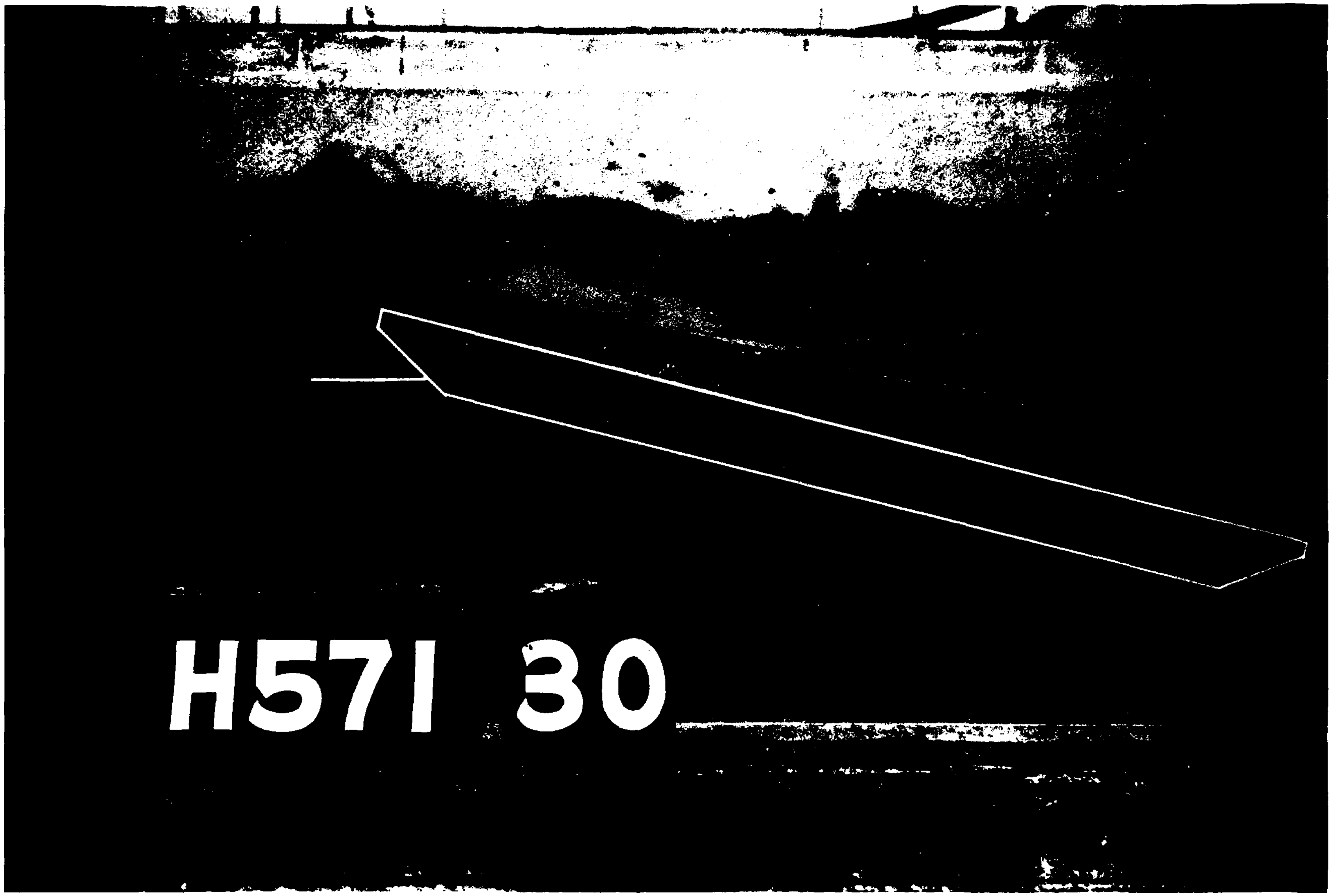

Photo 23. Side view of 72.3-ft SFB under attack of 10-sec, 8-ft spectral waves in a water depth of 15 ft

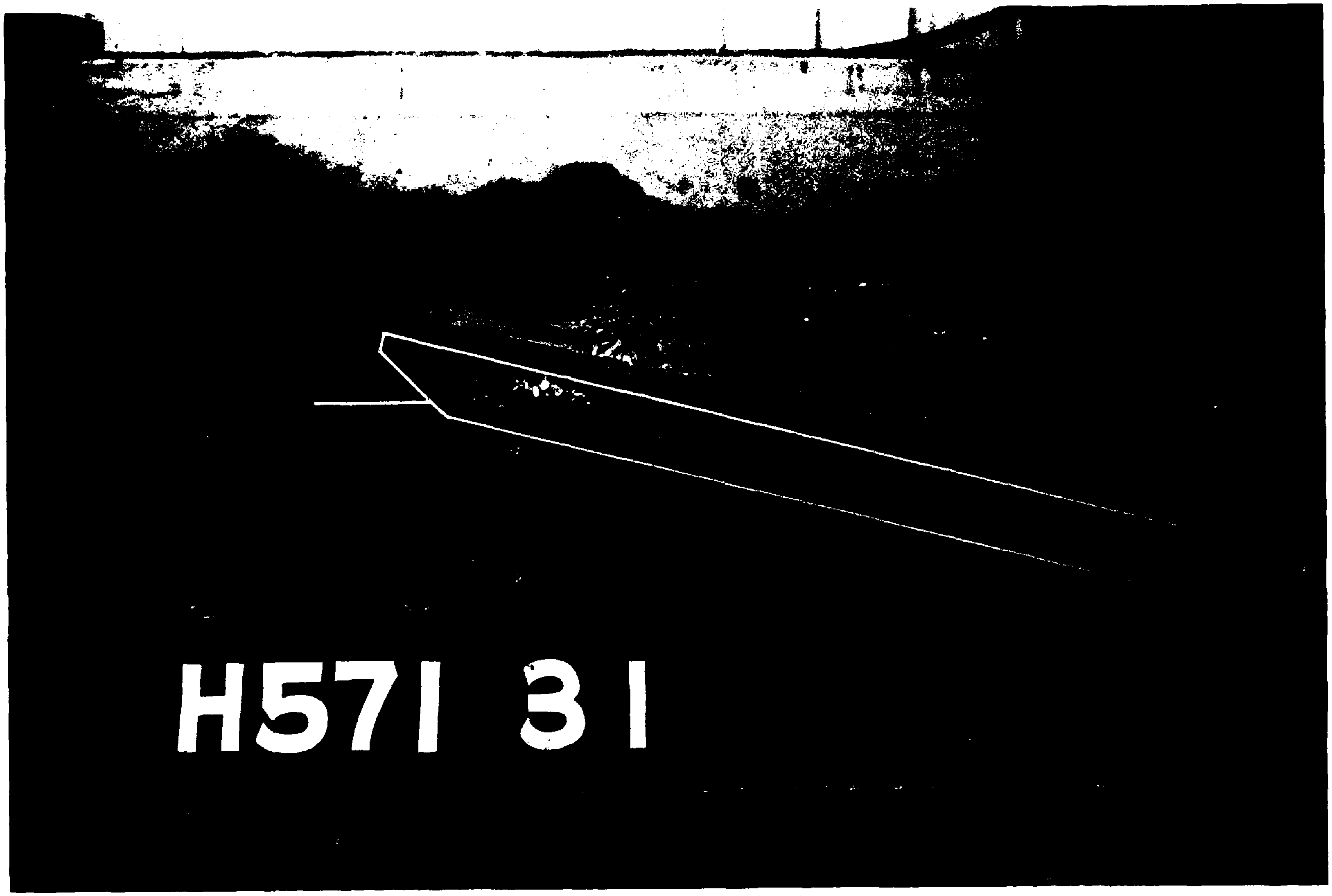

Photo 24. Side view of 72.3-ft SFB under attack of 14-sec, 4-ft spectral waves in a water depth of 15 ft

Photo 25. Side view of 72.3-ft SFB under attack of 14-sec, 8-ft spectral waves in a water depth of 15 ft

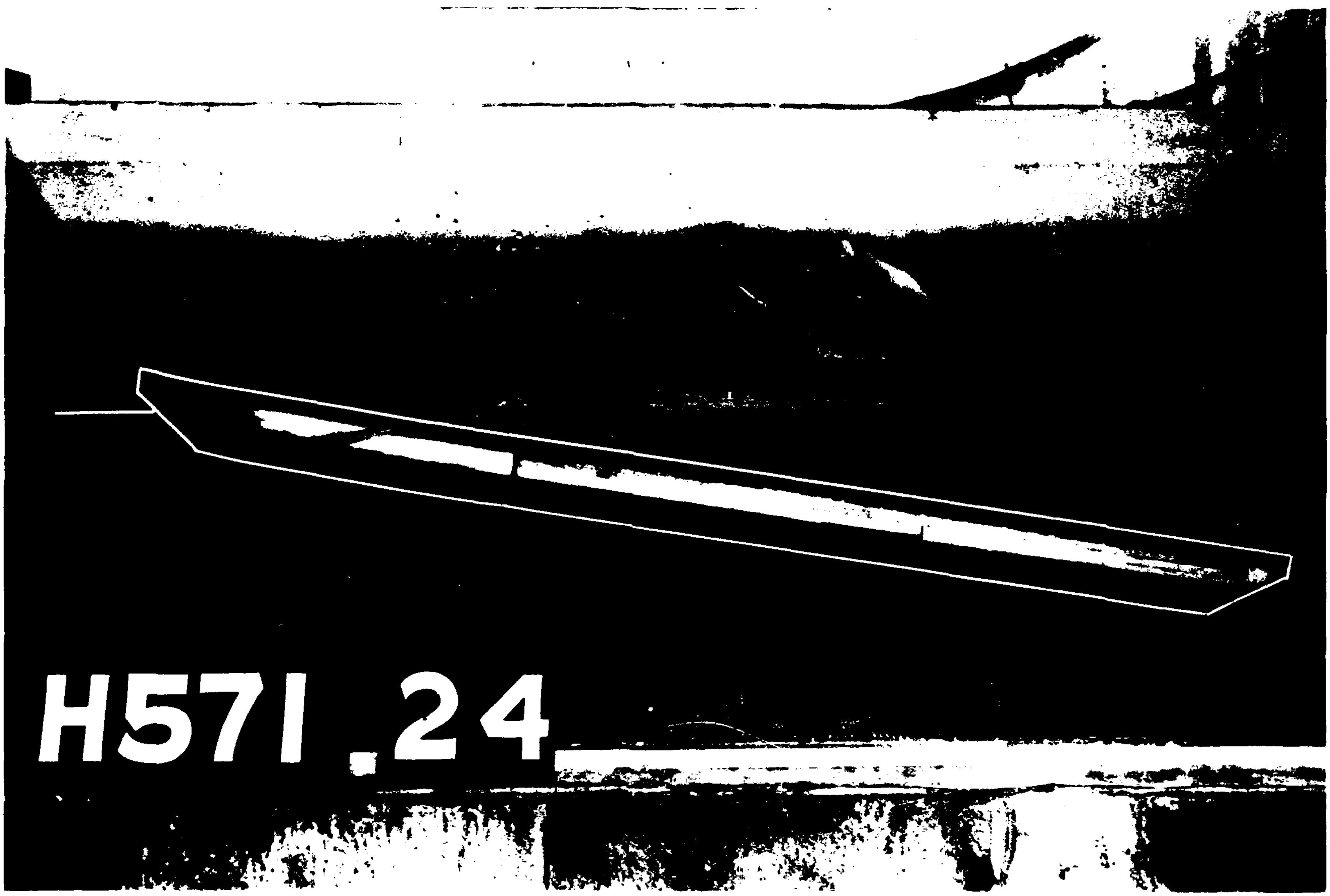

Photo 26. Side view of 89.6-ft SFB under attack of 6-sec, 4-ft spectral waves in a *water depth of 15 ft*

Photo 27. Side view of 89.6-ft SFB under attack of 6-sec, 6-ft spectral waves in a water depth of 15 ft

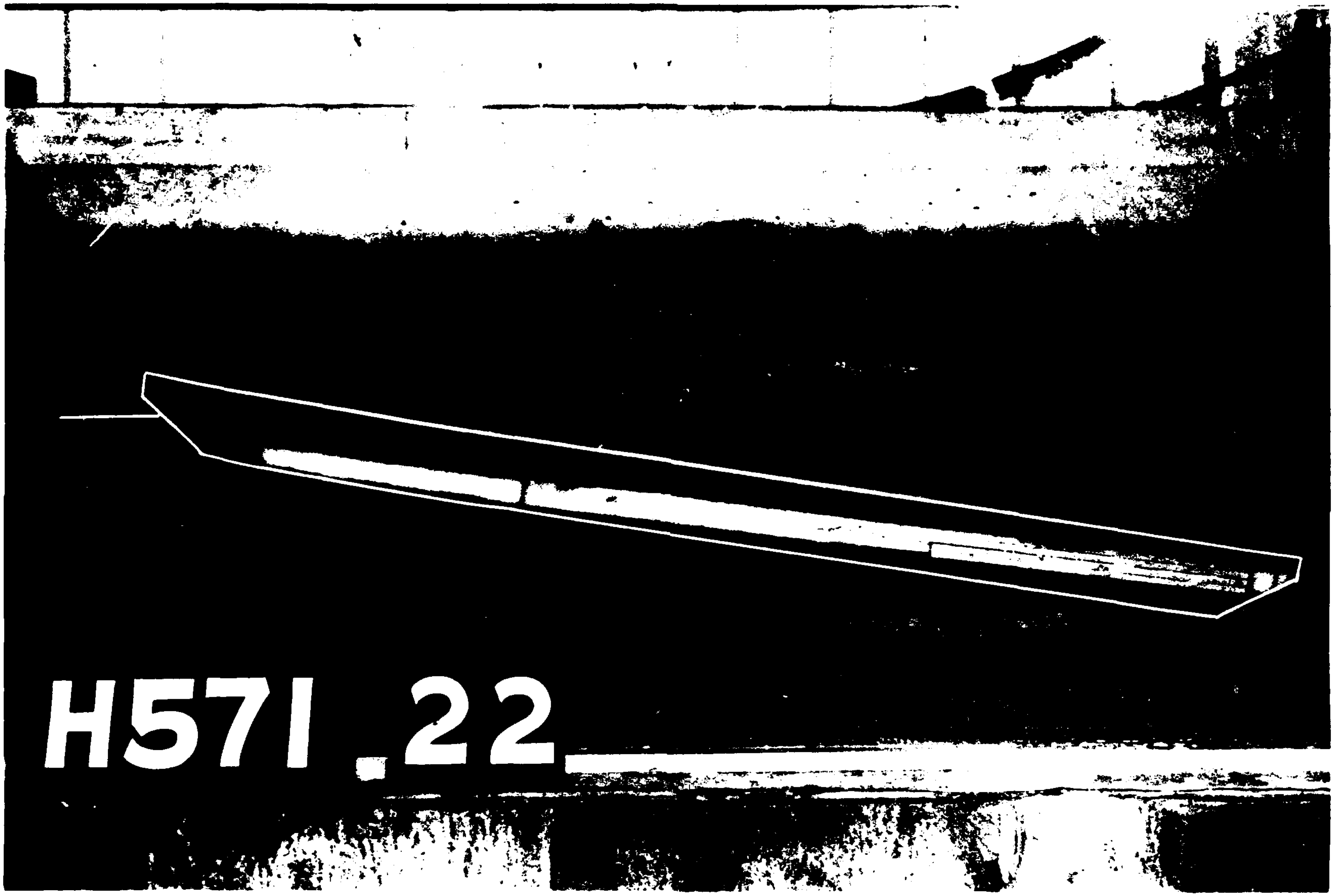

Photo 28. Side view of 89.6-ft SFB under attack of 10-sec, 4-ft spectral waves in a water depth of 15 ft

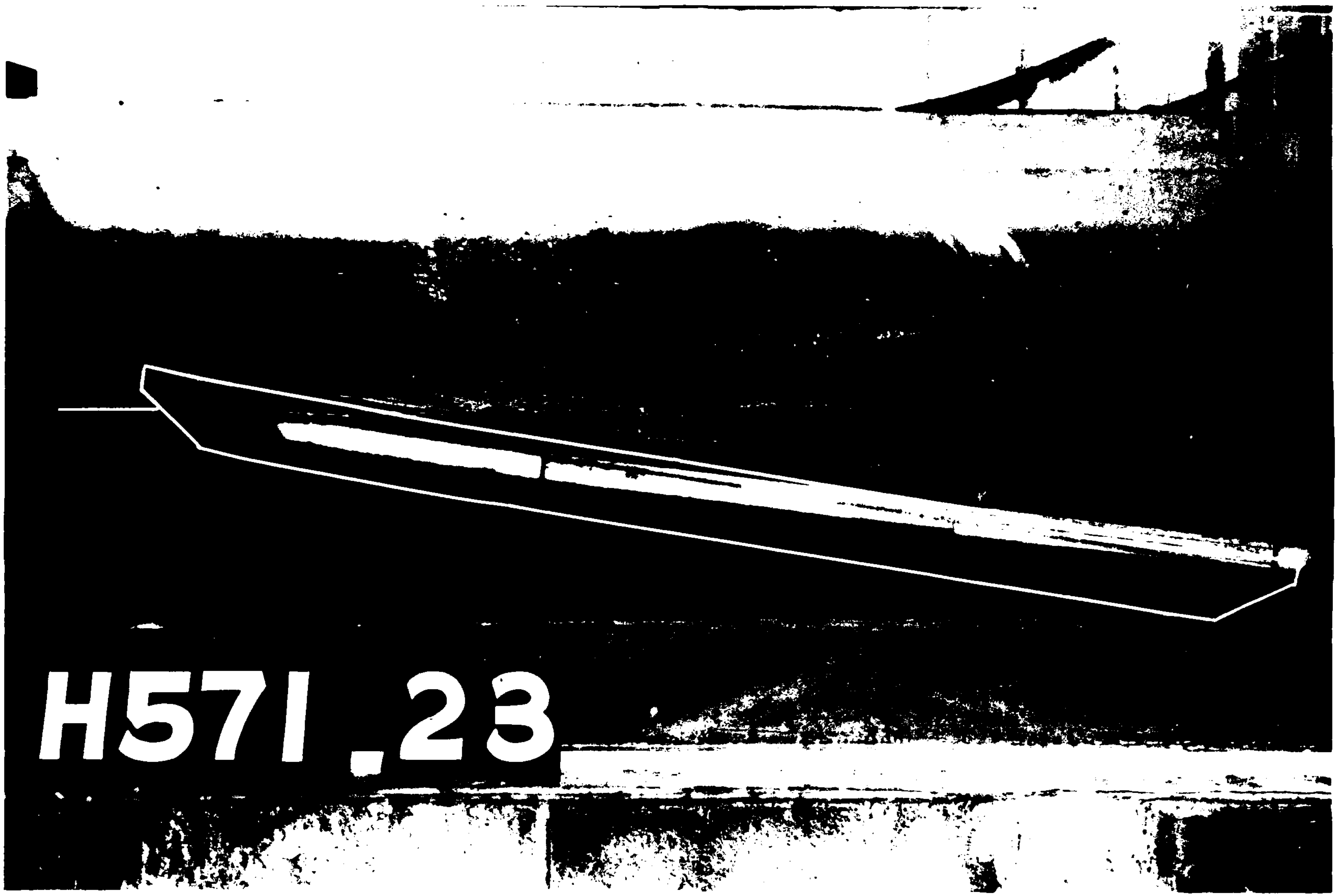

Photo 29. Side view of 89.6-ft SFB under attack of 10-sec, 8-ft spectral waves in a water depth of 15 ft

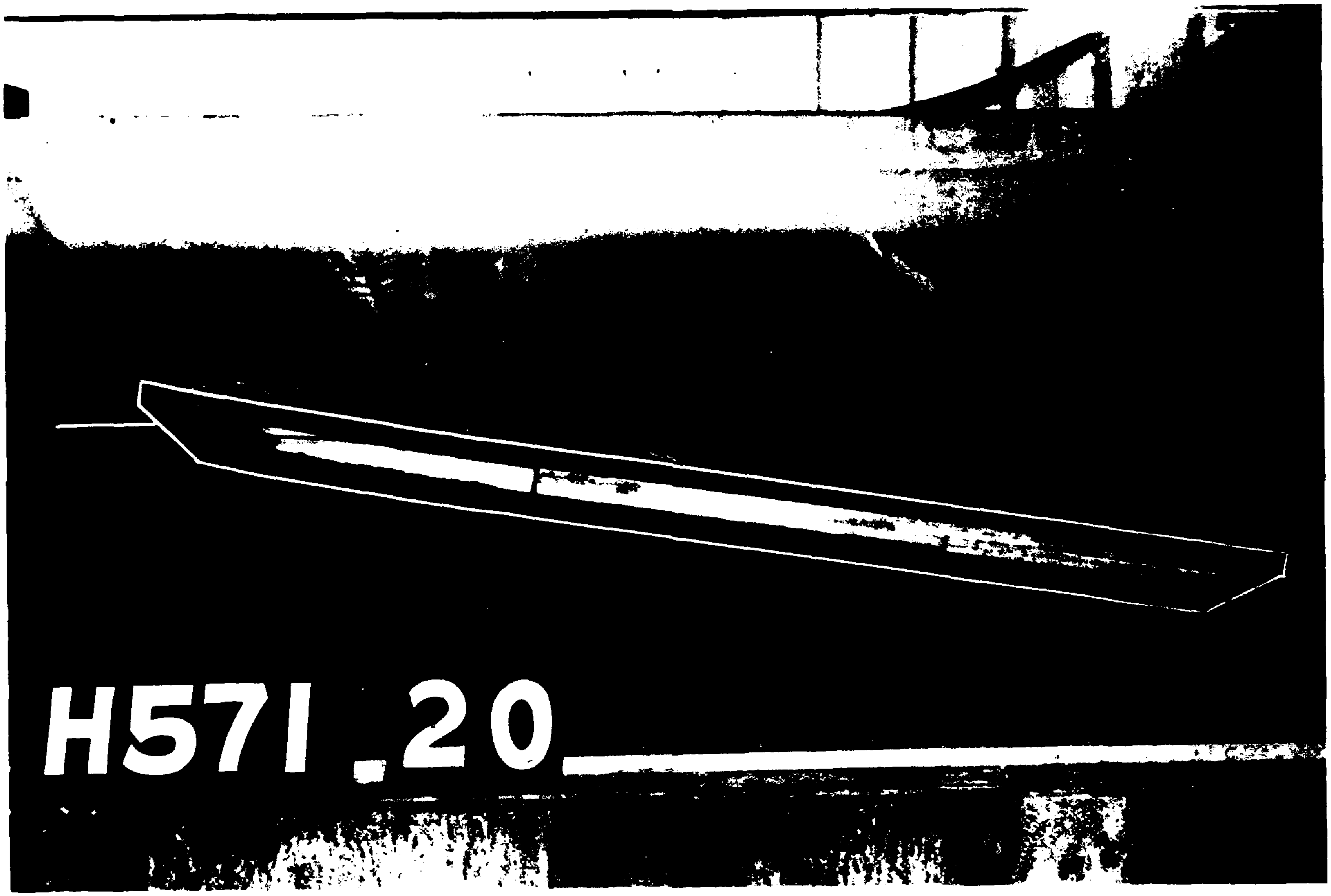

Photo 30. Side view of 89.6-ft SFB under attack of 14-sec, 4-ft spectral waves in a water depth of 15 ft

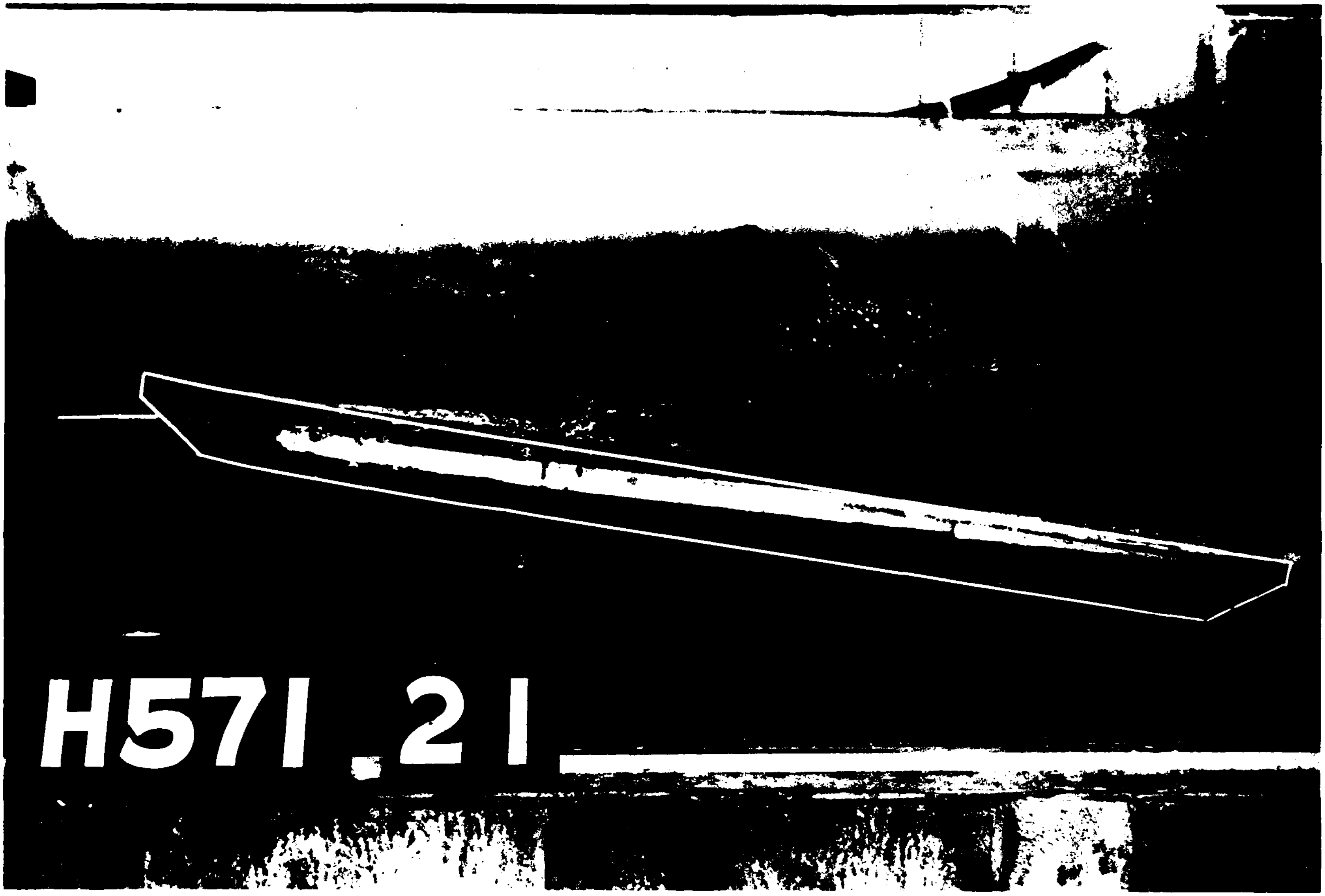

Photo 31. Side view of 89.6-ft SFB under attack of 14-sec, 8-ft spectral waves in a water depth of 15 ft

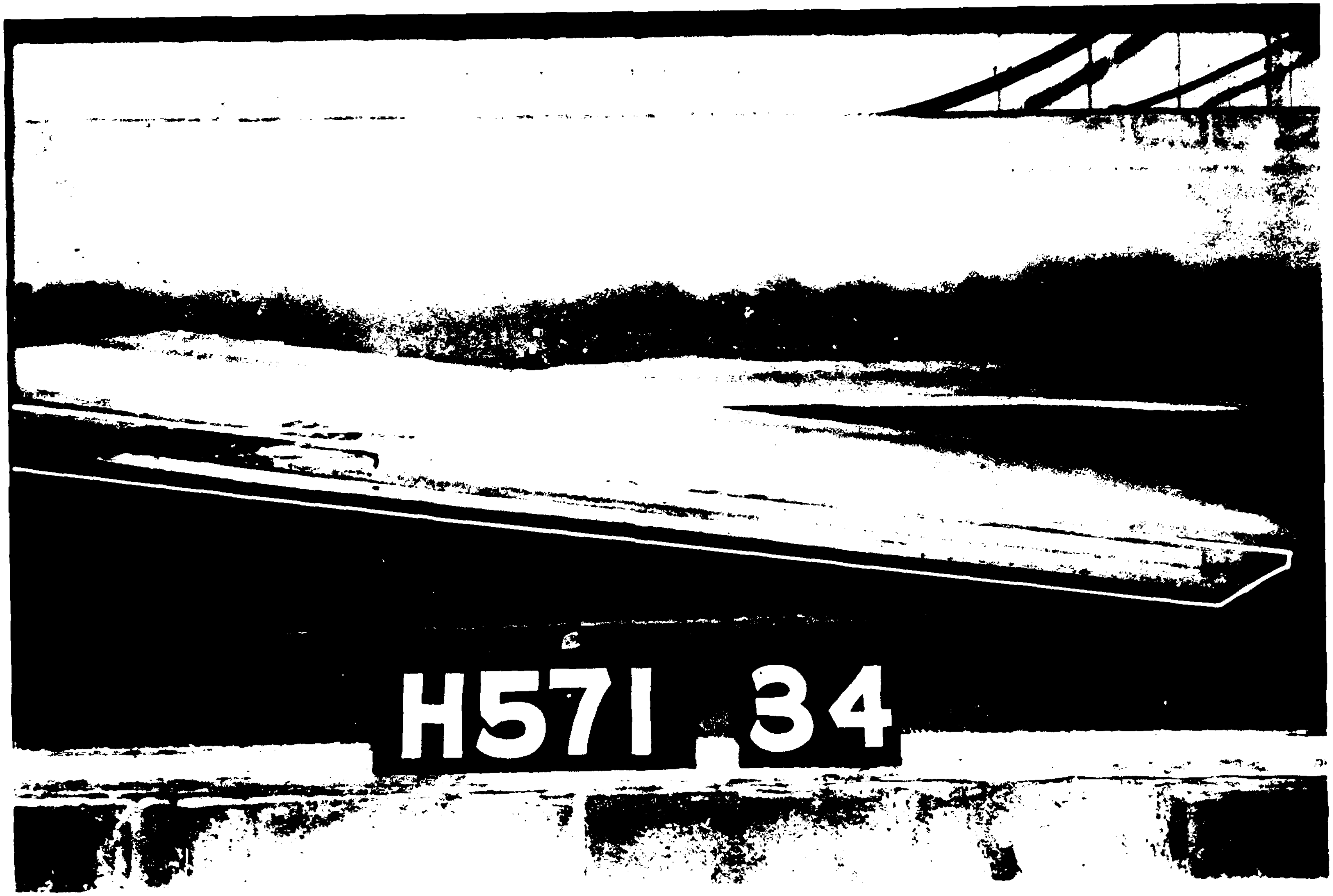

Photo 32. Side view of 118.4-ft SFB under attack of 6-sec, 4-ft spectral waves in a water depth of 15 ft

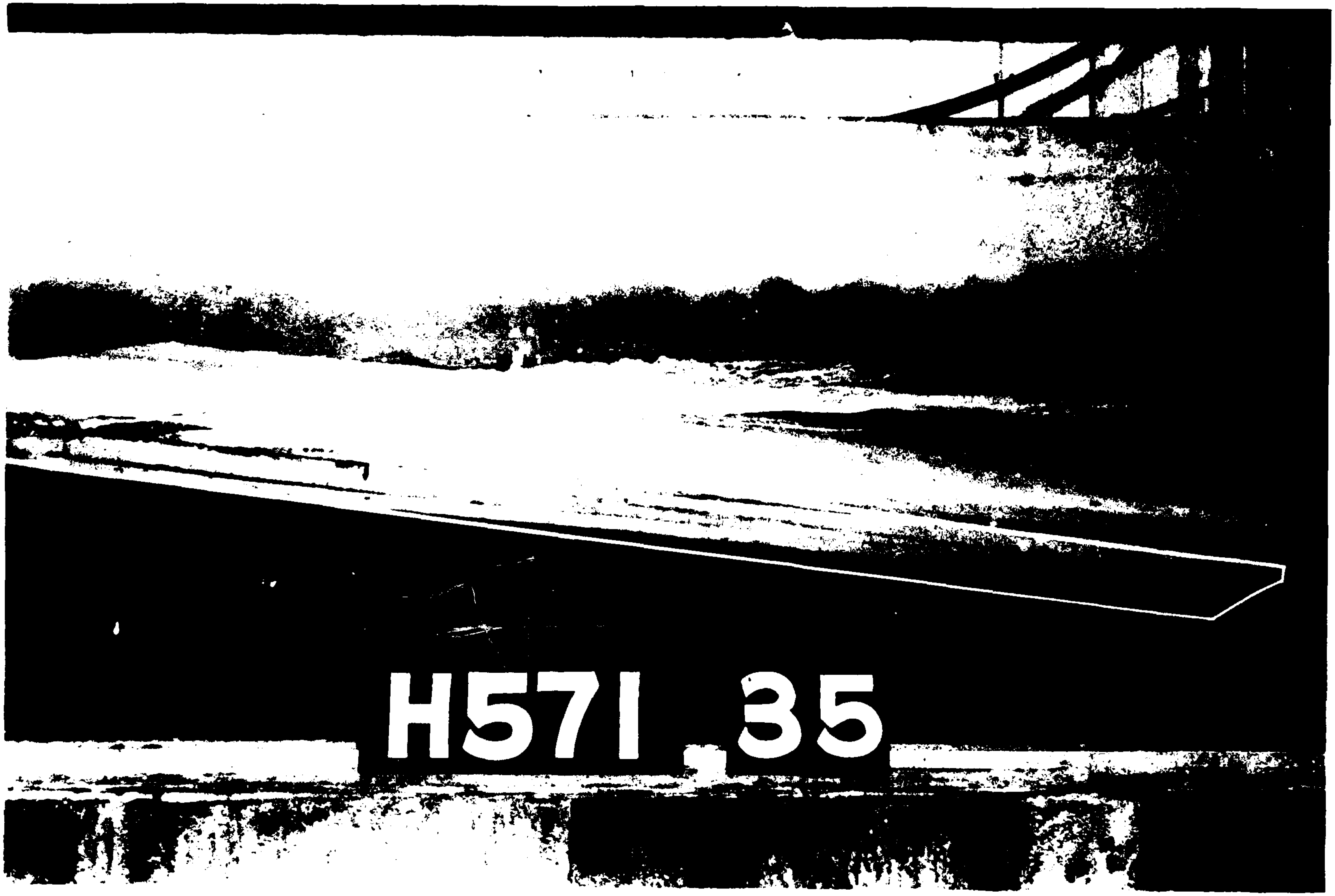

Photo 33. Side view of 118.4-ft SFB under attack of 6-sec, 6-ft spectral waves in a water depth of 15 ft

Photo 34. Side view of 118.4-ft SFB under attack of 10-sec, 4-ft spectral waves in a water depth of 15 ft

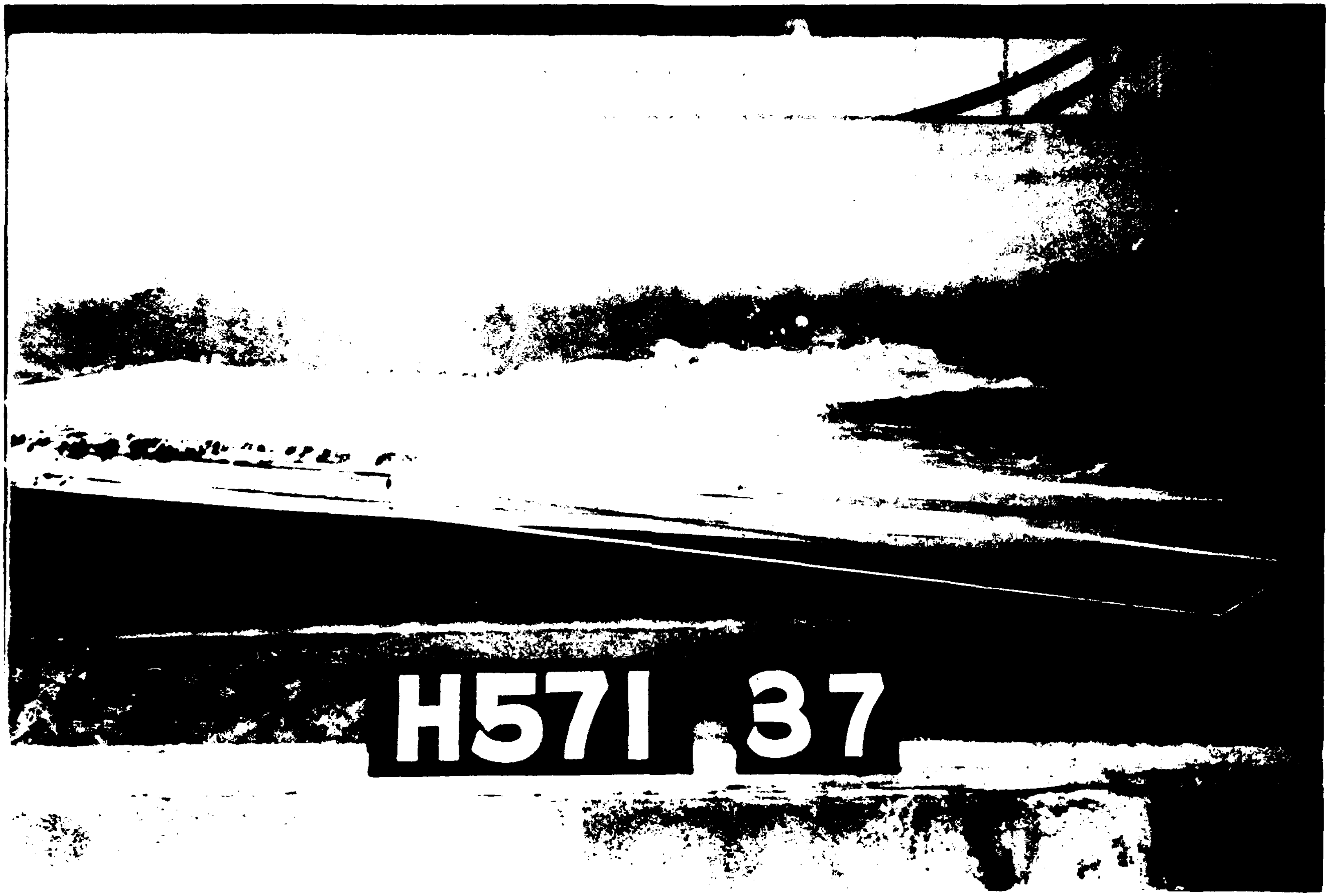

Photo 35. Side view of 118.4-ft SFB under attack of 10-sec, 8-ft spectral waves in a water depth of 15 ft

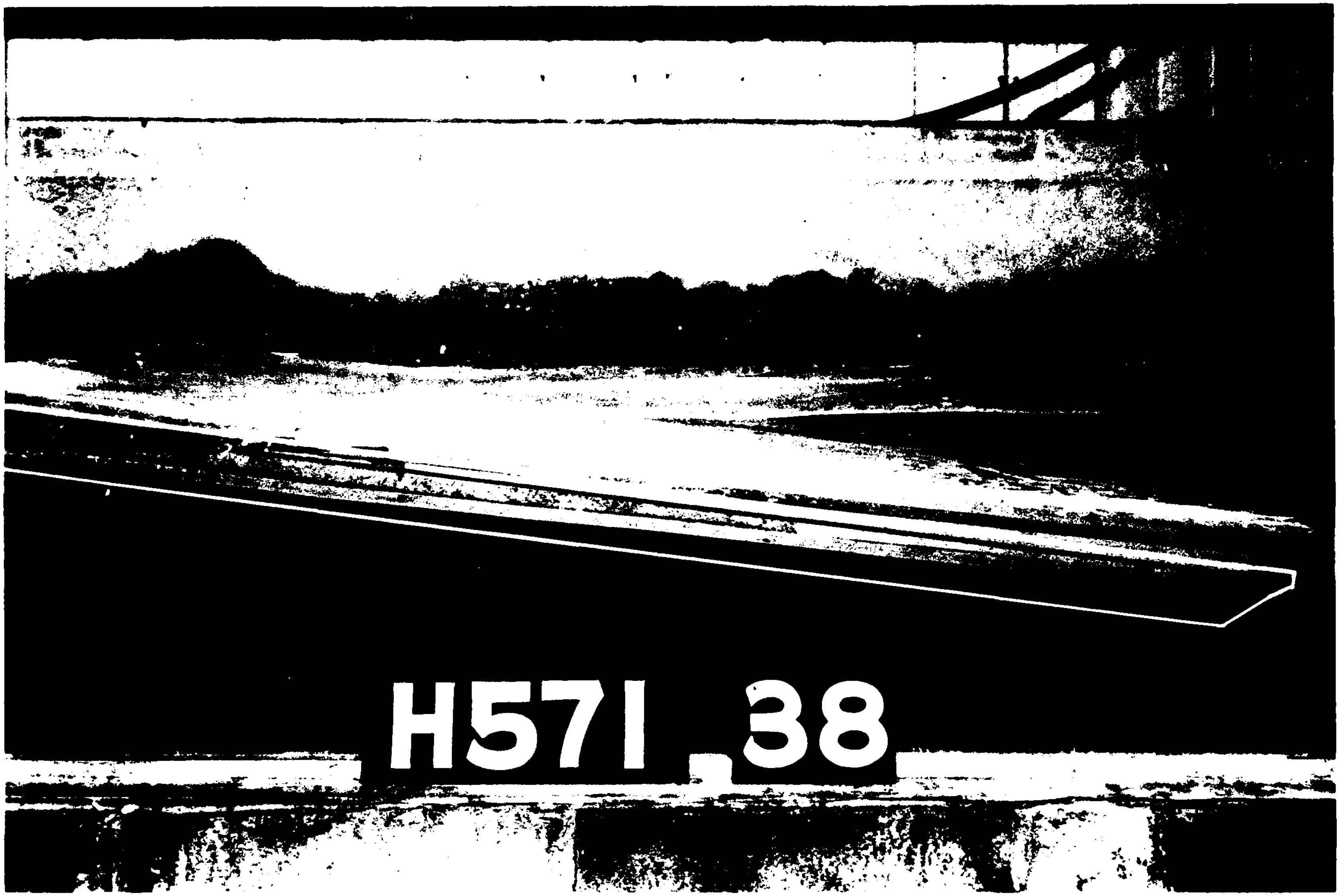

Photo 36. Side view of 118.4-ft SFB under attack of 14-sec, 4-ft spectral waves in a water depth of 15 ft

Photo 37. Side view of 118.4-ft SFB under attack of 14-sec, 8-ft spectral waves in a water depth of 15 ft

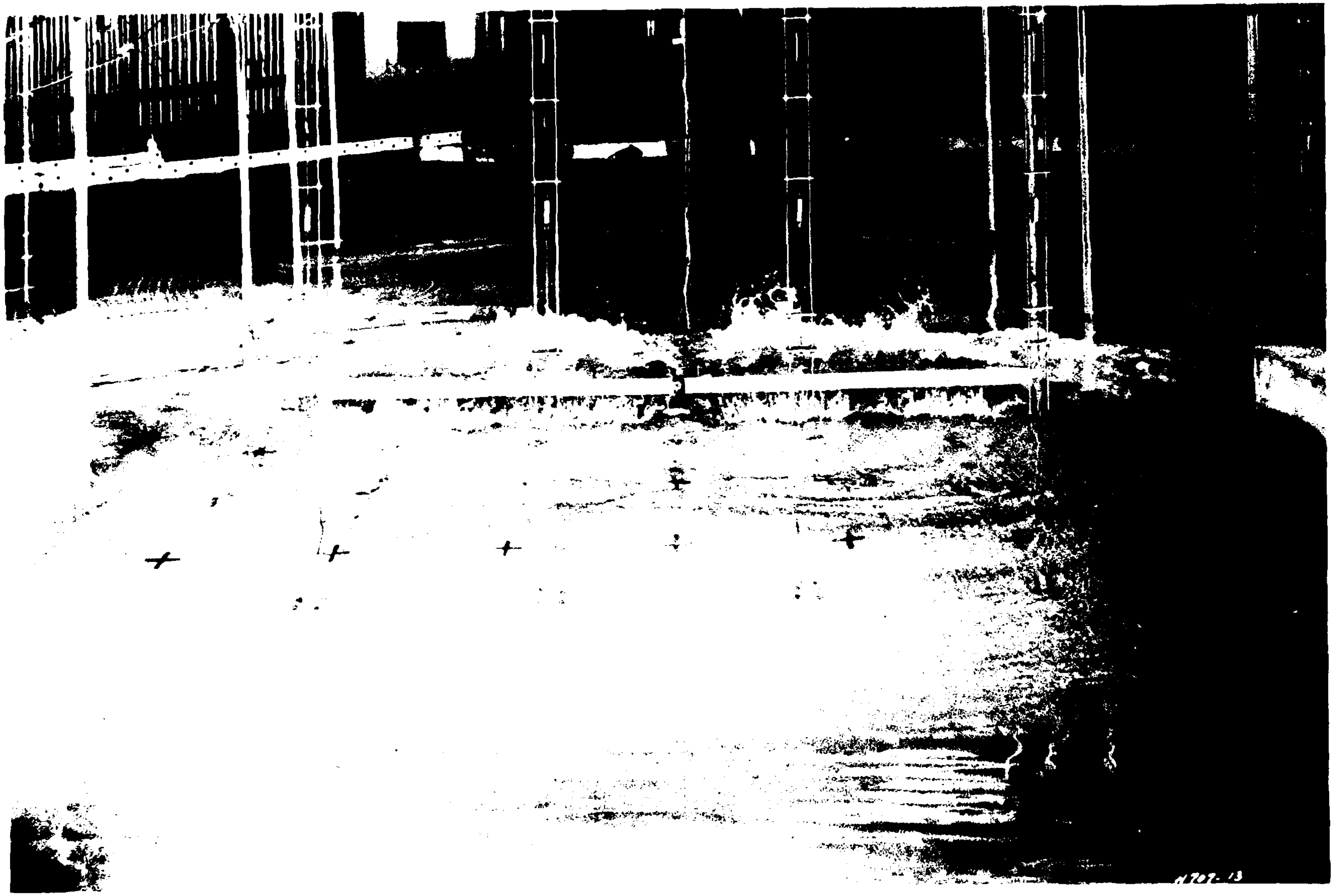

Photo 38. Seaside view of SFB during 90-deg monochromatic wave attack (side-connector tests)

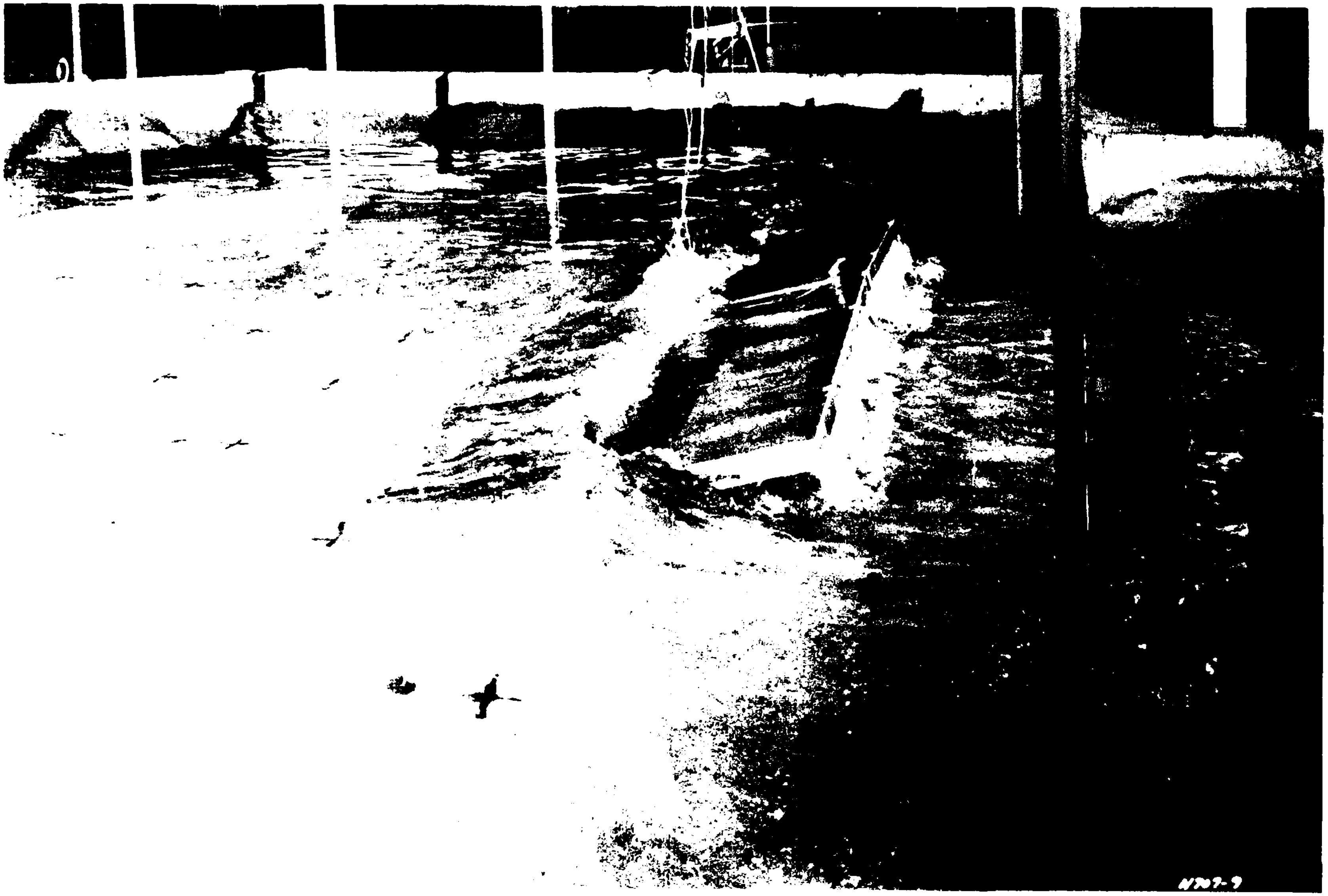

Photo 39. Side view of SFB during 90-deg monochromatic wave attack (side-connector tests)

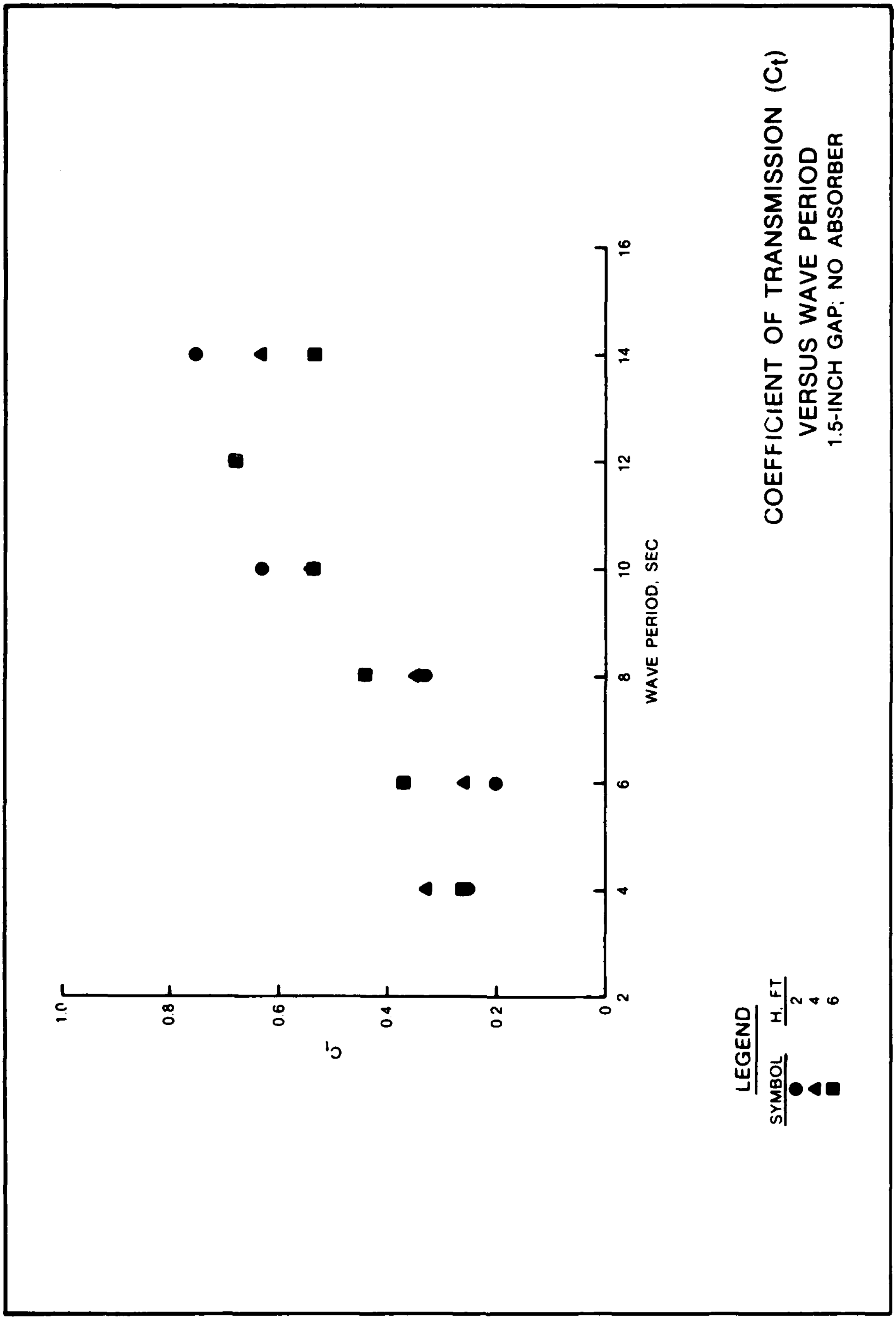
COEFFICIENT OF TRANSMISSION (C_t)
VERSUS WAVE PERIOD
1.5-INCH GAP; NO ABSORBER
C_t
0
0.2
0.4
0.6
0.8
1.0
2
4
6
8
10
12
14
16
WAVE PERIOD, SEC
LEGEND
SYMBOL H, FT
● 2
▲ 4
■ 6

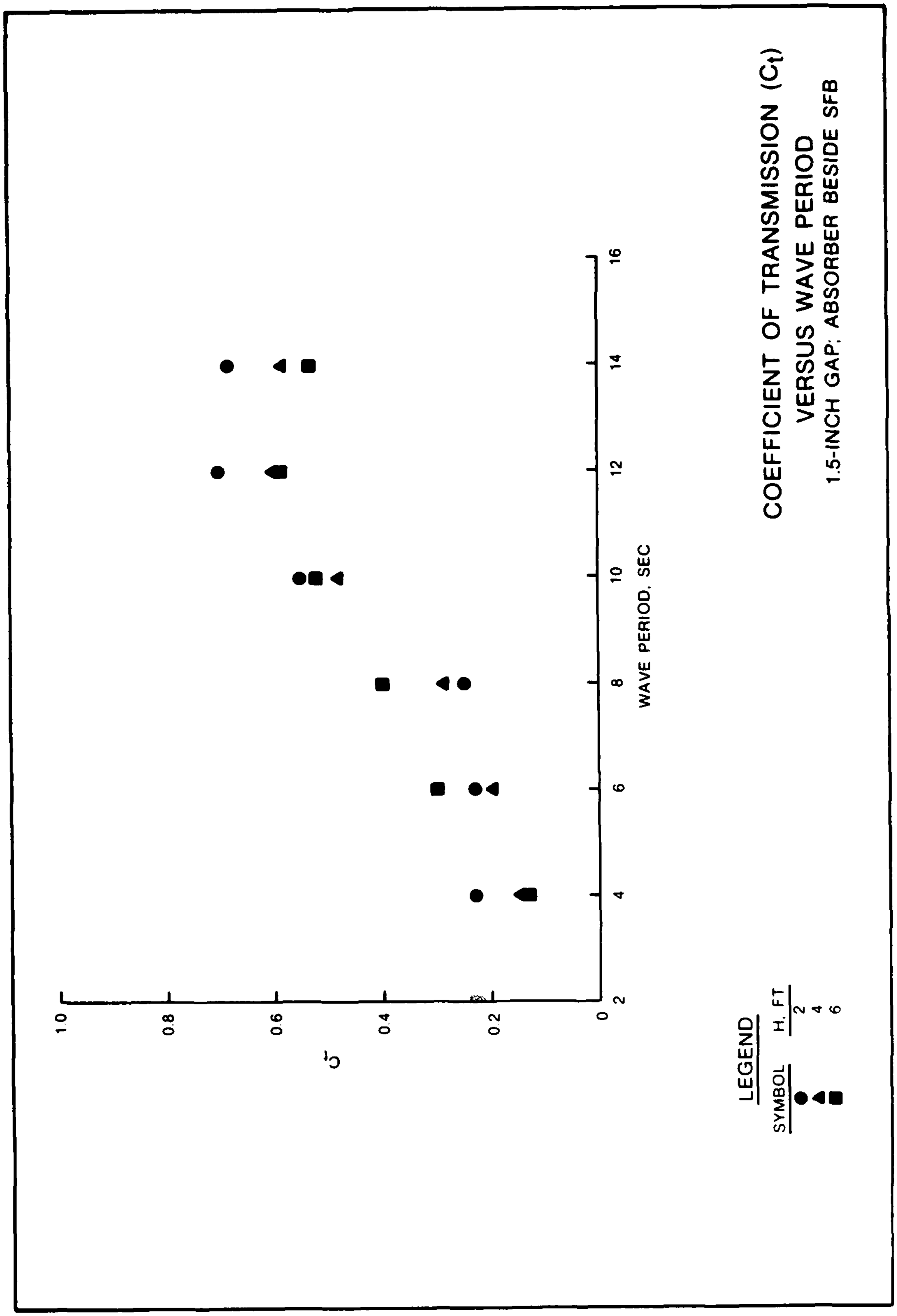
COEFFICIENT OF TRANSMISSION (C_t)
VERSUS WAVE PERIOD
1.5-INCH GAP; ABSORBER BESIDE SFB
C_t
1.0
0.8
0.6
0.4
0.2
0
2
4
6
8
10
12
14
16
WAVE PERIOD, SEC
LEGEND
SYMBOL
H, FT
2
4
6

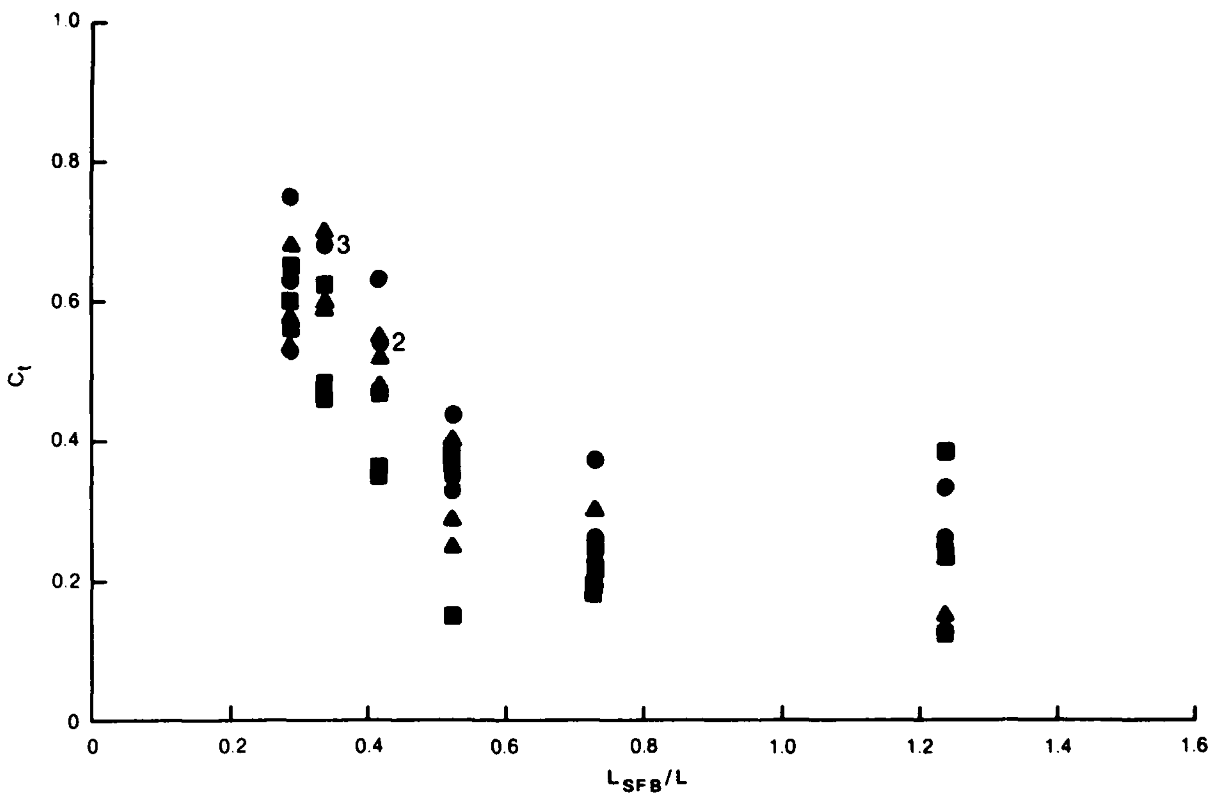

NOTE: NUMBERS BESIDE DATA POINTS INDICATE THAT THE NUMBER OF DATA POINTS EXCEEDS ONE.

LEGEND

SYMBOL	CONDITION
●	1 (1.5-INCH GAP, NO ABSORBER)
▲	2 (1.5-INCH GAP, ABSORBER BESIDE SFB)
■	3 (RAICHLEN, 1981)

COEFFICIENT OF TRANSMISSION (C_t) VERSUS RELATIVE STRUCTURE WIDTH (L_{SFB}/L)

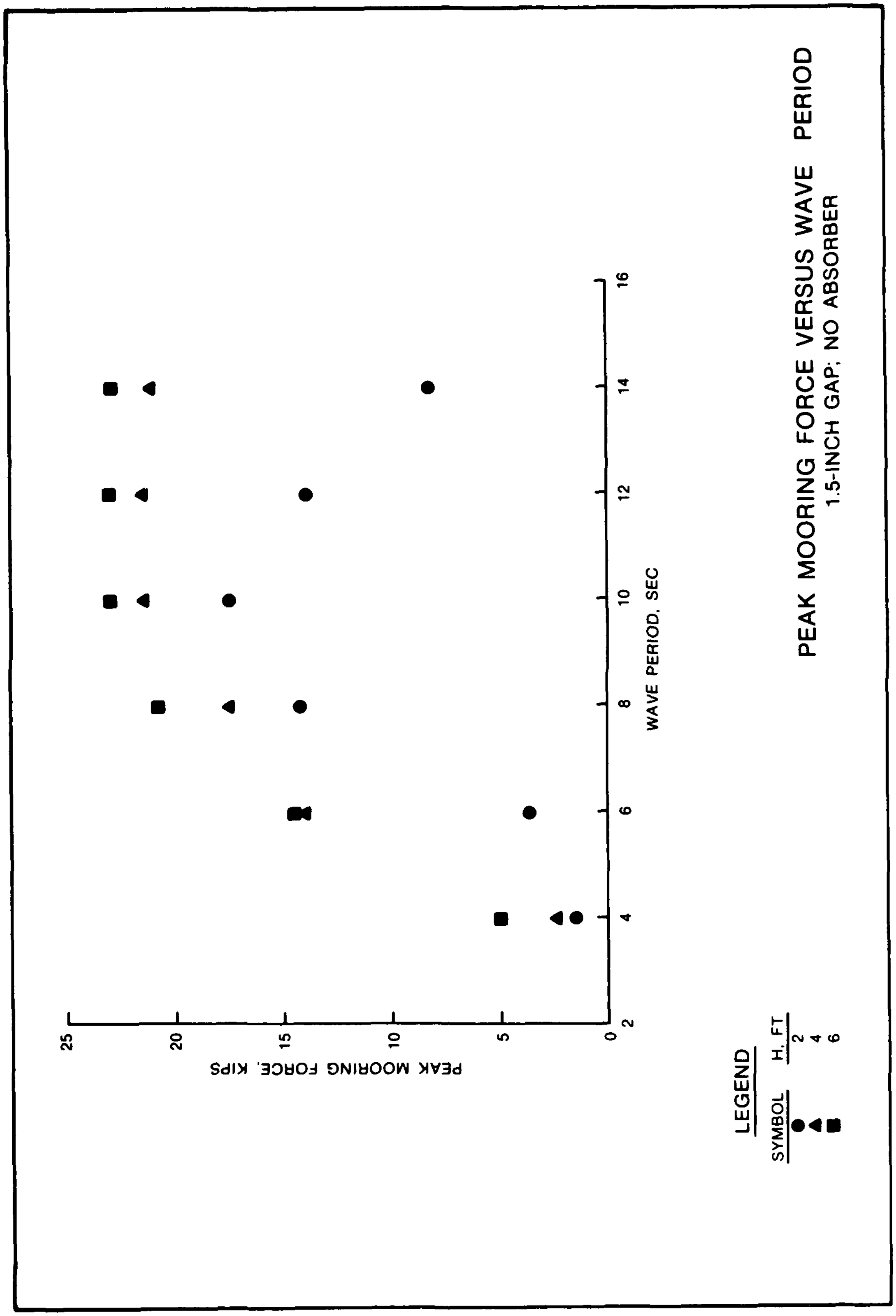

PEAK MOORING FORCE VERSUS WAVE PERIOD

1.5-INCH GAP; NO ABSORBER

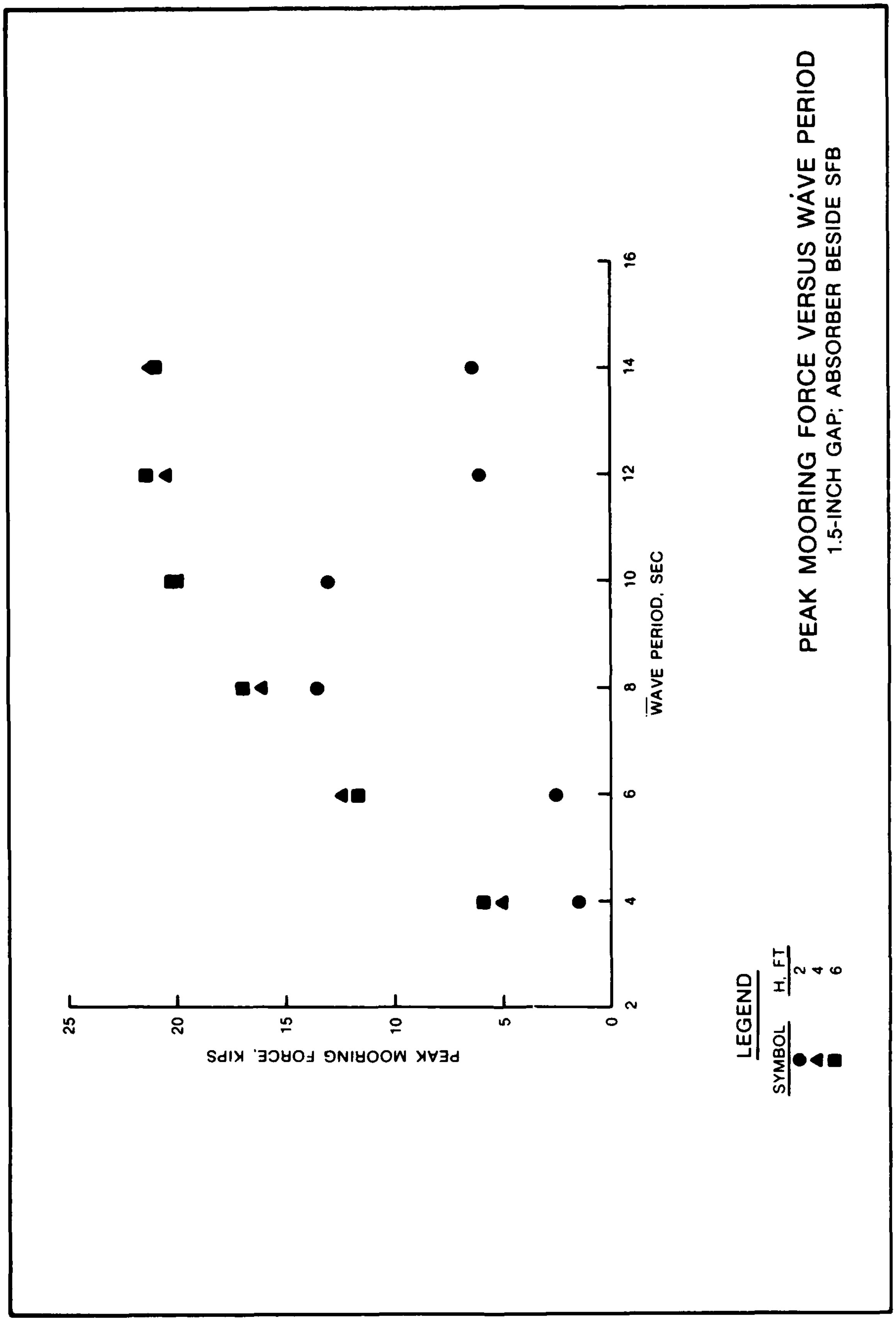

PEAK MOORING FORCE VERSUS WAVE PERIOD
1.5-INCH GAP; ABSORBER BESIDE SFB

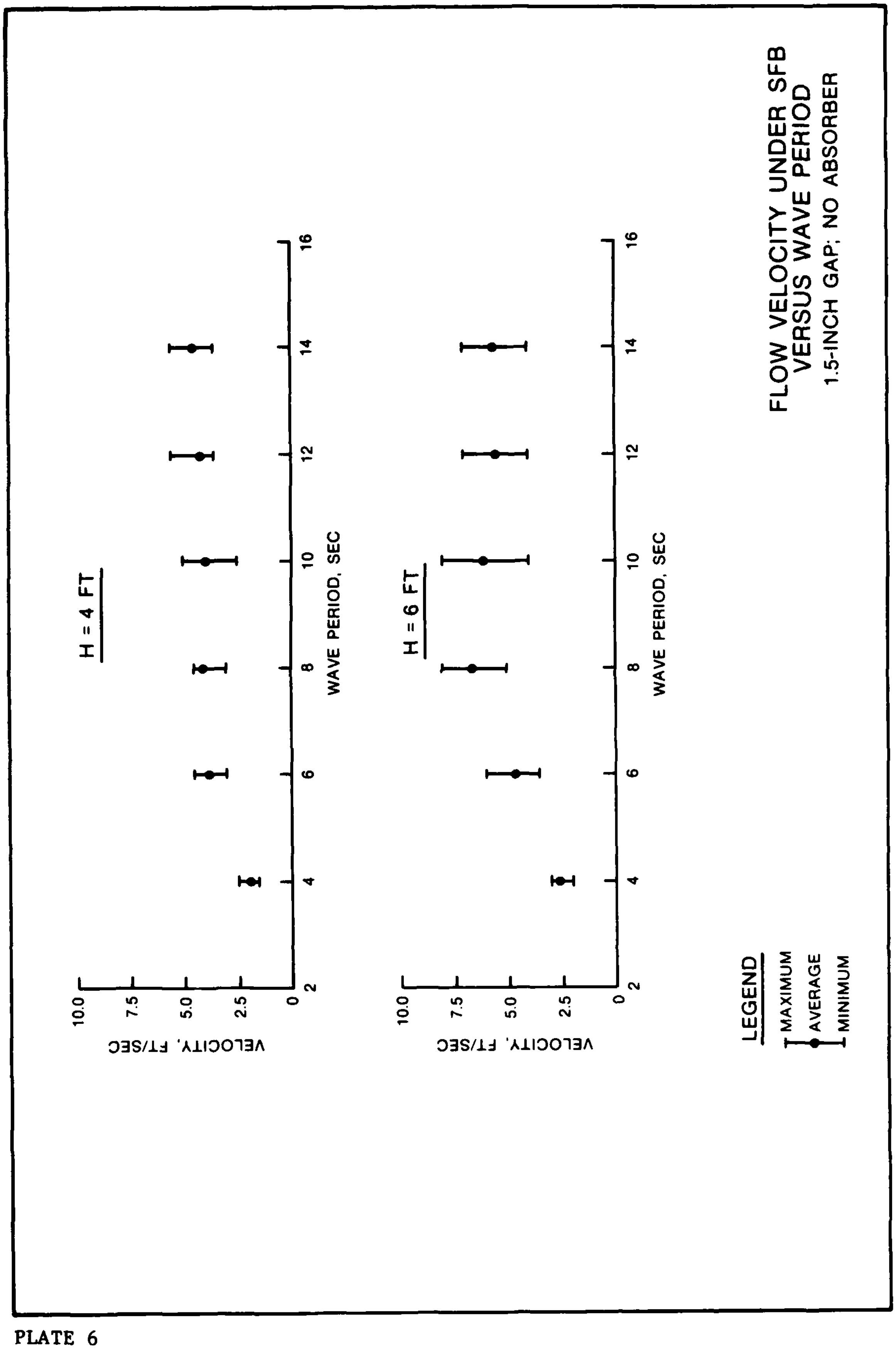
FLOW VELOCITY UNDER SFB
VERSUS WAVE PERIOD
1.5-INCH GAP; NO ABSORBER
H = 4 FT
H = 6 FT
VELOCITY, FT/SEC
10.0
7.5
5.0
2.5
0
WAVE PERIOD, SEC
2
4
6
8
10
12
14
16
LEGEND
MAXIMUM
AVERAGE
MINIMUM

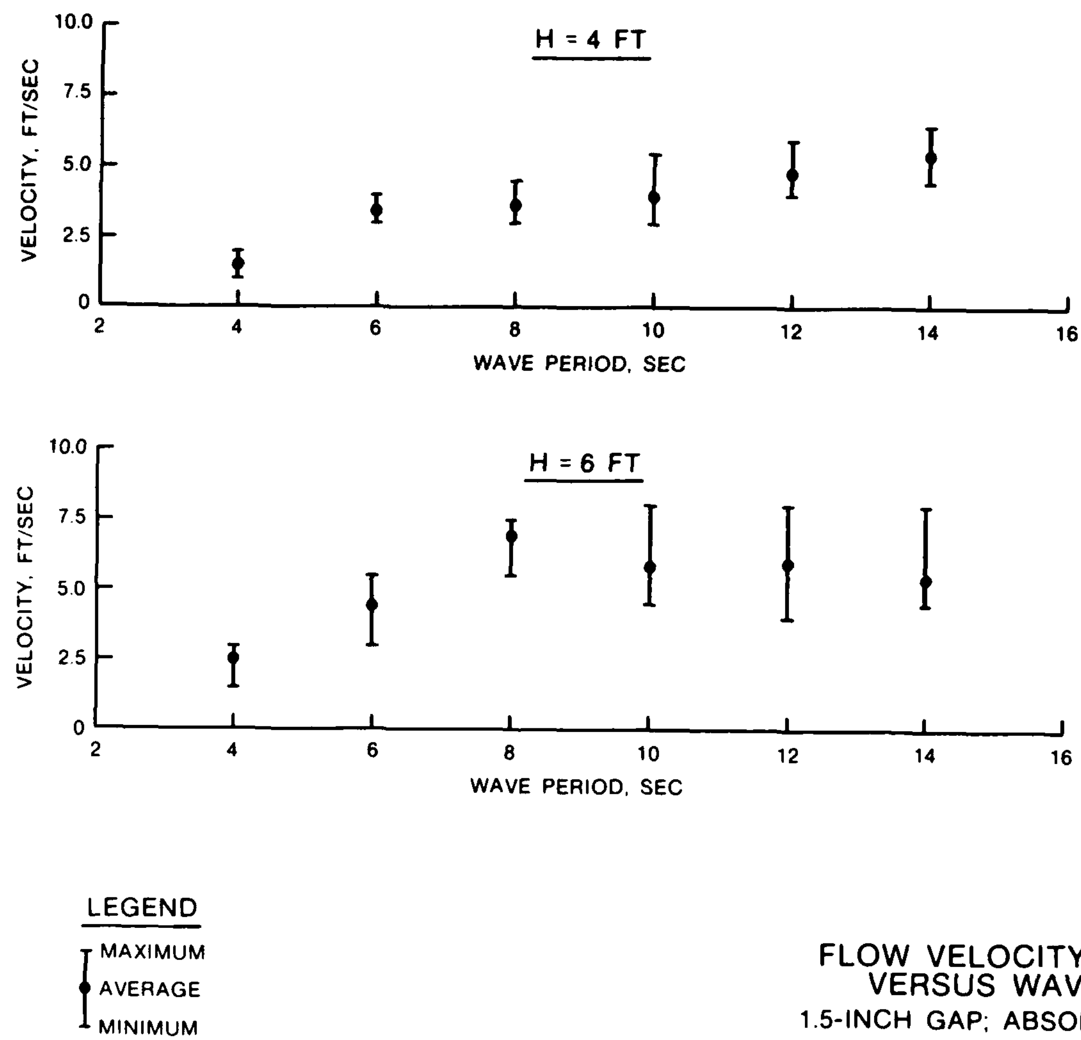

FLOW VELOCITY UNDER SFB
VERSUS WAVE PERIOD
1.5-INCH GAP; ABSORBER BESIDE SFB

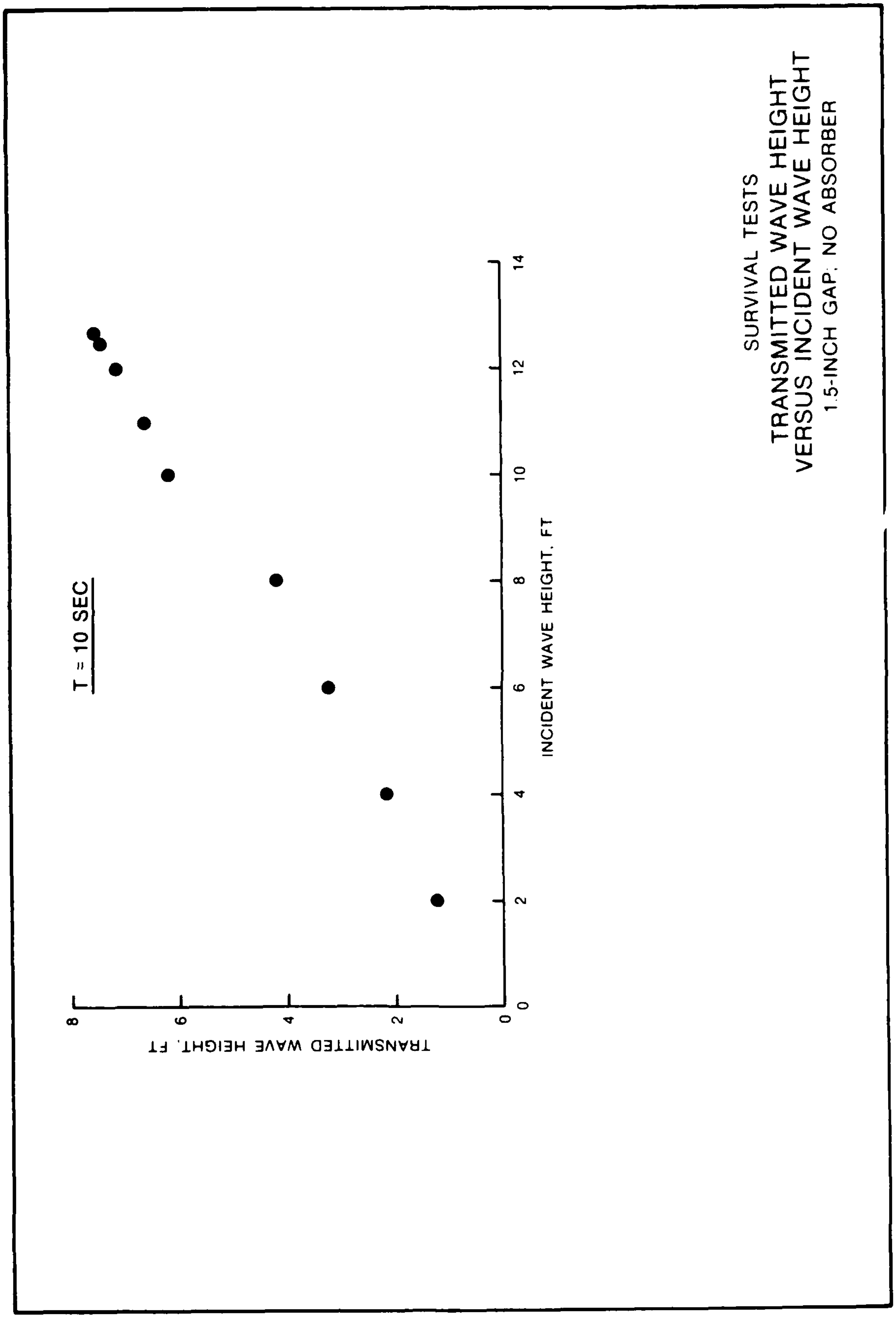
SURVIVAL TESTS
TRANSMITTED WAVE HEIGHT
VERSUS INCIDENT WAVE HEIGHT
1.5-INCH GAP; NO ABSORBER
T = 10 SEC
INCIDENT WAVE HEIGHT, FT
TRANSMITTED WAVE HEIGHT, FT
0
2
4
6
8
10
12
14

PLATE 8

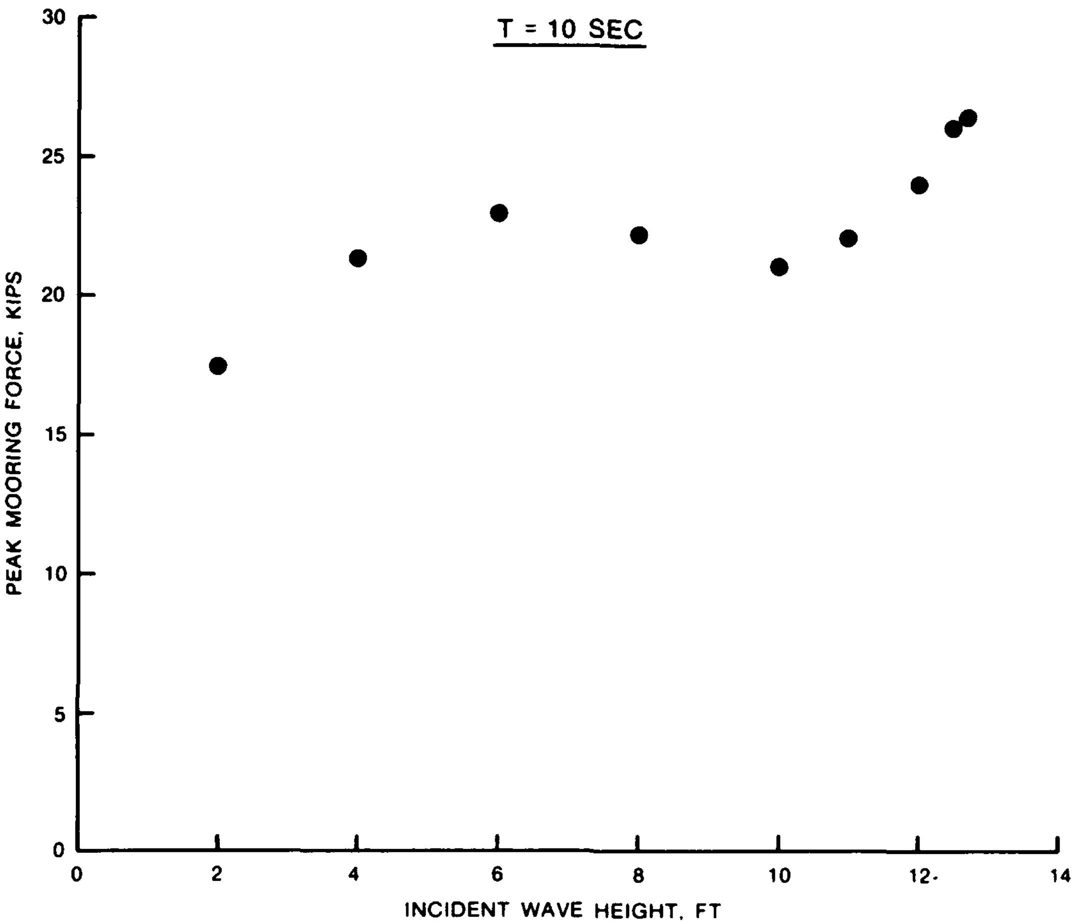

SURVIVAL TESTS
PEAK MOORING FORCE
VERSUS INCIDENT WAVE HEIGHT
1.5-INCH GAP; NO ABSORBER

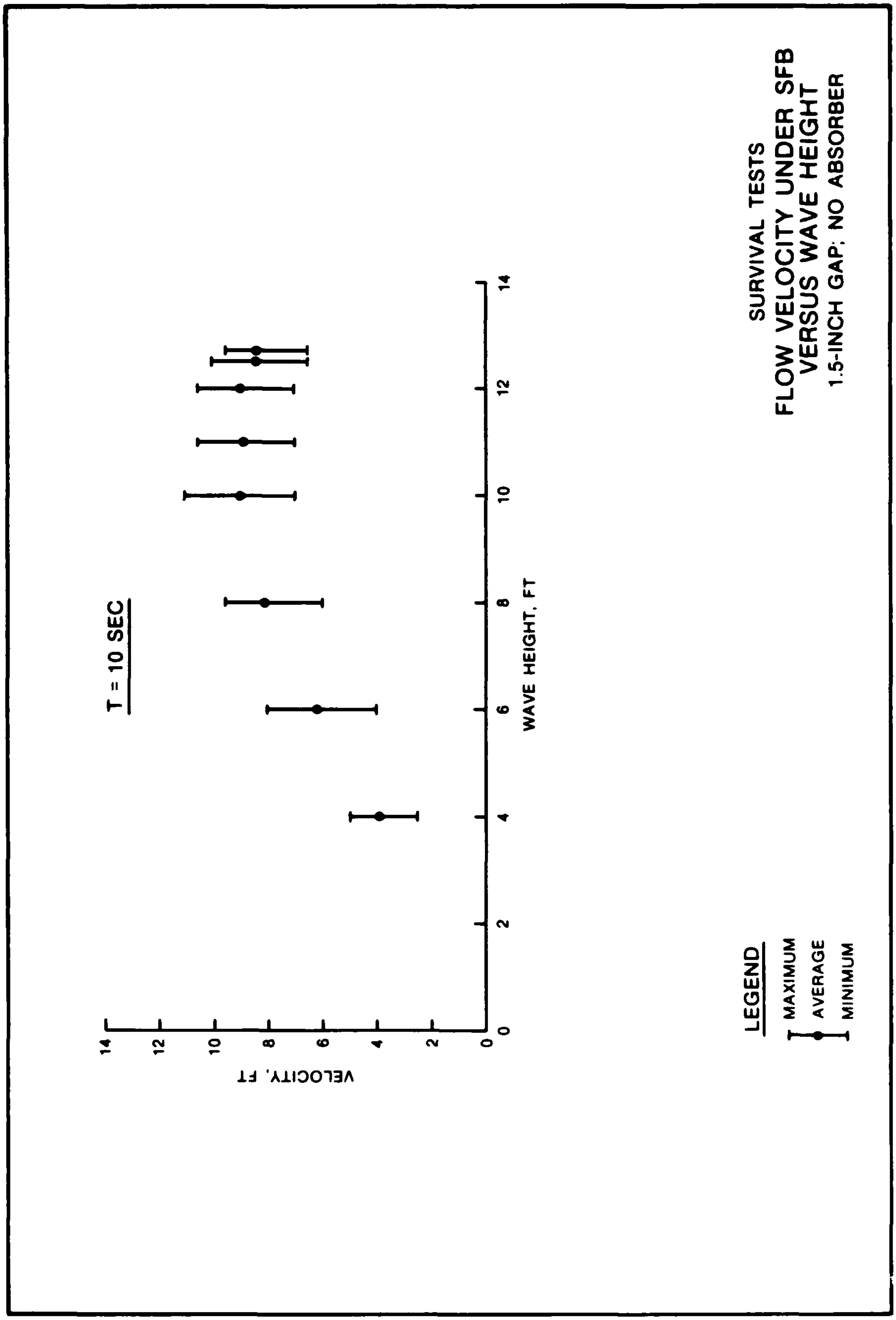

SURVIVAL TESTS
FLOW VELOCITY UNDER SFB
VERSUS WAVE HEIGHT
1.5-INCH GAP; NO ABSORBER
T = 10 SEC
LEGEND
MAXIMUM
AVERAGE
MINIMUM
VELOCITY, FT
0 2 4 6 8 10 12 14
WAVE HEIGHT, FT
0 2 4 6 8 10 12 14

PLATE 10

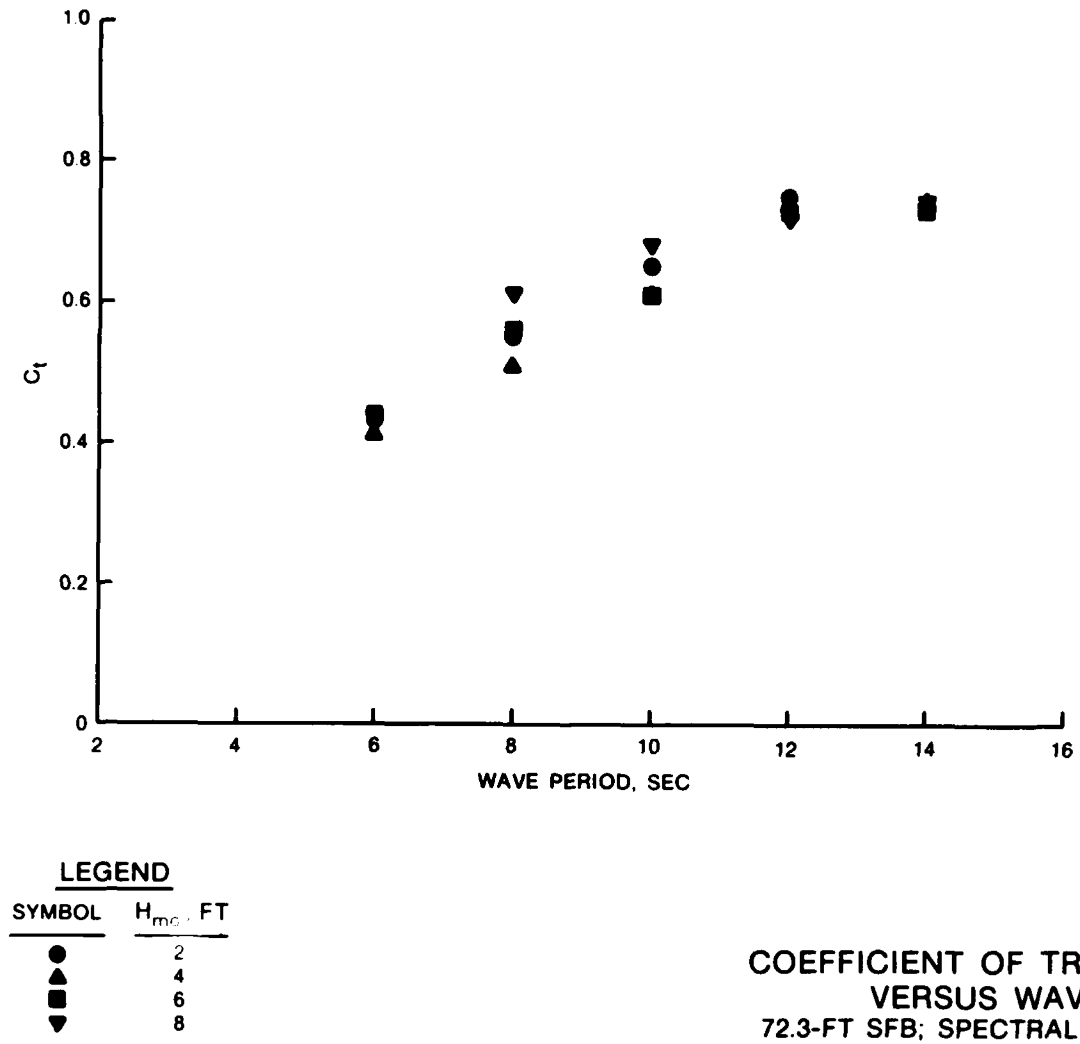

COEFFICIENT OF TRANSMISSION (C_t)
VERSUS WAVE PERIOD
72.3-FT SFB; SPECTRAL WAVES; d = 15.0 FT

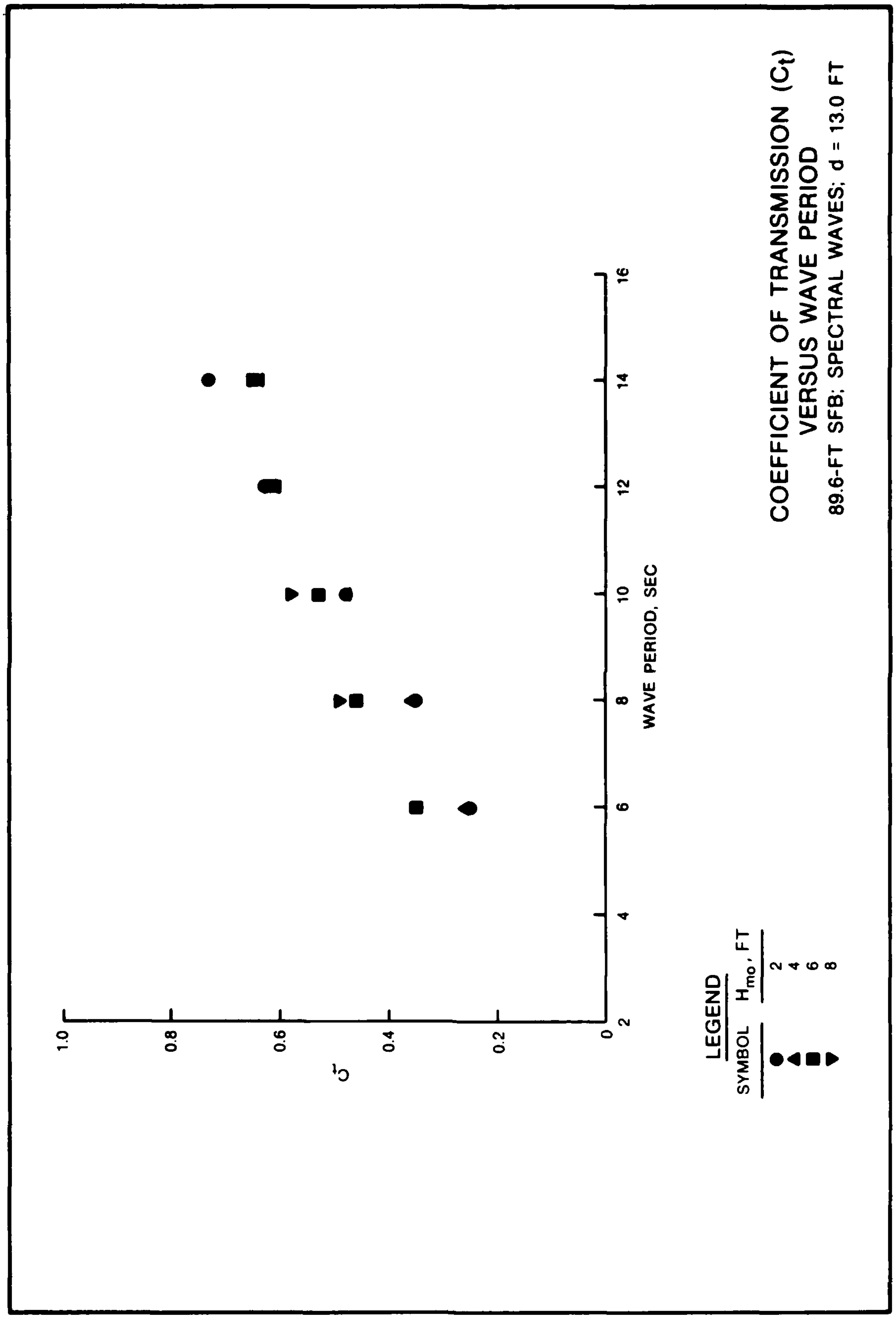
COEFFICIENT OF TRANSMISSION (C_t)
VERSUS WAVE PERIOD
89.6-FT SFB; SPECTRAL WAVES; d = 13.0 FT
C_t
1.0
0.8
0.6
0.4
0.2
0
2
4
6
8
10
12
14
16
WAVE PERIOD, SEC
LEGEND
SYMBOL
H_{mo}, FT
2
4
6
8

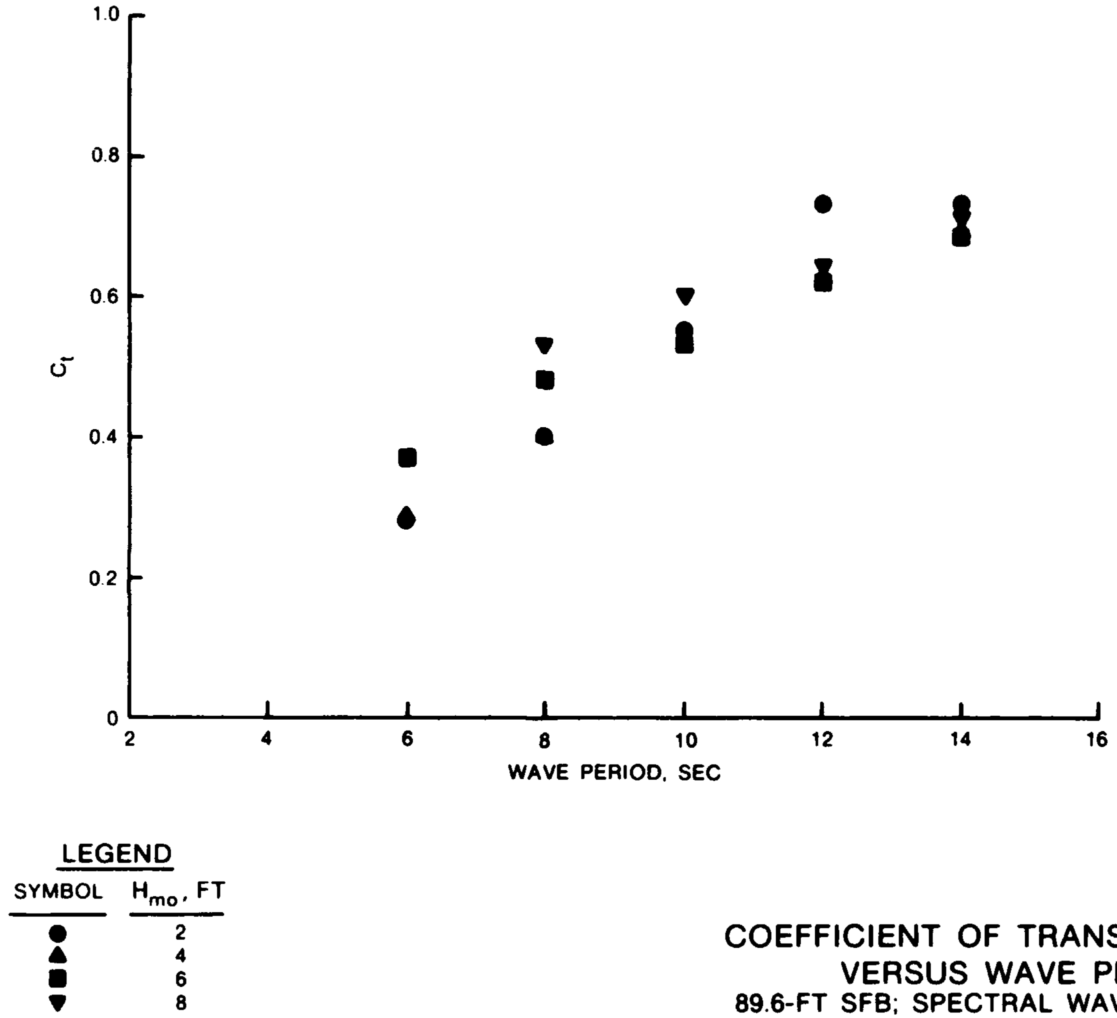

COEFFICIENT OF TRANSMISSION (C_t)
VERSUS WAVE PERIOD
89.6-FT SFB; SPECTRAL WAVES; d = 15.0 FT

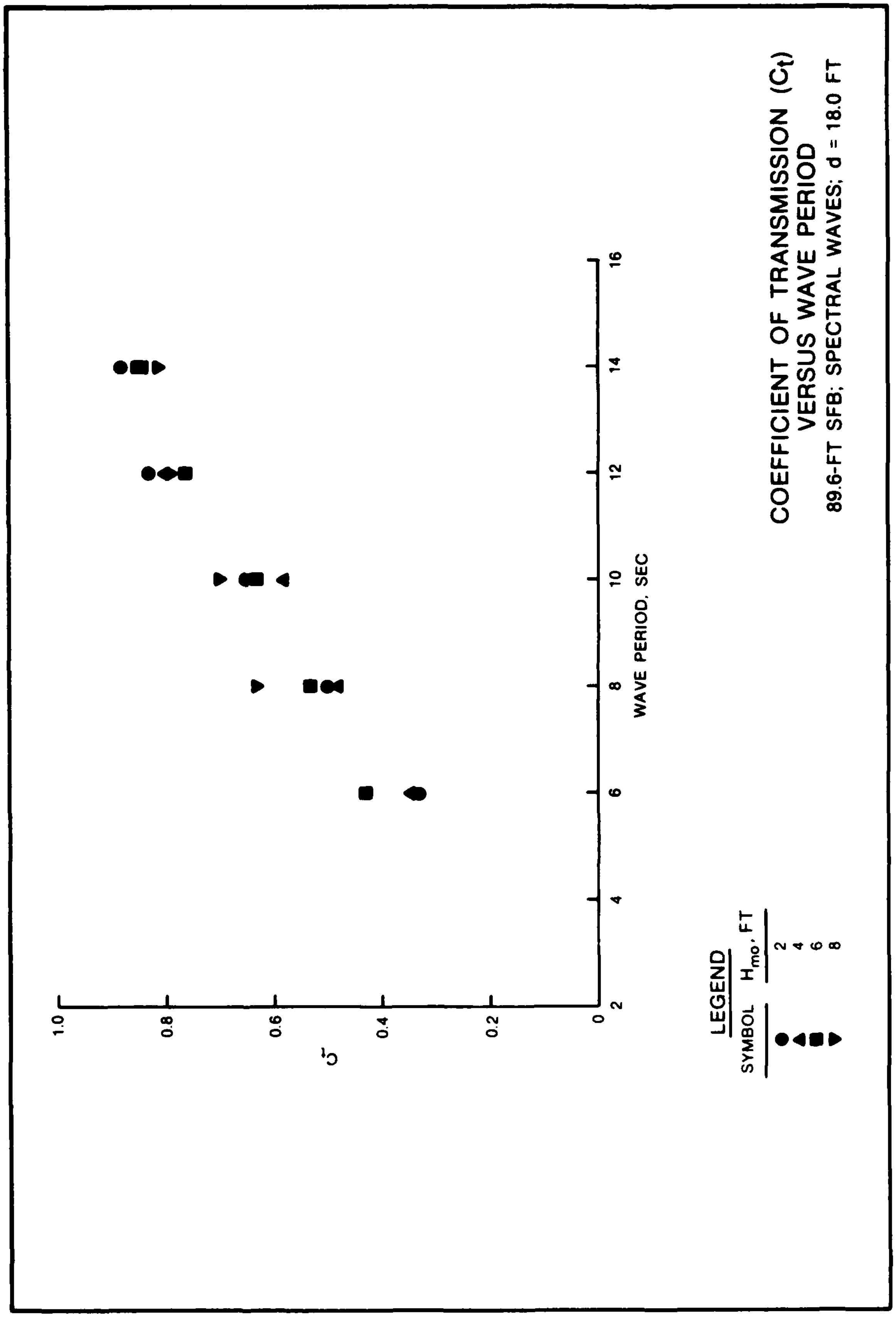

COEFFICIENT OF TRANSMISSION (C_t)
VERSUS WAVE PERIOD
89.6-FT SFB; SPECTRAL WAVES; d = 18.0 FT

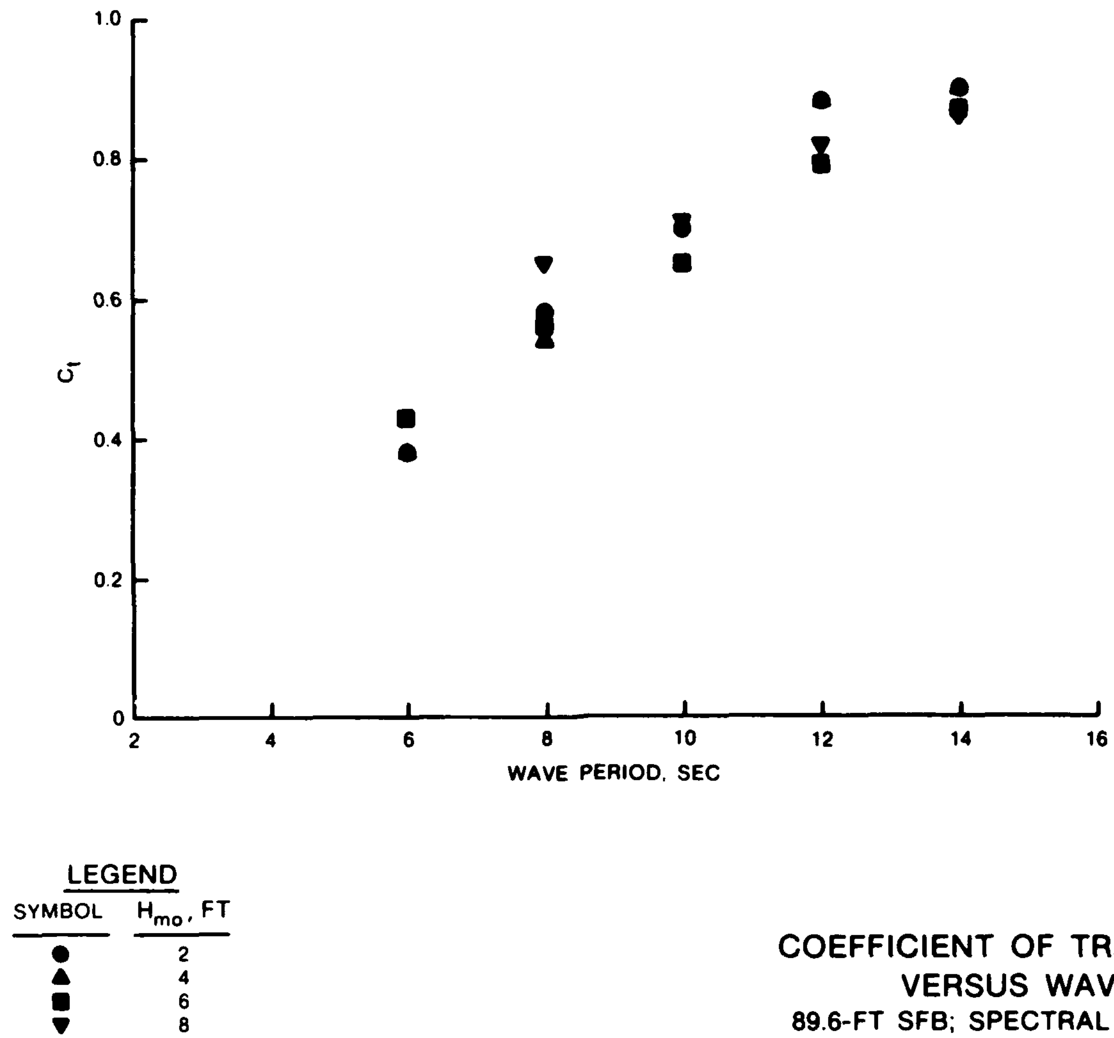

COEFFICIENT OF TRANSMISSION (C_t)
VERSUS WAVE PERIOD
89.6-FT SFB; SPECTRAL WAVES; d = 21.0 FT

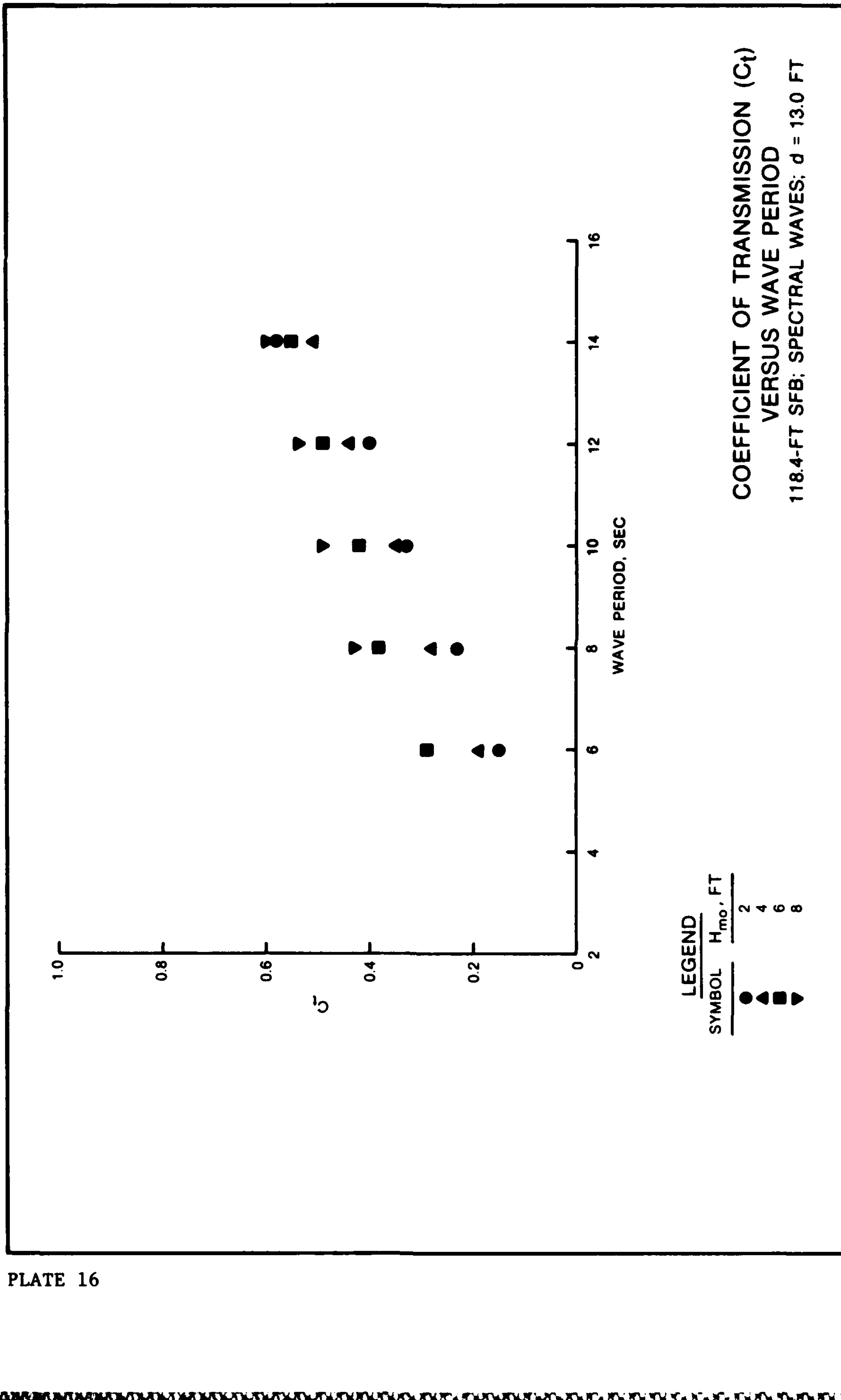
COEFFICIENT OF TRANSMISSION (C_t)
VERSUS WAVE PERIOD
118.4-FT SFB; SPECTRAL WAVES; d = 13.0 FT
C_t
WAVE PERIOD, SEC
LEGEND
SYMBOL
H_{mo}, FT
2
4
6
8
1.0
0.8
0.6
0.4
0.2
0
2
4
6
8
10
12
14
16

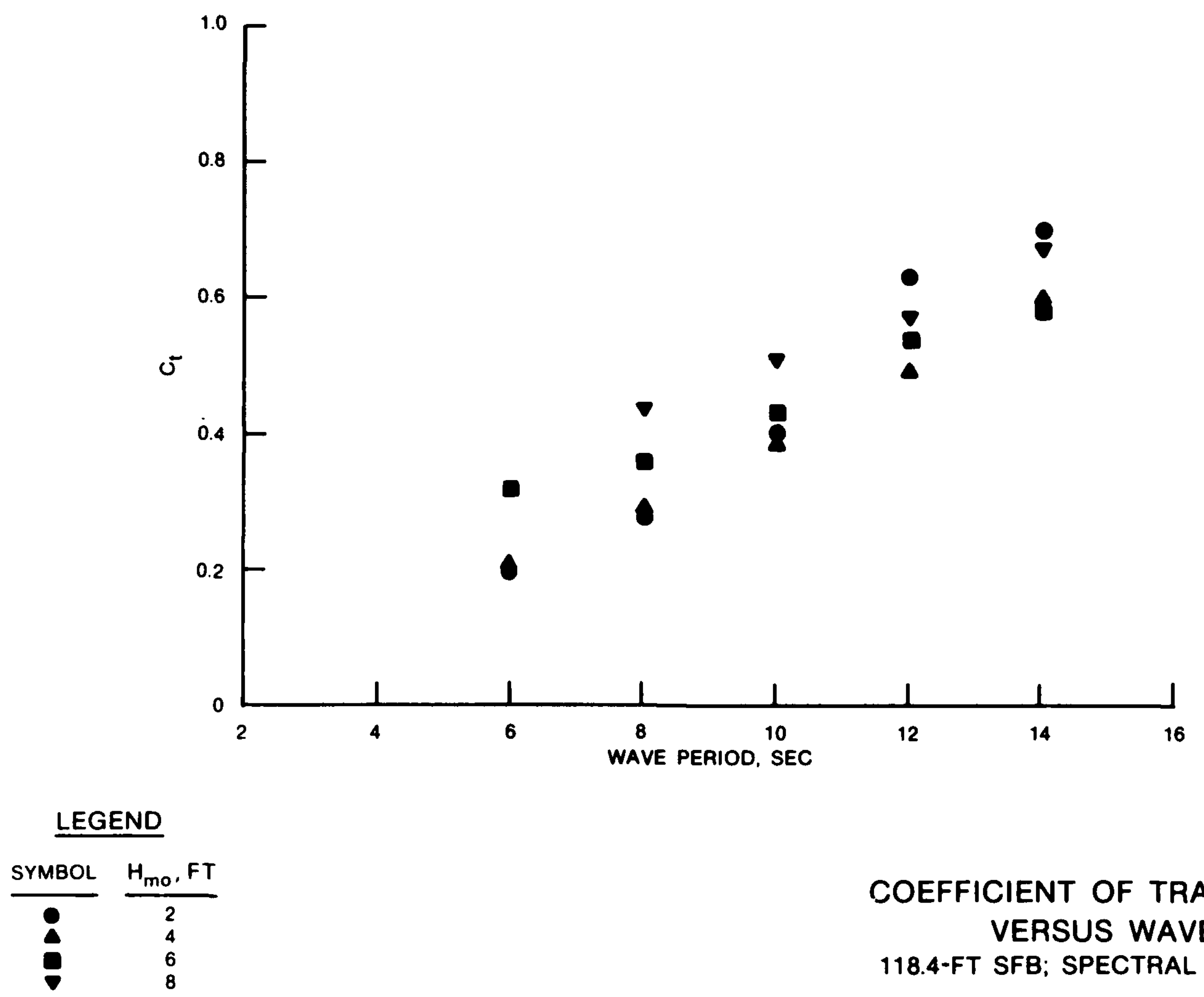

COEFFICIENT OF TRANSMISSION (C_t)
VERSUS WAVE PERIOD
118.4-FT SFB; SPECTRAL WAVES; d = 15.0 FT

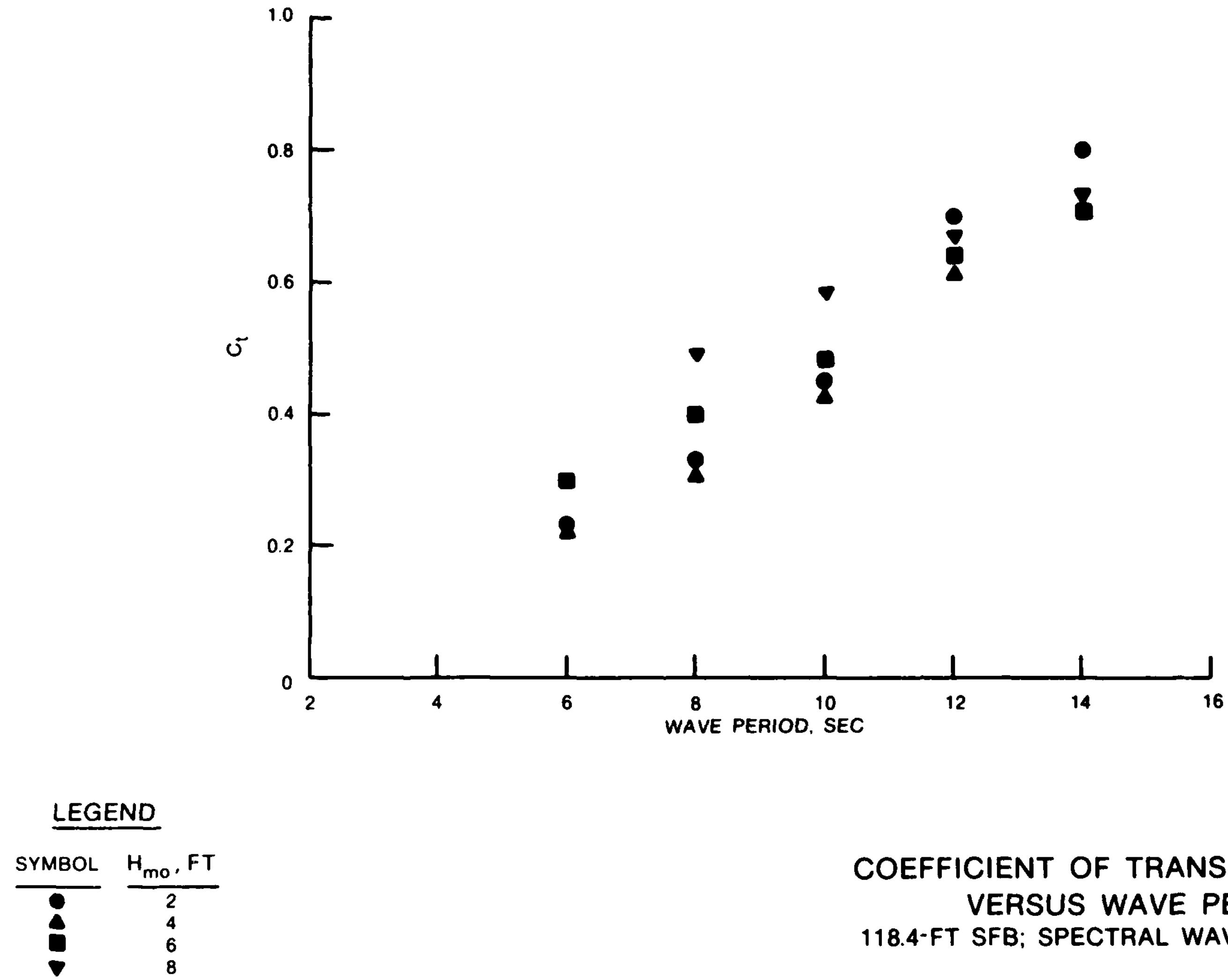

COEFFICIENT OF TRANSMISSION (C_t)
VERSUS WAVE PERIOD
118.4-FT SFB; SPECTRAL WAVES; d = 18.0 FT

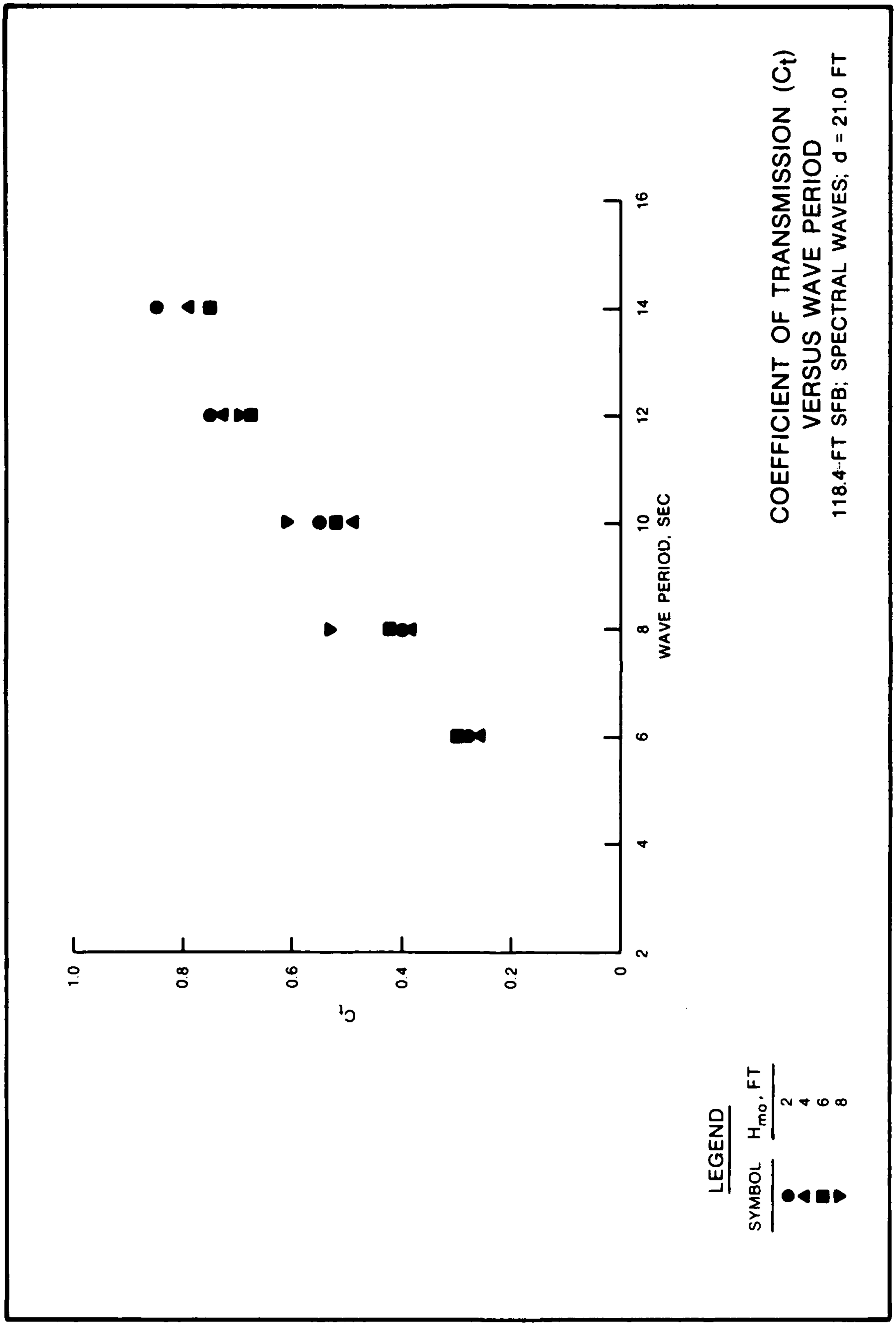
COEFFICIENT OF TRANSMISSION (C_t)
VERSUS WAVE PERIOD
118.4-FT SFB; SPECTRAL WAVES; d = 21.0 FT
LEGEND
SYMBOL
H_{mo}, FT
2
4
6
8
C_t
1.0
0.8
0.6
0.4
0.2
0
2
4
6
8
10
12
14
16
WAVE PERIOD, SEC

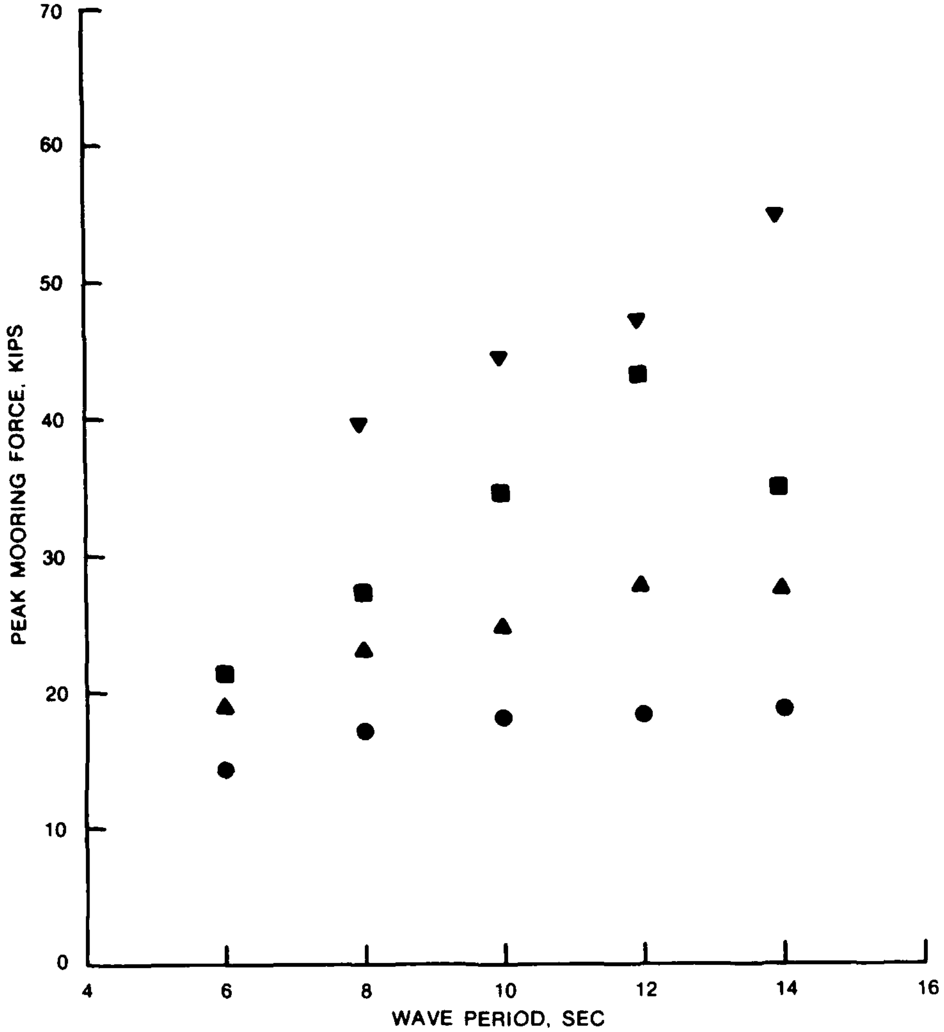

LEGEND

SYMBOL	H_{mo}, FT
●	2
▲	4
■	6
▼	8

PEAK MOORING FORCE VERSUS WAVE PERIOD
72.3-FT SFB; SPECTRAL WAVES; d = 15.0 FT

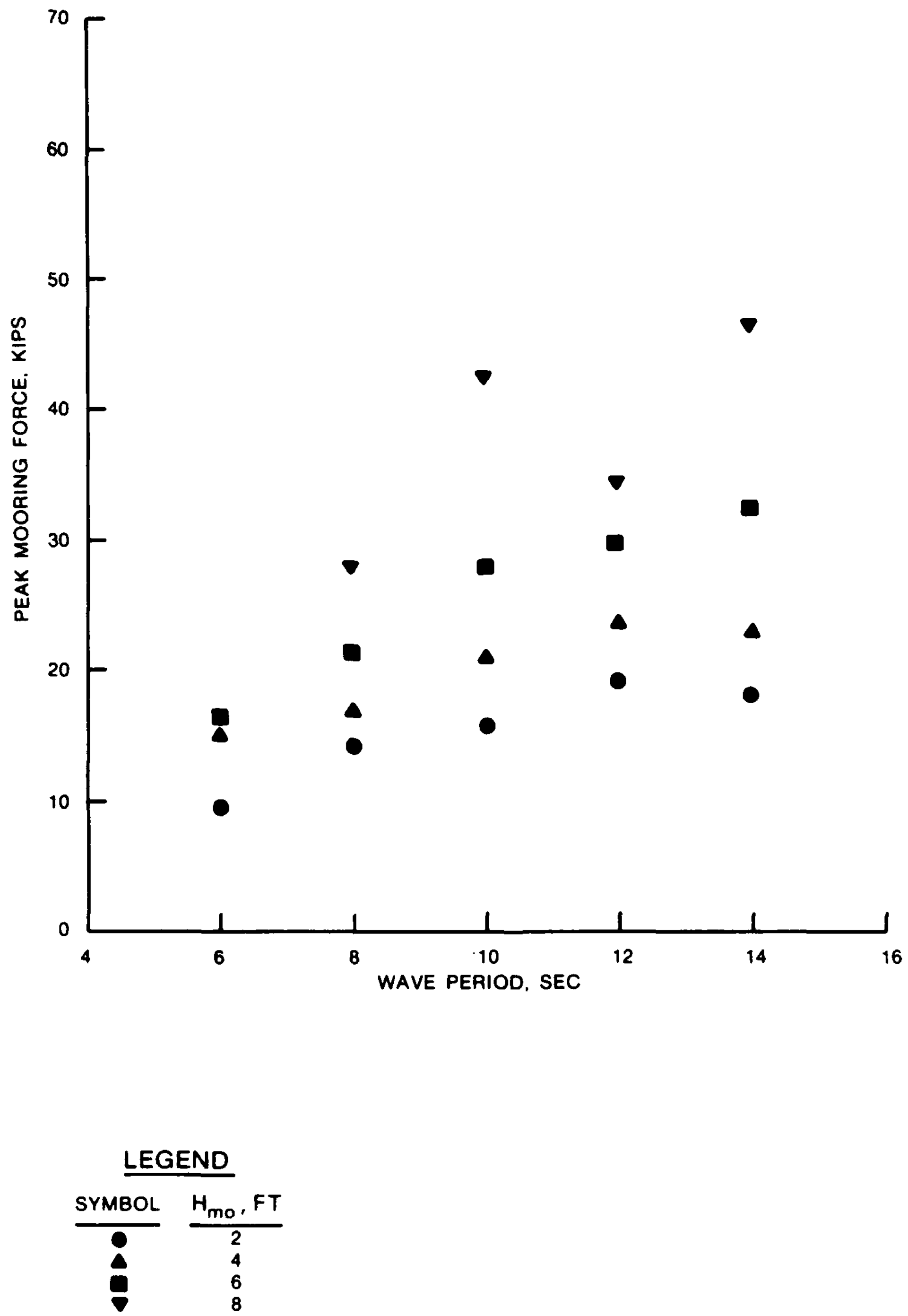

PEAK MOORING FORCE
VERSUS WAVE PERIOD
89.6-FT SFB; SPECTRAL
WAVES; d = 13.0 FT

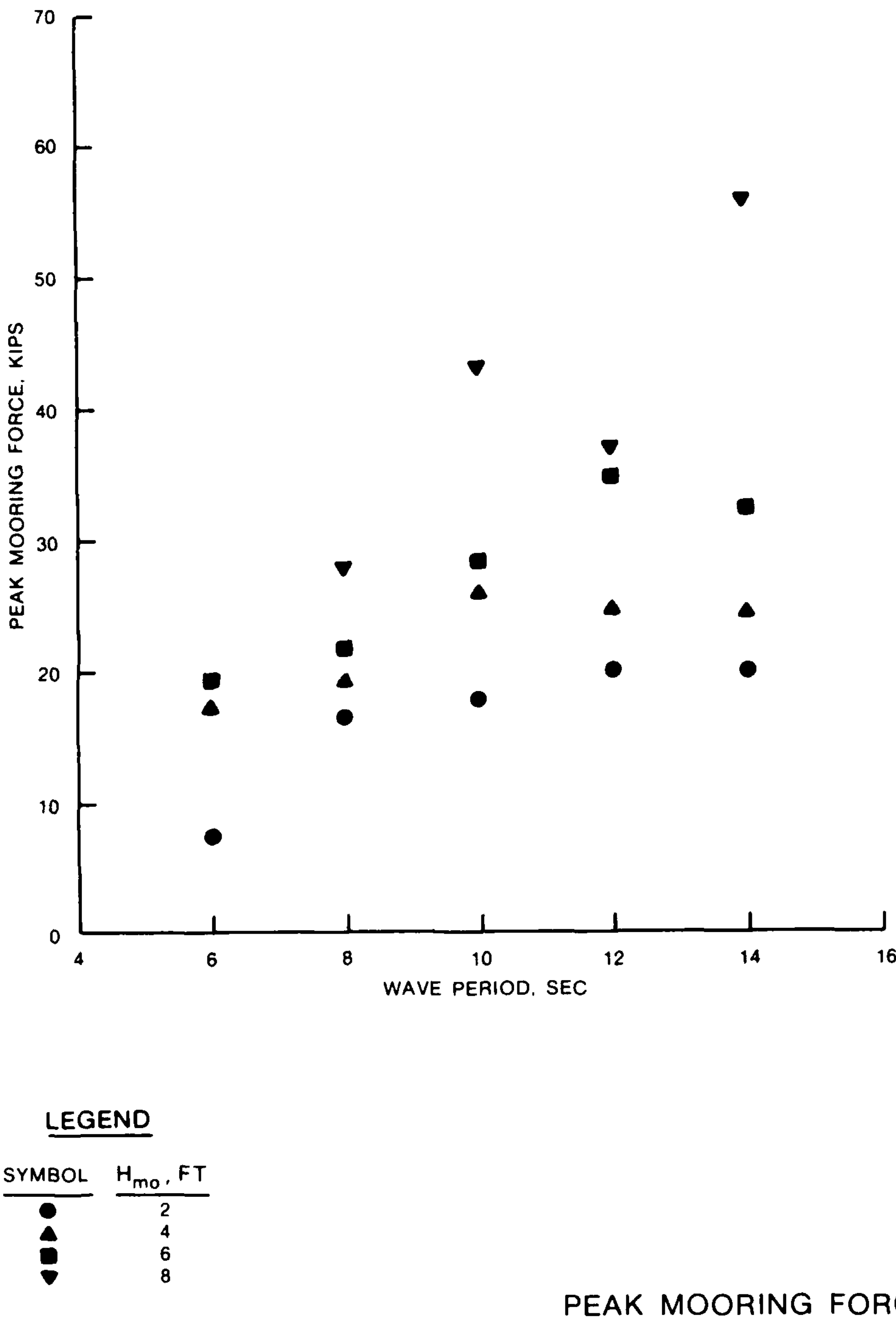

PEAK MOORING FORCE
VERSUS WAVE PERIOD
89.6-FT SFB; SPECTRAL
WAVES; d = 15.0 FT

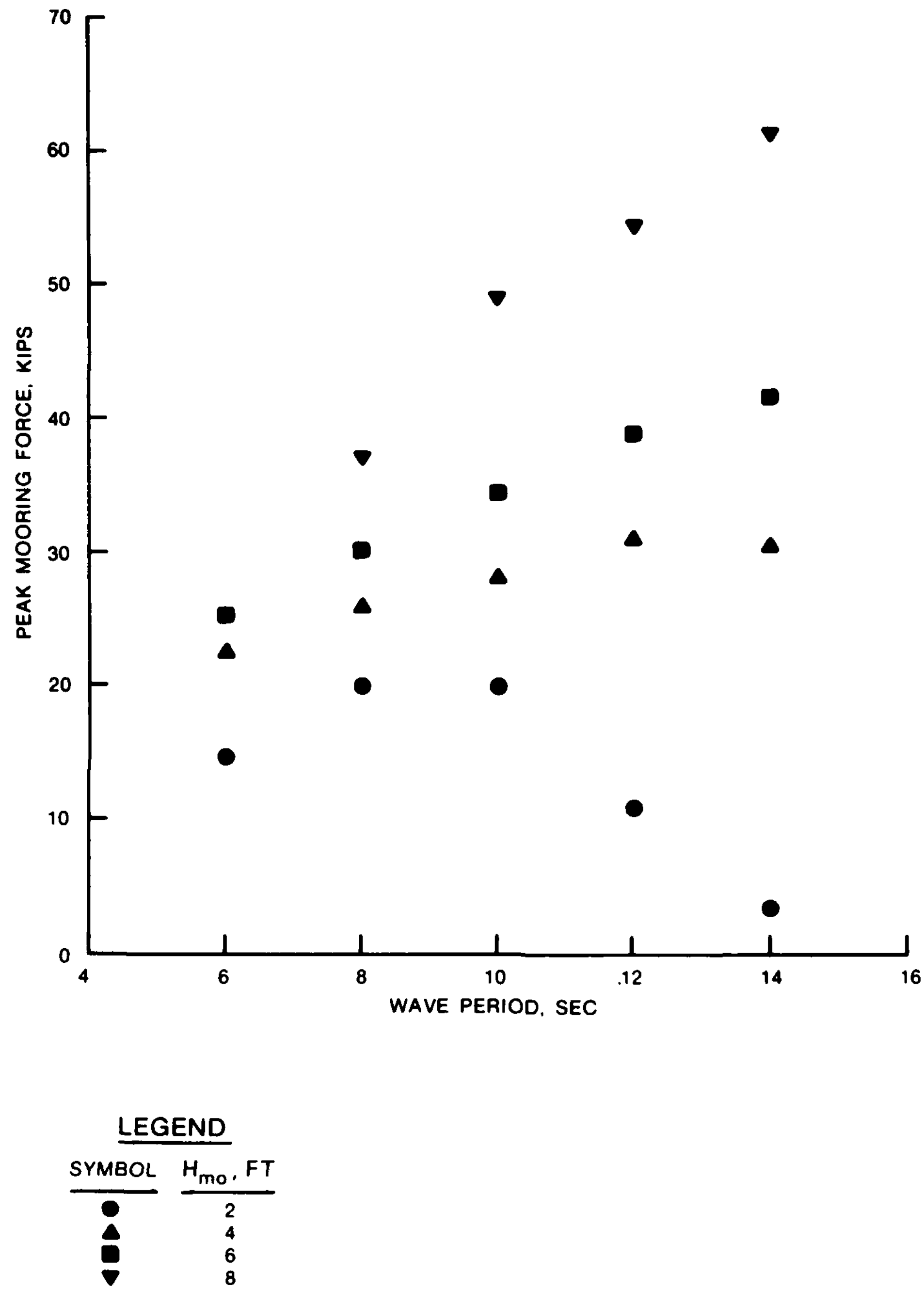

PEAK MOORING FORCE VERSUS WAVE PERIOD
89.6-FT SFB; SPECTRAL WAVES; d = 18.0 FT

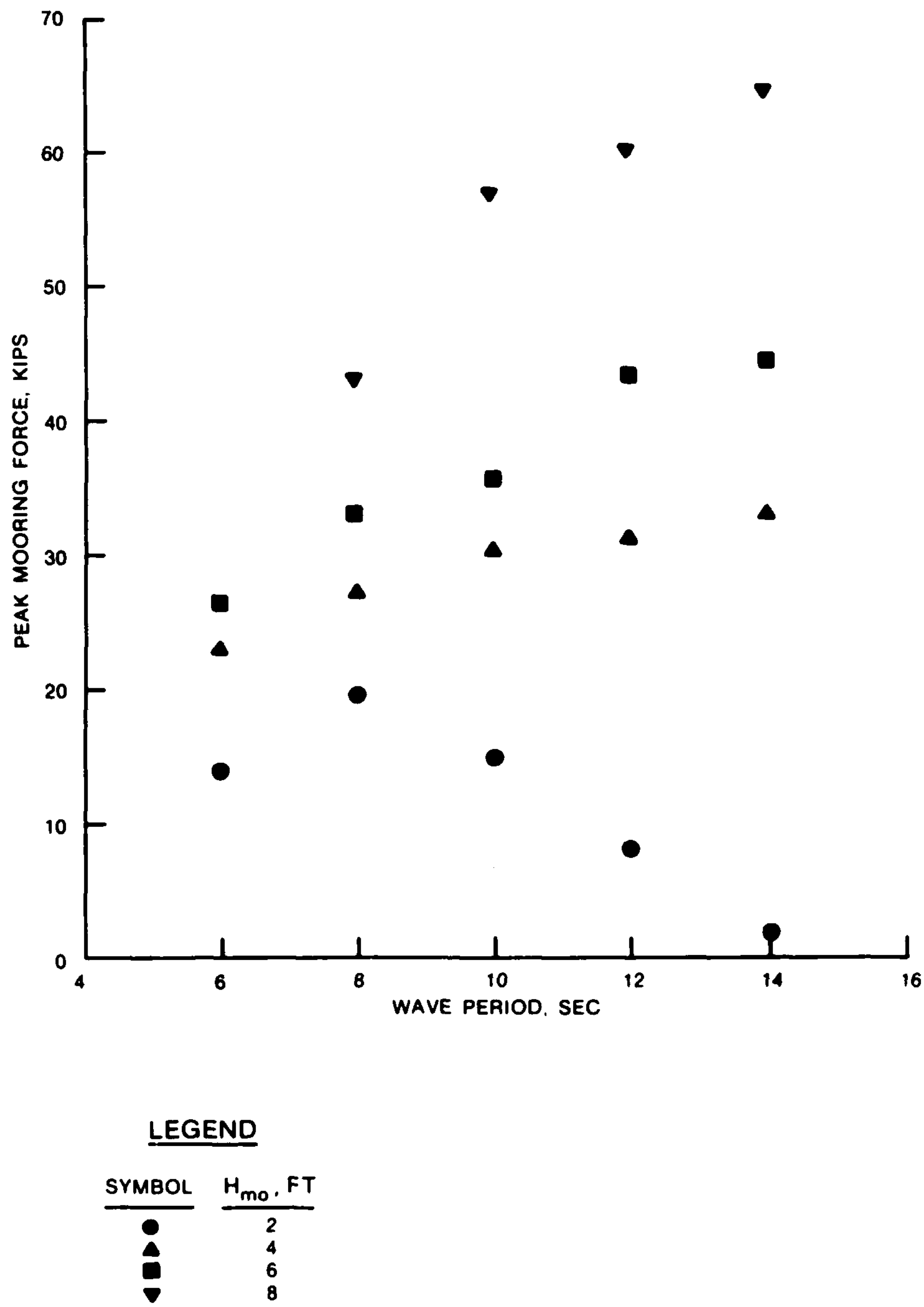

PEAK MOORING FORCE VERSUS WAVE PERIOD

89.6-FT SFB; SPECTRAL WAVES; d = 21.0 FT

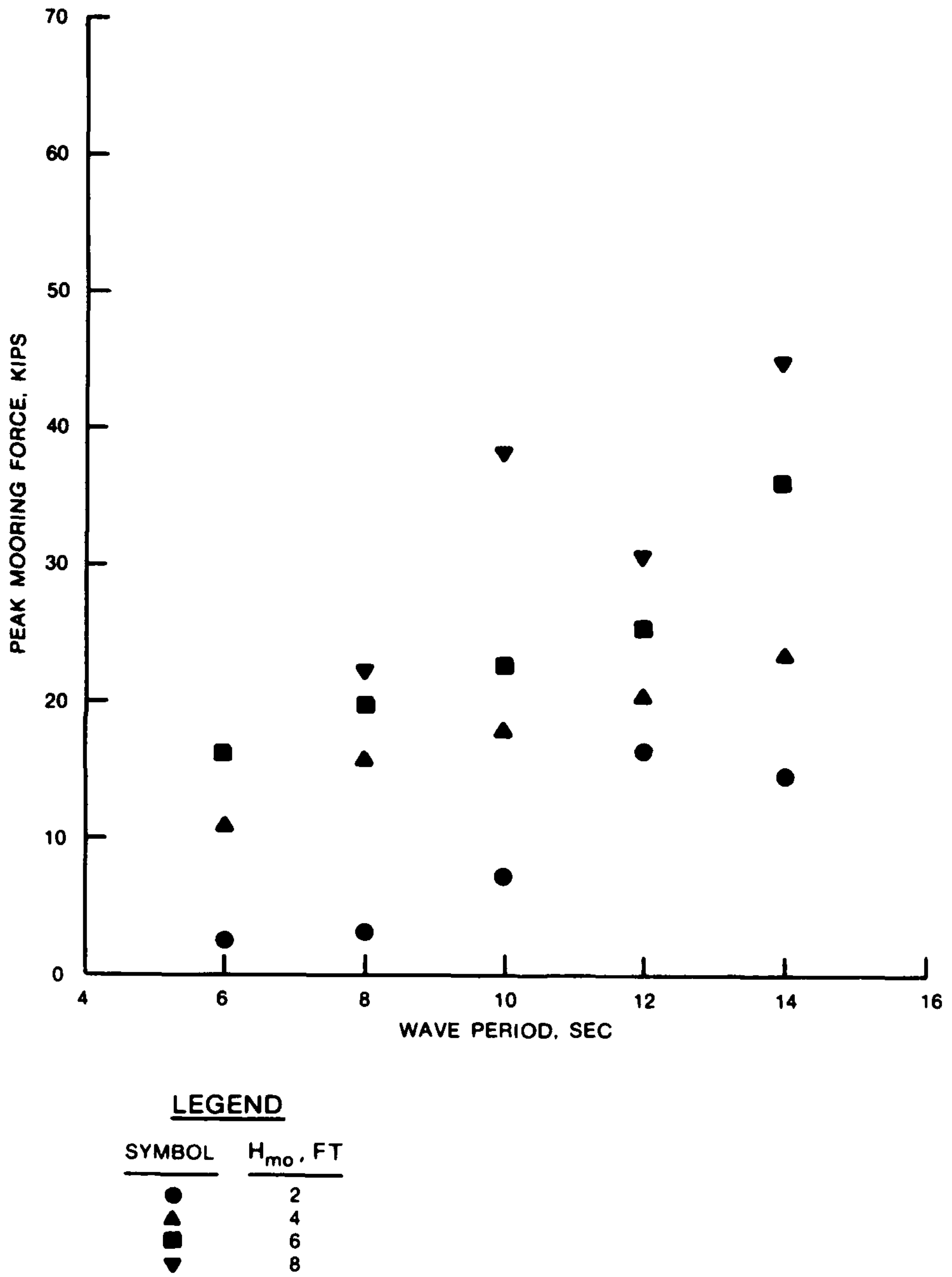

PEAK MOORING FORCE
VERSUS WAVE PERIOD
118.4-FT SFB; SPECTRAL
WAVES; d = 13.0 FT

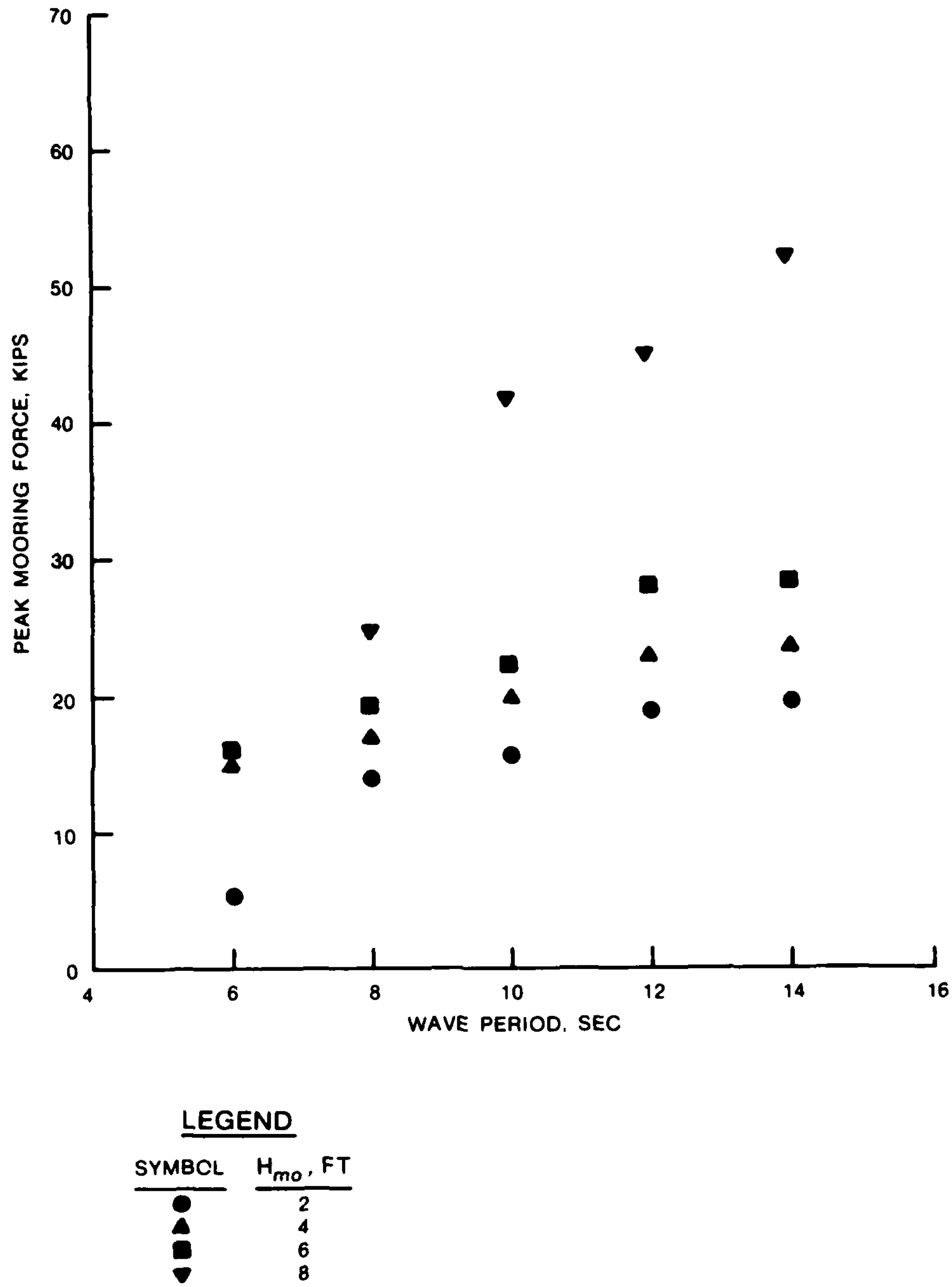

PEAK MOORING FORCE
VERSUS WAVE PERIOD
118.4-FT SFB; SPECTRAL
WAVES; d = 15.0 FT

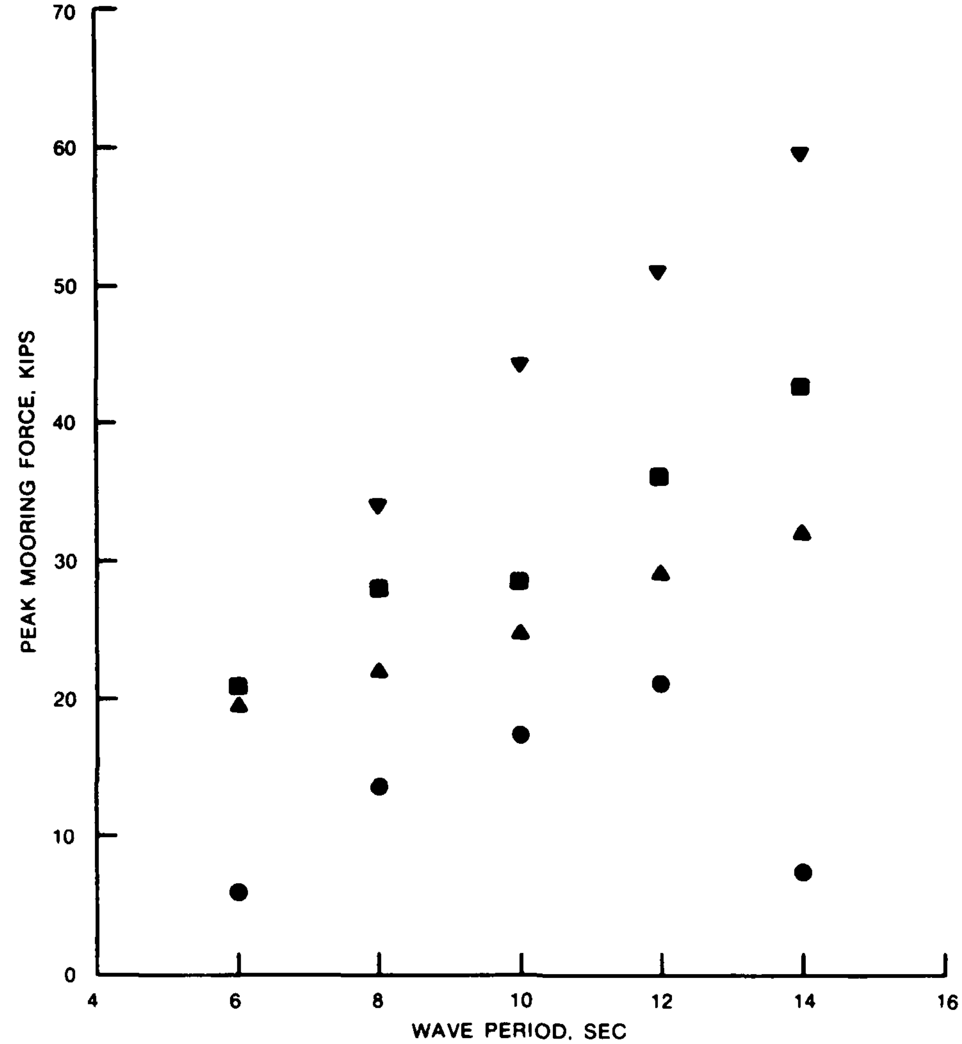

LEGEND

SYMBOL	H_{mo}, FT
●	2
▲	4
■	6
▼	8

PEAK MOORING FORCE VERSUS WAVE PERIOD

118.4-FT SFB; SPECTRAL WAVES; d = 18.0 FT

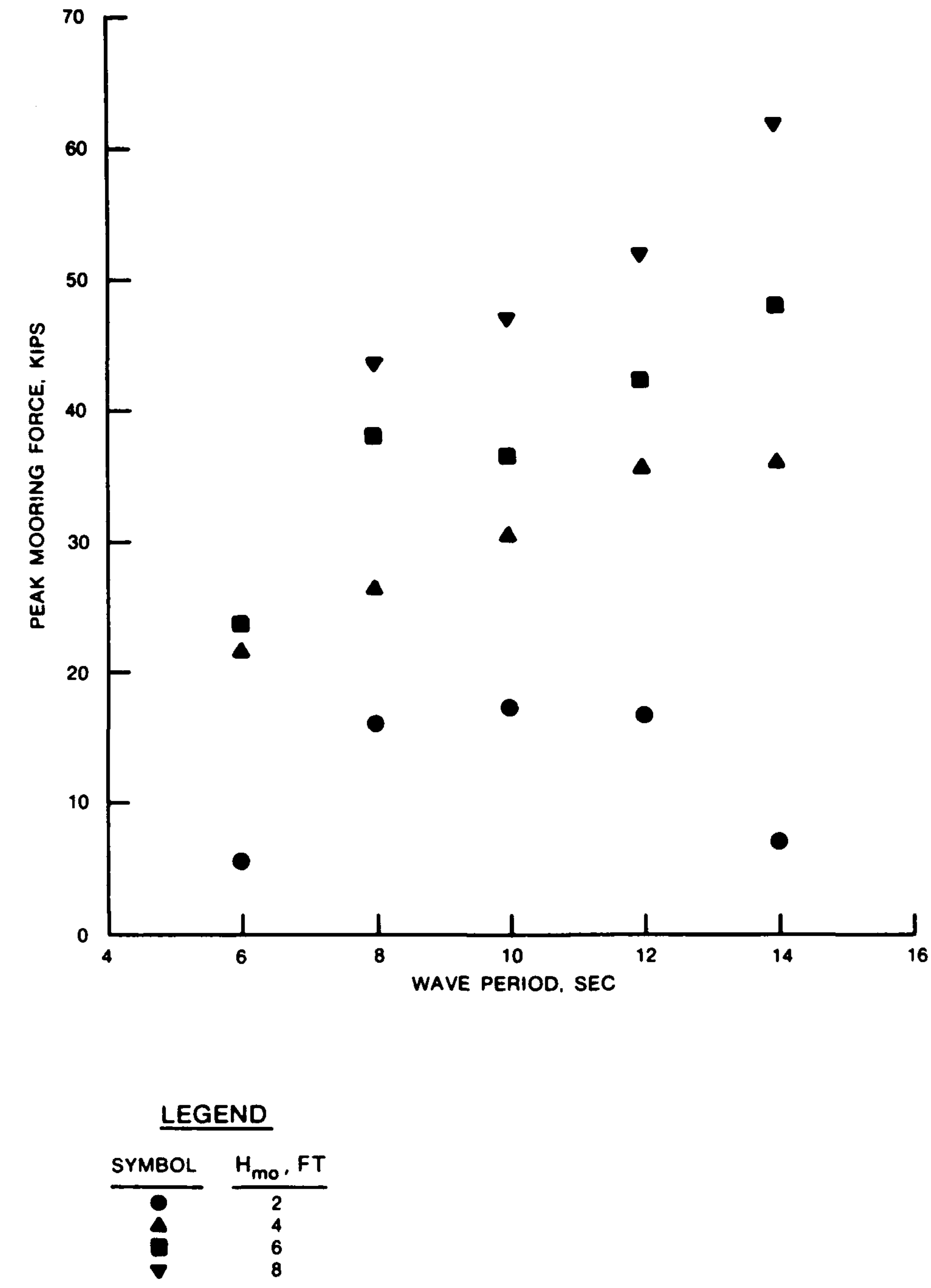

PEAK MOORING FORCE VERSUS WAVE PERIOD

118.4-FT SFB; SPECTRAL WAVES; d = 21.0 FT

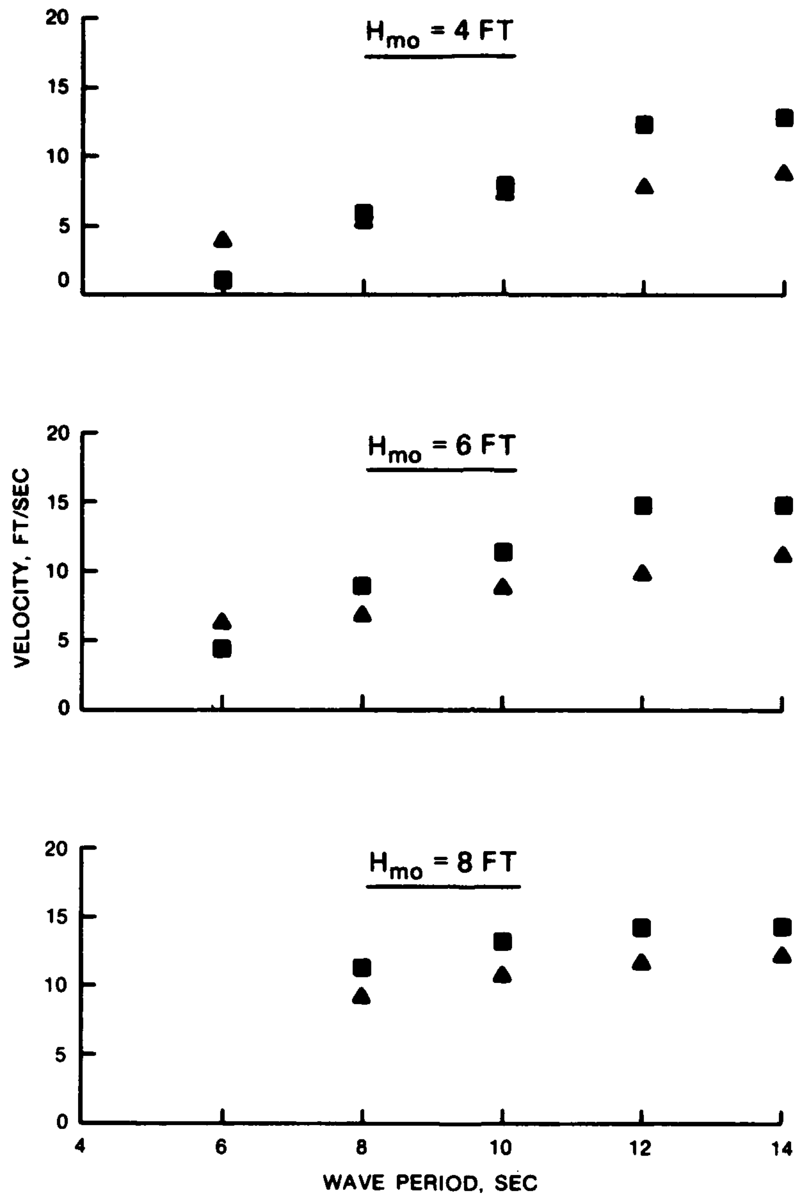

LEGEND

SYMBOL	SFB LENGTH, FT
▲	89.6
■	118.4

PEAK FLOW VELOCITY UNDER SFB VERSUS WAVE PERIOD

SPECTRAL WAVES; d = 13 FT

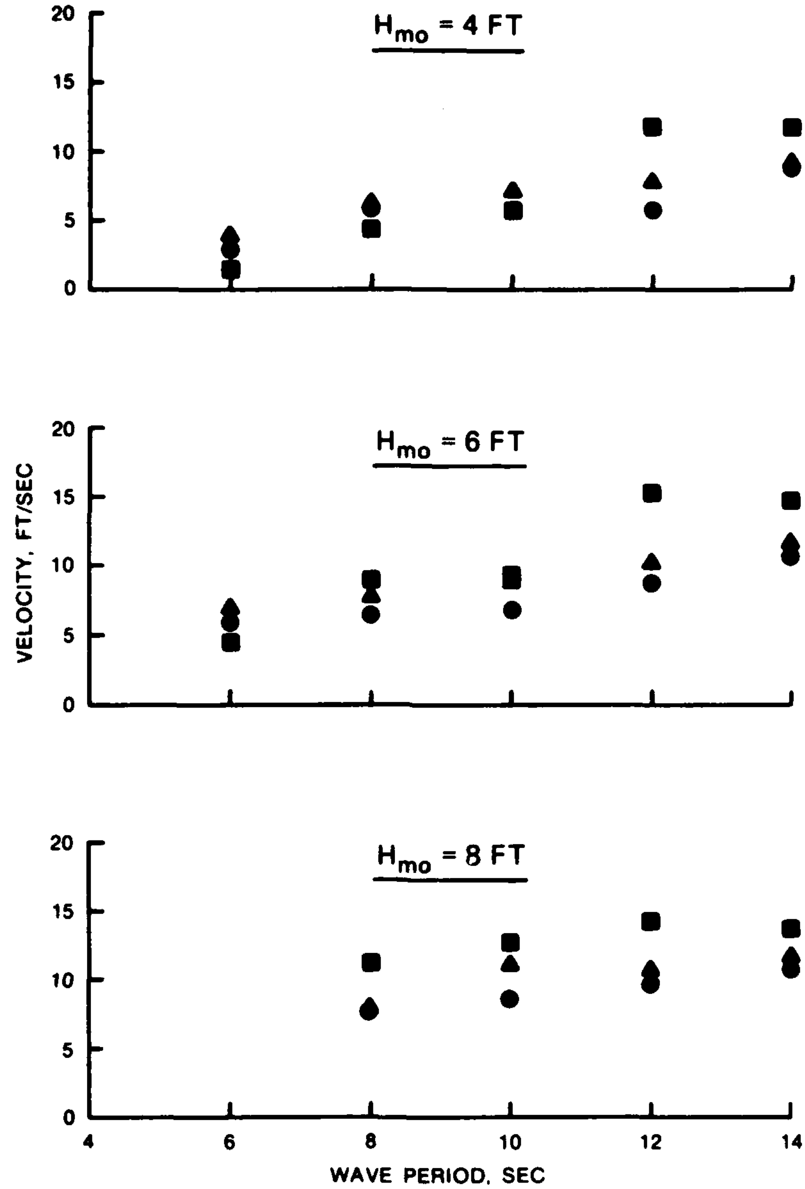

LEGEND

SYMBOL	SFB LENGTH, FT
●	72.3
▲	89.6
■	118.4

PEAK FLOW VELOCITY UNDER SFB VERSUS WAVE PERIOD

SPECTRAL WAVES; d = 15 FT

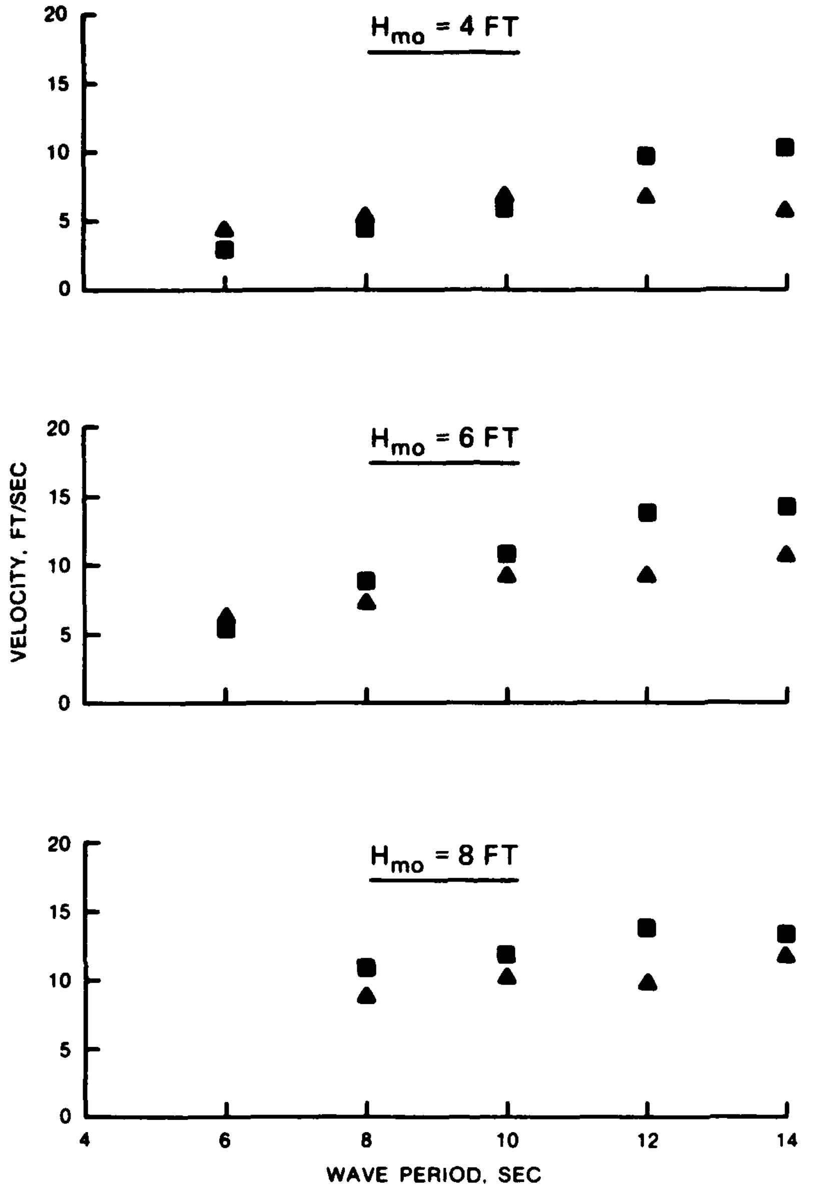

LEGEND

SYMBOL	SFB LENGTH, FT
▲	89.6
■	118.4

PEAK FLOW VELOCITY UNDER SFB VERSUS WAVE PERIOD
SPECTRAL WAVES; d = 18 FT

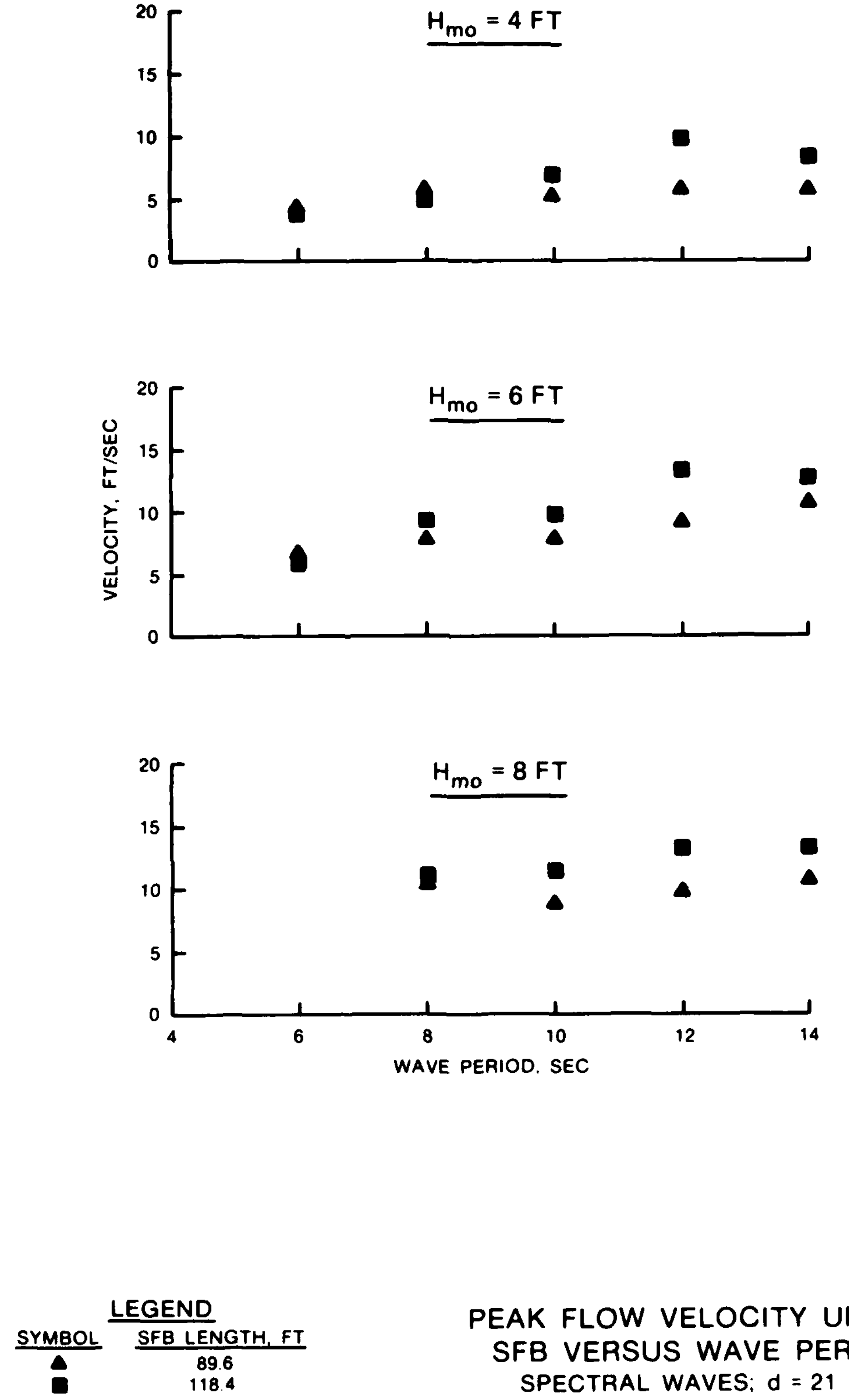

PEAK FLOW VELOCITY UNDER SFB VERSUS WAVE PERIOD
SPECTRAL WAVES; d = 21 FT

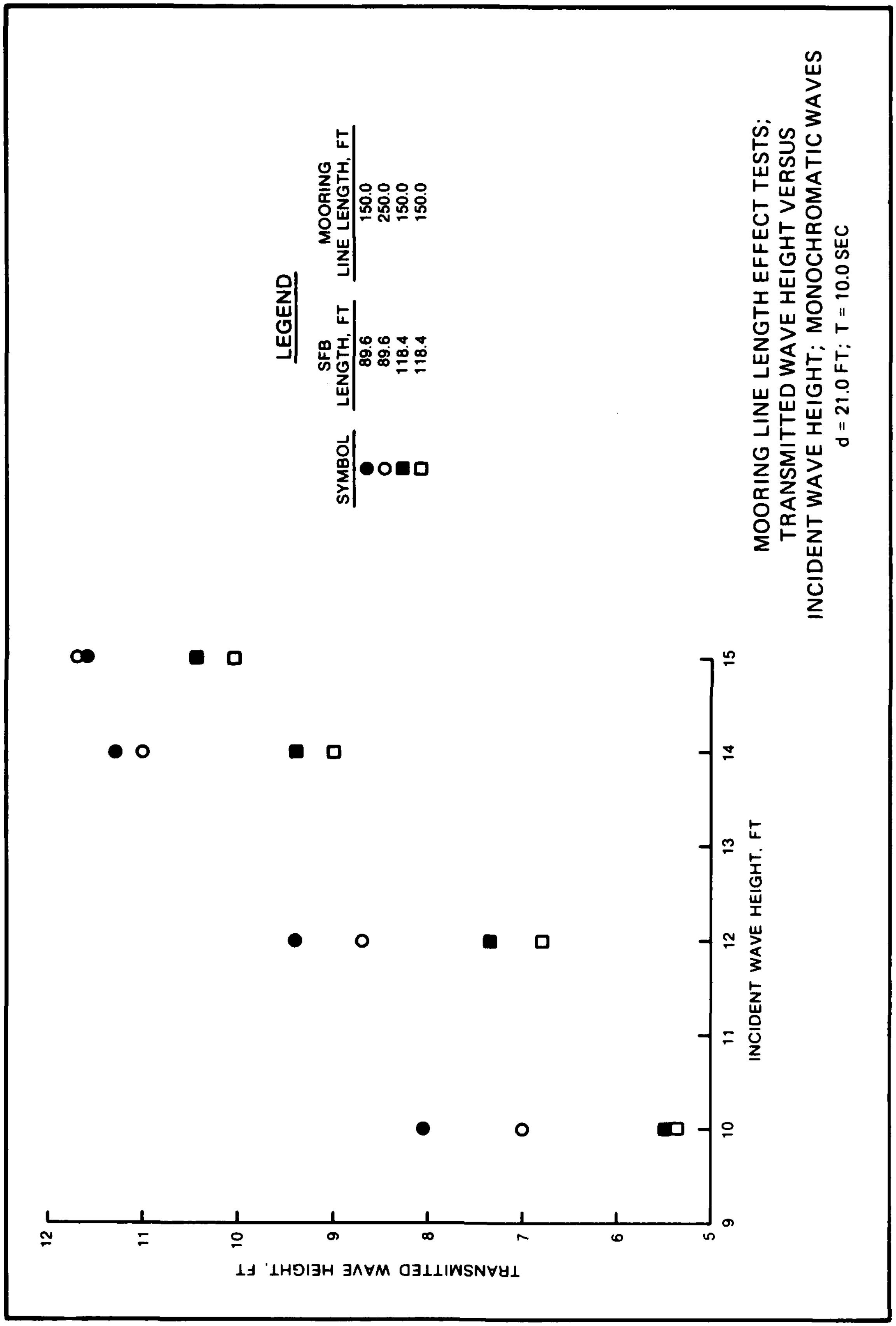

MOORING LINE LENGTH EFFECT TESTS;
TRANSMITTED WAVE HEIGHT VERSUS
INCIDENT WAVE HEIGHT; MONOCHROMATIC WAVES
d = 21.0 FT; T = 10.0 SEC

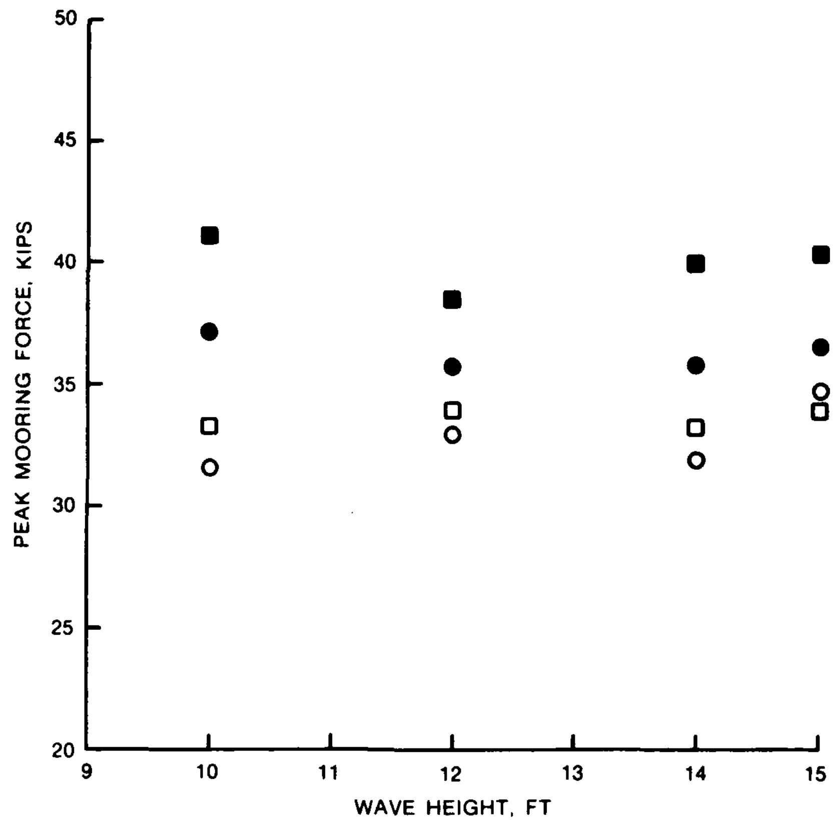

LEGEND

SYMBOL	SFB LENGTH, FT	MOORING LINE LENGTH, FT
●	89.6	150.0
○	89.6	250.0
■	118.4	150.0
□	118.4	250.0

MOORING LINE LENGTH EFFECT TESTS;
PEAK MOORING FORCE VERSUS
WAVE HEIGHT; MONOCHROMATIC WAVES
d = 21.0 FT; T = 10.0 SEC

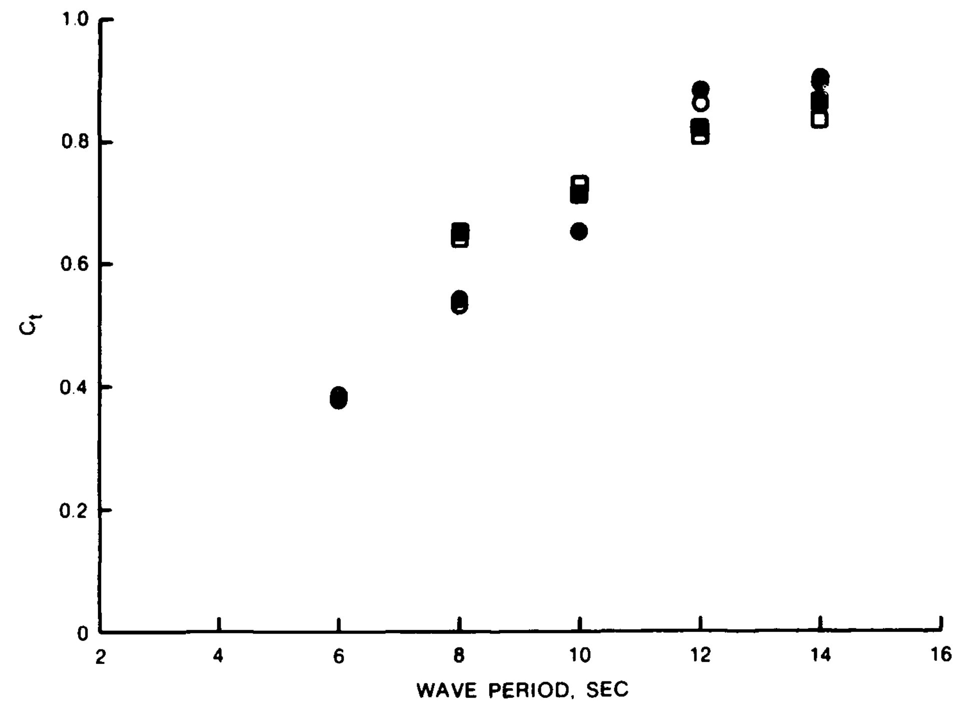

LEGEND

SYMBOL	H_{mo}, FT	MOORING LINE LENGTH, FT
●	4	150.0
○	4	250.0
■	8	150.0
□	8	250.0

MOORING LINE LENGTH EFFECT TESTS;
COEFFICIENT OF TRANSMISSION (C_t)
VERSUS WAVE PERIOD;
89.6-FT SFB; d = 21.0 FT;
SPECTRAL WAVES

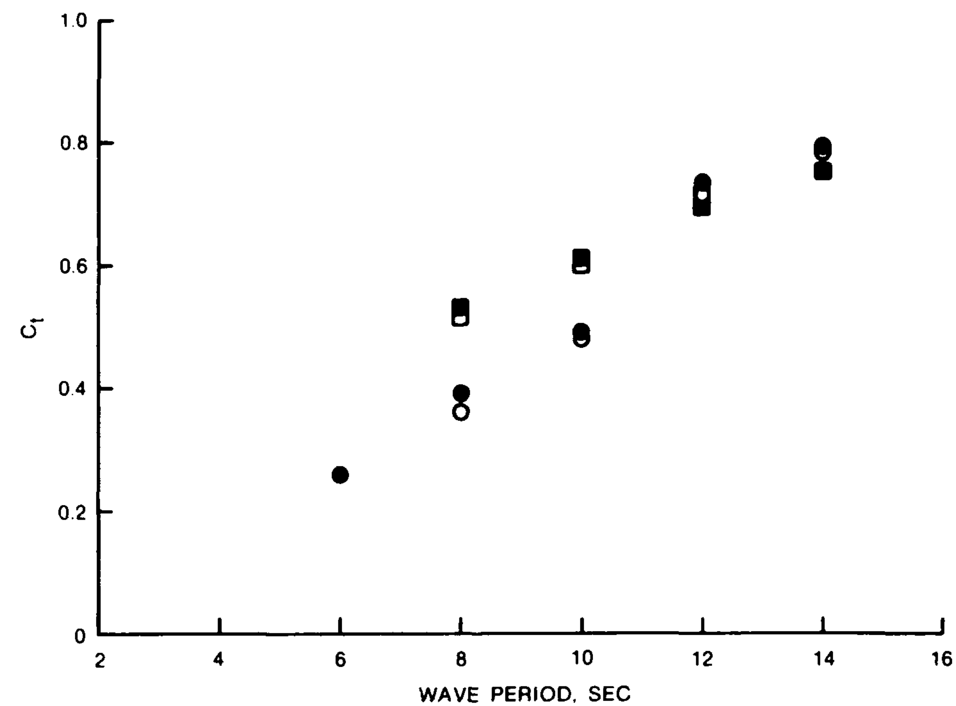

LEGEND

SYMBOL	H_{mo}, FT	MOORING LINE LENGTH, FT
●	4	150.0
○	4	250.0
■	8	150.0
□	8	250.0

MOORING LINE LENGTH EFFECT TESTS;
COEFFICIENT OF TRANSMISSION (C_t)
VERSUS WAVE PERIOD;
118.4-FT SFB; d = 21.0 FT;
SPECTRAL WAVES

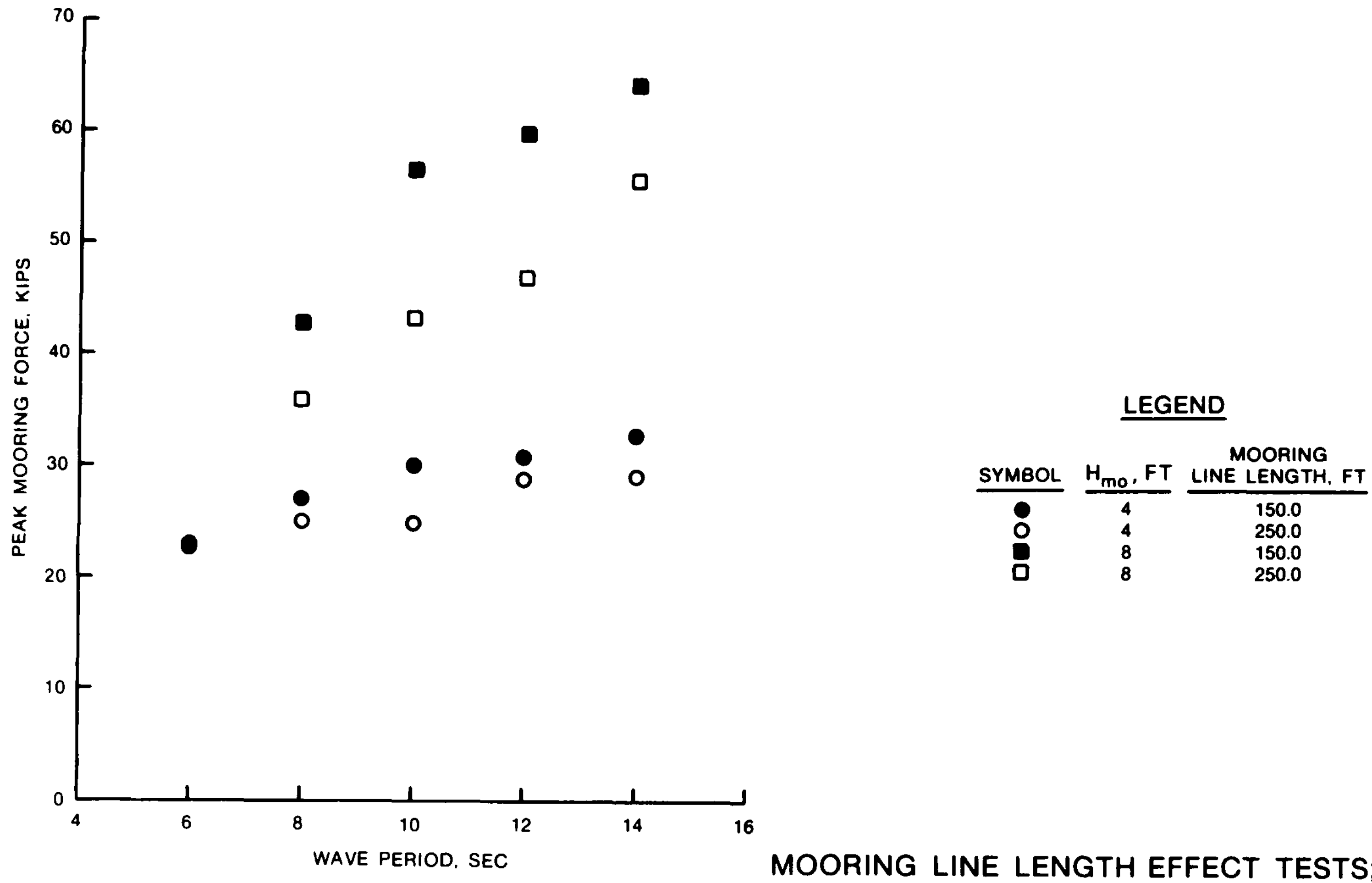

MOORING LINE LENGTH EFFECT TESTS; PEAK MOORING FORCE VERSUS WAVE PERIOD;
89.6-FT SFB; d = 21.0 FT;
SPECTRAL WAVES

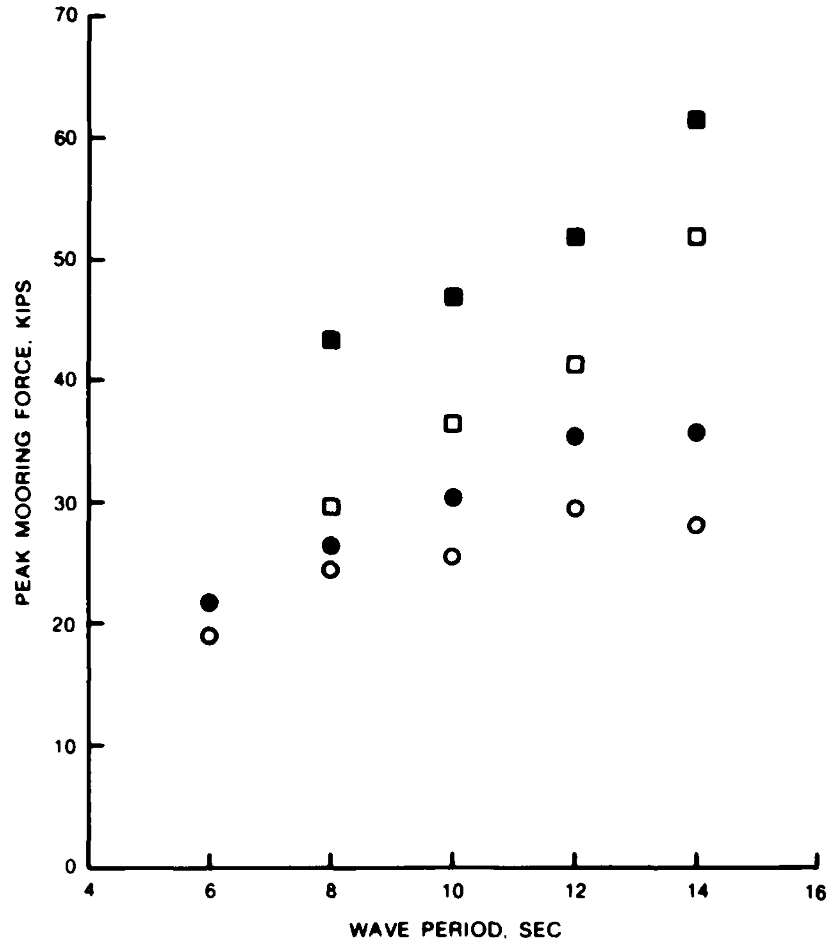

LEGEND

SYMBOL	H_{mo}, FT	MOORING LINE LENGTH, FT
●	4	150.0
○	4	250.0
■	8	150.0
□	8	250.0

MOORING LINE LENGTH EFFECT TESTS; PEAK MOORING FORCE VERSUS WAVE PERIOD; 118.4-FT SFB; d = 21.0 FT; SPECTRAL WAVES

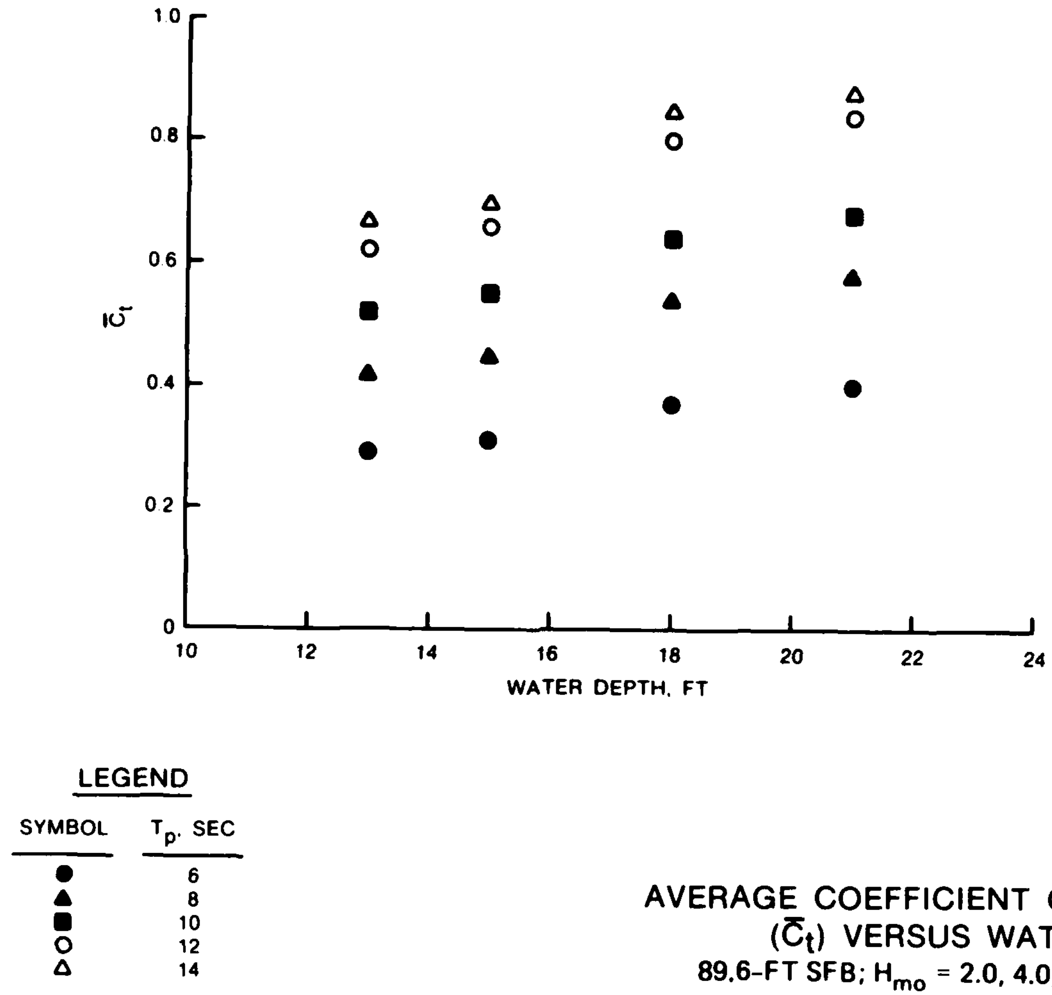

AVERAGE COEFFICIENT OF TRANSMISSION ($\bar{C}_t$) VERSUS WATER DEPTH

89.6-FT SFB; H_{mo} = 2.0, 4.0, 6.0, AND 8.0 FT

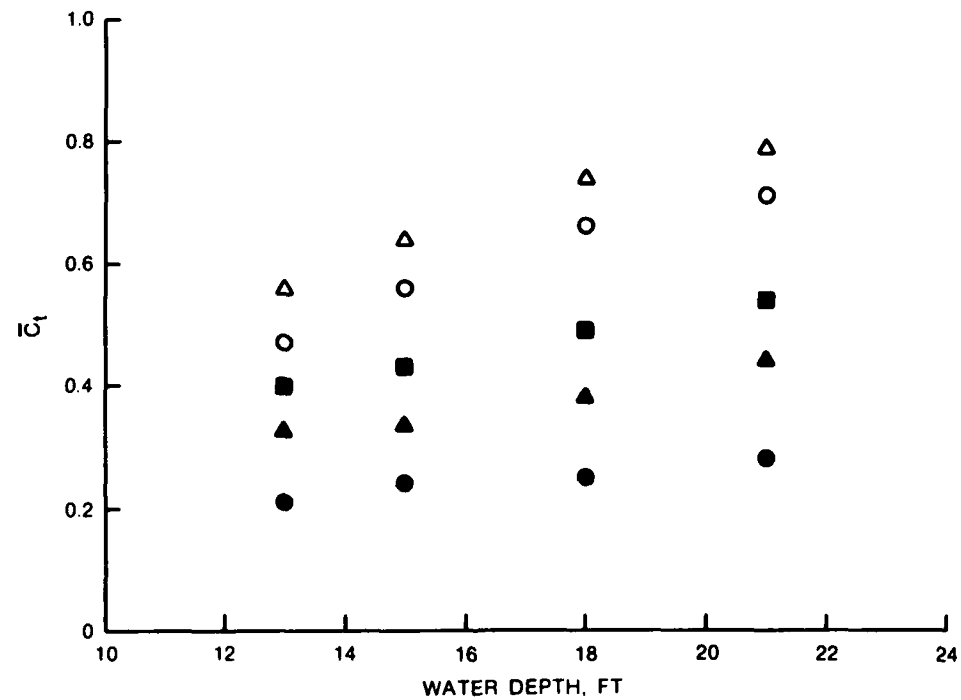

LEGEND

SYMBOL	T_p, SEC
●	6
▲	8
■	10
○	12
△	14

AVERAGE COEFFICIENT OF TRANSMISSION ($\bar{C}_t$) VERSUS WATER DEPTH

118.4-FT SFB; H_{mo} = 2.0, 4.0, 6.0, AND 8.0 FT

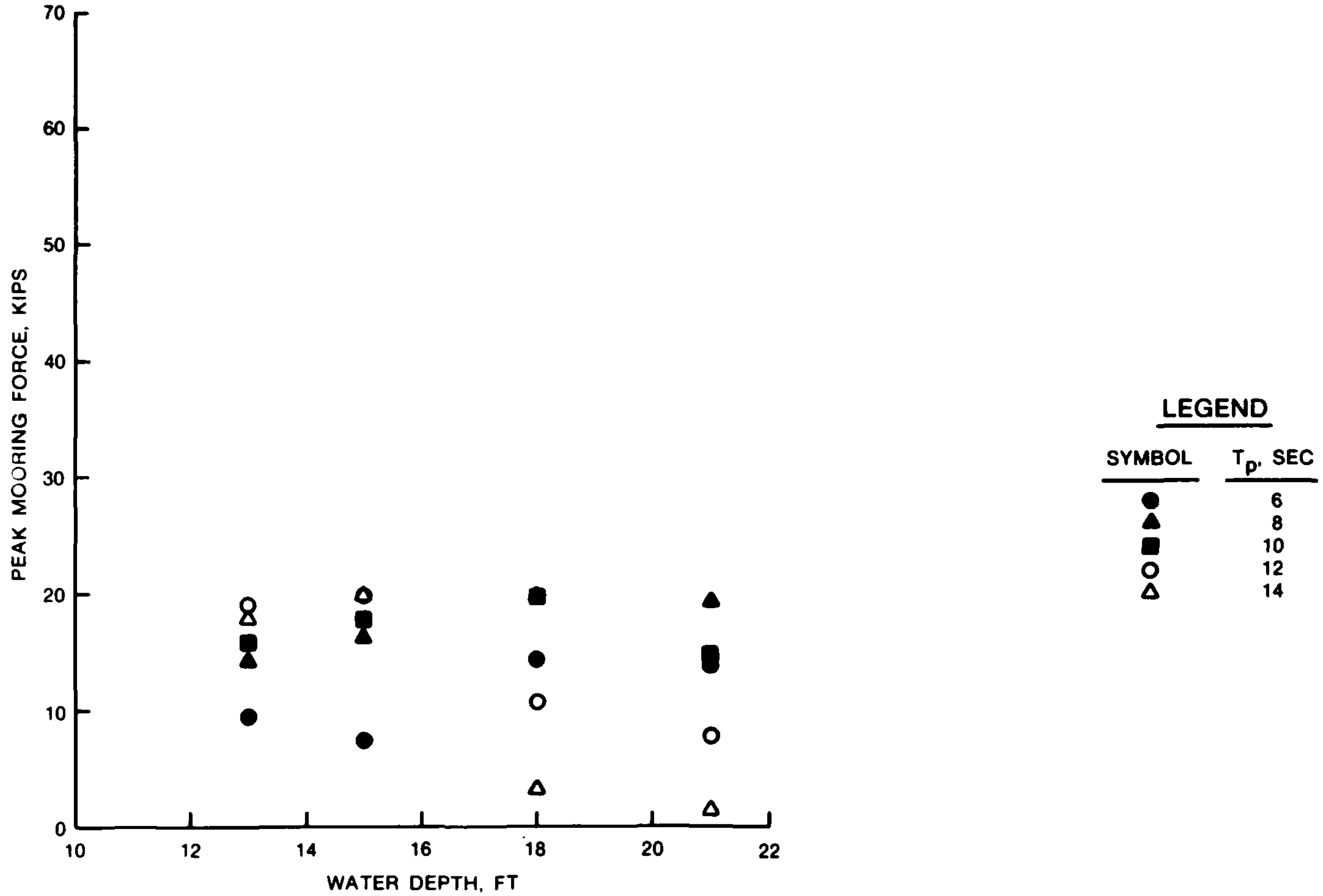

PEAK MOORING FORCE VERSUS WATER DEPTH
89.6-FT SFB; SPECTRAL WAVES; H_{mo} = 2.0 FT

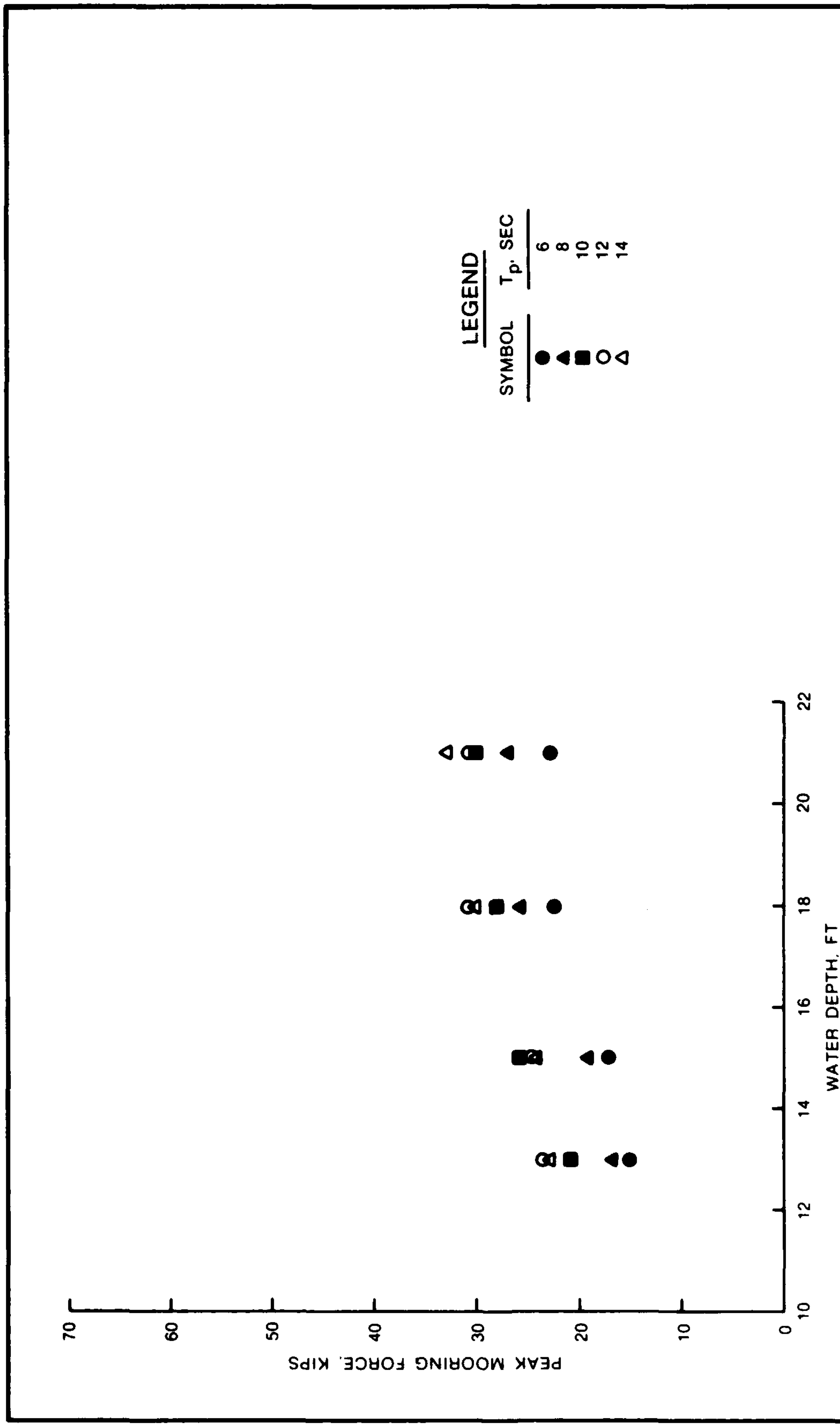

PEAK MOORING FORCE VERSUS WATER DEPTH
89.6-FT SFB; SPECTRAL WAVES; H_{mo} = 4.0 FT

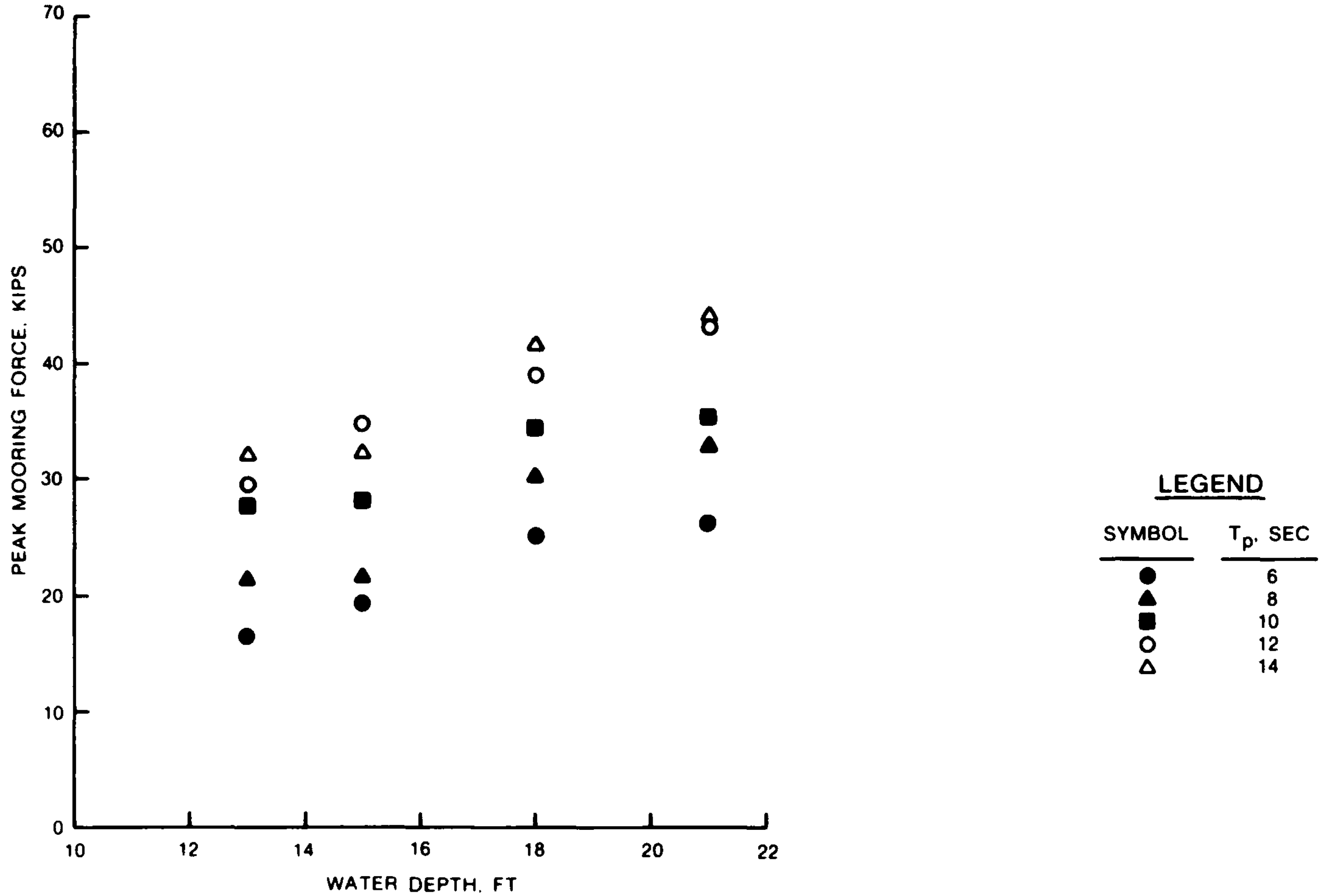

PEAK MOORING FORCE VERSUS WATER DEPTH
89.6-FT SFB; SPECTRAL WAVES; H_{mo} = 6.0 FT

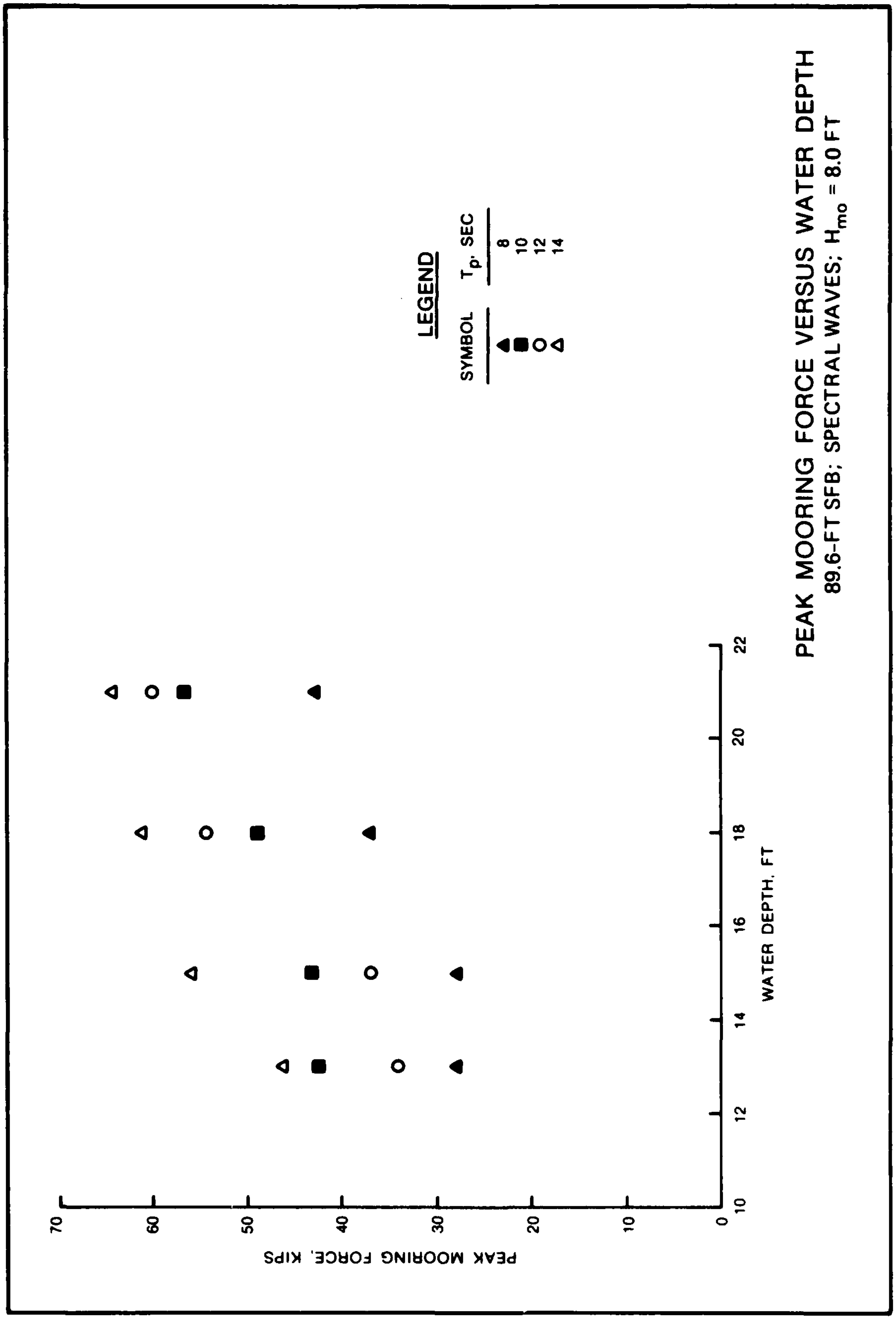

PEAK MOORING FORCE VERSUS WATER DEPTH
89.6-FT SFB; SPECTRAL WAVES; H_{mo} = 8.0 FT

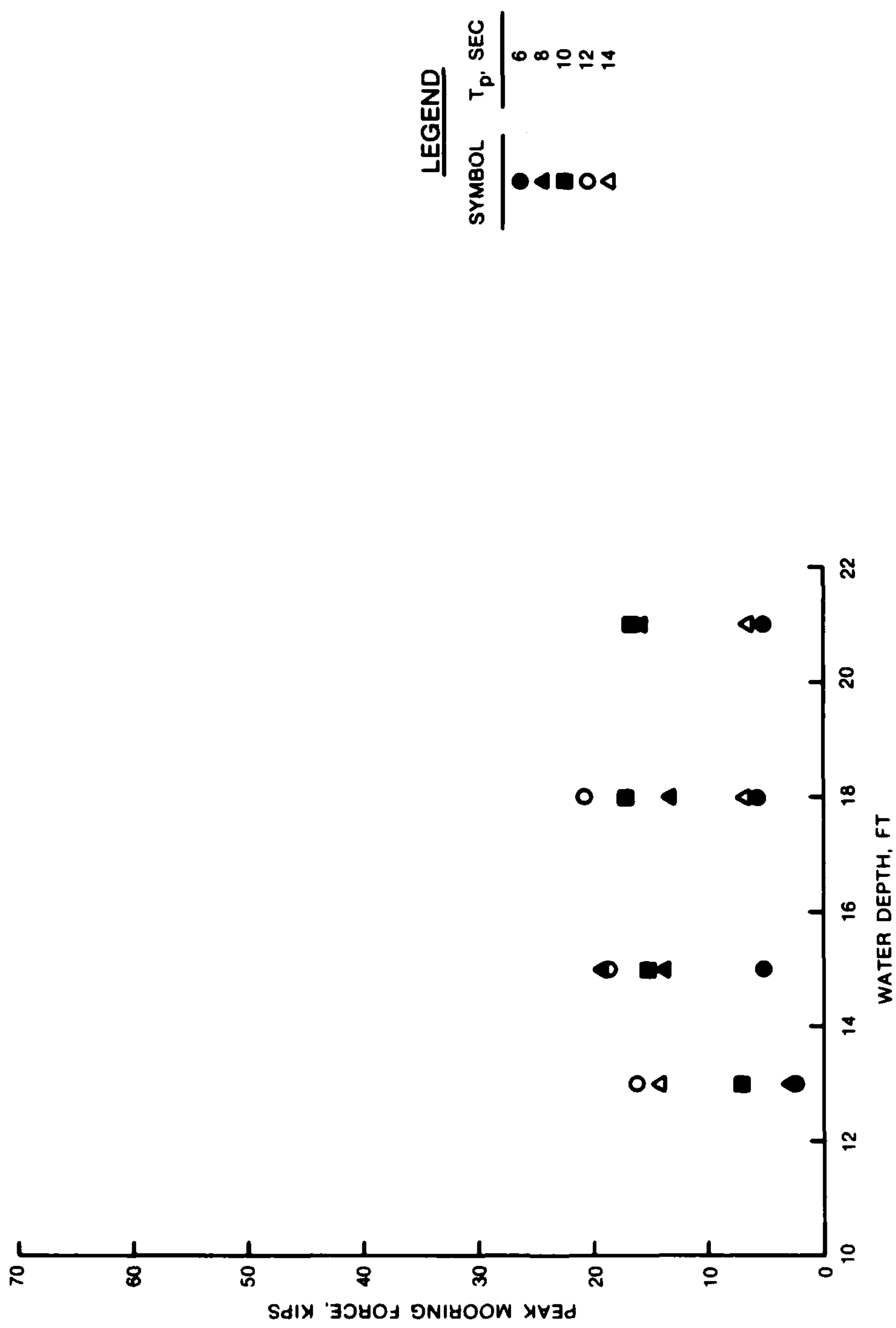

PEAK MOORING FORCE VERSUS WATER DEPTH
118.4-FT SFB; SPECTRAL WAVES; H_{mo} = 2.0 FT

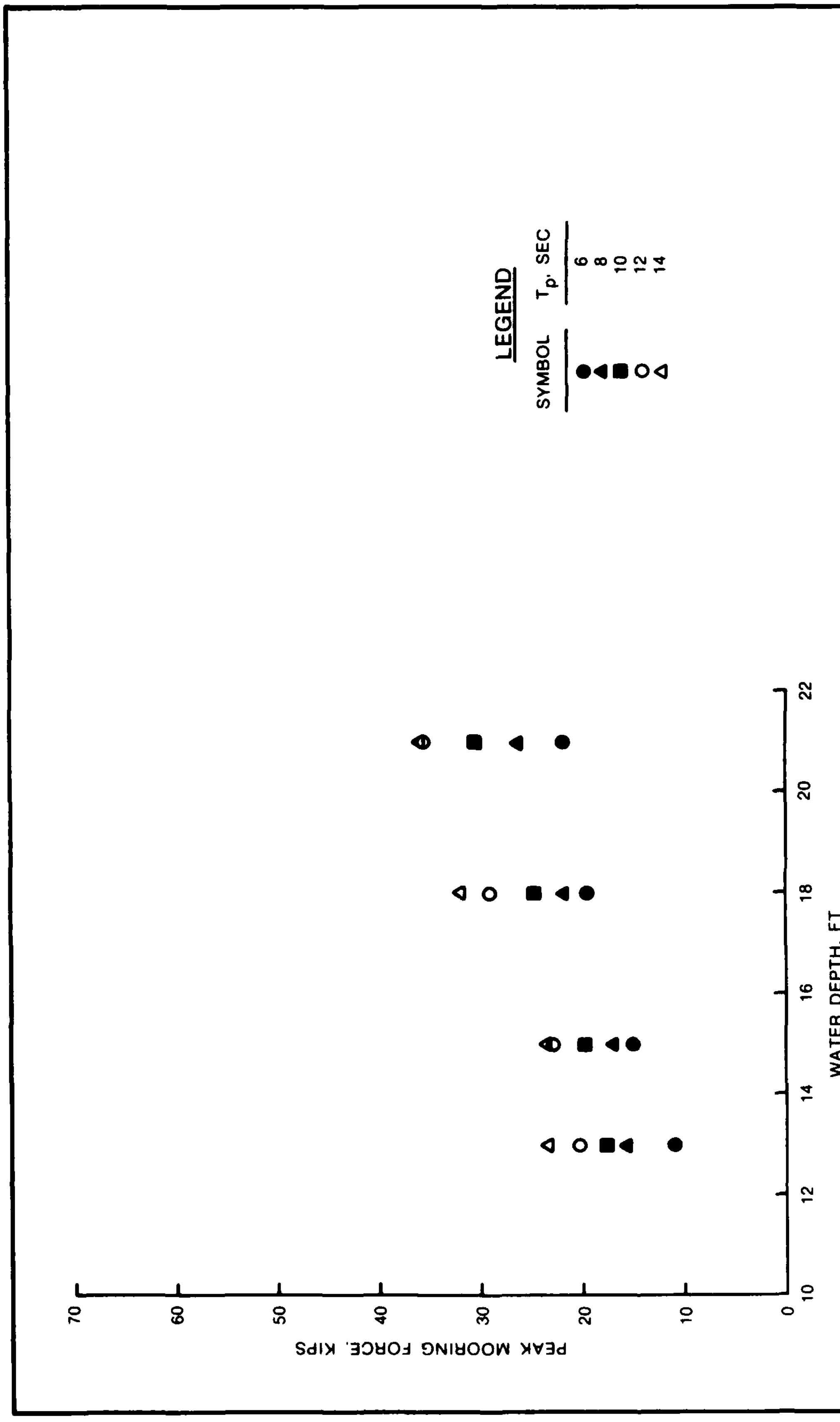

PEAK MOORING FORCE VERSUS WATER DEPTH
118.4-FT SFB; SPECTRAL WAVES; H_{mo} = 4.0 FT

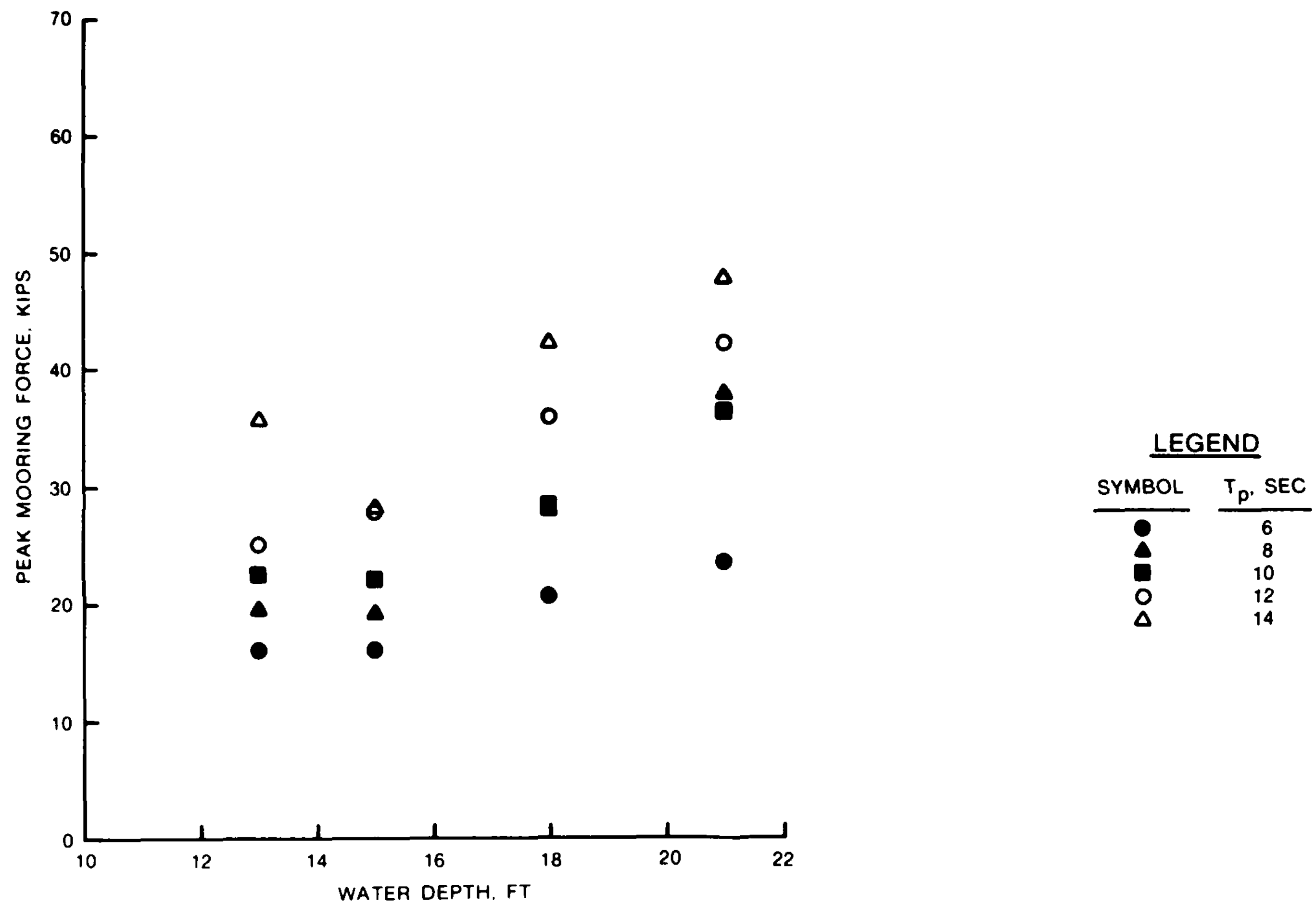

PEAK MOORING FORCE VERSUS WATER DEPTH
118.4-FT SFB; SPECTRAL WAVES; H_{mo} = 6.0 FT

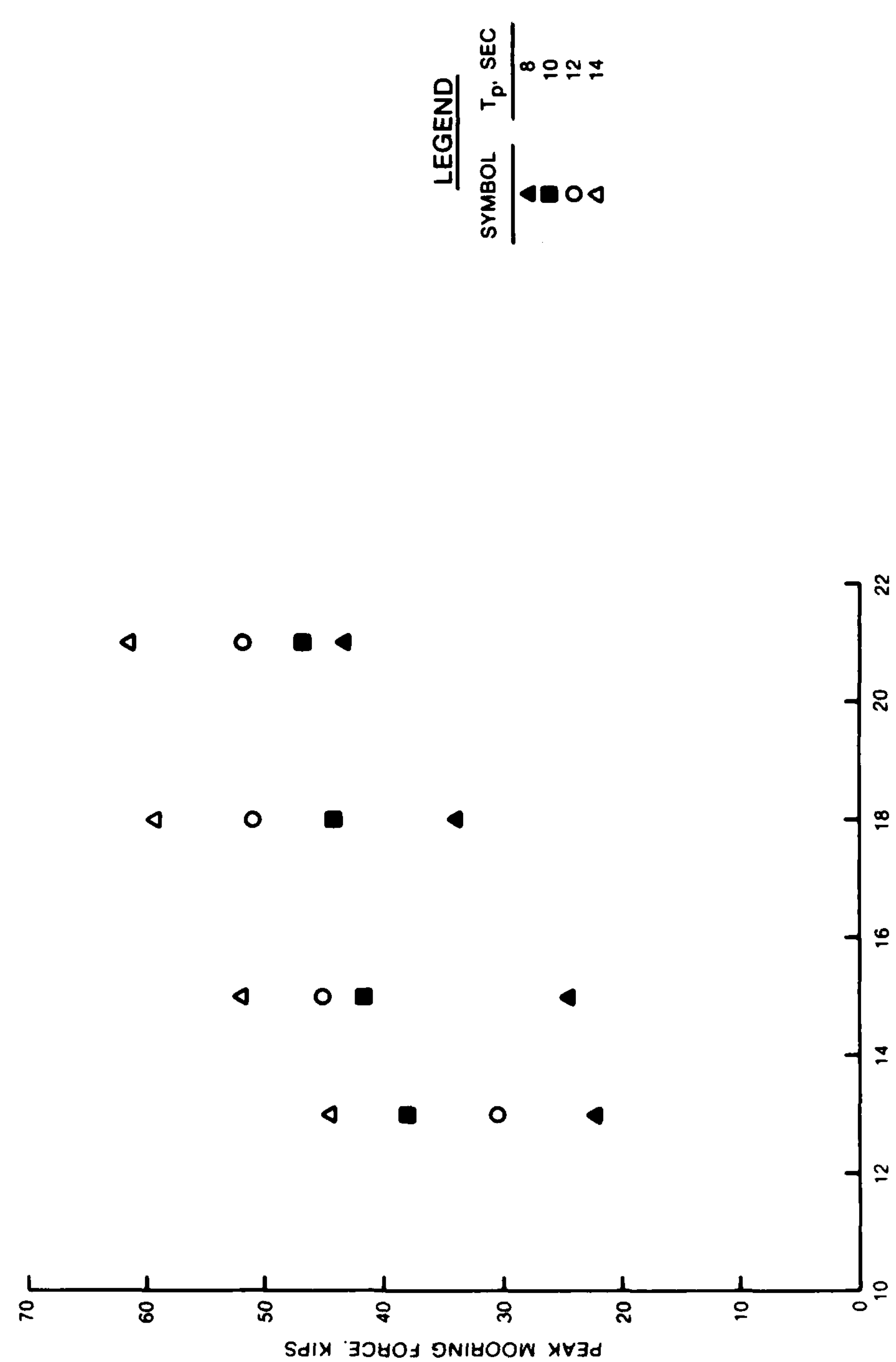

PEAK MOORING FORCE VERSUS WATER DEPTH
118.4-FT SFB; SPECTRAL WAVES; H_{mo} = 8.0 FT

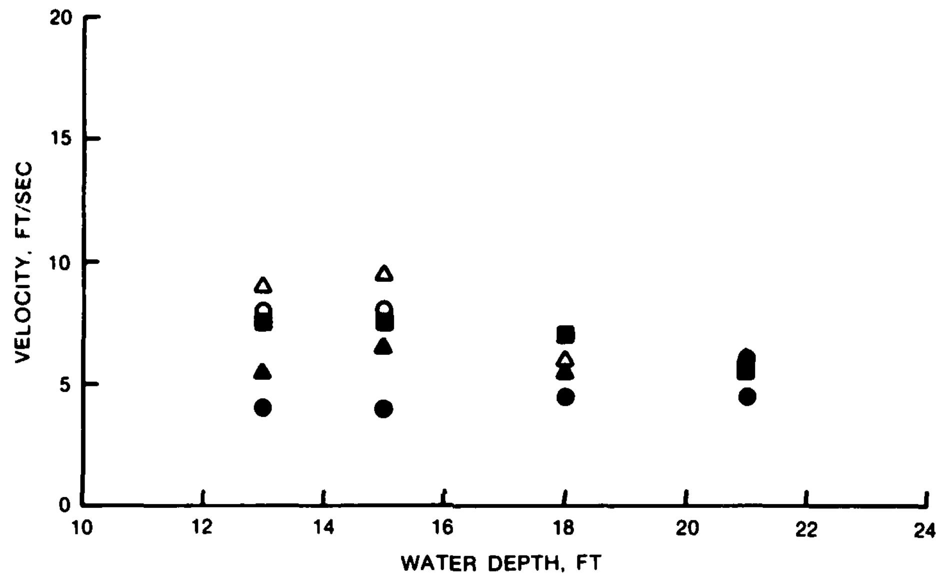

LEGEND

SYMBOL	T_p, SEC
●	6
▲	8
■	10
○	12
△	14

PEAK FLOW VELOCITY UNDER SFB VERSUS WATER DEPTH

89.6-FT SFB; SPECTRAL WAVES; H_{mo} = 4.0 FT

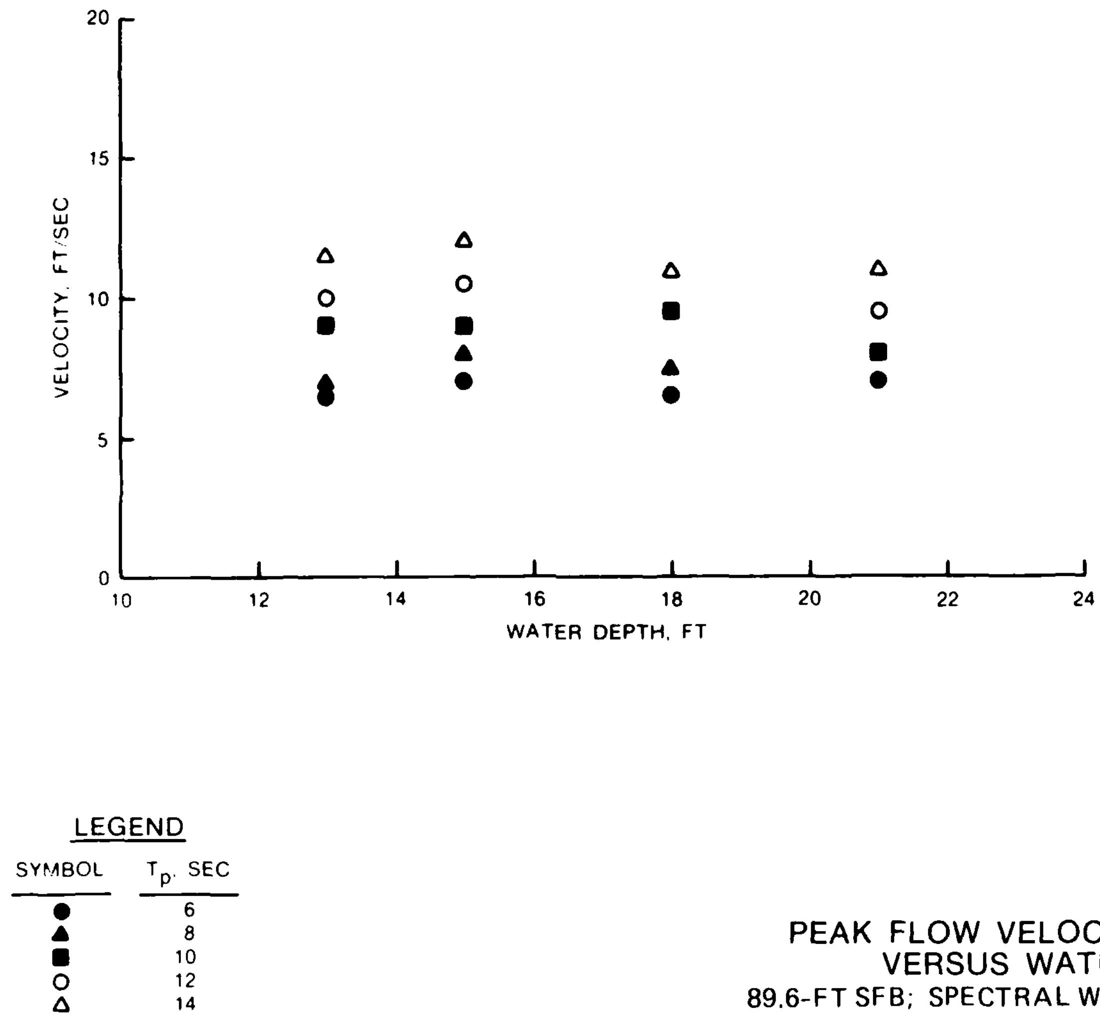

PEAK FLOW VELOCITY UNDER SFB
VERSUS WATER DEPTH
89.6-FT SFB; SPECTRAL WAVES; H_{mo} = 6.0 FT

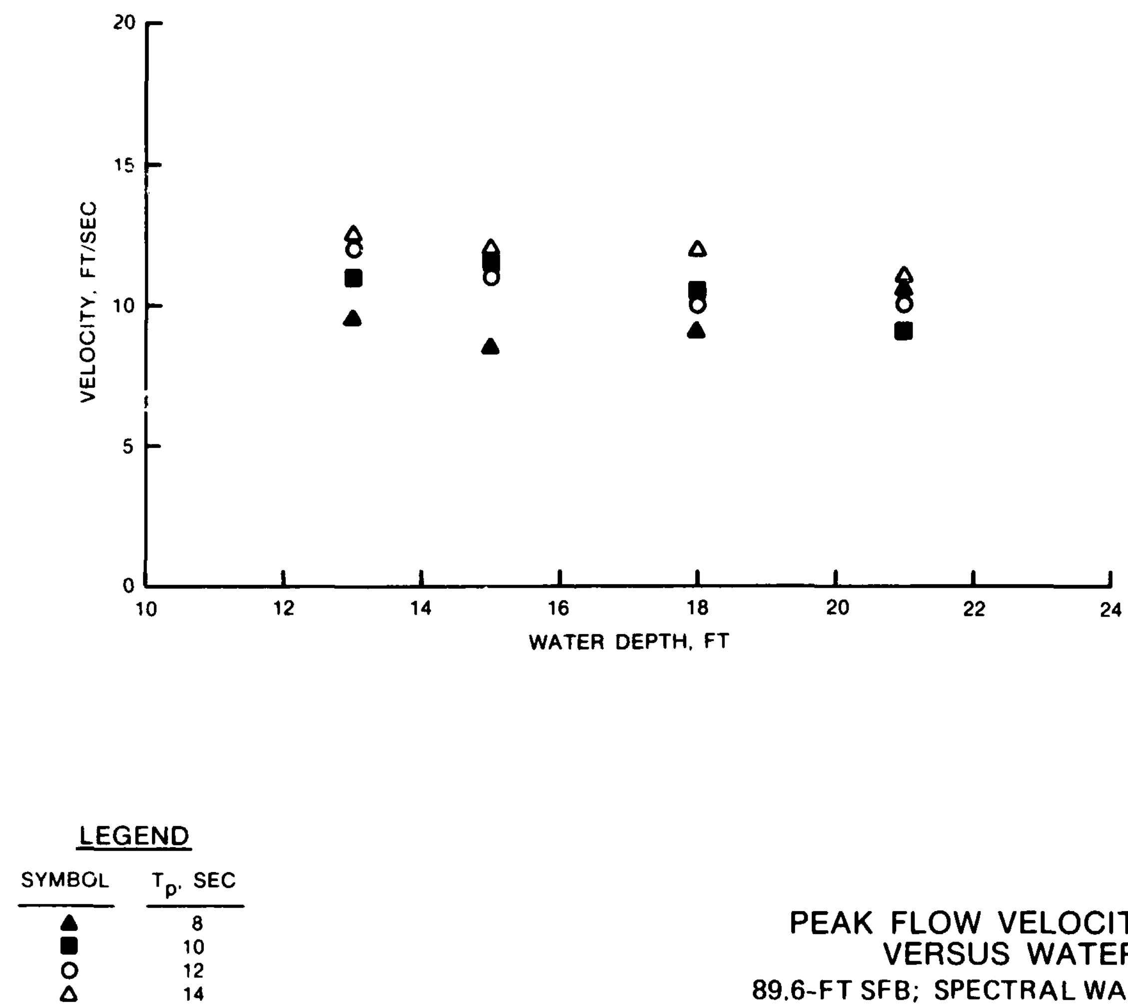

PEAK FLOW VELOCITY UNDER SFB
VERSUS WATER DEPTH

89.6-FT SFB; SPECTRAL WAVES; H_{mo} = 8.0 FT

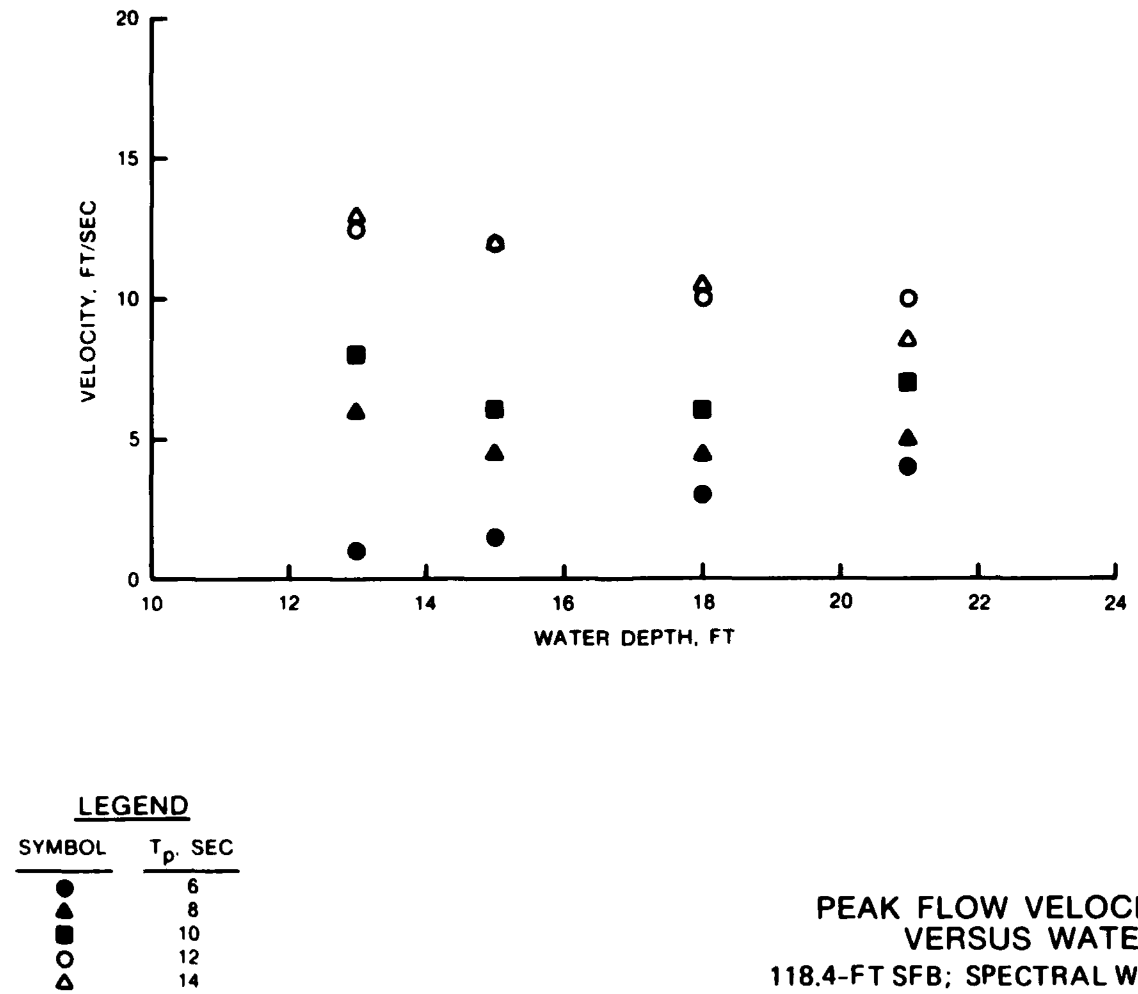

PEAK FLOW VELOCITY UNDER SFB
VERSUS WATER DEPTH

118.4-FT SFB; SPECTRAL WAVES; H_{mo} = 4.0 FT

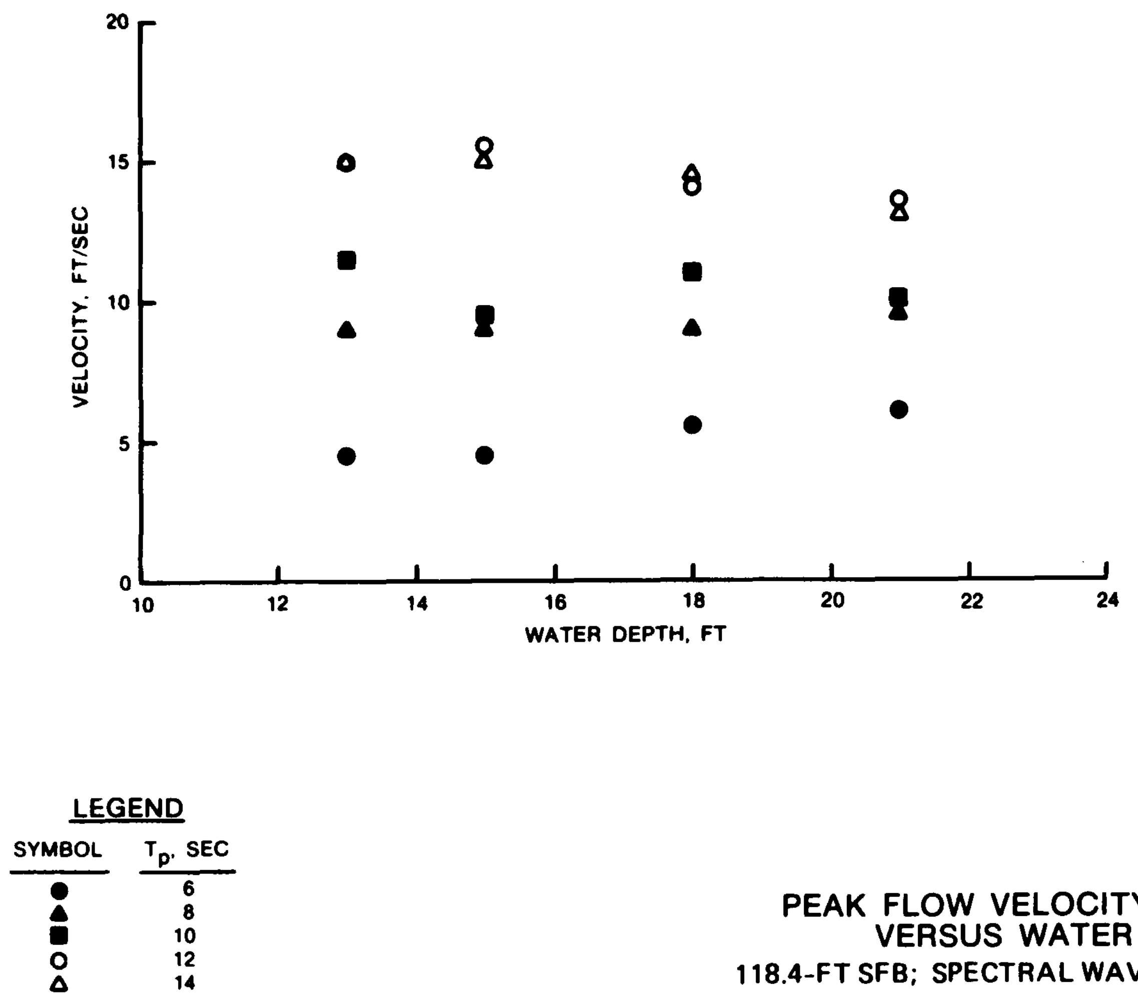

PEAK FLOW VELOCITY UNDER SFB VERSUS WATER DEPTH

118.4-FT SFB; SPECTRAL WAVES; H_{mo} = 6.0 FT

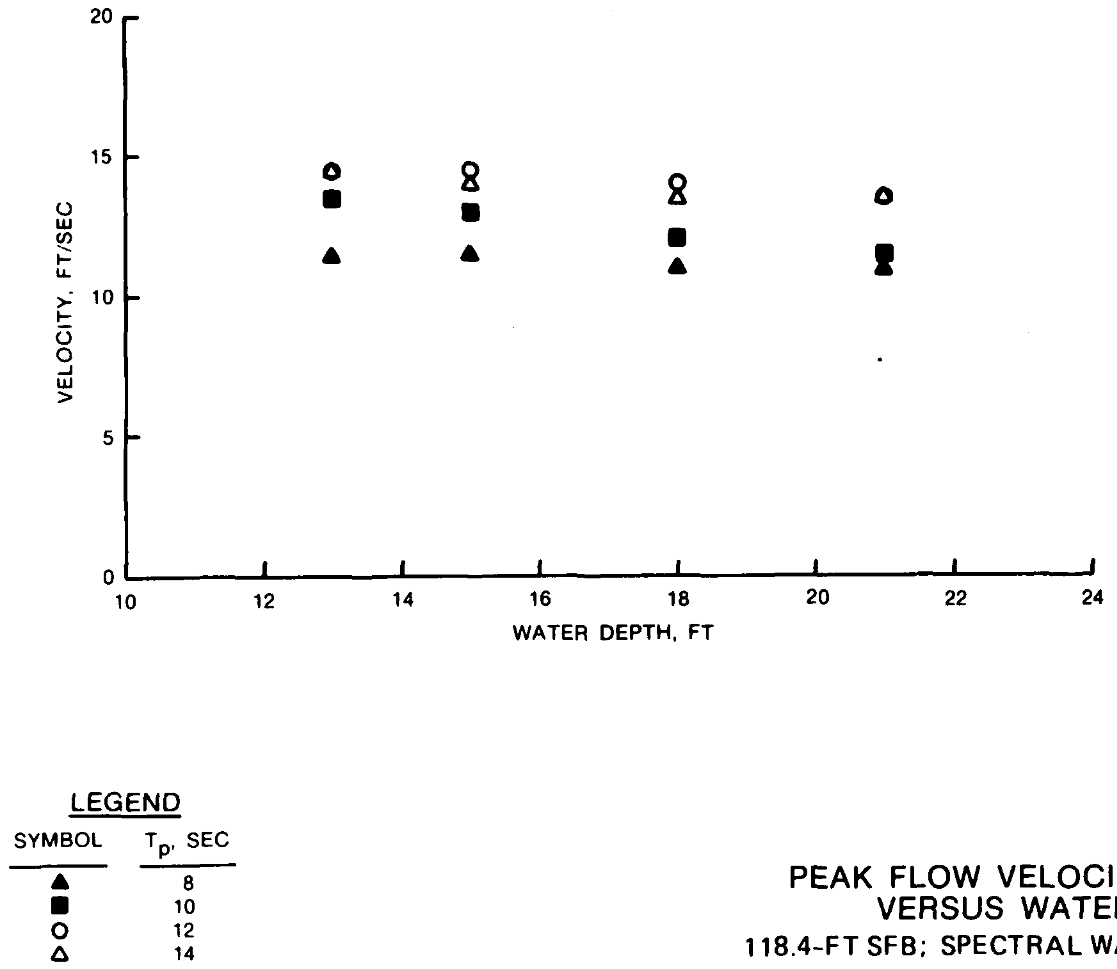

PEAK FLOW VELOCITY UNDER SFB
VERSUS WATER DEPTH

118.4-FT SFB; SPECTRAL WAVES; H_{mo} = 8.0 FT

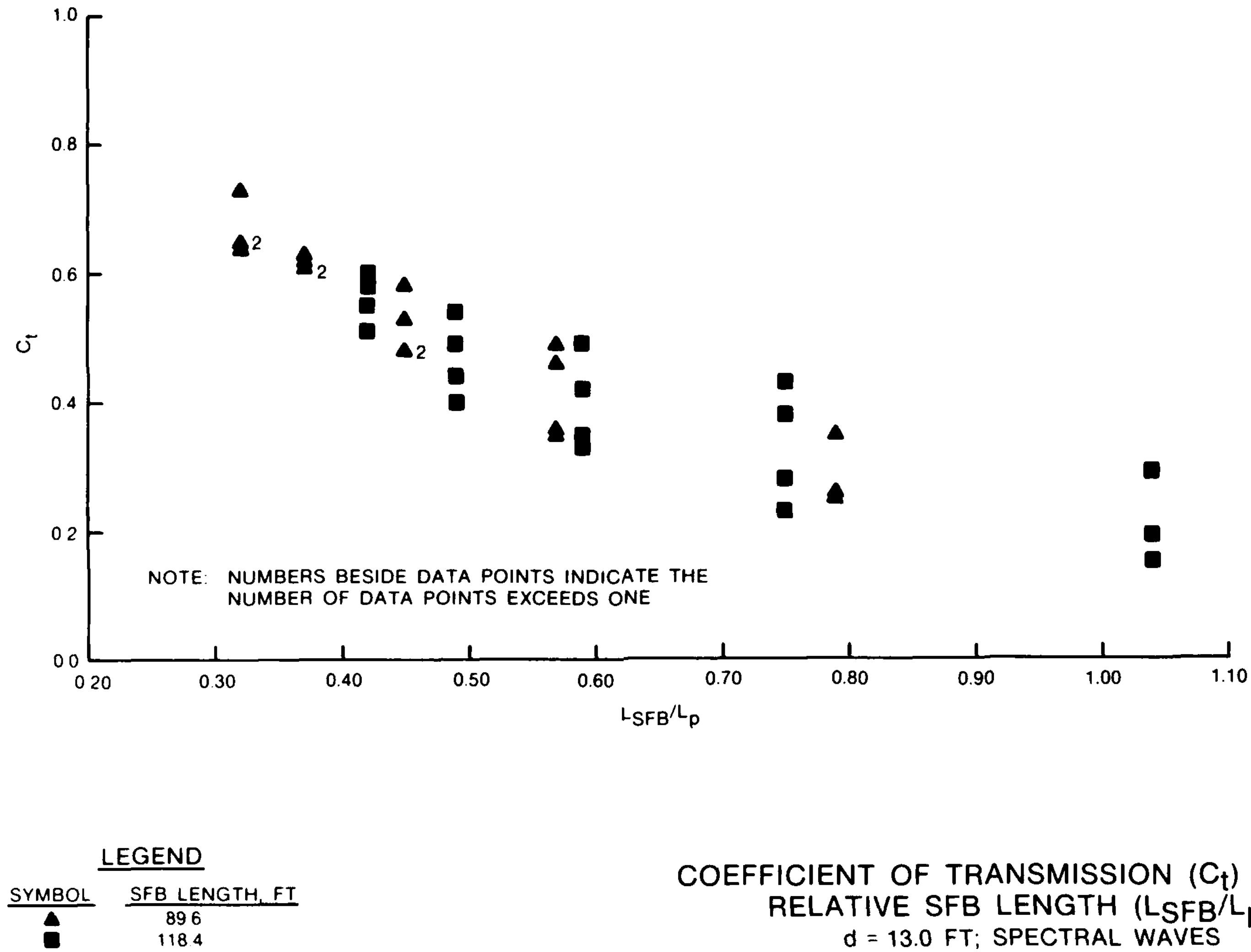

COEFFICIENT OF TRANSMISSION (C_t) VERSUS RELATIVE SFB LENGTH (L_{SFB}/L_p);
d = 13.0 FT; SPECTRAL WAVES

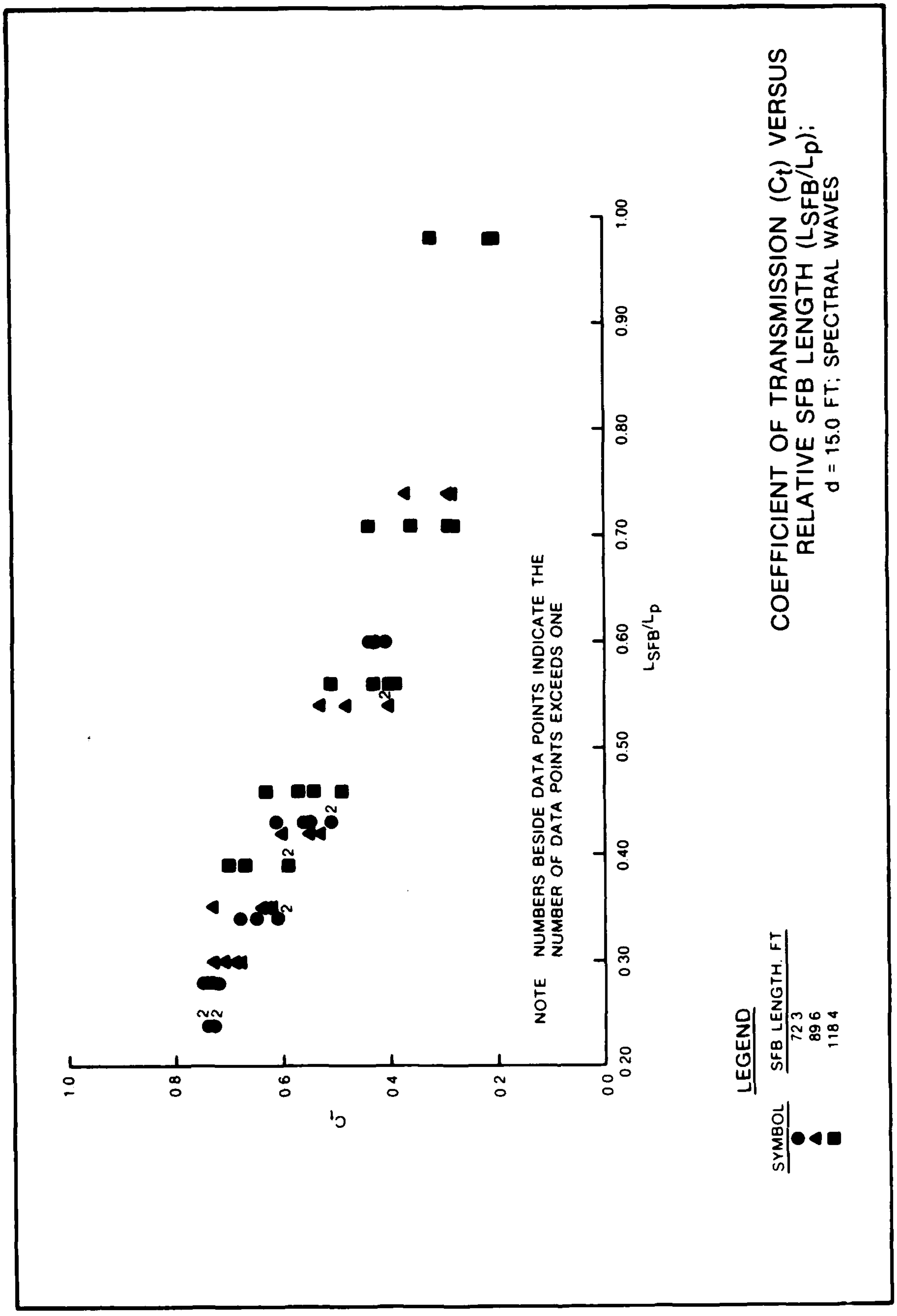

COEFFICIENT OF TRANSMISSION (C_t) VERSUS RELATIVE SFB LENGTH (L_{SFB}/L_p);
d = 15.0 FT; SPECTRAL WAVES

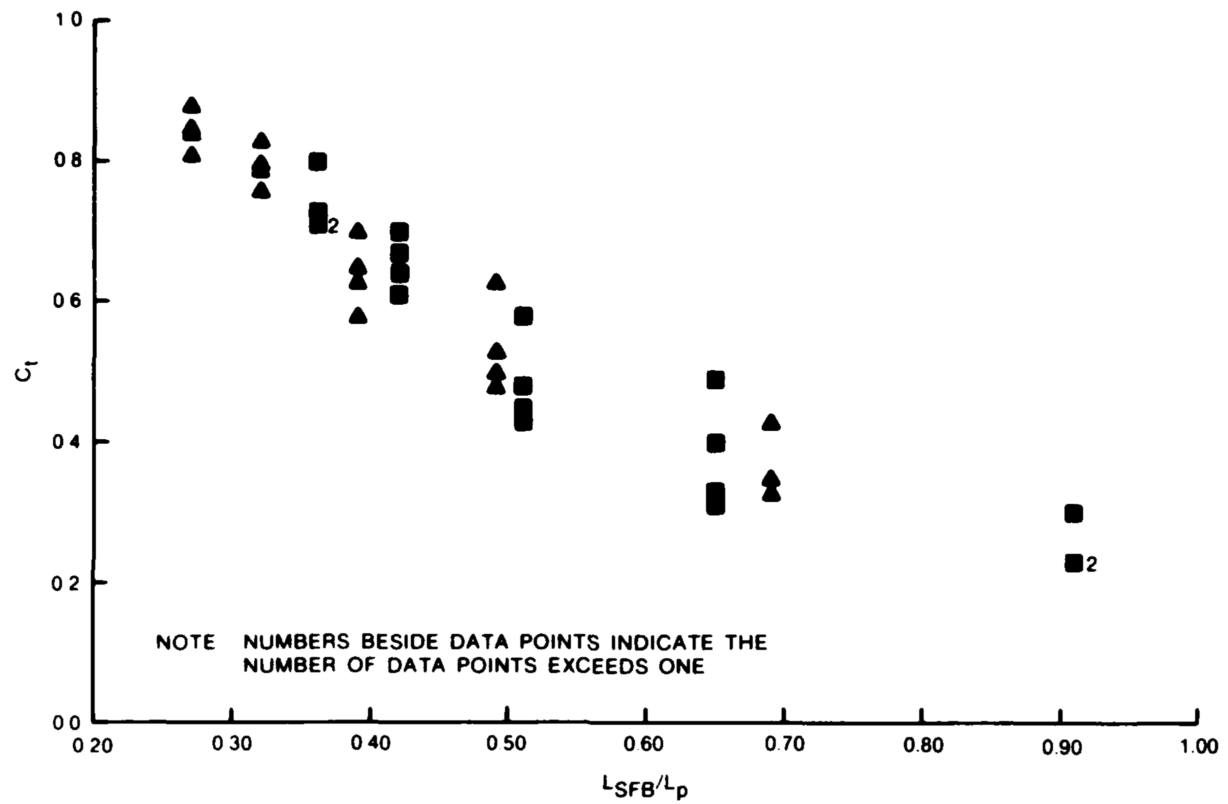

LEGEND

SYMBOL	SFB LENGTH, FT
▲	89.6
■	118.4

COEFFICIENT OF TRANSMISSION (C_t) VERSUS RELATIVE SFB LENGTH (L_{SFB}/L_p);
d = 18.0 FT; SPECTRAL WAVES

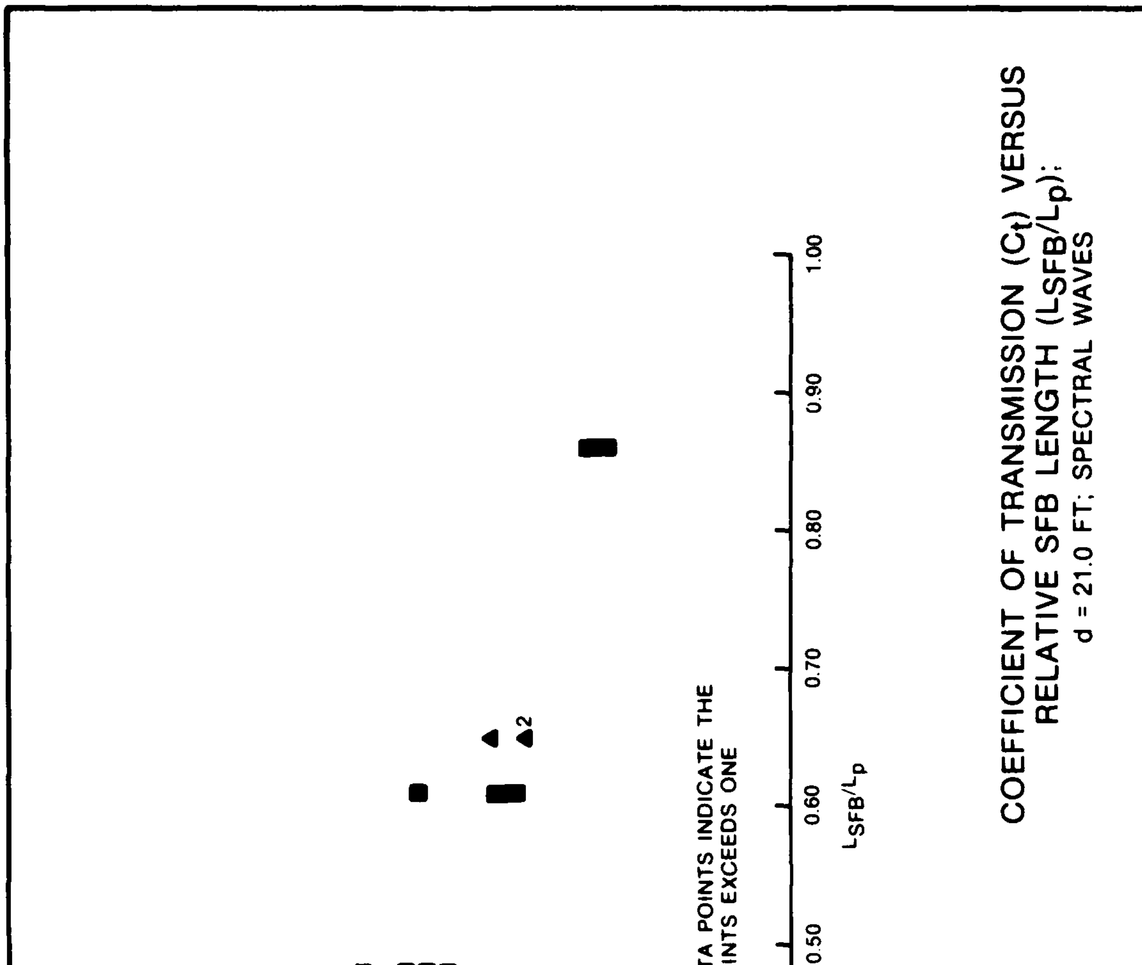

COEFFICIENT OF TRANSMISSION (C_t) VERSUS RELATIVE SFB LENGTH (L_{SFB}/L_p);
d = 21.0 FT; SPECTRAL WAVES

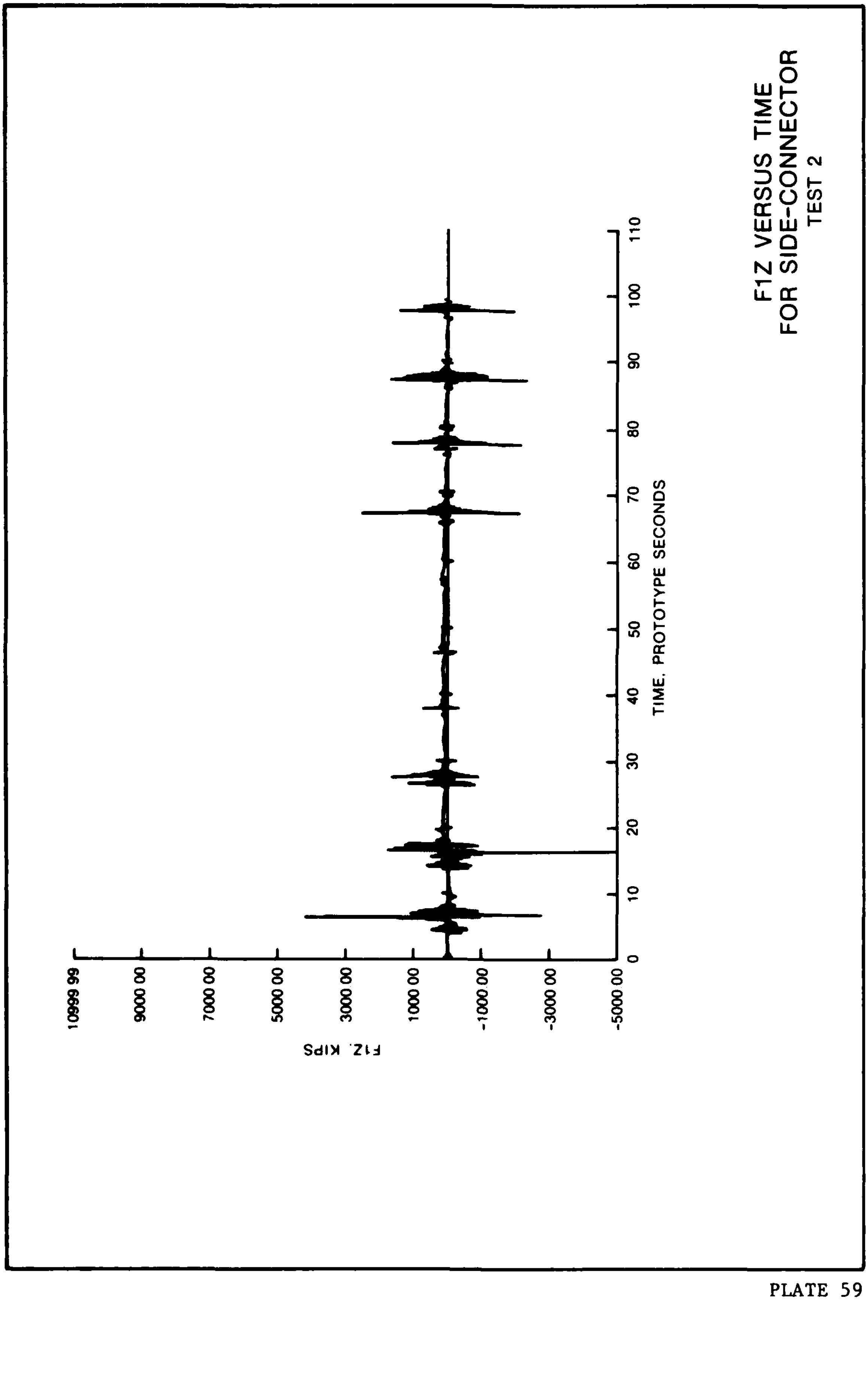
F1Z VERSUS TIME
FOR SIDE-CONNECTOR
TEST 2
F1Z, KIPS
10999.99
9000.00
7000.00
5000.00
3000.00
1000.00
-1000.00
-3000.00
-5000.00
0
10
20
30
40
50
60
70
80
90
100
110
TIME, PROTOTYPE SECONDS

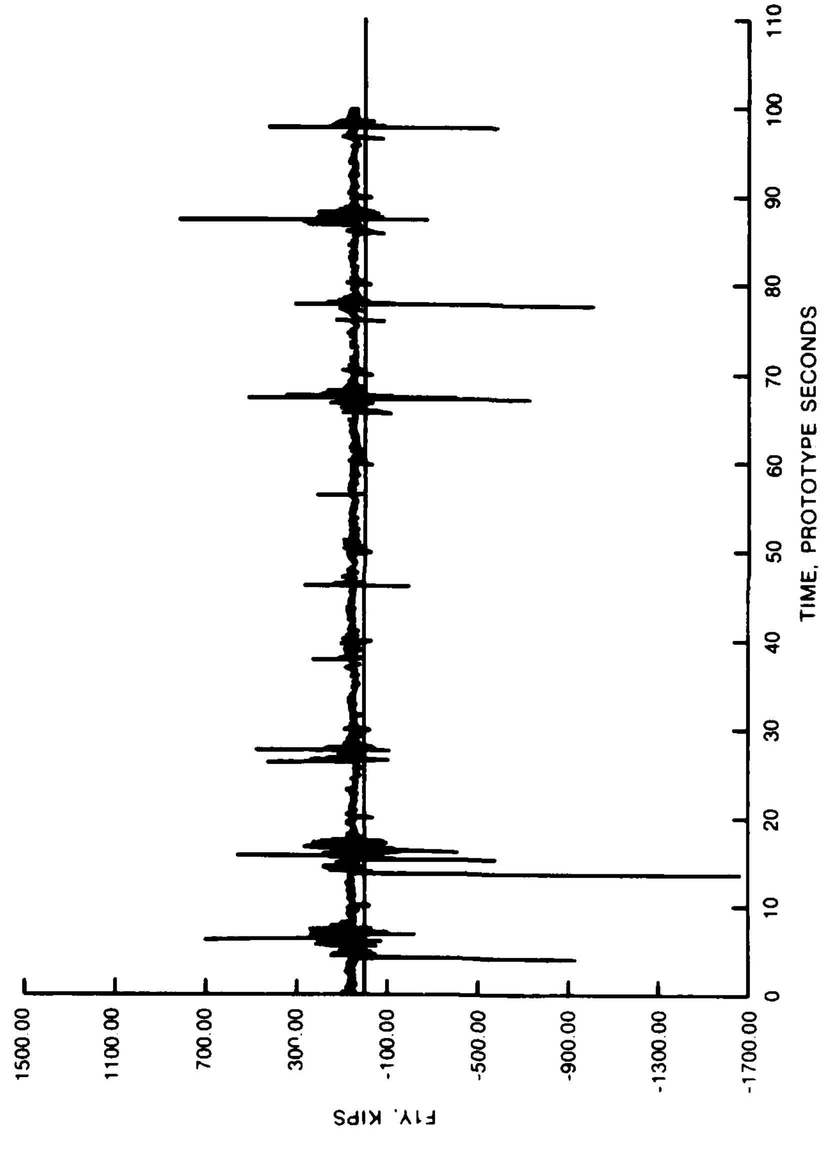

F1Y VERSUS TIME
FOR SIDE-CONNECTOR
TEST 2

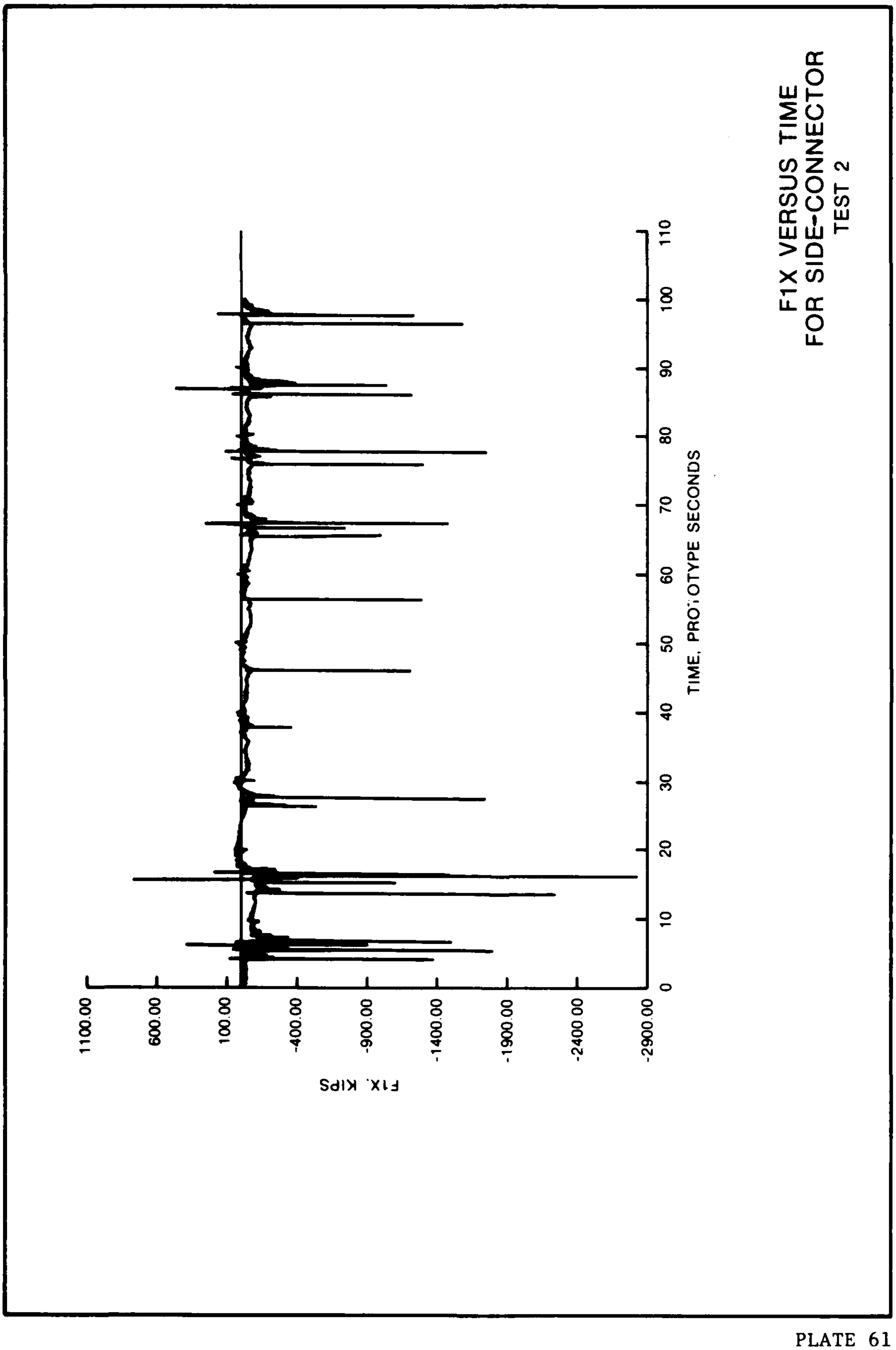
F1X VERSUS TIME
FOR SIDE-CONNECTOR
TEST 2
F1X, KIPS
1100.00
600.00
100.00
-400.00
-900.00
-1400.00
-1900.00
-2400.00
-2900.00
TIME, PROTOTYPE SECONDS
0
10
20
30
40
50
60
70
80
90
100
110

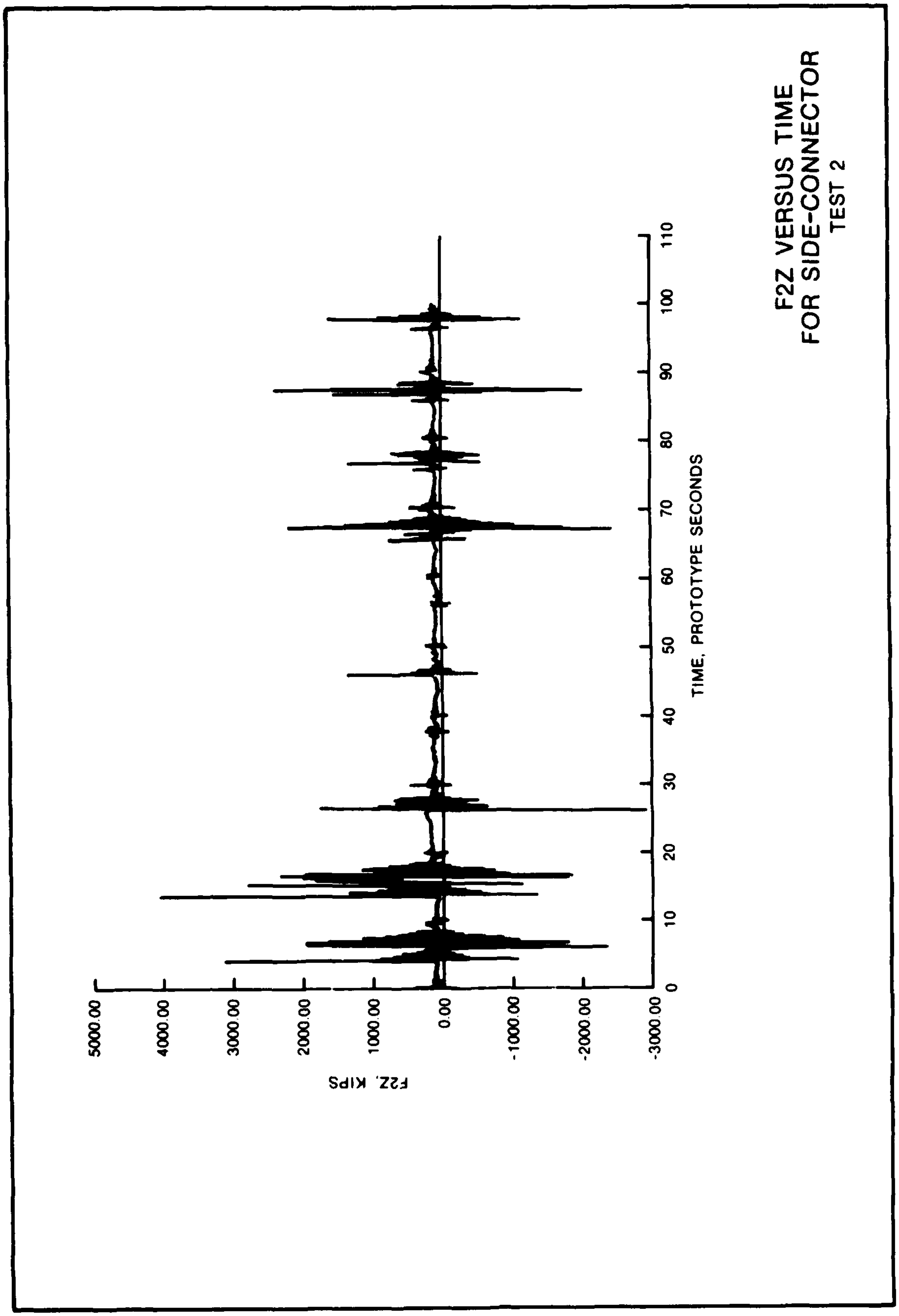

F2Z VERSUS TIME
FOR SIDE-CONNECTOR
TEST 2

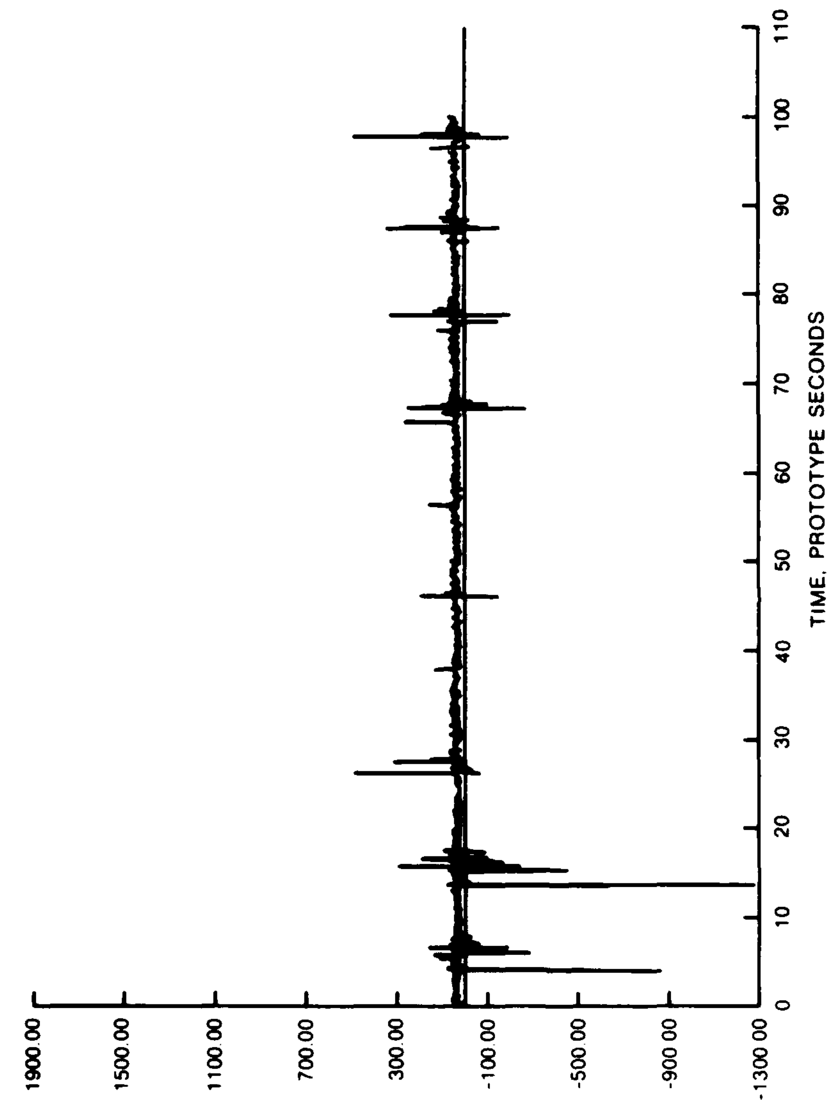

F2Y VERSUS TIME
FOR SIDE-CONNECTOR
TEST 2

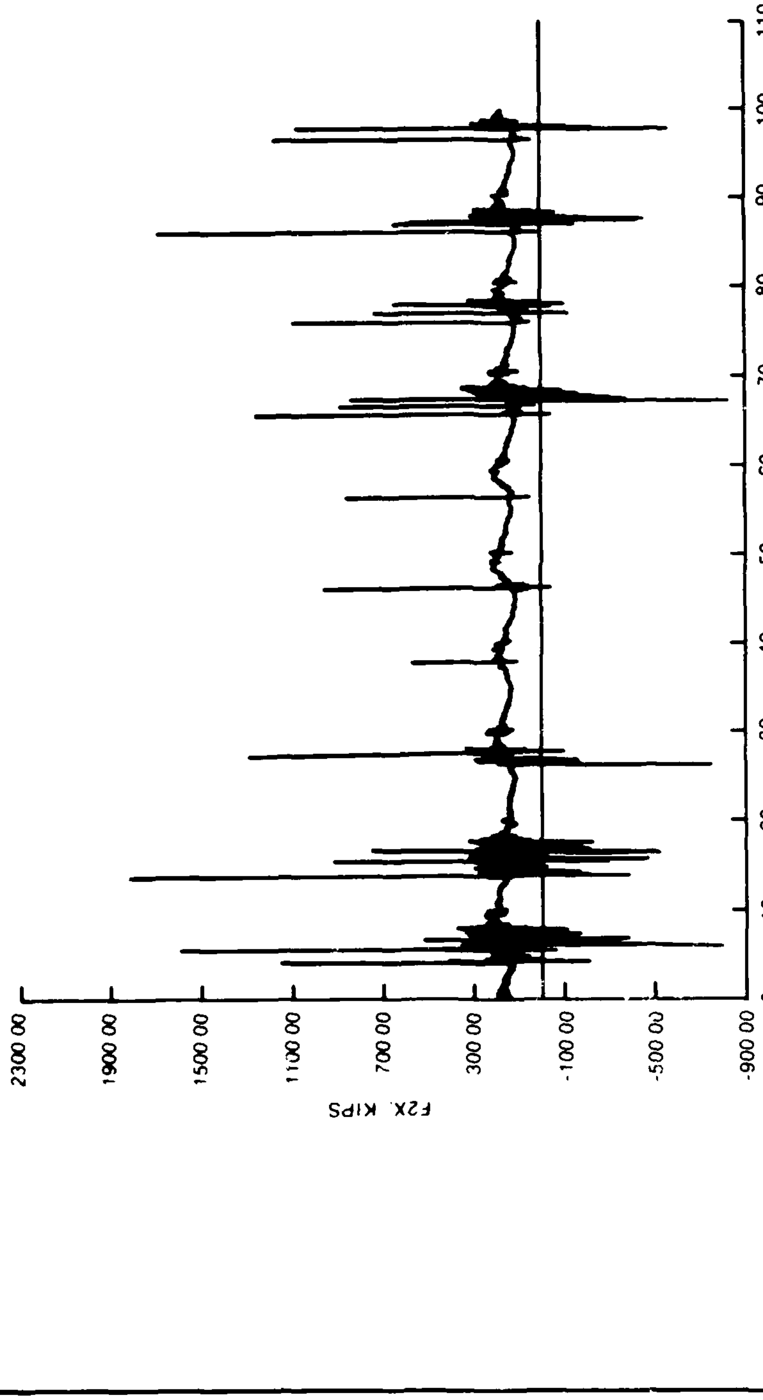

F2X VERSUS TIME
FOR SIDE-CONNECTOR
TEST 2

AD-A181 776 SLOPING FLOAT BREAKWATER STUDY OREGON INLET NORTH CAROLINA COASTAL MODEL INVESTIGATION(U) COASTAL ENGINEERING RESEARCH CENTER VICKSBURG MS 3/3

UNCLASSIFIED R D CARVER ET AL. APR 87 CERC-TR-87-5 F/G 13/2 NL

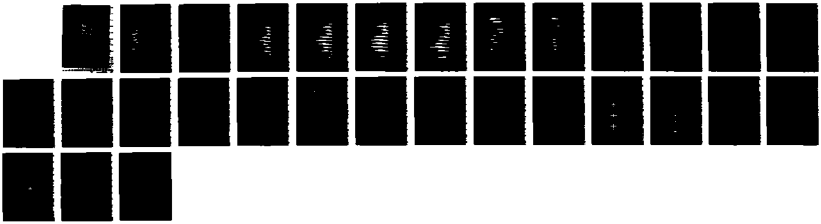

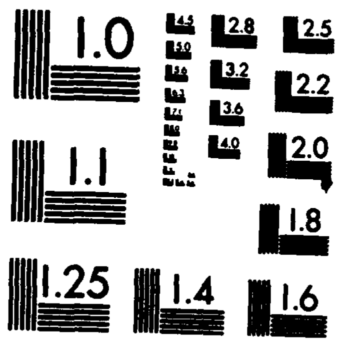

MICROCOPY RESOLUTION TEST CHART
NATIONAL BUREAU OF STANDARDS-1963-A

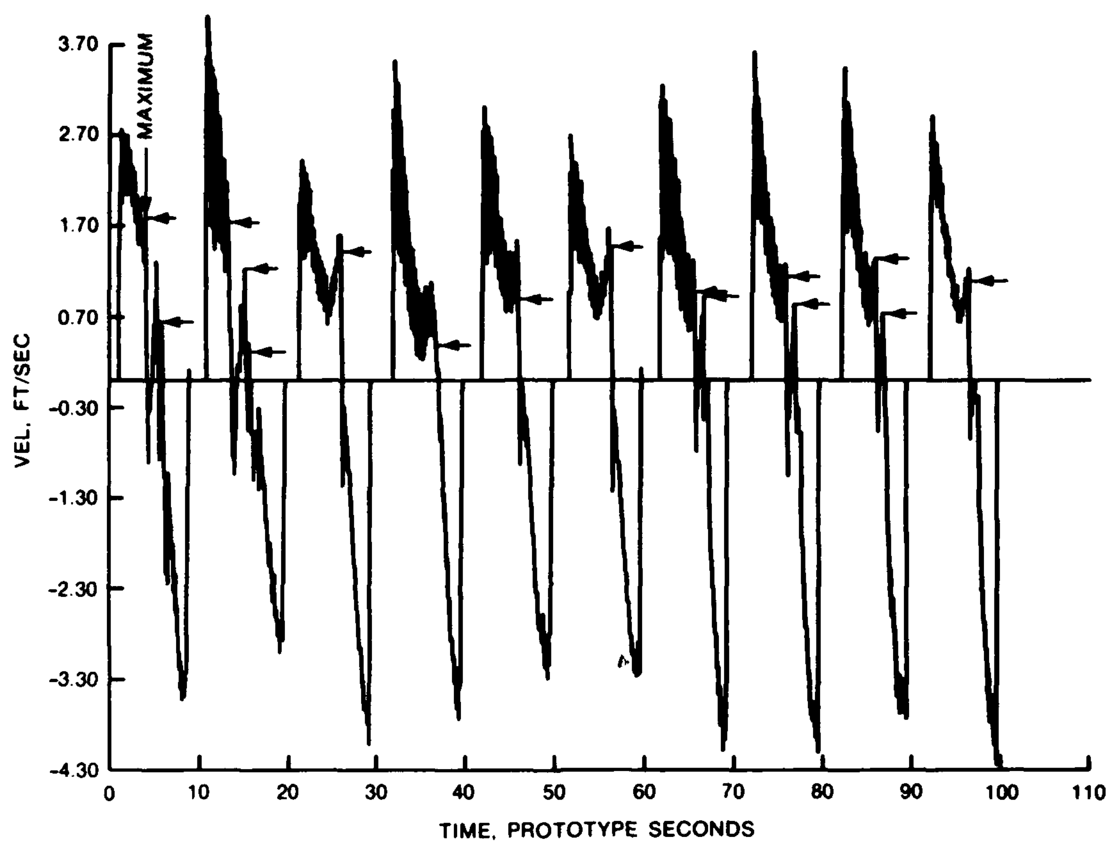

← INDICATES PROBABLE IMPACT VELOCITIES. IT APPEARS THAT MAXIMUM OCCURRED AT ~2.0 TO 3.0 SEC PROTOTYPE AND HAD A VALUE OF ~1.8 FT/SEC/PROTOTYPE.

VEL VERSUS TIME
FOR SIDE-CONNECTOR
TEST 2

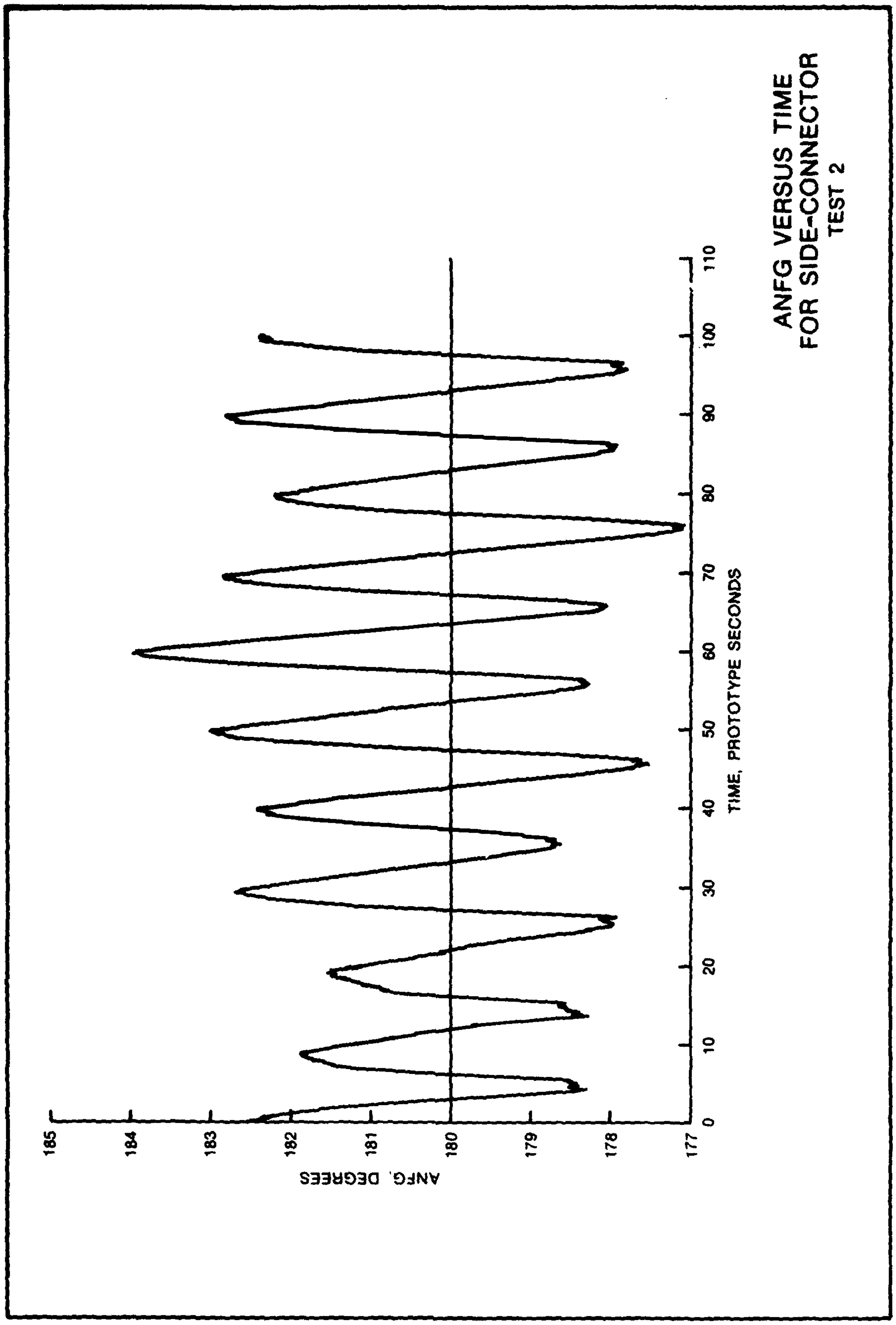
ANFG VERSUS TIME
FOR SIDE-CONNECTOR
TEST 2
ANFG, DEGREES
TIME, PROTOTYPE SECONDS
185
184
183
182
181
180
179
178
177
0
10
20
30
40
50
60
70
80
90
100
110

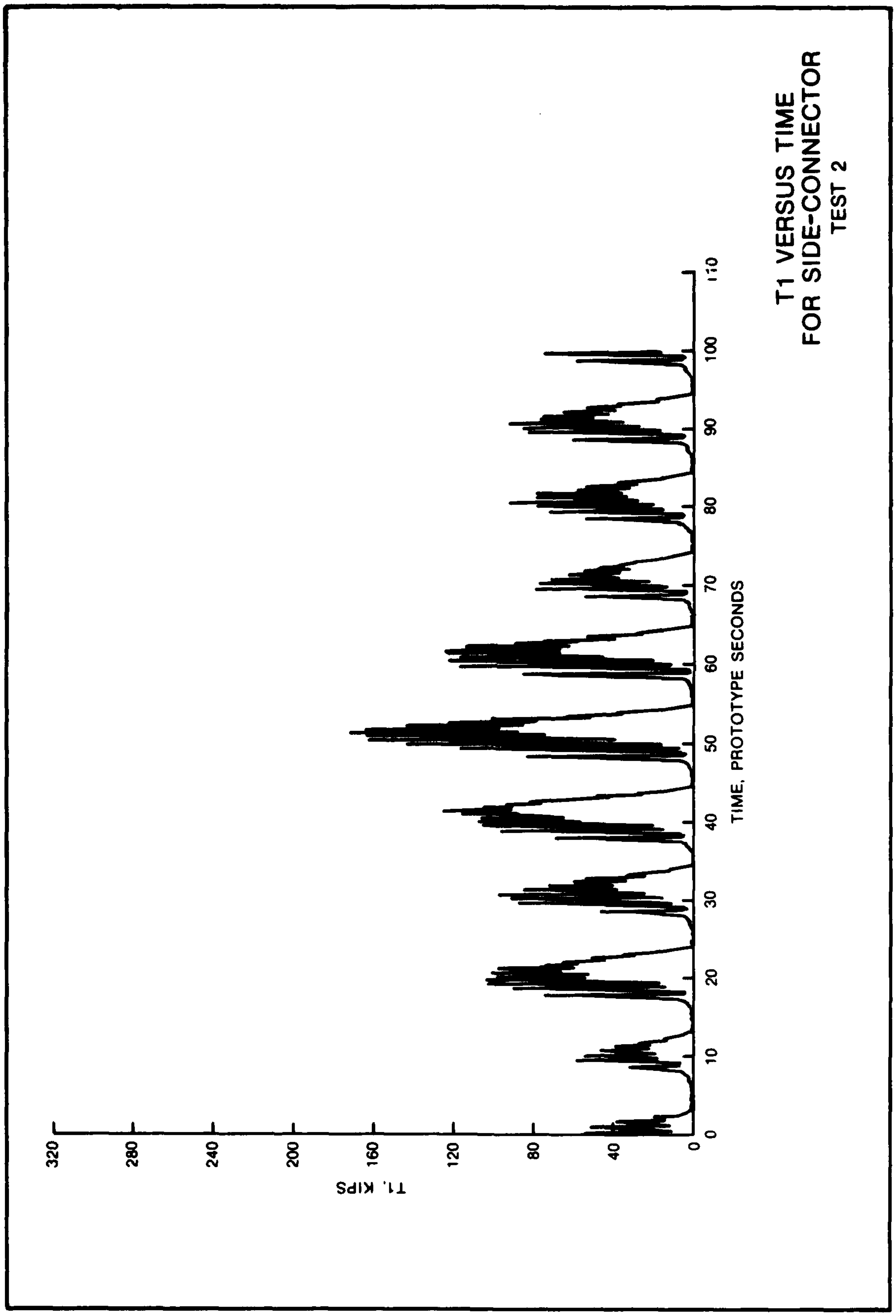

T1 VERSUS TIME
FOR SIDE-CONNECTOR
TEST 2
T1, KIPS
TIME, PROTOTYPE SECONDS
0
40
80
120
160
200
240
280
320
0
10
20
30
40
50
60
70
80
90
100
110

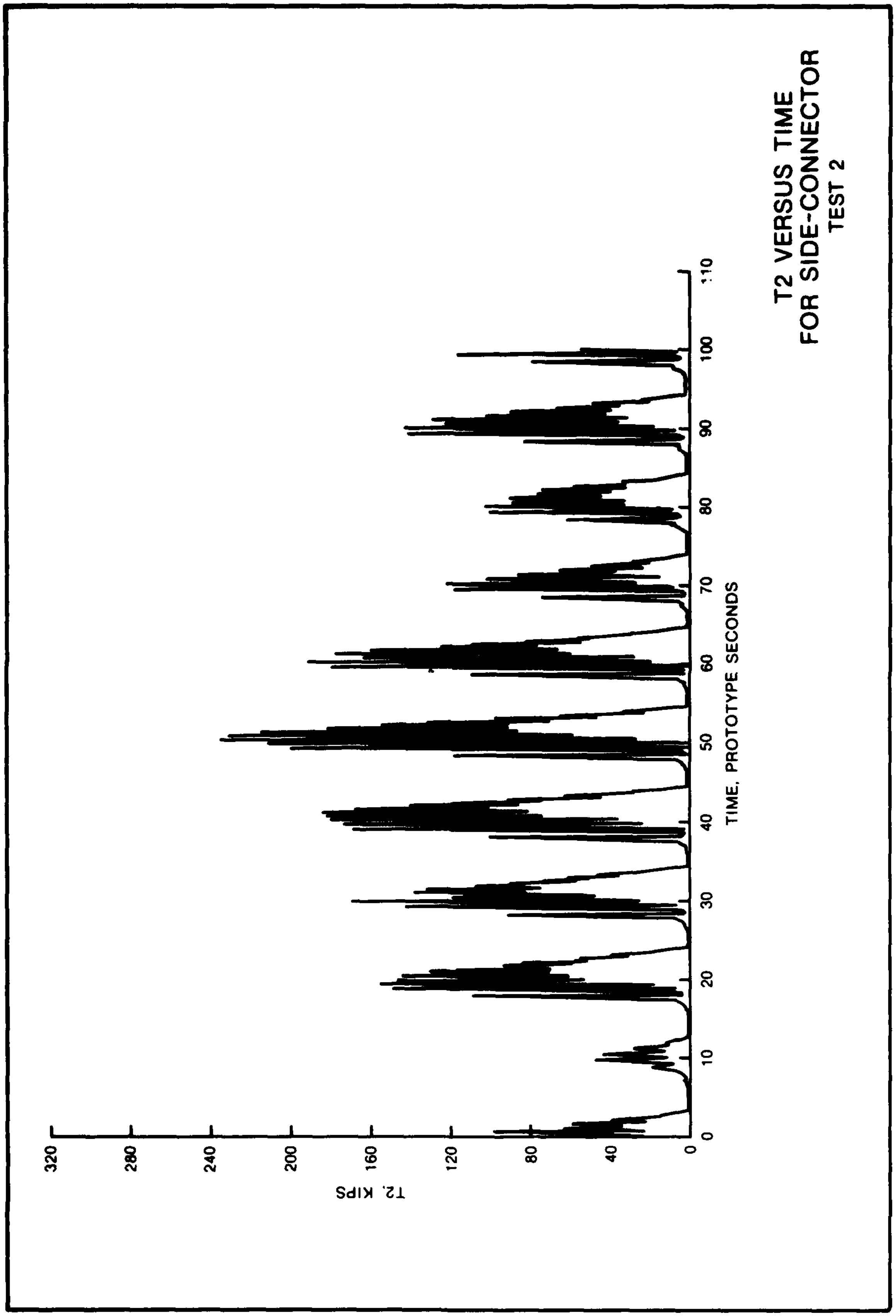
T2 VERSUS TIME
FOR SIDE-CONNECTOR
TEST 2
T2, KIPS
320
280
240
200
160
120
80
40
0
0
10
20
30
40
50
60
70
80
90
100
110
TIME, PROTOTYPE SECONDS

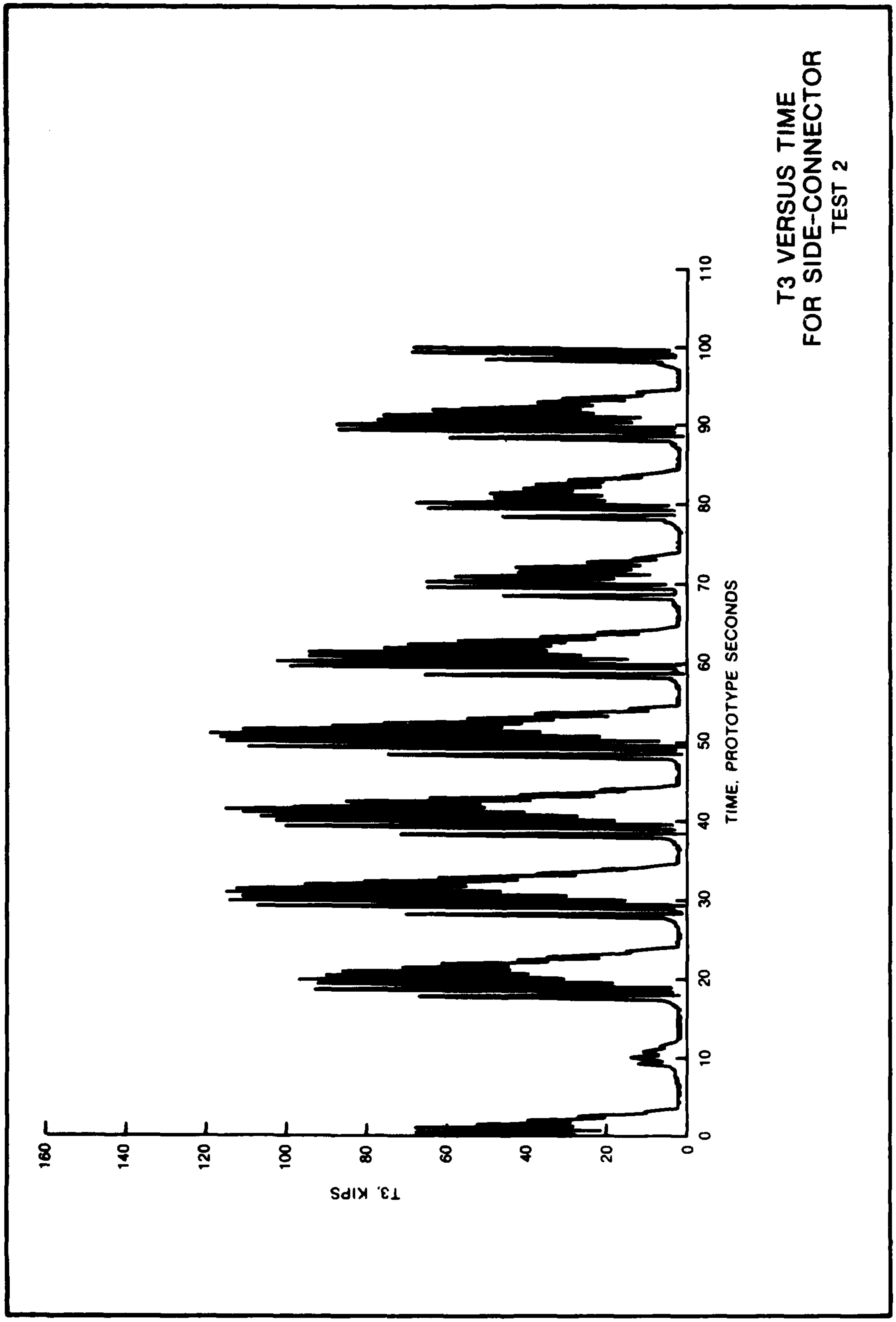

T3 VERSUS TIME
FOR SIDE-CONNECTOR
TEST 2
T3, KIPS
0
20
40
60
80
100
120
140
160
0
10
20
30
40
50
60
70
80
90
100
110
TIME, PROTOTYPE SECONDS

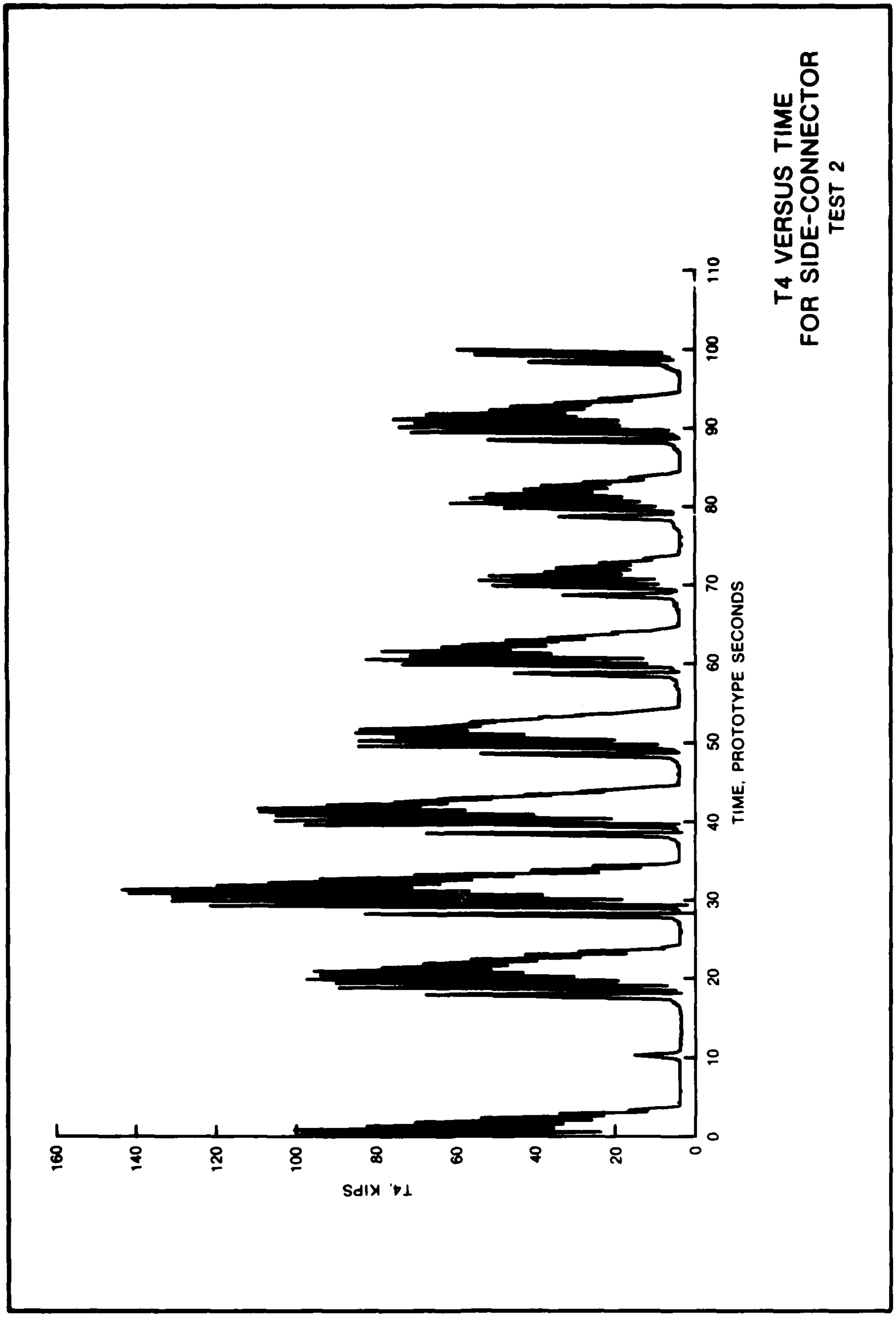
T4 VERSUS TIME
FOR SIDE-CONNECTOR
TEST 2
T4, KIPS
0
20
40
60
80
100
120
140
160
TIME, PROTOTYPE SECONDS
0
10
20
30
40
50
60
70
80
90
100
110

PLATE 72

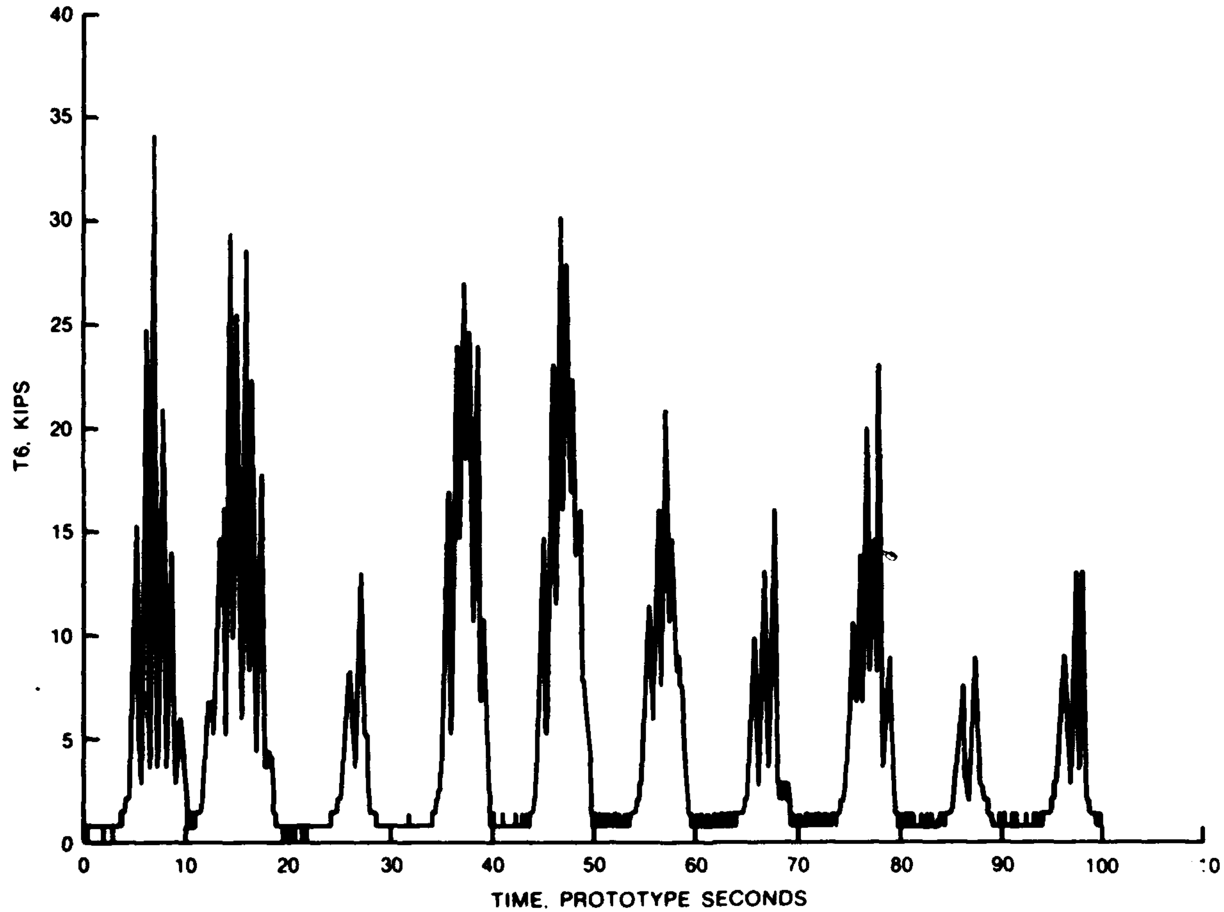

T6 VERSUS TIME
FOR SIDE-CONNECTOR
TEST 2

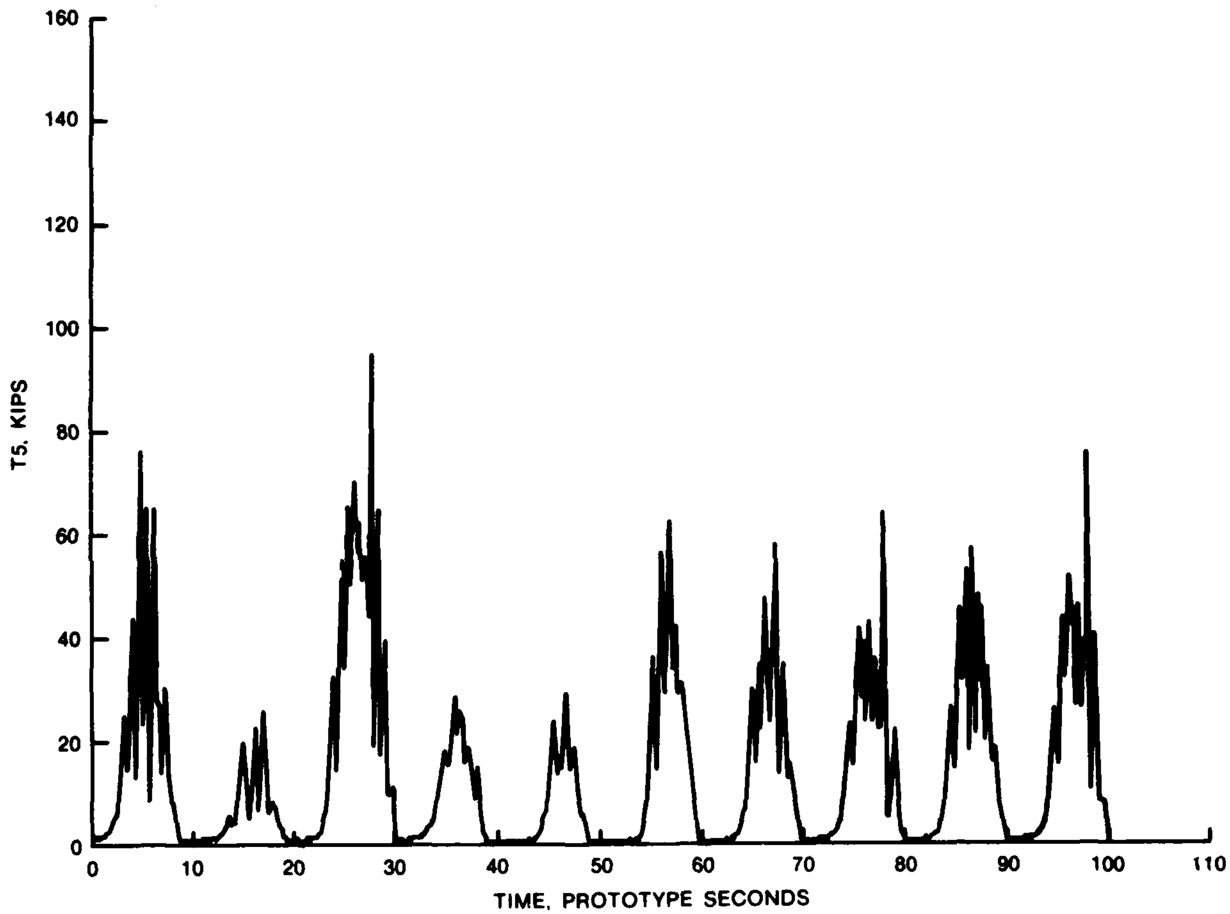

T5 VERSUS TIME
FOR SIDE-CONNECTOR
TEST 2

POSITIVE MAXIMUM -- TIME	6.2667	GAGE	MODEL		PROTOTYPE	
		> F1Z	264.1267	LB	4232.7988	KIPS
		F1Y	43.9586	LB	704.4648	KIPS
		F1X	-42.7794	LB	-685.5674	KIPS
		F2Z	-139.4329	LB	-2234.5015	KIPS
		F2Y	3.6397	LB	58.3291	KIPS
		F2X	-30.2207	LB	-484.3067	KIPS
		VEL	-.4028	FT/SEC	-2.0141	FT/SEC
		ANFG	180.1103	DEGREES	180.1103	DEGREES
		T1	.1000	LB	1.6026	KIPS
		T2	.0996	LB	1.5965	KIPS
		T3	.1311	LB	2.1006	KIPS
		T4	.2323	LB	3.7235	KIPS
		T5	3.0929	LB	49.5656	KIPS
		T6	1.1559	LB	18.5247	KIPS
NEGATIVE MAXIMUM -- TIME	16.2000	GAGE	MODEL		PROTOTYPE	
		> F1Z	-310.5099	LB	-4976.1201	KIPS
		F1Y	-16.5121	LB	-264.6163	KIPS
		F1X	-176.0784	LB	-2821.7690	KIPS
		F2Z	94.2527	LB	1510.4600	KIPS
		F2Y	-7.0359	LB	-112.7547	KIPS
		F2X	-8.9813	LB	-143.9312	KIPS
		VEL	-.2013	FT/SEC	-1.0063	FT/SEC
		ANFG	180.1483	DEGREES	180.1483	DEGREES
		T1	.1000	LB	1.6026	KIPS
		T2	.0996	LB	1.5965	KIPS
		T3	.1311	LB	2.1006	KIPS
		T4	.2323	LB	3.7235	KIPS
		T5	1.3028	LB	20.8781	KIPS
		T6	.6178	LB	9.9011	KIPS

F1Z MAXIMUMS FOR SIDE-CONNECTOR

TEST 2

NEGATIVE MAXIMUM -- TIME 13.6000

GAGE	MODEL		PROTOTYPE	
F1Z	-19.6529	LB	-314.9503	KIPS
>F1Y	-103.2018	LB	-1653.8752	KIPS
F1X	-139.5917	LB	-2237.0459	KIPS
F2Z	195.5755	LB	3134.2227	KIPS
F2Y	-79.6626	LB	-1276.6433	KIPS
F2X	113.5269	LB	1819.3416	KIPS
VEL	.0000	FT/SEC	.0000	FT/SEC
ANFG	178.2734	DEGREES	178.2734	DEGREES
T1	.0500	LB	8013	KIPS
T2	.0498	LB	.7982	KIPS
T3	.1311	LB	2.1006	KIPS
T4	.1936	LB	3.1029	KIPS
T5	.3282	LB	5.2594	KIPS
T6	.9168	LB	14.6920	KIPS

POSITIVE MAXIMUM -- TIME 87.3667

GAGE	MODEL		PROTOTYPE	
F1Z	95.9459	LB	1537.5942	KIPS
>F1Y	51.5037	LB	825.3795	KIPS
F1X	-9.5866	LB	-153.6320	KIPS
F2Z	-63.6131	LB	-1019.4404	KIPS
F2Y	21.3448	LB	342.0643	KIPS
F2X	18.4874	LB	296.2717	KIPS
VEL	-.3372	FT/SEC	-1.6859	FT/SEC
ANFG	180.1825	DEGREES	180.1825	DEGREES
T1	.2300	LB	3.6859	KIPS
T2	.3287	LB	5.2684	KIPS
T3	.2319	LB	3.7165	KIPS
T4	.3195	LB	5.1198	KIPS
T5	2.0785	LB	33.3094	KIPS
T6	.5182	LB	8.3042	KIPS

F1Y MAXIMUMS FOR
SIDE-CONNECTOR
TEST 2

POSITIVE MAXIMUM -- TIME	15.6667	GAGE	MODEL		PROTOTYPE	
		F1Z	14.8538	LB	238.0417	KIPS
		F1Y	34.8826	LB	559.0166	KIPS
		> F1X	47.7195	LB	764.7349	KIPS
		F2Z	60.3031	LB	966.3964	KIPS
		F2Y	18.7343	LB	300.2290	KIPS
		F2X	-12.1585	LB	-194.8472	KIPS
		VEL	-.0059	FT/SEC	-.0297	FT/SEC
		ANFG	179.1862	DEGREES	179.1862	DEGREES
		T1	.0500	LB	.8013	KIPS
		T2	.0996	LB	1.5965	KIPS
		T3	.1311	LB	2.1006	KIPS
		T4	.2323	LB	3.7235	KIPS
		T5	.3779	LB	6.0562	KIPS
		T6	1.0563	LB	16.9277	KIPS
NEGATIVE MAXIMUM -- TIME	16.2000	GAGE	MODEL		PROTOTYPE	
		F1Z	-310.5099	LB	-4976.1201	KIPS
		F1Y	-16.5121	LB	-264.6163	KIPS
		> F1X	-176.0784	LB	-2821.7690	KIPS
		F2Z	94.2527	LB	1510.4600	KIPS
		F2Y	-7.0359	LB	-112.7547	KIPS
		F2X	-8.9813	LB	-143.9312	KIPS
		VEL	-.2013	FT/SEC	-1.0063	FT/SEC
		ANFG	180.1483	DEGREES	180.1483	DEGREES
		T1	.1000	LB	1.6026	KIPS
		T2	.0996	LB	1.5965	KIPS
		T3	.1311	LB	2.1006	KIPS
		T4	.2323	LB	3.7235	KIPS
		T5	1.3028	LB	20.8781	KIPS
		T6	.6178	LB	9.9011	KIPS

F1X MAXIMUMS FOR
SIDE-CONNECTOR
TEST 2

POSITIVE MAXIMUM -- TIME	13.6667	GAGE	MODEL		PROTOTYPE	
		F1Z	-28.9738	LB	-464.3237	KIPS
		F1Y	-51.7154	LB	-828.7729	KIPS
		F1X	-108.6582	LB	-1741.3171	KIPS
		> F2Z	253.1905	LB	4057.5386	KIPS
		F2Y	-45.7755	LB	-733.5817	KIPS
		F2X	72.4740	LB	1161.4426	KIPS
		VEL	.0684	FT/SEC	.3422	FT/SEC
		ANFG	178.3495	DEGREES	178.3495	DEGREES
		T1	.0500	LB	.8013	KIPS
		T2	.0498	LB	.7982	KIPS
		T3	.0907	LB	1.4543	KIPS
		T4	.1936	LB	3.1029	KIPS
		T5	.3282	LB	5.2594	KIPS
		T6	1.0065	LB	16.1292	KIPS
NEGATIVE MAXIMUM -- TIME	26.2333	GAGE	MODEL		PROTOTYPE	
		F1Z	24.7565	LB	396.7388	KIPS
		F1Y	18.9177	LB	303.1682	KIPS
		F1X	-17.9271	LB	-287.2926	KIPS
		> F2Z	-182.3000	LB	-2921.4746	KIPS
		F2Y	19.5021	LB	312.5335	KIPS
		F2X	-39.8773	LB	-639.0593	KIPS
		VEL	-.0012	FT/SEC	-.0063	FT/SEC
		ANFG	178.0148	DEGREES	178.0148	DEGREES
		T1	.0500	LB	.8013	KIPS
		T2	.0996	LB	1.5965	KIPS
		T3	.1311	LB	2.1006	KIPS
		T4	.2323	LB	3.7235	KIPS
		T5	3.8686	LB	61.9969	KIPS
		T6	.3288	LB	5.2699	KIPS

F2Z MAXIMUMS FOR
SIDE-CONNECTOR
TEST 2

NEGATIVE MAXIMUM -- TIME	13.6000	GAGE	MODEL		PROTOTYPE	
		F1Z	-19.6529	LB	-314.9503	KIPS
		F1Y	-103.2018	LB	-1653.8752	KIPS
		F1X	-139.5917	LB	-2237.0459	KIPS
		F2Z	195.5755	LB	3134.2227	KIPS
		> F2Y	-79.6626	LB	-1276.6433	KIPS
		F2X	113.5269	LB	1819.3416	KIPS
		VEL	.0000	FT/SEC	.0000	FT/SEC
		ANFG	178.2734	DEGREES	178.2734	DEGREES
		T1	.0500	LB	.8013	KIPS
		T2	.0498	LB	.7982	KIPS
		T3	.1311	LB	2.1006	KIPS
		T4	.1936	LB	3.1029	KIPS
		T5	.3282	LB	5.2594	KIPS
		T6	.9168	LB	14.6920	KIPS
POSITIVE MAXIMUM -- TIME	26.1333	GAGE	MODEL		PROTOTYPE	
		F1Z	12.1581	LB	194.8409	KIPS
		F1Y	26.3534	LB	422.3305	KIPS
		F1X	-28.4423	LB	-455.8065	KIPS
		F2Z	-102.5259	LB	-1643.0430	KIPS
		> F2Y	30.3281	LB	486.0267	KIPS
		F2X	-24.1166	LB	-386.4839	KIPS
		VEL	.2212	FT/SEC	1.1062	FT/SEC
		ANFG	178.0719	DEGREES	178.0719	DEGREES
		T1	.0500	LB	.8013	KIPS
		T2	.0996	LB	1.5965	KIPS
		T3	.1311	LB	2.1006	KIPS
		T4	.2323	LB	3.7235	KIPS
		T5	3.8686	LB	61.9969	KIPS
		T6	.3787	LB	6.0684	KIPS

F2Y MAXIMUMS FOR SIDE-CONNECTOR
TEST 2

POSITIVE MAXIMUM -- TIME 67.2667

GAGE	MODEL		PROTOTYPE	
F1Z	-19.6529	LB	-314.9503	KIPS
F1Y	-103.2018	LB	-1653.8752	KIPS
F1X	-139.5917	LB	-2237.0459	KIPS
F2Z	195.5755	LB	3134.2227	KIPS
F2Y	-79.6626	LB	-1276.6433	KIPS
> F2X	113.5269	LB	1819.3416	KIPS
VEL	.0000	FT/SEC	.0000	FT/SEC
ANFG	178.2734	DEGREES	178.2734	DEGREES
T1	.0500	LB	.8013	KIPS
T2	.0498	LB	.7982	KIPS
T3	.1311	LB	2.1006	KIPS
T4	.1936	LB	3.1029	KIPS
T5	.3282	LB	5.2594	KIPS
T6	.9168	LB	14.6920	KIPS

NEGATIVE MAXIMUM -- TIME 13.6000

GAGE	MODEL		PROTOTYPE	
F1Z	160.4235	LB	2570.8882	KIPS
F1Y	22.6356	LB	362.7493	KIPS
F1X	-15.1399	LB	-242.6263	KIPS
F2Z	-151.2386	LB	-2423.6948	KIPS
F2Y	4.0441	LB	64.8095	KIPS
> F2X	-51.4852	LB	-825.0833	KIPS
VEL	-.2913	FT/SEC	-1.4563	FT/SEC
ANFG	180.0912	DEGREES	180.0912	DEGREES
T1	.1800	LB	2.8846	KIPS
T2	.2291	LB	3.6719	KIPS
T3	.1815	LB	2.9086	KIPS
T4	.3195	LB	5.1198	KIPS
T5	2.4166	LB	38.7281	KIPS
T6	.3787	LB	6.0684	KIPS

F2X MAXIMUMS FOR
SIDE-CONNECTOR
TEST 2

PLATE 78

POSITIVE MAXIMUM -- TIME 11.0667

GAGE	MODEL		PROTOTYPE	
F1Z	-1.8157	LB	-29.0983	KIPS
F1Y	3.3901	LB	54.3292	KIPS
F1X	-5.0469	LB	-80.8800	KIPS
F2Z	5.8436	LB	93.6474	KIPS
F2Y	2.4266	LB	38.8877	KIPS
F2X	11.6577	LB	186.8223	KIPS
> VEL	.7978	FT/SEC	3.9891	FT/SEC
ANFG	180.5552	DEGREES	180.5552	DEGREES
T1	1.6500	LB	26.4423	KIPS
T2	1.4445	LB	23.1489	KIPS
T3	.5243	LB	8.4025	KIPS
T4	.2323	LB	3.7235	KIPS
T5	.0497	LB	.7969	KIPS
T6	.0897	LB	1.4373	KIPS

POSITIVE VELOCITY INDICATES THAT BARGE MOTION IS IN THE NEGATIVE Z DIRECTION (TOWARD BOTTOM). THIS OUTPUT GIVES MAXIMUM VELOCITIES, BUT IT MUST BE COMPARED WITH TIME HISTORY PLOT TO DETERMINE MAXIMUM IMPACT VELOCITES.

NEGATIVE MAXIMUM -- TIME 99.4667

GAGE	MODEL		PROTOTYPE	
F1Z	4.3459	LB	69.6465	KIPS
F1Y	2.4060	LB	38.5577	KIPS
F1X	-1.7530	LB	-28.0925	KIPS
F2Z	5.5514	LB	88.9653	KIPS
F2Y	3.2354	LB	51.8486	KIPS
F2X	11.5326	LB	184.8178	KIPS
> VEL	-.8497	FT/SEC	-4.2484	FT/SEC
ANFG	182.2818	DEGREES	182.2818	DEGREES
T1	1.4000	LB	22.4359	KIPS
T2	7.2324	LB	115.9040	KIPS
T3	1.1192	LB	17.9361	KIPS
T4	1.0746	LB	17.2210	KIPS
T5	.5271	LB	8.4469	KIPS
T6	.0498	LB	.7985	KIPS

NEGATIVE VELOCITY INDICATES THAT BARGE MOTION IS IN THE POSITIVE Z DIRECTION

VEL MAXIMUMS FOR SIDE-CONNECTOR
TEST 2

NEGATIVE MAXIMUM -- TIME	59.7667	GAGE	MODEL		PROTOTYPE		
		F1Z	6.2165	LB	99.6226	KIPS	
		F1Y	2.8434	LB	45.5672	KIPS	
		F1X	-2.2597	LB	-36.2136	KIPS	
		F2Z	7.8303	LB	125.4859	KIPS	
		F2Y	2.8310	LB	45.3682	KIPS	
		F2X	12.8585	LB	206.0662	KIPS	
		VEL	-.0012	FT/SEC	-.0063	FT/SEC	
		> ANFG	183.9551	DEGREES	183.9551	DEGREES	← MAXIMUM CONCAVE UPWARDS
		T1	2.0900	LB	33.4936	KIPS	
		T2	.0000	LB	.0000	KIPS	
		T3	.1815	LB	2.9086	KIPS	
		T4	4.5791	LB	73.3832	KIPS	
		T5	.0497	LB	.7969	KIPS	
		T6	.0897	LB	1.4373	KIPS	
POSITIVE MAXIMUM -- TIME	76.0000	GAGE	MODEL		PROTOTYPE		
		F1Z	-3.4112	LB	-54.6662	KIPS	
		F1Y	8.2015	LB	131.4342	KIPS	
		F1X	-2.8721	LB	-46.0267	KIPS	
		F2Z	14.9591	LB	239.7298	KIPS	
		F2Y	4.0441	LB	64.8095	KIPS	
		F2X	3.9525	LB	63.3410	KIPS	
		VEL	-.2103	FT/SEC	-1.0516	FT/SEC	
		> ANFG	177.0679	DEGREES	177.0679	DEGREES	← MAXIMUM CONVEX UPWARDS
		T1	.0500	LB	.8013	KIPS	
		T2	.0996	LB	1.5965	KIPS	
		T3	.1311	LB	2.1006	KIPS	
		T4	.2323	LB	3.7235	KIPS	
		T5	2.4664	LB	39.5250	KIPS	
		T6	.8670	LB	13.8935	KIPS	

ANFG RANGE LIMITS FOR
SIDE-CONNECTOR
TEST 2

NEGATIVE MAXIMUM -- TIME	51.1667	GAGE	MODEL		PROTOTYPE	
		F1Z	-15.2171	LB	-243.8630	KIPS
		F1Y	-3.5545	LB	-56.9624	KIPS
		F1X	-67.8429	LB	-1087.2263	KIPS
		F2Z	159.3471	LB	2553.6382	KIPS
		F2Y	-3.0730	LB	-49.2463	KIPS
		F2X	21.6645	LB	347.1877	KIPS
		VEL	.0531	FT/SEC	.2656	FT/SEC
		ANFG	178.4218	DEGREES	178.4218	DEGREES
		> T1	.0000	LB	.0000	KIPS
		T2	.0996	LB	1.5965	KIPS
		T3	.1311	LB	2.1006	KIPS
		T4	.2323	LB	3.7235	KIPS
		T5	2.7050	LB	43.3500	KIPS
		T6	.0897	LB	1.4373	KIPS
POSITIVE MAXIMUM -- TIME	4.1000	GAGE	MODEL		PROTOTYPE	
		F1Z	7.0417	LB	112.8474	KIPS
		F1Y	1.4910	LB	23.8939	KIPS
		F1X	-1.0139	LB	-16.2491	KIPS
		F2Z	4.9671	LB	79.6010	KIPS
		F2Y	1.6178	LB	25.9268	KIPS
		F2X	10.3068	LB	165.1730	KIPS
		VEL	.0000	FT/SEC	.0000	FT/SEC
		ANFG	181.8939	DEGREES	181.8939	DEGREES
		> T1	10.6800	LB	171.1538	KIPS
		T2	8.7466	LB	140.1704	KIPS
		T3	5.2028	LB	83.3786	KIPS
		T4	5.3342	LB	85.4845	KIPS
		T5	.0497	LB	.7969	KIPS
		T6	.0498	LB	.7985	KIPS

T1 MAXIMUM FOR
SIDE-CONNECTOR
TEST 2

NEGATIVE MAXIMUM -- TIME 50.3667

GAGE	MODEL		PROTOTYPE	
F1Z	7.3168	LB	117.2556	KIPS
F1Y	3.9369	LB	63.0911	KIPS
F1X	-1.5418	LB	-24.7087	KIPS
F2Z	6.6617	LB	106.7574	KIPS
F2Y	3.2354	LB	51.8486	KIPS
F2X	13.3589	LB	214.0845	KIPS
VEL	-.5188	FT/SEC	-2.5938	FT/SEC
ANFG	182.0764	DEGREES	182.0764	DEGREES
T1	.2800	LB	4.4872	KIPS
> T2	.0000	LB	.0000	KIPS
T3	.1311	LB	2.1006	KIPS
T4	3.3496	LB	53.6799	KIPS
T5	.2287	LB	3.6656	KIPS
T6	1.0065	LB	16.1292	KIPS

POSITIVE MAXIMUM -- TIME 48.5333

GAGE	MODEL		PROTOTYPE	
F1Z	1.6502	LB	26.4456	KIPS
F1Y	2.4060	LB	38.5577	KIPS
F1X	-1.2251	LB	-19.6329	KIPS
F2Z	3.5674	LB	57.1268	KIPS
F2Y	2.8310	LB	45.3682	KIPS
F2X	9.3311	LB	149.5374	KIPS
VEL	.0000	FT/SEC	.0000	FT/SEC
ANFG	182.5974	DEGREES	182.5974	DEGREES
T1	5.5100	LB	88.3013	KIPS
> T2	14.6740	LB	235.1607	KIPS
T3	2.3998	LB	38.4576	KIPS
T4	1.2198	LB	19.5482	KIPS
T5	.0000	LB	.0000	KIPS
T6	.0498	LB	.7985	KIPS

T2 MAXIMUM FOR SIDE-CONNECTOR

TEST 2

		GAGE	MODEL		PROTOTYPE	
NEGATIVE MAXIMUM -- TIME	51.0667					
		F1Z	7.5918	LB	121.6639	KIPS
		F1Y	3.3901	LB	54.3292	KIPS
		F1X	-2.2597	LB	-36.2136	KIPS
		F2Z	6.3695	LB	102.0752	KIPS
		F2Y	2.8310	LB	45.3682	KIPS
		F2X	13.6090	LB	218.0936	KIPS
		VEL	-.6300	FT/SEC	-3.1500	FT/SEC
		ANFG	182.9131	DEGREES	182.9131	DEGREES
		T1	1.1600	LB	18.5897	KIPS
		T2	.6176	LB	9.8981	KIPS
		> T3	.0000	LB	.0000	KIPS
		T4	4.9567	LB	79.4338	KIPS
		T5	.0497	LB	.7969	KIPS
		T6	.2790	LB	4.4715	KIPS
POSITIVE MAXIMUM -- TIME	49.5333	GAGE	MODEL		PROTOTYPE	
		F1Z	7.0417	LB	112.8474	KIPS
		F1Y	2.8434	LB	45.5672	KIPS
		F1X	-1.8585	LB	-29.7844	KIPS
		F2Z	7.5382	LB	120.8037	KIPS
		F2Y	2.8310	LB	45.3682	KIPS
		F2X	11.2825	LB	180.8087	KIPS
		VEL	.0000	FT/SEC	.0000	FT/SEC
		ANFG	182.0764	DEGREES	182.0764	DEGREES
		T1	8.6300	LB	138.3013	KIPS
		T2	3.8354	LB	61.4643	KIPS
		> T3	7.4211	LB	118.9277	KIPS
		T4	4.4339	LB	71.0560	KIPS
		T5	.0497	LB	.7969	KIPS
		T6	.0498	LB	.7985	KIPS

T3 MAXIMUM FOR
SIDE-CONNECTOR
TEST 2

NEGATIVE MAXIMUM -- TIME	31.2667	GAGE	MODEL		PROTOTYPE	
		F1Z	18.0447	LB	289.1774	KIPS
		F1Y	6.1239	LB	98.1388	KIPS
		F1X	-.1905	LB	-3.0522	KIPS
		F2Z	6.3695	LB	102.0752	KIPS
		F2Y	2.0222	LB	32.4073	KIPS
		F2X	11.6577	LB	186.8223	KIPS
		VEL	-.6147	FT/SEC	-3.0734	FT/SEC
		ANFG	182.0042	DEGREES	182.0042	DEGREES
		T1	1.5000	LB	24.0385	KIPS
		T2	3.2974	LB	52.8433	KIPS
		T3	.0907	LB	1.4543	KIPS
		> T4	.0000	LB	.0000	KIPS
		T5	3.8288	LB	61.3594	KIPS
		T6	.0897	LB	1.4373	KIPS

POSITIVE MAXIMUM -- TIME	28.3667	GAGE	MODEL		PROTOTYPE	
		F1Z	2.7505	LB	44.0787	KIPS
		F1Y	2.8434	LB	45.5672	KIPS
		F1X	-2.1542	LB	-34.5217	KIPS
		F2Z	9.8170	LB	157.3243	KIPS
		F2Y	2.0222	LB	32.4073	KIPS
		F2X	10.4319	LB	167.1776	KIPS
		VEL	.0000	FT/SEC	.0000	FT/SEC
		ANFG	181.5402	DEGREES	181.5402	DEGREES
		T1	5.1200	LB	82.0513	KIPS
		T2	6.4554	LB	103.4515	KIPS
		T3	6.5338	LB	104.7081	KIPS
		> T4	8.9743	LB	143.8187	KIPS
		T5	.0497	LB	.7969	KIPS
		T6	.0498	LB	.7985	KIPS

T4 MAXIMUM FOR
SIDE-CONNECTOR
TEST 2

		GAGE	MODEL		PROTOTYPE	
NEGATIVE MAXIMUM -- TIME	27.7000	GAGE	MODEL		PROTOTYPE	
		F1Z	-13.5887	LB	-217.7676	KIPS
		F1Y	2.8434	LB	45.5672	KIPS
		F1X	-7.3062	LB	-117.0868	KIPS
		F2Z	14.3748	LB	230.3656	KIPS
		F2Y	2.0222	LB	32.4073	KIPS
		F2X	14.5847	LB	233.7292	KIPS
		VEL	.0000	FT/SEC	.0000	FT/SEC
		ANFG	181.5022	DEGREES	181.5022	DEGREES
		T1	3.6000	LB	57.6923	KIPS
		T2	.9663	LB	15.4858	KIPS
		T3	.5747	LB	9.2104	KIPS
		T4	.2323	LB	3.7235	KIPS
		> T5	.0000	LB	.0000	KIPS
		T6	.3787	LB	6.0684	KIPS
POSITIVE MAXIMUM -- TIME	9.4667	GAGE	MODEL		PROTOTYPE	
		F1Z	66.1278	LB	1059.7397	KIPS
		F1Y	11.4820	LB	184.0058	KIPS
		F1X	-3.0832	LB	-49.4105	KIPS
		F2Z	40.9034	LB	655.5029	KIPS
		F2Y	.0812	LB	1.3012	KIPS
		F2X	18.2372	LB	292.2625	KIPS
		VEL	-.4453	FT/SEC	-2.2266	FT/SEC
		ANFG	181.1865	DEGREES	181.1865	DEGREES
		T1	.2300	LB	3.6859	KIPS
		T2	.3786	LB	6.0666	KIPS
		T3	.4336	LB	6.9482	KIPS
		T4	.4647	LB	7.4469	KIPS
		> T5	5.9173	LB	94.8281	KIPS
		T6	.1295	LB	2.0760	KIPS

T5 MAXIMUM FOR SIDE-CONNECTOR
TEST 2

NEGATIVE MAXIMUM -- TIME 6.9333	GAGE	MODEL		PROTOTYPE	
	F1Z	-7.2072	LB	-115.5001	KIPS
	F1Y	3.3901	LB	54.3292	KIPS
	F1X	.6119	LB	9.8062	KIPS
	F2Z	10.4014	LB	166.6886	KIPS
	F2Y	1.6178	LB	25.9268	KIPS
	F2X	10.9072	LB	174.7950	KIPS
	VEL	.0000	FT/SEC	.0000	FT/SEC
	ANFG	182.4111	DEGREES	182.4111	DEGREES
	T1	.7200	LB	11.5385	KIPS
	T2	3.8354	LB	61.4643	KIPS
	T3	3.9223	LB	62.8571	KIPS
	T4	3.1560	LB	50.5770	KIPS
	T5	.0497	LB	.7969	KIPS
	> T6	.0000	LB	.0000	KIPS
POSITIVE MAXIMUM -- TIME 0.4667	GAGE	MODEL		PROTOTYPE	
	F1Z	70.4198	LB	1128.5085	KIPS
	F1Y	12.4661	LB	199.7773	KIPS
	F1X	-9.1643	LB	-146.8643	KIPS
	F2Z	-112.3257	LB	-1800.0918	KIPS
	F2Y	.0812	LB	1.3012	KIPS
	F2X	-20.8144	LB	-333.5633	KIPS
	VEL	-.3875	FT/SEC	-1.9375	FT/SEC
	ANFG	181.2436	DEGREES	181.2436	DEGREES
	T1	.1400	LB	2.2436	KIPS
	T2	.1395	LB	2.2351	KIPS
	T3	.1311	LB	2.1006	KIPS
	T4	.2323	LB	3.7235	KIPS
	T5	.8652	LB	13.8656	KIPS
	> T6	2.1325	LB	34.1748	KIPS

T6 MAXIMUM FOR
SIDE CONNECTOR
TEST 2

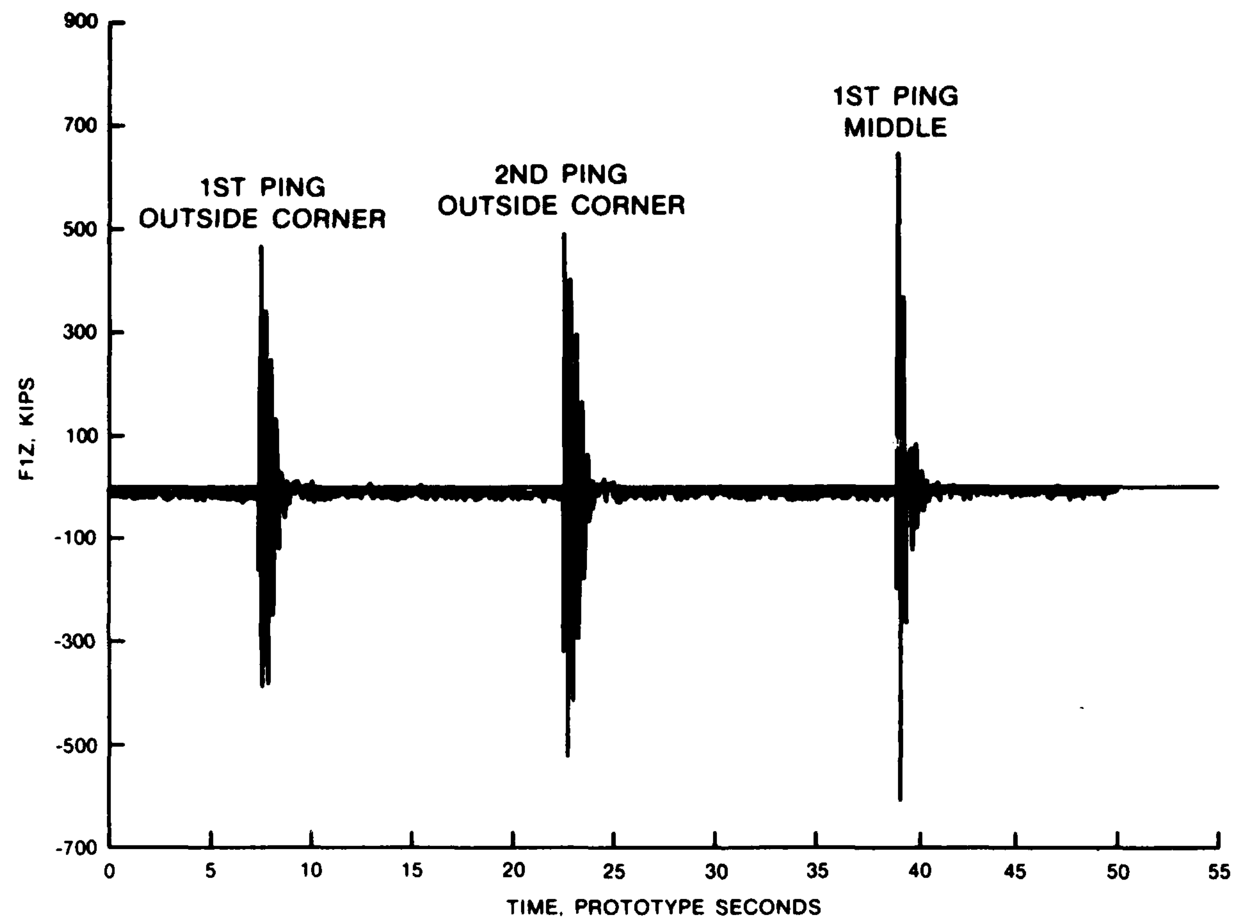

F1Z VERSUS TIME
FOR FIRST HALF OF
SIDE-CONNECTOR TEST 16

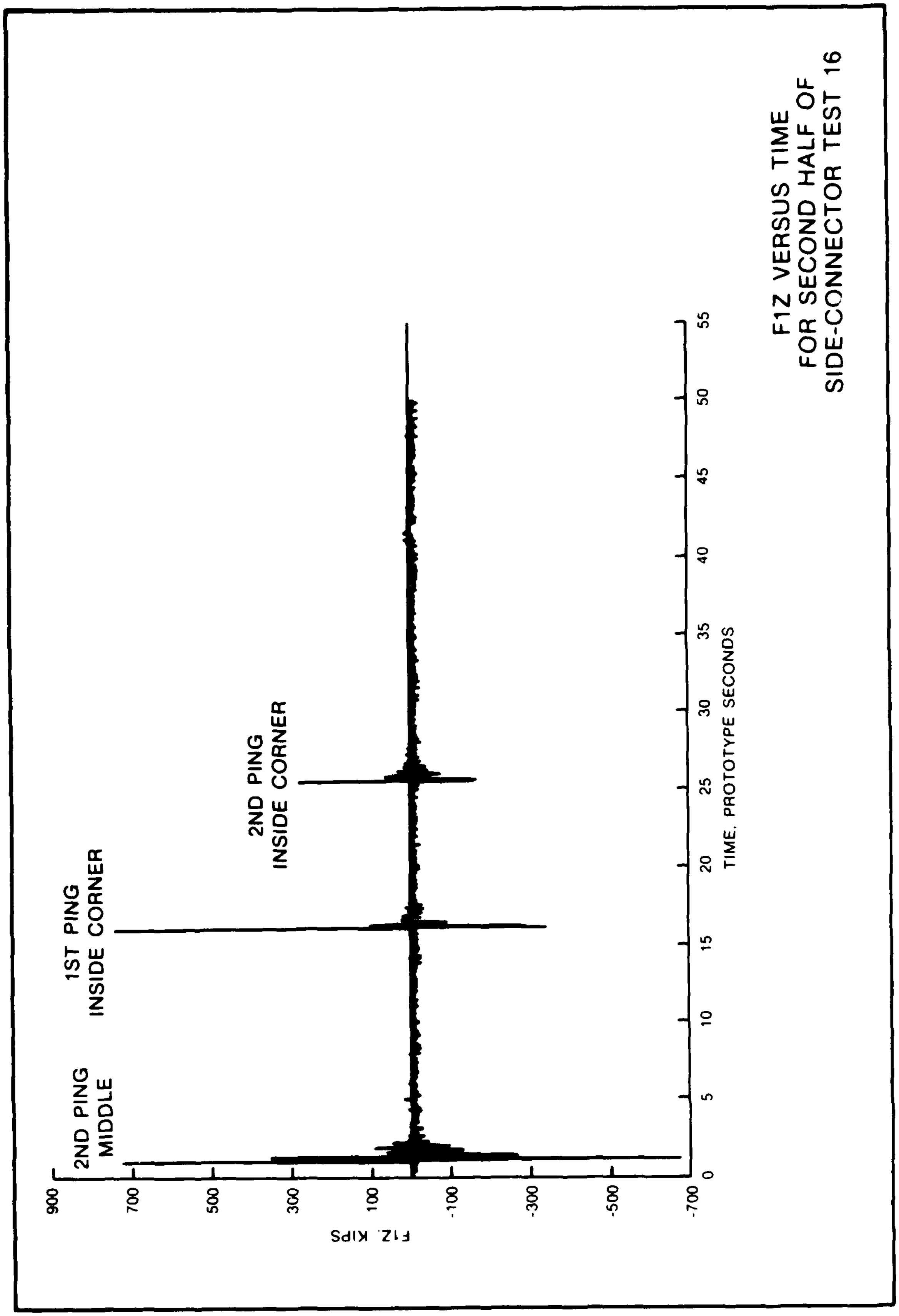

F1Z VERSUS TIME
FOR SECOND HALF OF
SIDE-CONNECTOR TEST 16

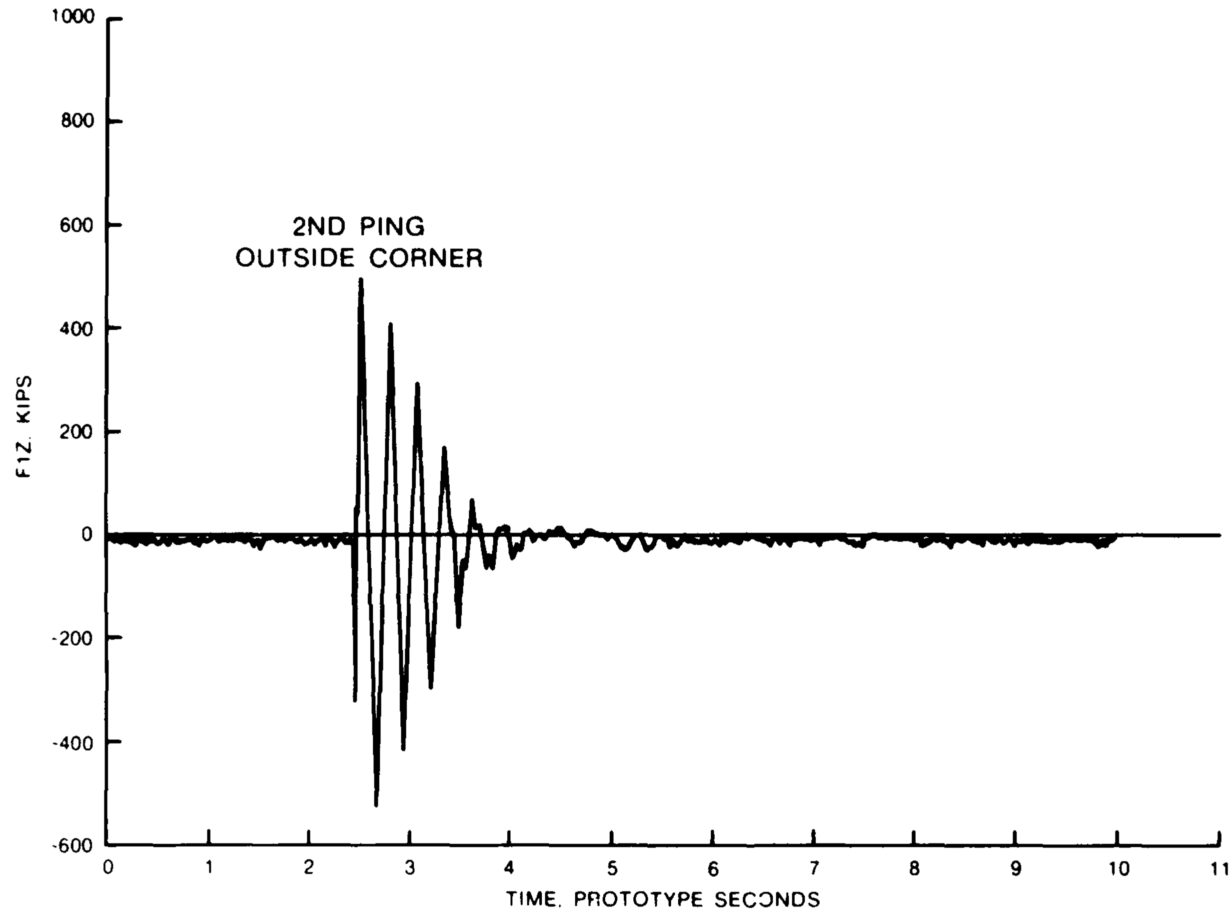

F1Z VERSUS TIME FOR SECOND PING OF OUTSIDE CORNER DURING SIDE-CONNECTOR TEST 16

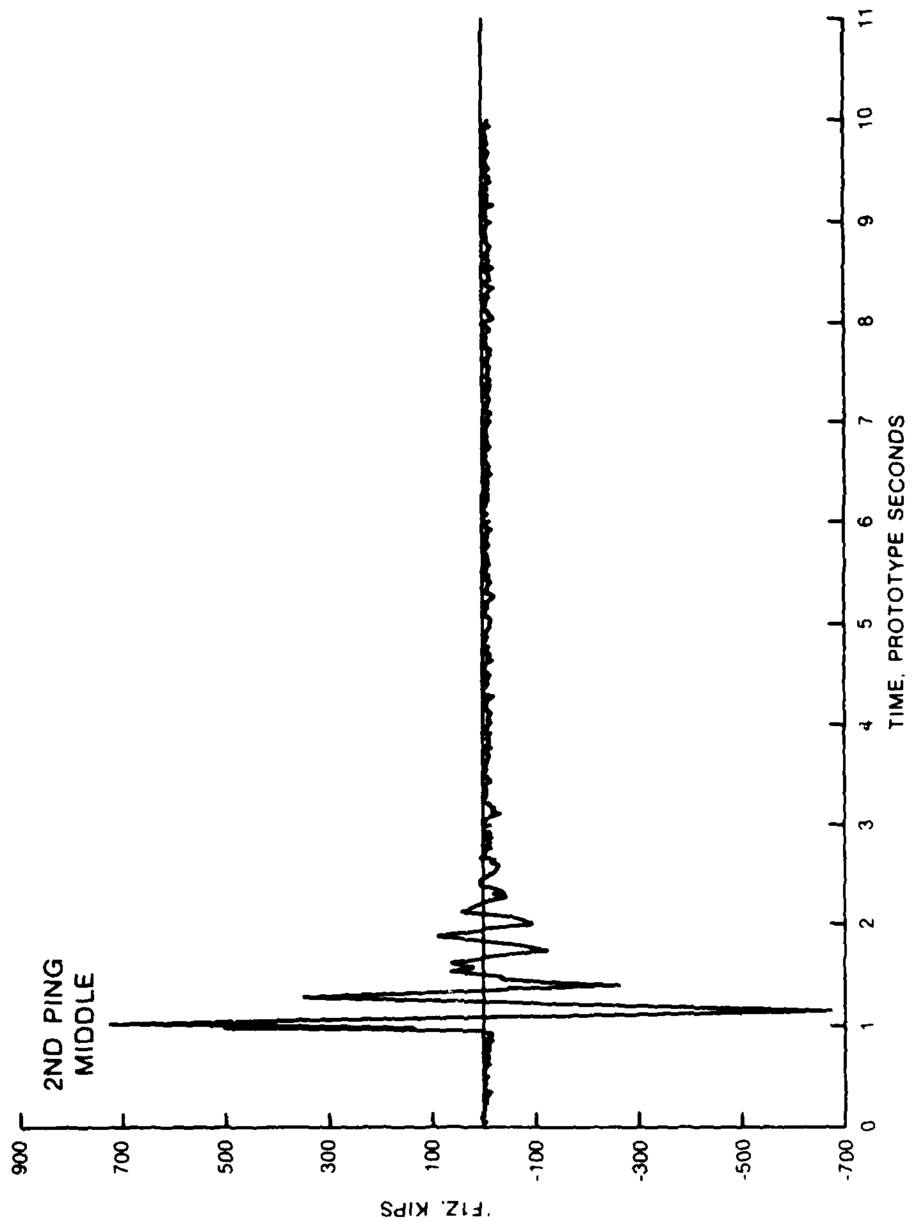

F1Z VERSUS TIME FOR SECOND
PING OF MIDDLE DURING
SIDE-CONNECTOR TEST 16

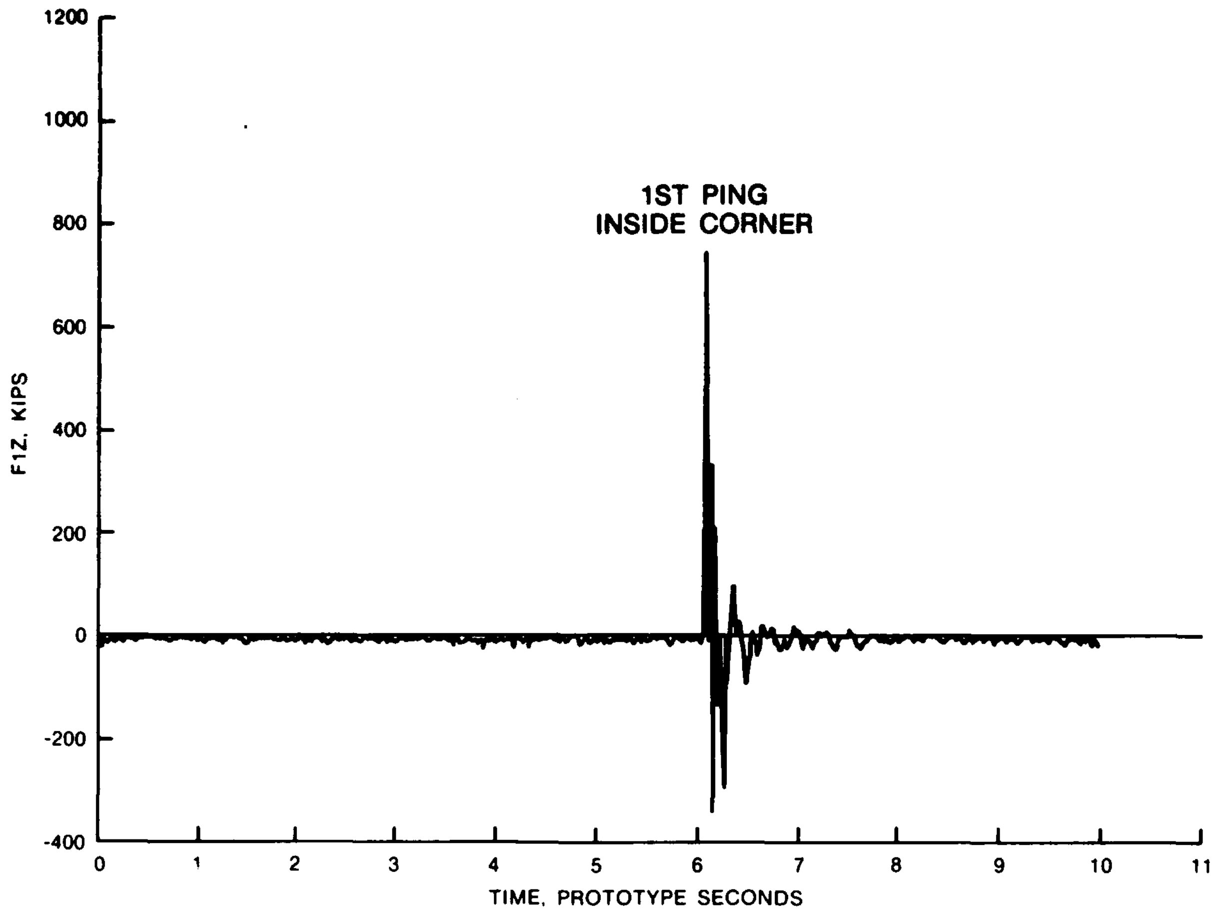

F1Z VERSUS TIME FOR FIRST PING OF INSIDE CORNER DURING SIDE-CONNECTOR TEST 16

APPENDIX A: NOTATION

A	Area, ft^2
$\bar{C}_t$	Average wave transmission coefficient
C_t	Wave transmission coefficient
d	Water depth, ft
$E(f)$	Spectral energy density function
E_o	Spectral energy
f	Frequency, sec^{-1}
f_m	Peak frequency, sec^{-1}
F	Force, lb or kips
g	Gravity, ft/sec^2
H_{mo}	Deep-water significant wave height, ft
H	Wave height, ft
H_s	Significant wave height, ft
H_t	Transmitted wave height, ft
I	Mass moment of inertia, lb (mass)/ft^2
L	Length or wavelength, ft
L_p	Wavelength of peak spectral period
T or t	Time or wave period, sec
T_p	Spectral peak wave period
V	Volume, ft^3
W	Width, ft

END

7-87

DTIC